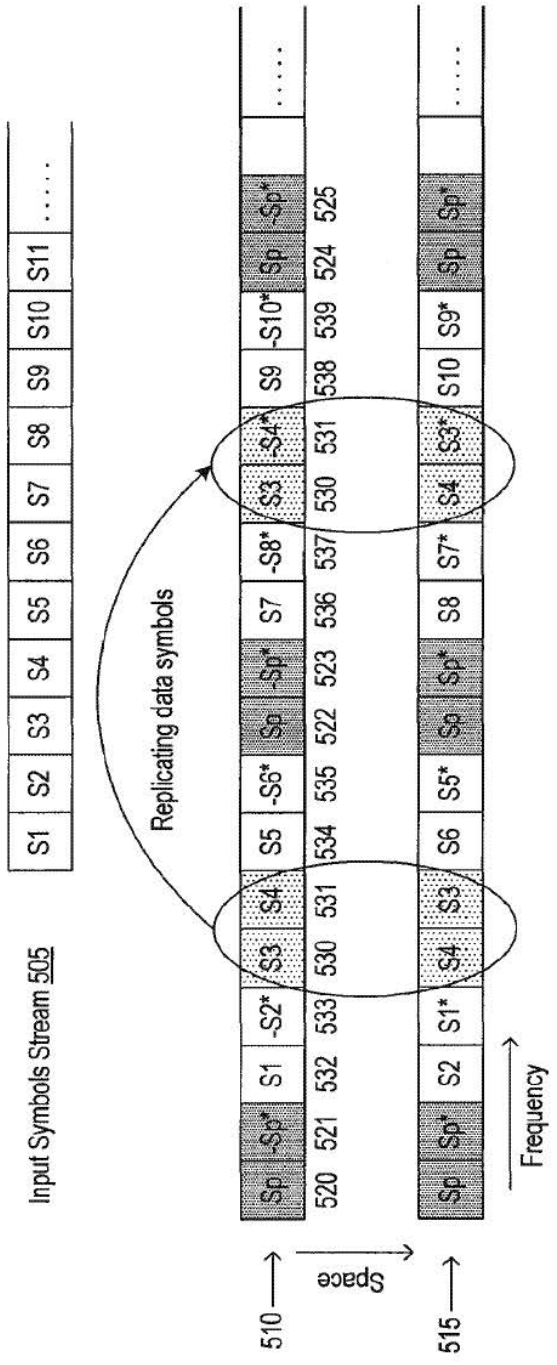


Figure 5

Petitioner Samsung Ex-1004, 0105

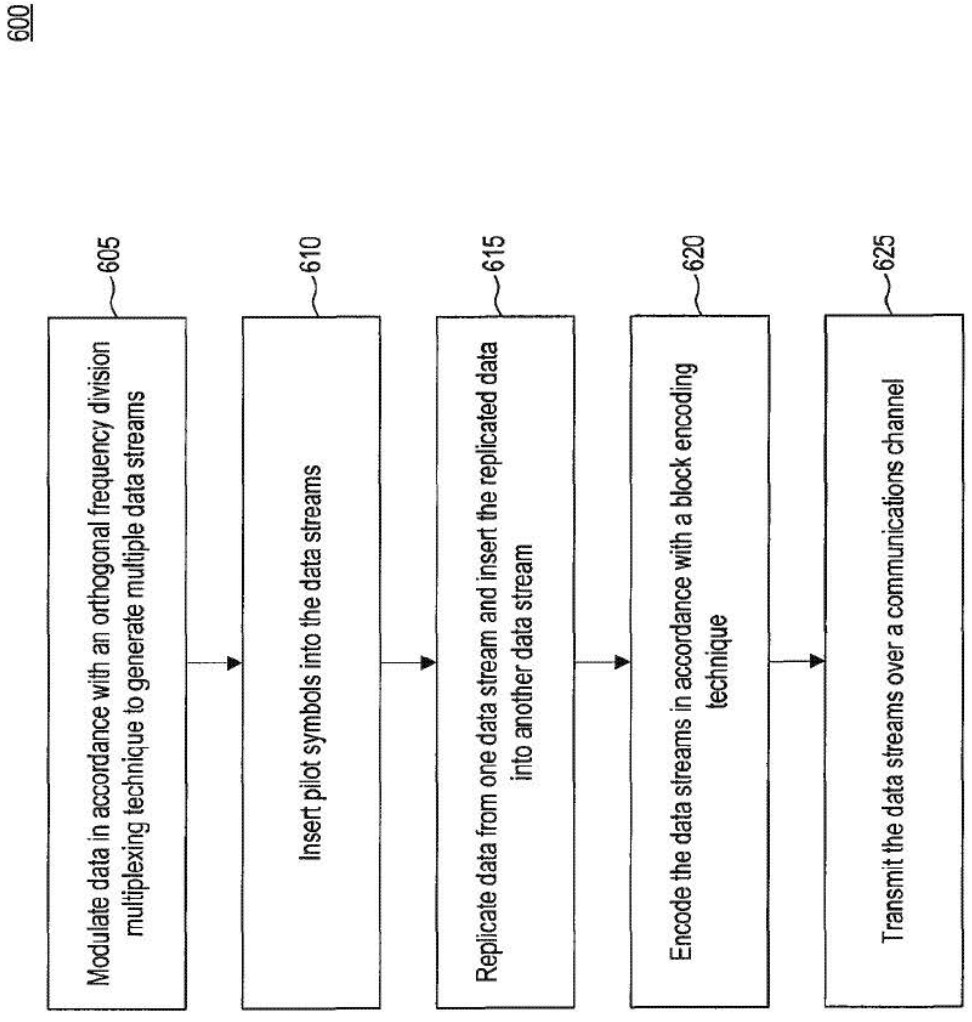


Figure 6

Petitioner Samsung Ex-1004, 0106

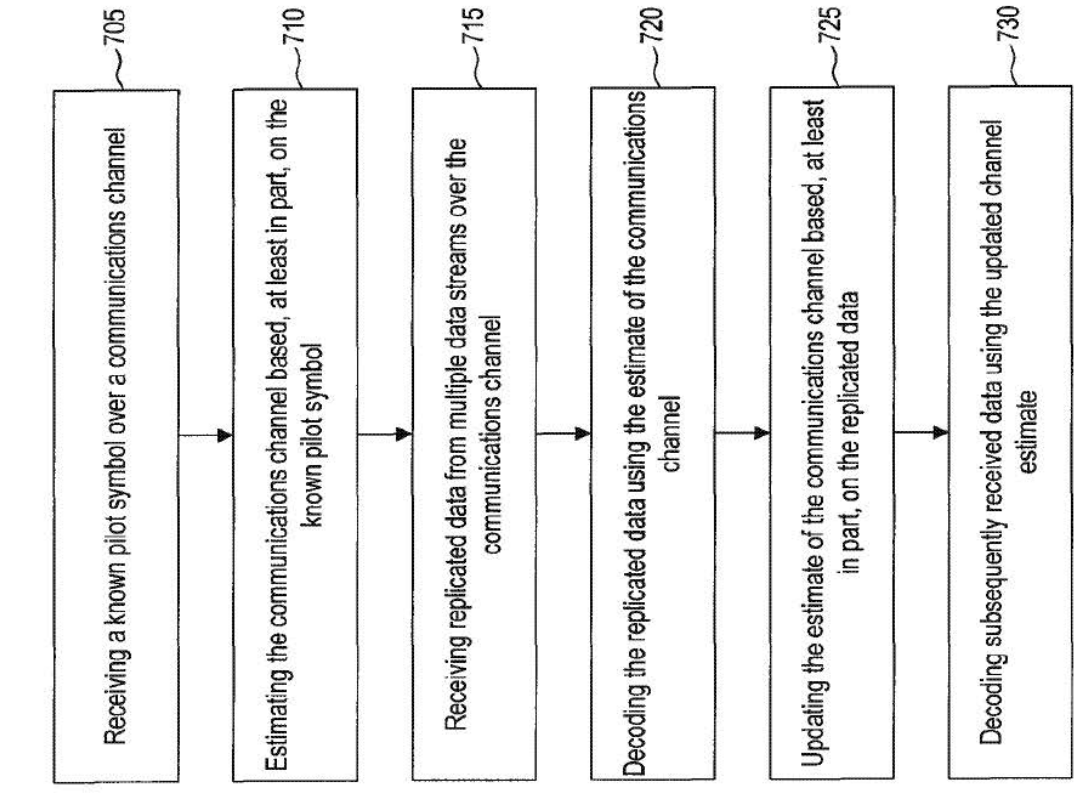


Figure 7

Petitioner Samsung Ex-1004, 0107

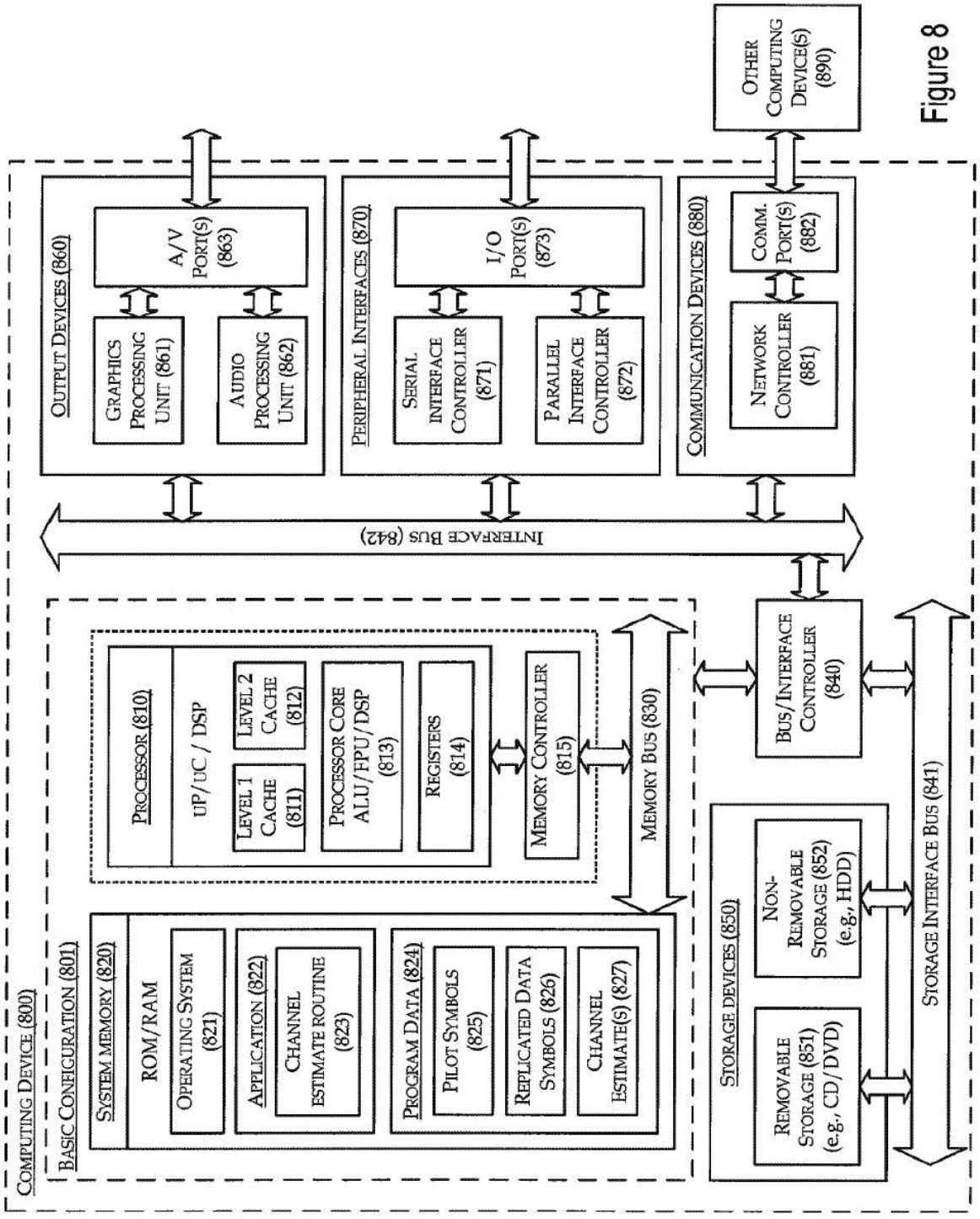


Figure 8

Petitioner Samsung Ex-1004, 0108

INTERNATIONAL SEARCH REPORT

International application No.
PCT/US2010/046106

A. CLASSIFICATION OF SUBJECT MATTER

Int. Cl.

H04L 27/28 (2006.01) ***H04J 11/00*** (2006.01)
H04B 7/04 (2006.01) ***H04K 1/10*** (2006.01)

According to International Patent Classification (IPC) or to both national classification and IPC

B. FIELDS SEARCHED

Minimum documentation searched (classification system followed by classification symbols)

Documentation searched other than minimum documentation to the extent that such documents are included in the fields searched

Electronic data base consulted during the international search (name of data base and, where practicable, search terms used)
EPODOC, WPI: mimo, miso, ofdm, multiple antenna, first, second stream, insert, embed, overlap, replicat, pilot and similar terms.
INSPEC: mimo, miso, ofdm, multiple antenna, first stream, second stream, insert, embed, overlap, replicat, pilot and similar terms.
GOOGLE, GOOGLE SCHOLAR: mimo, ofdm, first, second, (insert or embed or overlap), stream, pilot

C. DOCUMENTS CONSIDERED TO BE RELEVANT

Category*	Citation of document, with indication, where appropriate, of the relevant passages	Relevant to claim No.
A	US 7778337 B2 (TONG et al.) 17 August 2010 Abstract; Col. 4 line 12-Col. 6 line 21	1-20
A	US 7397862 B2 (OUYANG et al.) 8 July 2008 Abstract; Col. 1 line 64-Col. 2 line 19	1-20
A	US 2002/0122381 A1 (WU et al.) 5 September 2002 Abstract; Paras [0011]-[0015]	1-20

☐ Further documents are listed in the continuation of Box C ☒ See patent family annex

* Special categories of cited documents:
"A" document defining the general state of the art which is not considered to be of particular relevance
"E" earlier application or patent but published on or after the international filing date
"L" document which may throw doubts on priority claim(s) or which is cited to establish the publication date of another citation or other special reason (as specified)
"O" document referring to an oral disclosure, use, exhibition or other means
"P" document published prior to the international filing date but later than the priority date claimed
"T" later document published after the international filing date or priority date and not in conflict with the application but cited to understand the principle or theory underlying the invention
"X" document of particular relevance; the claimed invention cannot be considered novel or cannot be considered to involve an inventive step when the document is taken alone
"Y" document of particular relevance; the claimed invention cannot be considered to involve an inventive step when the document is combined with one or more other such documents, such combination being obvious to a person skilled in the art
"&" document member of the same patent family

Date of the actual completion of the international search	Date of mailing of the international search report
03 November 2010	09 NOV 2010
Name and mailing address of the ISA/AU AUSTRALIAN PATENT OFFICE PO BOX 200, WODEN ACT 2606, AUSTRALIA E-mail address: pct@ipaustralia.gov.au Facsimile No. +61 2 6283 7999	Authorized officer **JUZER KHANBHAI** AUSTRALIAN PATENT OFFICE (ISO 9001 Quality Certified Service) Telephone No : +61 2 6283 2176

Form PCT/ISA/210 (second sheet) (July 2009)

Petitioner Samsung Ex-1004, 0109

INTERNATIONAL SEARCH REPORT

Information on patent family members

International application No.
PCT/US2010/046106

This Annex lists the known "A" publication level patent family members relating to the patent documents cited in the above-mentioned international search report. The Australian Patent Office is in no way liable for these particulars which are merely given for the purpose of information.

Patent Document Cited in Search Report		Patent Family Member					
US	7778337	CN	1605172	CN	101188597	EP	1442549
		US	2003072254	US	7248559	US	2007253324
		US	7545734	US	2007053282	US	2009225891
		US	2010271930	WO	03034644		
US	7397862	US	2007086538				
US	2002/0122381	CA	2351140	CA	2355433	EP	1185001
		EP	1185048	EP	1686703	US	6850481
		US	2002122383	US	6985434	US	2002122382
		US	7009931	US	2002041635	US	7233625
		US	2006104196	US	7336601	US	2007274408
		US	7403570	US	2008002568	US	7688710
		US	2007036069	US	7801019		

Due to data integration issues this family listing may not include 10 digit Australian applications filed since May 2001.

END OF ANNEX

Petitioner Samsung Ex-1004, 0110

PCT REQUEST

Original (for **SUBMISSION**)

0	**For receiving Office use only**	
0-1	International Application No.	PCT/US10/46106
0-2	International Filing Date	20 AUG 2010(20.08.2010)
0-3	Name of receiving Office and "PCT International Application"	RO/US

0-4	**Form PCT/RO/101 PCT Request**	
0-4-1	Prepared Using	PCT-SAFE [EASY/EFS-Web mode] Version 3.51.045.221 MT/FOP 20100401/0.20.5.18
0-5	**Petition** The undersigned requests that the present international application be processed according to the Patent Cooperation Treaty	
0-6	**Receiving Office (specified by the applicant)**	United States Patent and Trademark Office (USPTO) (RO/US)
0-7	**Applicant's or agent's file reference**	P215801WO01
I	**Title of Invention**	INSERTING AND DECODING REPLICATED DATA SYMBOLS IN WIRELESS COMMUNICATIONS
II	**Applicant**	
II-1	This person is	Applicant only
II-2	Applicant for	All designated States except US
II-4	Name	THE BOARD OF REGENTS OF THE UNIVERSITY OF TEXAS SYSTEM
II-5	Address	201 W. 7th Street Austin, Texas 78701 United States of America
II-6	State of nationality	US
II-7	State of residence	US
III-1	**Applicant and/or inventor**	
III-1-1	This person is	Applicant and inventor
III-1-2	Applicant for	US only
III-1-4	Name (LAST, First)	ALI, Yazdan Panah
III-1-5	Address	502 Elmwood Place #101 Austin, Texas 78705 United States of America
III-1-6	State of nationality	IR
III-1-7	State of residence	US

PCT REQUEST

Original (for **SUBMISSION**)

III-2	**Applicant and/or inventor**	
III-2-1	This person is	Applicant and inventor
III-2-2	Applicant for	US only
III-2-4	Name (LAST, First)	HEATH, JR., Robert W.
III-2-5	Address	2143 Barton Hills Drive Austin, Texas 78704 United States of America
III-2-6	State of nationality	US
III-2-7	State of residence	US
IV-1	**Agent or common representative; or address for correspondence** The person identified below is hereby/ has been appointed to act on behalf of the applicant(s) before the competent International Authorities as:	Agent
IV-1-1	Name	DORSEY AND WHITNEY LLP
IV-1-2	Address	IP Docket - SE 701 Fifth Avenue, Suite 6100 Seattle, Washington 98104-7043 United States of America
IV-1-3	Telephone No.	206-903-8800
IV-1-4	Facsimile No.	206-299-9288
IV-1-5	e-mail	ipdocket-se@dorsey.com
IV-1-5(a)	E-mail authorization The receiving Office, the International Searching Authority, the International Bureau and the International Preliminary Examining Authority are authorized to use this e-mail address, if the Office or Authority so wishes, to send notifications issued in respect of this international application:	as advance copies followed by notifi-cations
IV-2	**Additional agent(s)**	additional agent(s) with same address as first named agent
IV-2-1	Name(s)	BULCHIS,Edward W.(26847); MEIKLEJOHN,Paul T.(26569); PARK,Brian C.(45519); ENG,Kimton N.(43605); STEWART,Douglas(51060); BROWN,James Fearon(60837); MEYER,Ryan(61435); LANE,Jennifer M.(51916)
V	**DESIGNATIONS**	
V-1	**The filing of this request constitutes under Rule 4.9(a), the designation of all Contracting States bound by the PCT on the international filing date, for the grant of every kind of protection available and, where applicable, for the grant of both regional and national patents.**	
VI-1	**Priority Claim**	NONE
VII-1	**International Searching Authority Chosen**	Australian Patent Office (ISA/AU)

PCT REQUEST

Original (for **SUBMISSION**)

VIII	**Declarations**	Number of declarations	
VIII-1	Declaration as to the identity of the inventor	–	
VIII-2	Declaration as to the applicant's entitlement, as at the international filing date, to apply for and be granted a patent	–	
VIII-3	Declaration as to the applicant's entitlement, as at the international filing date, to claim the priority of the earlier application	–	
VIII-4	Declaration of inventorship (only for the purposes of the designation of the United States of America)	–	
VIII-5	Declaration as to non-prejudicial disclosures or exceptions to lack of novelty	–	
IX	**Check list**	Number of sheets	Electronic file(s) attached
IX-1	Request (including declaration sheets)	4	✓
IX-2	Description	21	–
IX-3	Claims	4	–
IX-4	Abstract	1	✓
IX-5	Drawings	7	–
IX-7	TOTAL	37	
	Accompanying Items	Paper document(s) attached	Electronic file(s) attached
IX-8	Fee calculation sheet	✓	–
IX-20	**Figure of the drawings which should accompany the abstract**	1	
IX-21	**Language of filing of the international application**	English	
X-1	**Signature of applicant, agent or common representative**	/Jennifer M. Lane 51916/	
X-1-1	Name (LAST, First)	LANE, Jennifer M.	
X-1-2	Name of signatory		
X-1-3	Capacity		

PCT REQUEST

Original (for **SUBMISSION**)

FOR RECEIVING OFFICE USE ONLY

20-08-2010

10-1	**Date of actual receipt of the purported international application**	20 AUG 2010
10-2	**Drawings:**	
10-2-1	Received	
10-2-2	Not received	
10-3	**Corrected date of actual receipt due to later but timely received papers or drawings completing the purported international application**	
10-4	**Date of timely receipt of the required corrections under PCT Article 11(2)**	
10-5	**International Searching Authority**	ISA/AU
10-6	**Transmittal of search copy delayed until search fee is paid**	

FOR INTERNATIONAL BUREAU USE ONLY

11-1	**Date of receipt of the record copy by the International Bureau**	

To: ipdocket-se@dorsey.com,IPDocket_SE@dorsey.foundationip.com,pogson.phoebe@dorsey.com
From: PAIR_eOfficeAction@uspto.gov
Cc: PAIR_eOfficeAction@uspto.gov
Subject: Private PAIR Correspondence Notification for Customer Number 27076

Feb 24, 2012 05:28:32 AM

Dear PAIR Customer:

DORSEY & WHITNEY LLP
INTELLECTUAL PROPERTY DEPARTMENT
Columbia Center
701 Fifth Avenue, Suite 6100
SEATTLE, WA 98104-7043
UNITED STATES

The following USPTO patent application(s) associated with your Customer Number, 27076 , have new outgoing correspondence. This correspondence is now available for viewing in Private PAIR.

The official date of notification of the outgoing correspondence will be indicated on the form PTOL-90 accompanying the correspondence.

Disclaimer:
The list of documents shown below is provided as a courtesy and is not part of the official file wrapper. The content of the images shown in PAIR is the official record.

Application	Document	Mailroom Date	Attorney Docket No.
12999029	NTC.PUB	02/23/2012	P215801.WO-US.01

To view your correspondence online or update your email addresses, please visit us anytime at https://sportal.uspto.gov/secure/myportal/privatepair.

If you have any questions, please email the Electronic Business Center (EBC) at EBC@uspto.gov with 'e-Office Action' on the subject line or call 1-866-217-9197 during the following hours:

Monday - Friday 6:00 a.m. to 12:00 a.m.

Thank you for prompt attention to this notice,

UNITED STATES PATENT AND TRADEMARK OFFICE

PATENT APPLICATION INFORMATION RETRIEVAL SYSTEM

Doc code: IDS
Doc description: Information Disclosure Statement (IDS) Field

PTO/SB/08a (01-10)
Approved for use through 07/31/2012. OMB 0651-0031
U.S. Patent and Trademark Office; U.S. DEPARTMENT OF COMMERCE
Under the Paperwork Reduction Act of 1995, no persons are required to respond to a collection of information unless it contains a valid OMB control number.

INFORMATION DISCLOSURE STATEMENT BY APPLICANT (Not for submission under 37 CFR 1.99)		
	Application Number	12/999,029
	Filing Date	December 14, 2010
	First Named Inventor	Ali Yazdan Panah
	Art Unit	2611
	Examiner Name	Shuwang Liu
	Attorney Docket Number	P215801.WO-US.01

U.S.PATENTS

Examiner Initial*	Cite No	Patent Number	Kind Code[1]	Issue Date	Name of Patentee or Applicant of cited Document	Pages, Columns, Lines, Where Relevant Passages or Relevant Figures Appear
		US-6519296B2		Feb 11, 2003	Hladik	
		US-7522682B2		Apr 21, 2009	Obernosterer et al.	

FOREIGN PATENT DOCUMENTS

Examiner Initial*	Cite No	Foreign Document Number[3]	Country Code[2]	Kind Code[4]	Publication Date	Name of Patentee or Applicant of cited Document	Pages,Columns,Lines where Relevant Passages or Relevant Figures Appear	T[5]

NON-PATENT LITERATURE DOCUMENTS

Examiner Initials*	Cite No	Include name of the author (in CAPITAL LETTERS), title of the article (when appropriate), title of the item (book, magazine, journal, serial, symposium, catalog, etc.), date, page(s), volume-issue number(s), publisher, city and/or country where published.	T[5]
		CHEON, H. et al., "PERFORMANCE ANALYSIS OF SPACE-TIME BLOCK CODES IN TIME-VARYING RAYLEIGH FADING CHANNELS", IEEE International Conference on Acoustics, Speech, and Signal Processing, 2002. Proceedings. (ICASSP '02)., Volume: 3, pp. III-2357-III-2360	
		CIRPAN, H. A. et al., "Nondata-Aided Channel Estimation for OFDM Systems With Space-Frequency Transmit Diversity", IEEE Transactions on Vehicular Technology, March 2006, Vol: 55, no: 2, pp: 449-457	
		KLEIDER, J. E. , "MISO joint synchronization-pilot design for OFDM systems", IEEE International Conference on Acoustics, Speech and Signal Processing, 2008. ICASSP 2008., March 31 2008-April 4 2008, pp: 3033-3036	
		LEE, K. F. et al., "A Space-Frequency Transmitter Diversity Technique for OFDM Systems", Proc. IEEE Global Telecommunications Conf. (GLOBECOM), 2000, Vol.3, pp: 1473-1477	
		LI, W. et al., "Effects of channel-estimation errors on receiver selection-combining schemes for Alamouti MIMO systems with BPSK", IEEE Transactions on Communications, Jan 2006, Volume: 54, no. 1, pp: 169-178	

INFORMATION DISCLOSURE STATEMENT BY APPLICANT (Not for submission under 37 CFR 1.99)		
	Application Number	12/999,029
	Filing Date	December 14, 2010
	First Named Inventor	Ali Yazdan Panah
	Art Unit	2611
	Examiner Name	Shuwang Liu
	Attorney Docket Number	P215801.WO-US.01

		LU, H. , "PHY 45-4- Reduced-Complexity ICI Mitigation for Mobile SFBC-OFDM with Application to DVB-H", IEEE Wireless Communications and Networking Conference, 2008. WCNC 2008., March 31 2008-April 3, 2008, pp.1183-1187	
		STAMOULIS, A. et al., "Intercarrier Interference in MIMO OFDM", IEEE Transactions on Signal Processing, Oct 2002, Volume: 50, Issue.10, pp: 2451-2464	
		SUN, Y. et al., "EM-based iterative receiver design with carrier-frequency offset estimation for MIMO OFDM systems", IEEE Transactions on Communications, April 2005, Volume: 53, Issue: 4, pp: 581-586	
		XIAOQIANG, M. A. et al., "AN EM-BASED CHANNEL ESTIMATION ALGORITHM FOR SPACE-TIME AND SPACE-FREQUENCY BLOCK CODED OFDM", IEEE International Conference on Acoustics, Speech, and Signal Processing, 2003. Proceedings. (ICASSP'03)., 6-10 April 2003, Vol.4, pp: IV-389-92,	
		YANG, H., "A road to future broadband wireless access: MIMO-OFDM-Based air interface", Communications Magazine, IEEE, Jan. 2005, Volume: 43, Issue: 1, pp: 53-60	

EXAMINER SIGNATURE

Examiner Signature		Date Considered	

*EXAMINER: Initial if reference considered, whether or not citation is in conformance with MPEP 609. Draw line through a citation if not in conformance and not considered. Include copy of this form with next communication to applicant.

[1] See Kind Codes of USPTO Patent Documents at www.USPTO.GOV or MPEP 901.04. [2] Enter office that issued the document, by the two-letter code (WIPO Standard ST.3). [3] For Japanese patent documents, the indication of the year of the reign of the Emperor must precede the serial number of the patent document.
[4] Kind of document by the appropriate symbols as indicated on the document under WIPO Standard ST.16 if possible. [5] Applicant is to place a check mark here if English language translation is attached.

PERFORMANCE ANALYSIS OF SPACE-TIME BLOCK CODES IN TIME-VARYING RAYLEIGH FADING CHANNELS

Hyunsoo Cheon and Daesik Hong

Information & Telecommunications Lab
Dept. of Electrical/Electronic Engineering, Yonsei University
134 Shinchondong Seodaemungu, Seoul, 120-749, Korea
e-mail: hscheon@catseye.yonsei.ac.kr

ABSTRACT

In this paper, we provide the performance analysis of pilot symbol assisted modulation (PSAM) for transmit diversity with space-time block codes (STBC) in time-varying Rayleigh fading channels. For the performance evaluation, the average bit error rate of transmit diversity with STBC is derived when the channel estimation error exists. Using the result, the average BER in time-varying channels is evaluated when the PSAM is employed.

1. INTRODUCTION

The transmit diversity scheme, which is also known as space-time block codes (STBC), has been proposed by Alamouti [1], and it is one of the most simple and efficient ways to exploit full diversity in wireless channels. Particularly, the STBC provide the full diversity when it is hard to equip more than one receive antennas due to physical constraints, such as the cost of multiple RF down-converters, additional power consumption and size limitations.

To exploit the STBC in mobile communications, rapid fading is an inevitable impediment, which causes an irreducible error floor. To suppress the error floor, pilot symbol assisted modulation (PSAM) is one of the most likely solution [2].

In PSAM, the pilot symbol is inserted periodically in order to enable the coherent detection. Moreover, to detect the symbols received from multiple Tx antennas, the minimum number of pilot symbols per one Tx antenna is equal to the number of Tx antennas. In this case, the received pilot symbols may lose consistency due to rapid fading, and the estimated channel responses may harm the orthogonality of the received STBC symbols.

This work is supported by a grant from the Brain Korea (BK) 21 program and pnpnetwork corp. in Korea.

In this paper, we examine the pilot symbol assisted modulation with the Alamouti's scheme in rapid fading channels. We analyze the effect of the channel estimation error and time variations of the channel.

This paper is organized as follows. The next section describes the signal model and a brief review of the STBC. In section 3, the effect of the channel estimation error and time-variations of the channel are described. The performance evaluation is provided in section 4. In the final section, conclusions are drawn.

2. SYSTEM MODELING

In the following, boldface symbols denote matrices (in capital letters) and vectors (lower case). The index is used for the sample sequence number. A complex conjugation, matrix transpose and hermitian operator are denoted as the superscript *, ^{T}, and ^{H}, respectively.

2.1. Space-Time Block Codes

For simplicity, we consider a transmit diversity system with 2 TX antennas. The STBC symbol is transmitted from 2 TX antennas during two symbol periods $2T$.

$$\mathbf{x} = \begin{bmatrix} \overset{space}{\longrightarrow} \\ s_1 & s_2 \\ -s_2^* & s_1^* \end{bmatrix} \Big\downarrow time \tag{1}$$

In a flat fading channel, the received signal vector, whose elements are the symbols received at time t and $t+T$, is given as

$$\mathbf{r} = \begin{bmatrix} r_1 \\ r_2^* \end{bmatrix} = \frac{1}{\sqrt{2}} \underbrace{\begin{bmatrix} h_1 & h_2 \\ h_2^* & -h_1^* \end{bmatrix}}_{\mathbf{H}} \underbrace{\begin{bmatrix} s_1 \\ s_2 \end{bmatrix}}_{\mathbf{s}} + \underbrace{\begin{bmatrix} n_1 \\ n_2^* \end{bmatrix}}_{\mathbf{n}}, \tag{2}$$

where h_i is the channel response of the signal received from TX antenna i, s_i is the transmitted symbol with

Petitioner Samsung Ex-1004, 0118

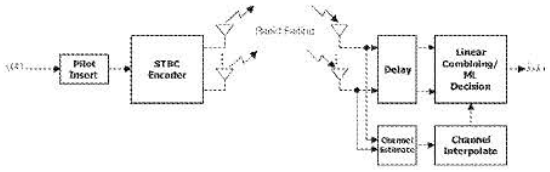


Figure 1: PSAM using Transmit diversity with STBC

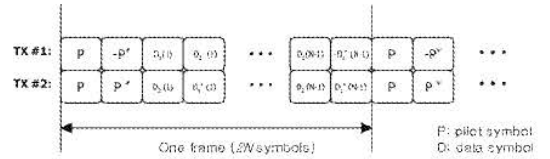


Figure 2: Transmitted symbol frame structure

variance σ_s^2, and n_1 and n_2 are the additive noise with variance σ_n^2.

The combined signal vector is written as

$$\mathbf{z} = \mathbf{H}^H \mathbf{r} = \frac{|h_1|^2 + |h_2|^2}{\sqrt{2}} \mathbf{s} + \mathbf{H}^H \mathbf{n}. \tag{3}$$

We assume that the channel response is normalized, *i.e.*, $E\{|h_i|^2\} = 1$ for $i = 1, 2$, so that the average received SNR is $\bar{\gamma} = \sigma_s^2/\sigma_n^2$.

2.2. Pilot Symbol Aided Modulation (PSAM)

Figure 1 shows a block diagram of a transmit diversity system exploiting PSAM. Known pilot symbols are inserted periodically for frequency channel estimation, and the channel interpolation is performed in the receiver for the compensation of the channel variations.

We assume that the pilot symbol block is an orthogonal matrix $\mathbf{U}$, *i.e.*, $\mathbf{U}^H\mathbf{U} = \mathbf{I}$, and it is transmitted with power P. The resulting frame structure can be shown in Fig 2. In this case, the received pilot symbol block at one Rx antenna can be written as

$$\mathbf{r}_P = \begin{bmatrix} r_{P1} \\ r_{P2} \end{bmatrix} = \sqrt{P}\mathbf{U} \begin{bmatrix} h_1 \\ h_2 \end{bmatrix} + \mathbf{n}. \tag{4}$$

The channel response vector is directly estimated as

$$\hat{\mathbf{h}} = \frac{1}{\sqrt{P}} \mathbf{U}^H \mathbf{r}_P = \mathbf{h} + \underbrace{\frac{1}{\sqrt{P}} \mathbf{U}^H \mathbf{n}}_{\boldsymbol{\epsilon}}, \tag{5}$$

where $\boldsymbol{\epsilon}$ is 2×1 channel estimation error vector, whose elements are mutually uncorrelated complex Gaussian r.v.s with variance σ_ϵ^2.

3. PSAM FOR STBC IN TIME-VARYING CHANNELS

3.1. Channel Estimation Error

In a time-varying Rayleigh fading channel, the received symbol vector is rewritten as

$$\mathbf{r}(k) = \underbrace{\frac{1}{\sqrt{2}} \begin{bmatrix} h_{1,0}(k) & h_{2,0}(k) \\ h_{2,1}^*(k) & -h_{1,1}^*(k) \end{bmatrix}}_{\mathbf{H}(k)} \begin{bmatrix} s_1(k) \\ s_2(k) \end{bmatrix} + \begin{bmatrix} n_1(k) \\ n_2^*(k) \end{bmatrix}, \tag{6}$$

where k denotes the STBC symbol index within one symbol frame, and $h_{i,j}(k)$ is i-th channel respouse at $(2k + j)T$.

In this case, the channel response is estimated from the observation $\mathbf{r}(0)$, and the estimated channel response vector is

$$\hat{\mathbf{h}} = \frac{1}{2} \begin{bmatrix} h_{1,0}(0) + h_{1,1}(0) \\ h_{2,0}(0) + h_{2,1}(0) \end{bmatrix} + \frac{1}{2} \begin{bmatrix} h_{2,0}(0) - h_{2,1}(0) \\ h_{1,0}(0) - h_{1,1}(0) \end{bmatrix} + \boldsymbol{\epsilon}. \tag{7}$$

The channel responses $h_{i,0}(0)$ and $h_{i,1}(0)$ are mutually correlated complex Gaussian r.v.s, and can be expressed using a standard transformation of r.v.s. as follows.

$$\begin{aligned} h_{i,0}(0) &= \sqrt{\frac{1+\rho}{2}} p_i(0) + \sqrt{\frac{1-\rho}{2}} q_i(0) \\ h_{i,1}(0) &= \sqrt{\frac{1+\rho}{2}} p_i(0) - \sqrt{\frac{1-\rho}{2}} q_i(0), \end{aligned} \tag{8}$$

where $p_i(0)$ and $q_i(0)$ are mutually uncorrelated complex Gaussian r.v.s with variance 1, and the correlation coefficient ρ is

$$\rho = \frac{\mathrm{Cov}(|h_{i,0}(0)|^2, |h_{i,1}(0)|^2)}{\sqrt{\mathrm{Var}(h_{i,0}(0))\mathrm{Var}(h_{i,1}(0))}}. \tag{9}$$

Substituting (8) into (7), the estimated channel response vector can be rewritten as

$$\hat{\mathbf{h}}(0) = \sqrt{\frac{1+\rho}{2}} \begin{bmatrix} p_1(0) \\ p_2(0) \end{bmatrix} + \sqrt{\frac{1-\rho}{2}} \begin{bmatrix} q_2(0) \\ q_1(0) \end{bmatrix} + \boldsymbol{\epsilon}. \tag{10}$$

Assuming that the desired channel response is $h_{i,0}(0)$, the channel mismatch is rewritten as

$$\tilde{\epsilon}_i = |\hat{h}_{i,0}(0) - h_{i,0}(0)| = \sqrt{\frac{1-\rho}{2}} |q_1(0) - q_2(0)| + \epsilon_i(0), \tag{11}$$

and its variance is $\sigma_{\tilde{\epsilon}}^2 = (1 - \rho) + \sigma_n^2/P$.

The correlation coefficient is determined by the channel model, the maximum doppler frequency f_d and time interval. We consider three channel models - classic [3],

Petitioner Samsung Ex-1004, 0119

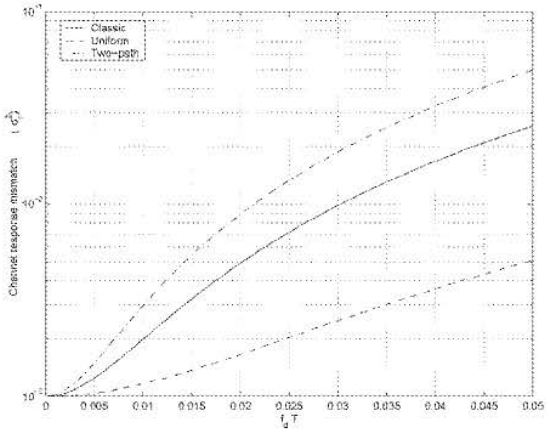


Figure 3: Channel response mismatch due to the loss of orthogonality (pilot SNR = 30 dB)

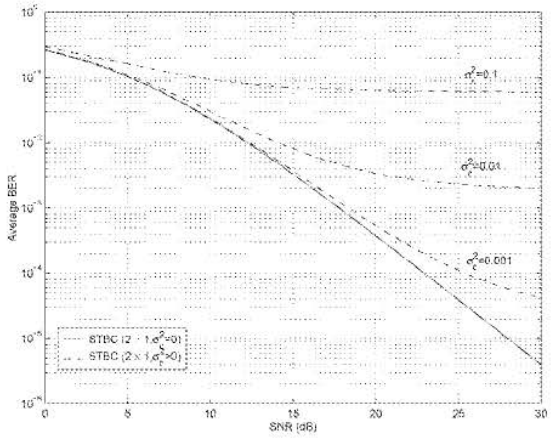


Figure 4: BER of QPSK in transmit diversity using STBC when the channel estimation error exists.

uniform, and two-path model, in which the correlation coefficients are given as

$$\rho = \begin{cases} J_0(2\pi f_d T) & \text{(classic model)} \\ \mathrm{sinc}(f_d T) & \text{(uniform model)} \\ \cos(2\pi f_d T) & \text{(two-path model)} \end{cases} \tag{12}$$

where $J_0(x)$ is the zeroth-order Bessel function of the first kind, and $\mathrm{sinc}(x) = \sin(\pi x)/\pi x$.

Figure 3 shows the channel response mismatch in time-varying Rayleigh channels.

3.2. Channel Response Interpolation

The combined symbol vector can be written as

$$\mathbf{z}(k) = \frac{1}{\sqrt{2}} \underbrace{\tilde{\mathbf{H}}^H(k)\mathbf{H}(k)}_{\mathbf{\Omega}} \begin{bmatrix} s_1(k) \\ s_2(k) \end{bmatrix} + \tilde{\mathbf{H}}(k)\mathbf{n}(k) \tag{13}$$

where $\tilde{\mathbf{H}}(k)$ is interpolated channel response matrix.

In this case, the channel response interpolation should be performed for each symbol interval T to reduce the degradation due to the loss of orthogonality. Thus, 4 channel responses are interpolated in one STBC symbol duration, the interpolated channel response matrix becomes

$$\tilde{\mathbf{H}}(k) = \begin{bmatrix} \tilde{h}_{1,0}(k) & \tilde{h}_{2,0}(k) \\ \tilde{h}_{2,1}(k) & \tilde{h}_{1,1}(k) \end{bmatrix}, \tag{14}$$

and the matrix $\mathbf{\Omega}$ is written as

$$\mathbf{\Omega} = \begin{bmatrix} a_{1,2} & b_{1,2} \\ b_{2,1} & a_{2,1} \end{bmatrix} \tag{15}$$

where

$$\begin{aligned} a_{i,j}(k) &= \tilde{h}_{i,0}^*(k)h_{i,0}(k) + \tilde{h}_{j,1}(k)h_{j,1}^*(k), \\ b_{i,j}(k) &= \tilde{h}_{i,0}^*(k)h_{j,0}(k) - \tilde{h}_{j,1}(k)h_{i,1}^*(k). \end{aligned} \tag{16}$$

In the optimum linear channel interpolator (wiener filter) [2], the interpolation error is uncorrelated with $\tilde{h}_{i,j}(k)$ and $\hat{h}_{i,0}(k)$, and its variance becomes $\sigma_{\tilde{e}}^2$.

4. PERFORMANCE ANALYSIS

4.1. Effect of Channel Estimation Error

Assuming that the channel response is stationary and the transmitted symbols are uncorrelated, the effective SNR is a conditional expectation subject to the estimated channel responses $\hat{h}_1$ and $\hat{h}_2$, which can be written as

$$\gamma_e = \frac{(|h_1 + \epsilon_1|^2 + |h_2 + \epsilon_2|^2)\sigma_s^2}{(|\epsilon_1|^2 + |\epsilon_2|^2)\sigma_s^2 + 2\sigma_n^2}. \tag{17}$$

Let $\alpha = |\epsilon_1|^2 + |\epsilon_2|^2$. The channel estimation error ϵ_1 and ϵ_2 are mutually uncorrelated complex Gaussian r.v.s, so that α is a chi-square r.v. with 4 degrees of freedom.

For sufficiently small σ_ϵ^2, the channel estimation error ϵ_i and the estimated channel response $\hat{h}_i$ can be assumed to be uncorrelated. Under this assumption, BER of QPSK can be obtained as

$$P_E(\bar{\gamma}) = \int_0^\infty P(E|\alpha)p(\alpha)d\alpha. \tag{18}$$

Suppose that the channel response h_i is i.i.d. complex gaussian r.v, the conditional error probability is

$$P(E|\alpha) = \left(\frac{1-\xi(\alpha)}{2}\right)^2 \{2 + \xi(\alpha)\}, \tag{19}$$

Petitioner Samsung Ex-1004, 0120

where

$$\xi(\alpha) = \sqrt{\frac{\bar{\gamma}(1+\sigma_\epsilon^2)}{\bar{\gamma}(2\alpha+1+\sigma_\epsilon^2)+4}}. \quad (20)$$

Figure 4 shows the average BER of QPSK in 2×1 STBC when there is the channel estimation error. As shown in the figure, the channel estimation error causes the error floor.

4.2. Effect of Time-Varying Channels

To evaluate the optimum case, the frame length is chosen to be $N < 1/4f_dT$, and the pilot SNR is set to the average data SNR $\bar{\gamma}$. When the channel response interpolation is perfect, the performance is degraded by the channel estimation error at each pilot symbol blocks and the loss of orthogonality.

Though the effect of the channel estimation error at high SNR is small, the loss of orthogonality causes the irreducible error. Figure 5 and 6 show the average BER of QPSK when optimum channel interpolation is assumed in two channels (classic, uniform). As shown in the figures, the error floors are due to the initial channel estimation error and the loss of orthogonality of the pilot symbol block. The BER performance in the uniform channel model is shown to be better than that in classic channel model. This indicates that the error floor is mostly due to the correlation between the consecutive channel responses.

5. CONCLUSIONS

The STBC is simple and effective transmit diversity scheme, which exploits the orthogonality of the transmitted symbols. However, the loss of orthogonality due to the time-variation of the channel response increases the channel estimation error, which causes performance degradation.

For a performance evaluation of STBC in rapid Rayleigh fading channels, the impairments due to the channel estimation error and the time-varying channels are analyzed, and the average bit error probability is derived.

6. REFERENCES

[1] S. M. Alamouti, "A simple transmit diversity technique for wireless communications," *IEEE Journal of Selected Areas in Comm.*, vol. 16, pp. 1451–1458, Oct. 1998.

[2] J. K. Cavers, "An Analysis of Pilot-Symbol assisted modulation for Rayleigh-fading Channels," *IEEE Trans. on Vehicular Tech.*, vol. 40, pp. 686–693, Nov. 1991.

[3] W. C. Jakes, *Microwave Mobile Communication*. New York: John Wiley & Sons, 1974.

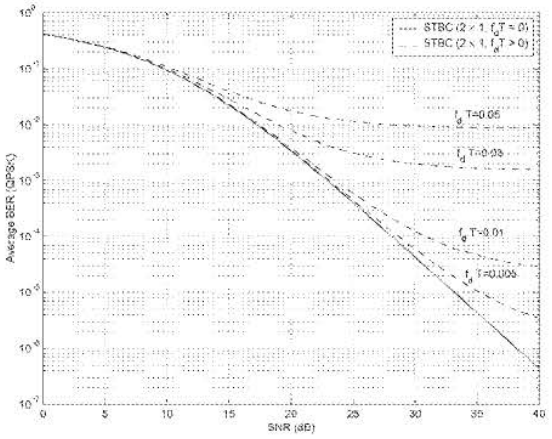


Figure 5: BER of QPSK in transmit diversity using STBC (PSAM, classic model)

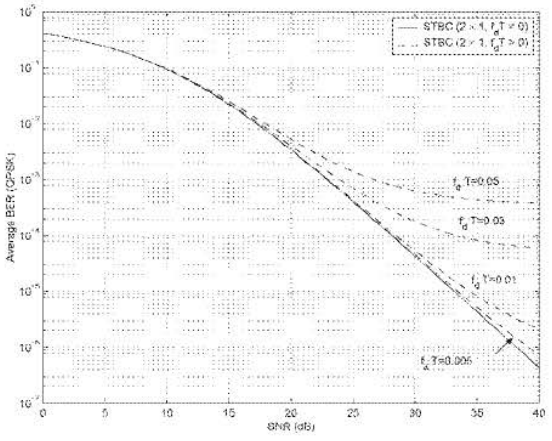


Figure 6: BER of QPSK in transmit diversity using STBC (PSAM, uniform model)

Petitioner Samsung Ex-1004, 0121

Nondata-Aided Channel Estimation for OFDM Systems With Space-Frequency Transmit Diversity

Hakan A. Çırpan, *Member, IEEE*, Erdal Panayırcı, *Fellow, IEEE*, and Hakan Doğan, *Student Member, IEEE*

***Abstract*—This paper proposes a computationally efficient nondata-aided maximum *a posteriori* (MAP) channel-estimation algorithm focusing on the space-frequency (SF) transmit diversity orthogonal frequency division multiplexing (OFDM) transmission through frequency-selective channels. The proposed algorithm properly averages out the data sequence and requires a convenient representation of the discrete multipath fading channel based on the Karhunen–Loeve (KL) orthogonal expansion and estimates the complex channel parameters of each subcarrier iteratively, using the expectation maximization (EM) method. To further reduce the computational complexity of the proposed MAP algorithm, the optimal truncation property of the KL expansion is exploited. The performance of the MAP channel estimator is studied based on the evaluation of the modified Cramer–Rao bound (CRB). Simulation results confirm the proposed theoretical analysis and illustrate that the proposed algorithm is capable of tracking fast fading and improving overall performance.**

***Index Terms*—Expectation maximization (EM) algorithm, maximum *a posteriori* (MAP) channel estimation, orthogonal frequency division multiplexing (OFDM) systems, space-frequency coding.**

I. Introduction

TRADITIONAL wireless technologies are not very well suited to meet the demanding requirements of providing very high data rates with ubiquity and mobility. Given the scarcity and exorbitant cost of the radio spectrum, such data rates dictate the need for extremely high spectral efficient coding and modulation schemes [1]. The combined application of transmit-antenna diversity and orthogonal frequency division multiplexing (OFDM) modulation appears to be capable of enabling the types of capacities and data rates needed for broadband wireless services [1], [2].

Transmit-antenna diversity has been exploited recently to develop high-performance space-time/frequency codes and simple maximum likelihood (ML) decoders for transmission over flat fading channels [3]–[5]. Unfortunately, their practical application can present a real challenge to channel-estimation algorithms, especially when the signal suffers from frequency-selective multipath channels. One of the solutions for alleviating frequency selectivity is through the use of OFDM together with transmit diversity which combats the long channel impulse response by transmitting parallel symbols over many orthogonal subcarriers, yielding unique reduced complexity physical layer capabilities [1].

Channel estimation for transmit-diversity OFDM systems has attracted much attention with the pioneering studies of Li [6], [7]. Among many other techniques, an iterative procedure based on the expectation maximization (EM) algorithm was also applied to the channel estimation problem in the context of space-time block coding (STBC) [8], [9] as well as transmit-diversity OFDM systems [10]–[13]. In [10], both the ML and the maximum *a posteriori* (MAP) iterative receivers for STBC-OFDM systems based on the EM algorithm are proposed to directly detect transmitted symbols under the assumption that fading processes remain constant across several OFDM words contained in one STBC code word. Note that even this approach pretends to bypass the channel-estimation process; it iterates between the ML data detection and the channel estimation consecutively until the convergence is reached. Although this approach is certainly optimal, its convergence rate is slow; the initial selection of the channel parameters is very critical and its implementation is quite complex.

An EM approach proposed for the general estimation from superimposed signals [15] is applied to the channel estimation for OFDM systems with transmitter- diversity systems and is compared with the space-alternating generalized EM (SAGE) version in [12]. Moreover, in [13], a modified version of [12] is proposed for STBC-OFDM and space-frequency (SF) block-coding (SFBC)-OFDM systems.

Unlike the EM approaches treated in [10]–[13], we adopt a two-step detection procedure: 1) Use the EM algorithm to estimate the channel, and 2) use the estimated channel to perform coherent detection. The major contribution of this paper is to obtain a new efficient nondata-aided MAP EM channel-estimation algorithm for OFDM systems with transmitter diversity using SFBC. A different approach is adapted here to explicitly model the channel parameters by a Karhunen–Loeve (KL) series representation, since a KL expansion allows one to tackle the estimation of correlated parameters as a parameter estimation problem of the uncorrelated coefficients. Note that

Manuscript received August 8, 2003; revised June 17, 2004 and August 2, 2005. This work was conducted within the NEWCOM Network of Excellence in Wireless COMmunications funded through the EC Sixth Framework Programme and was supported in part by the Research Fund of Istanbul University under Projects 220/29042004, UDP-599/28042005, and UDP-599/28072005, and The Scientific and Technological Research Council of Turkey (TUBITAK) under Grant 104E166. The review of this paper was coordinated by Dr. E. Larsson.

H. A. Çırpan and H. Doğan are with the Department of Electrical Engineering, Istanbul University, Avcilar 34850, Istanbul, Turkey (e-mail: hcirpan@istanbul.edu.tr; hdogan@istanbul.edu.tr).

E. Panayırcı is with the Department of Electrical and Electronics Engineering, Bilkent University, Bilkent 06800, Ankara, Turkey (e-mail: eepanay@ee.bilkent.edu.tr).

Digital Object Identifier 10.1109/TVT.2005.863427

0018-9545/$20.00 © 2006 IEEE

Petitioner Samsung Ex-1004, 0122

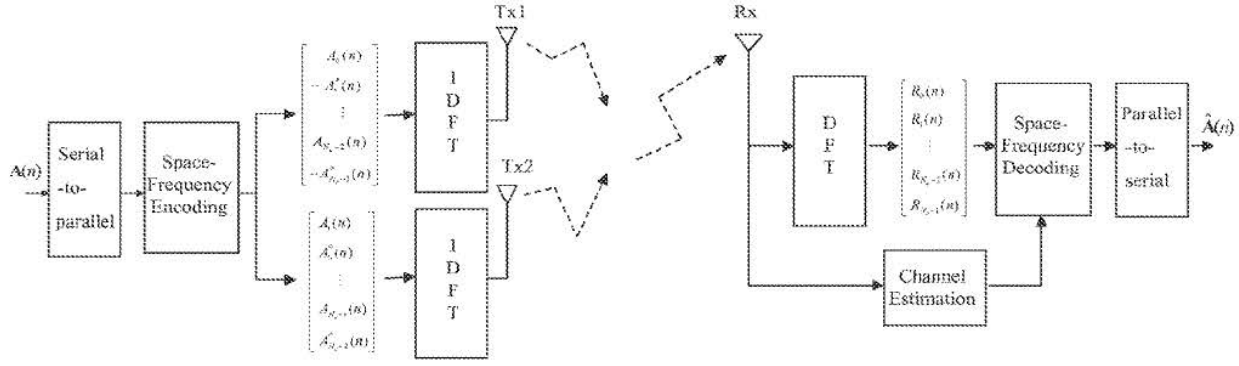


Fig. 1. SF block-coded OFDM scheme.

the KL expansion is well known for its optimal truncation property [19]. That is, the KL expansion requires the minimum number of terms among all possible series expansions in representing a random channel for a given mse. Thus, the optimal truncation property of the KL expansion results in a smaller computational load on the channel-estimation algorithm. Moreover, except for a few pilot symbols for initialization, the technique does not need any training sequence to acquire the channel and more information carrying signals can be transmitted.

Due to the orthogonality of the SFBC system based on the Alamouti orthogonal design, as well as the KL expansion of the multipath channel that yields simple exact iterative expressions for the unknown channel parameters in frequency domain which do not require any matrix inversion [18], [19]. Moreover, the optimal truncation property of the KL expansion can further reduce the computational load on the channel-estimation algorithm.

II. SFBC-OFDM Systems

Resorting to coding across tones, the set of generally correlated OFDM subchannels is first divided into groups of subchannels. This subchannel grouping with appropriate system parameters preserves the diversity gain while simplifying not only the code construction, but the decoding algorithm as well [14]. A block diagram of a two-branch SF OFDM transmitter-diversity system is shown in Fig. 1. To cast the received signal model, we first define $N_c \times 1$ the data vector $\mathbf{A}(n)$ as $\mathbf{A}(n) = [A(nN_c), A(nN_c+1), \ldots, A(nN_c + N_c - 1)]^T$. Following the notation of [14], let $A_k(n)$ denote the kth forward polyphase component of the serial data symbols, i.e, $A_k(n) = A(nN_c + k)$ for $k = 0, \ldots, N_c - 1$. The polyphase component $A_k(n)$ can also be viewed as the data symbol to be transmitted on the kth tone during the block instant n. The data symbol vector $\mathbf{A}(n)$ can therefore be expressed as $\mathbf{A}(n) = [A_0(n), A_1(n), \ldots, A_{N_c-1}]^T$. Resorting the subchannel grouping, $\mathbf{A}(n)$ is coded into two vectors $\mathbf{A}_e(n)$ and $\mathbf{A}_o(n)$ by the SF encoder as

$$\begin{aligned}\mathbf{A}_e(n) &= [A_0(n), A_2(n), \ldots, A_{N_c-4}(n), A_{N_c-2}(n)]^T \\ \mathbf{A}_o(n) &= [A_1(n), A_3(n), \ldots, A_{N_c-3}(n), A_{N_c-1}(n)]^T \end{aligned} \quad (1)$$

where $\mathbf{A}_e(n)$ and $\mathbf{A}_o(n)$ actually corresponds to the even and odd polyphase component vectors of $\mathbf{A}(n)$. Then, the SF block code transmission matrix may be represented by

$$\begin{matrix} & \text{frequency} \rightarrow \\ \text{space} \downarrow & \end{matrix} \begin{bmatrix} \mathbf{A}_e(n) & -\mathbf{A}_o^*(n) \\ \mathbf{A}_o(n) & \mathbf{A}_e^*(n) \end{bmatrix} \quad (2)$$

where * stands for the complex conjugation.

If the received signal sequence is also parsed in even and odd blocks of N_c tones, $\mathbf{R}_e(n) = [R_0(n), R_2(n), \ldots, R_{N_c-2}(n)]^T$ and $\mathbf{R}_o(n) = [R_1(n), R_3(n), \ldots, R_{N_c-1}(n)]^T$, the received signal can be expressed in vector form as

$$\begin{aligned}\mathbf{R}_e(n) &= \mathcal{A}_e(n)\mathbf{H}_{1,e}(n) + \mathcal{A}_o(n)\mathbf{H}_{2,e}(n) + \mathbf{W}_e(n) \\ \mathbf{R}_o(n) &= -\mathcal{A}_o^\dagger(n)\mathbf{H}_{1,o}(n) + \mathcal{A}_e^\dagger(n)\mathbf{H}_{2,o}(n) + \mathbf{W}_o(n) \end{aligned} \quad (3)$$

where $\mathcal{A}_e(n)$ and $\mathcal{A}_o(n)$ are $N_c/2 \times N_c/2$ diagonal matrices whose elements are $\mathbf{A}_e(n)$ and $\mathbf{A}_o(n)$, respectively, and † denotes the conjugate transpose. $\mathbf{H}_{\mu,e}(n) = [H_{\mu,0}(n), H_{\mu,2}(n), \ldots, H_{\mu,N_c-2}(n)]^T$ and $\mathbf{H}_{\mu,o}(n) = [H_{\mu,1}(n), H_{\mu,3}(n), \ldots, H_{\mu,N_c-1}(n)]^T$ are $N_c/2$ length vectors denoting the even and odd component vectors of the channel attenuations between the μth transmitter and the receiver. Finally, $\mathbf{W}_e(n)$ and $\mathbf{W}_o(n)$ are $N_c/2 \times 1$ zero mean and independent identically distributed (i.i.d.) Gaussian vectors that model additive noise in the N_c tones, with a variance of $\sigma^2/2$ per dimension.

Equation (3) shows that the information symbols $\mathcal{A}_e(n)$ and $\mathcal{A}_o(n)$ are transmitted twice in two consecutive adjacent subchannel groups through two different channels. In order to estimate the channels and decode $\mathcal{A}$ with the embedded diversity gain through the repeated transmission, for each n, we can write the following equation from (3) as

$$\begin{bmatrix} \mathbf{R}_e(n) \\ \mathbf{R}_o(n) \end{bmatrix} = \begin{bmatrix} \mathcal{A}_e(n) & \mathcal{A}_o(n) \\ -\mathcal{A}_o^\dagger(n) & \mathcal{A}_e^\dagger(n) \end{bmatrix} \begin{bmatrix} \mathbf{H}_{1,e}(n) \\ \mathbf{H}_{2,e}(n) \end{bmatrix} + \begin{bmatrix} \mathbf{W}_e(n) \\ \mathbf{W}_o(n) \end{bmatrix} \quad (4)$$

where the complex channel gains between the adjacent subcarriers are assumed to be approximately constant, i.e., $\mathbf{H}_{1,e}(n) \approx \mathbf{H}_{1,o}(n)$ and $\mathbf{H}_{2,e}(n) \approx \mathbf{H}_{2,o}(n)$. The effect of this assumption allows us to omit the dependence of $\mathbf{H}_{1,e}(n)$ and $\mathbf{H}_{2,e}(n)$ on

Petitioner Samsung Ex-1004, 0123

the even channel components. Using (4) and dropping subscript "$_e$," we have

$$\begin{bmatrix} \mathbf{R}_e(n) \\ \mathbf{R}_o(n) \end{bmatrix} = \begin{bmatrix} \mathcal{A}_e(n) & \mathcal{A}_o(n) \\ -\mathcal{A}_o^{\dagger}(n) & \mathcal{A}_e^{\dagger}(n) \end{bmatrix} \begin{bmatrix} \mathbf{H}_1(n) \\ \mathbf{H}_2(n) \end{bmatrix} + \begin{bmatrix} \mathbf{W}_e(n) \\ \mathbf{W}_o(n) \end{bmatrix} \tag{5}$$

or in a more succinct form

$$\mathbf{R}(n) = \mathcal{A}(n)\mathbf{H}(n) + \mathbf{W}(n). \tag{6}$$

Based on (6), our main objective in this paper is to develop a channel-estimation algorithm in accordance with the MAP criterion. The channel variations are considered as random processes and the KL orthogonal series expansion is applied. Prompted by the general applicability of the KL expansion, in this paper, we consider the components of $\mathbf{H}_\mu(n)$ to be expressed by a linear combination of orthonormal base vectors as $\mathbf{H}_\mu(n) = \mathbf{\Psi}\mathbf{G}_\mu(n)$, where $\mathbf{\Psi} = [\psi_0, \psi_1, \ldots, \psi_{N_c-1}]$, ψ_i's are the orthonormal basis vectors corresponding to the eigenvectors of the channel autocorrelation matrix $\mathbf{C}_{\mathbf{H}_\mu} = E[\mathbf{H}_\mu \mathbf{H}_\mu^{\dagger}]$. $\mathbf{G}_\mu(n)$ is an $N_c \times 1$ zero-mean i.i.d. Gaussian vector whose components $\mathbf{G}_\mu(n)[k] = \mathbf{G}_\mu(n,k)$, $k = 0, 1, \ldots, N_c - 1$ correspond to the weights of the KL expansion. Note that the covariance matrix of $\mathbf{G}_\mu(n)$ is $\mathbf{\Lambda} = \mathrm{diag}(\lambda_0, \lambda_1, \ldots, \lambda_{N_c-1})$, where λ_k's are the eigenvalues of $\mathbf{C}_{\mathbf{H}_\mu}$. Therefore, $\mathbf{C}_{\mathbf{H}_\mu}$ can be expressed as

$$\mathbf{C}_{\mathbf{H}_\mu} = \mathbf{\Psi}\mathbf{\Lambda}\mathbf{\Psi}^{\dagger}. \tag{7}$$

Thus, the channel estimation problem in this application is equivalent to estimating the i.i.d. Gaussian vector $\mathbf{G}_\mu$ of the KL expansion coefficients.

III. Nondata-Aided EM-Based MAP Channel Estimation

In the nondata-aided MAP estimation approach, we choose $\widehat{\mathbf{G}}$ to maximize the posterior probability density function (PDF), $\widehat{\mathbf{G}} = \arg\max_{\mathbf{G}} p(\mathbf{G}|\mathbf{R})$ where $\mathbf{G} = [\mathbf{G}_1^T, \mathbf{G}_2^T]^T$. To find the MAP estimator, we must equivalently maximize $p(\mathbf{R}|\mathbf{G})p(\mathbf{G})$. The prior PDF of the KL expansion coefficient r.v.'s of the fading channel can be expressed as $p(\mathbf{G}) \sim \exp(-\mathbf{G}^{\dagger}\widetilde{\mathbf{\Lambda}}^{-1}\mathbf{G})$, where $\widetilde{\mathbf{\Lambda}} = \mathrm{diag}(\mathbf{\Lambda}\ \mathbf{\Lambda})$.

Hence, the MAP estimator equivalently takes the form

$$\widehat{\mathbf{G}}_{\mathrm{MAP}} = \arg\max_{\mathbf{G}} [\ln p(\mathbf{R}|\mathbf{G}) + \ln p(\mathbf{G})] \tag{8}$$

where $p(\mathbf{R}|\mathbf{G}) = E_{\mathcal{A}}[p(\mathbf{R}|\mathbf{A}, \mathbf{G})]$.

Given the transmitted signals $\mathcal{A}$, coded according to the SF transmit-diversity scheme and the discrete channel orthonormal series expansion representation coefficients $\mathbf{G}$ and taking into account the independence of the noise components, the conditional PDF of the received signal $\mathbf{R}$ can be expressed as

$$p(\mathbf{R}|\mathcal{A}, \mathbf{G}) \sim \exp\left[-(\mathbf{R} - \mathcal{A}\widetilde{\mathbf{\Psi}}\mathbf{G})^{\dagger}\widetilde{\mathbf{\Sigma}}^{-1}(\mathbf{R} - \mathcal{A}\widetilde{\mathbf{\Psi}}\mathbf{G})\right] \tag{9}$$

where $\widetilde{\mathbf{\Sigma}}$ is an $N_c \times N_c$ diagonal matrix with $\widetilde{\mathbf{\Sigma}}[k,k] = \sigma^2$, for $k = 0, 1, \ldots, N_c - 1$ and $\widetilde{\mathbf{\Psi}} = \mathrm{diag}(\mathbf{\Psi}\ \mathbf{\Psi})$.

Obtaining the MAP estimate of $\mathbf{G}$ from (9) is a complicated optimization problem and does not yield a closed-form solution. The solution of such problems usually requires numerical methods, such as methods of scoring, Newton–Raphson, or some other gradient search algorithm. However, for the problem at hand, these numerical methods tend to be computationally complex. Fortunately, the solution can be easily obtained by means of the iterative EM algorithm. Since the EM algorithm has been studied and applied to a number of problems in communications over the years, the details of the algorithm will not be presented in this paper. See [20]–[22] for a general exposition to the EM algorithm and [18] its applications to the estimation problem related to this study. Basically, this algorithm inductively reestimates $\mathbf{G}$ so that a monotonic increase in the *a posteriori* conditional pdf in (9) is guaranteed. The monotonic increase is realized via the maximization of the auxiliary function

$$Q\left(\mathbf{G}|\mathbf{G}^{(i)}\right) = \sum_{\mathcal{A}} p\left(\mathbf{R}, \mathcal{A}, \mathbf{G}^{(i)}\right) \log p(\mathbf{R}, \mathcal{A}, \mathbf{G}) \tag{10}$$

where $\mathbf{G}^{(i)}$ is the estimation of $\mathbf{G}$ at the ith iteration.

Note that $p(\mathbf{R}, \mathcal{A}, \mathbf{G}) \sim p(\mathbf{R}|\mathcal{A}, \mathbf{G})p(\mathbf{G})$, since the data symbols $\mathcal{A} = \{A_k(n)\}$ are assumed to be independent of each other and are identically distributed and because of the fact that they are independent of $\mathbf{G}$. Therefore, (10) can be easily evaluated compared to a direct computation of (9).

Given the received signal $\mathbf{R}$, the EM algorithm starts with an initial value $\mathbf{G}^0$ of the unknown channel parameter $\mathbf{G}$. The $(i+1)$th estimate of $\mathbf{G}$ is obtained by the maximization step described by $\mathbf{G}^{(i+1)} = \arg\max_{\mathbf{G}} Q(\mathbf{G}|\mathbf{G}^{(i)})$. As described in Appendix I, the expression of the reestimated value of $\mathbf{G}_\mu^{(i+1)}$ $(\mu = 1, 2)$ can be obtained as follows:

$$\begin{aligned} \mathbf{G}_1^{(i+1)} &= (\mathbf{I} + \mathbf{\Sigma}\mathbf{\Lambda}^{-1})^{-1}\mathbf{\Psi}^{\dagger}\left[\mathbf{\Gamma}_1^{(i)\dagger}\mathbf{R}_e(n) - \mathbf{\Gamma}_2^{(i)}\mathbf{R}_o(n)\right] \\ \mathbf{G}_2^{(i+1)} &= (\mathbf{I} + \mathbf{\Sigma}\mathbf{\Lambda}^{-1})^{-1}\mathbf{\Psi}^{\dagger}\left[\mathbf{\Gamma}_2^{(i)\dagger}\mathbf{R}_e(n) + \mathbf{\Gamma}_1^{(i)}\mathbf{R}_o(n)\right] \end{aligned} \tag{11}$$

where it can be easily seen that

$$(\mathbf{I} + \mathbf{\Sigma}\mathbf{\Lambda}^{-1})^{-1} = \mathrm{diag}\left(\left[\left(\frac{1+\sigma^2}{\lambda_0}\right)^{-1}, \ldots, \left(\frac{1+\sigma^2}{\lambda_{N_c-1}}\right)^{-1}\right]\right) \tag{12}$$

and $\mathbf{\Gamma}_\mu^{(i)}$ in (11) is an $N_c/2 \times N_c/2$ dimensional diagonal matrix representing the *a posteriori* probabilities of the data symbols at the ith iteration step whose kth component is defined as

$$\Gamma_\mu^{(i)}(k) = \sum_{a_1} \sum_{a_2 \in S_k} a_\mu P\Big(A_{2k}(n) = a_1 \quad A_{2k+1}(n) = a_2 | \mathbf{R}, \mathbf{G}^{(i)}\Big), \qquad \mu = 1, 2 \tag{13}$$

where S_k denotes the alphabet set taken by the kth OFDM symbol.

Petitioner Samsung Ex-1004, 0124

A truncated expansion $\mathbf{G}_{\mu,r}$ can be formed by selecting r orthonormal basis vectors among all the basis vectors that satisfy $\mathbf{C}_{\mathbf{H}_\mu}\mathbf{\Psi} = \mathbf{\Psi}\mathbf{\Lambda}$. The optimal one that yields the smallest average mean-squared truncation error $1/(N_c/2)\, E[\boldsymbol{\epsilon}_r^\dagger \boldsymbol{\epsilon}_r]$ is the one expanded with the orthonormal basis vectors associated with the first largest r eigenvalues given by

$$\frac{1}{\frac{N_c}{2}-r} E\left[\boldsymbol{\epsilon}_r^\dagger \boldsymbol{\epsilon}_r\right] = \frac{1}{\frac{N_c}{2}-r} \sum_{i=r}^{\frac{N_c}{2}-1} \lambda_i \tag{14}$$

where $\boldsymbol{\epsilon}_r = \mathbf{G}_\mu - \mathbf{G}_{\mu,r}$. For the problem at hand, the truncation property of the KL expansion results in a low-rank approximation. Thus, a rank-r approximation of $\mathbf{\Lambda}_r$ is defined as $\mathbf{\Lambda}_r = \mathrm{diag}\{\lambda_0, \lambda_1, \ldots, \lambda_{r-1}, 0, \ldots, 0\}$. Since the trailing $N_c/2 - r$ variances $\{\lambda_l\}_{l=r}^{N_c/2-1}$ are small compared to the leading r variances $\{\lambda_l\}_{l=0}^{r-1}$, then the trailing $N_c/2 - r$ variances are set to zero to produce the approximation. However, the pattern of eigenvalues for $\mathbf{\Lambda}$ typically splits the eigenvectors into dominant and subdominant sets. Then, the choice of r is more or less obvious. The optimal truncated KL (rank-r) estimator of (11) can easily be obtained by replacing $\mathbf{\Lambda}_r$ with $\mathbf{\Lambda}$ in (11).

A. Initialization

In order to choose good initial values for the unknown channel parameters, the N_{PS} data symbols $\{A_k(n)\}$ for $k \in S_{PS}$ in each OFDM frame are inserted as pilot symbols known by the receiver. Corresponding to the pilot symbols, we focus on an under-sampled signal model and employ the least squares (LS) estimate to obtain under-sampled channel parameters. Then, the complete initial channel gains can easily be determined using an interpolation technique, i.e., a lowpass interpolation algorithm [16]. Finally, the initial values of $\mathbf{G}_\mu^{(0)}$ are used in the iterative EM algorithm to avoid divergence. The details of the initialization process is presented in [17] and [18].

B. Computation of $\Gamma_\mu^{(i)}(k)$ for QPSK

As the details are given in Appendix II, $\mathbf{\Gamma}_\mu^{(i)} = [\Gamma_\mu^{(i)}(0), \ldots, \Gamma_\mu^{(i)}((N_c/2)-1)]^T$ can be computed for QPSK signaling as follows:

$$\mathbf{\Gamma}_\mu^{(i)} = \frac{1}{2}\tanh\left[\frac{1}{\sigma^2}\mathrm{Re}\left(\mathbf{Z}_\mu^{(i)}\right)\right] + \frac{j}{2}\tanh\left[\frac{1}{\sigma^2}\mathrm{Im}\left(\mathbf{Z}_\mu^{(i)}\right)\right] \tag{15}$$

where

$$\mathbf{Z}_1^{(i)} = \mathcal{R}_e \mathbf{\Psi}^* \mathbf{G}_1^{*(i)} + \mathcal{R}_o^* \mathbf{\Psi} \mathbf{G}_2^{(i)}$$
$$\mathbf{Z}_2^{(i)} = \mathcal{R}_e \mathbf{\Psi}^* \mathbf{G}_2^{*(i)} - \mathcal{R}_o^* \mathbf{\Psi} \mathbf{G}_1^{(i)}$$

and $\mathcal{R}_e$ and $\mathcal{R}_o$ are $N_c/2 \times N_c/2$ diagonal matrices whose elements are $\mathbf{R}_e$ and $\mathbf{R}_o$, respectively.

IV. Modified Cramer–Rao Bound

In this section, we turn our attention to the analytical performance results and study the performance of the MAP channel estimator based on the evaluation of the modified CRB.

The mean-squared estimation error for the unbiased estimation of a nonrandom parameter has a lower bound, the CRB, which defines the ultimate accuracy of the unbiased estimation procedure. Suppose $\hat{\mathbf{G}}$ is an unbiased estimator of a vector of unknown parameters $\mathbf{G}$ (i.e., $E\{\hat{\mathbf{G}}\} = \mathbf{G}$), then the mse matrix is lower bounded by the inverse of the Fisher information matrix (FIM) $E\{(\mathbf{G} - \hat{\mathbf{G}})(\mathbf{G} - \hat{\mathbf{G}})^\dagger\} \geq \mathbf{J}^{-1}(\mathbf{G})$.

Since the estimation of unknown random parameters $\mathbf{G}'$ via the MAP approach is considered in this paper, the modified FIM needs to be taken into account in the derivation of the stochastic CRB [24]. Fortunately, the modified FIM can be obtained by a straightforward modification of the FIM as

$$\mathbf{J}_M(\mathbf{G}) \triangleq \mathbf{J}(\mathbf{G}) + \mathbf{J}_P(\mathbf{G}) \tag{16}$$

where $\mathbf{J}_P(\mathbf{G})$ represents the *a priori* information.

Under the assumption that $\mathbf{G}$ and $\mathbf{W}(n)$ are independent of each other and $\mathbf{W}(n)$ is a zero-mean, the A_k's are adopting finite complex values, from [24] and (9), the conditional PDF is given by

$$p(\mathbf{R}|\mathbf{G}) = E_{\mathcal{A}}\left\{p(\mathbf{R}|\mathcal{A}, \mathbf{G})\right\} \sim \frac{1}{\sigma^2} E_{\mathcal{A}}\left\{(\mathbf{R} - \mathcal{A}\tilde{\mathbf{\Psi}}\mathbf{G})^\dagger (\mathbf{R} - \mathcal{A}\tilde{\mathbf{\Psi}}\mathbf{G})\right\}. \tag{17}$$

Since $\ln p(\mathbf{R}|\mathbf{G})$ is required for the computation of $\mathbf{J}(\mathbf{G})$, it is unfortunately computationally intensive. However, an approximate of $\ln p(\mathbf{R}|\mathbf{G})$ can still be obtained from $\ln p(\mathbf{R}|\mathcal{A}, \mathbf{G})$. Since the logarithmic function is a concave, by Jensen's inequality, we have

$$\ln p(\mathbf{R}|\mathbf{G}) \leq E_{\mathcal{A}} \ln\left\{p(\mathbf{R}|\mathcal{A}, \mathbf{G})\right\}. \tag{18}$$

Therefore, we get a valid $\mathbf{J}(\mathbf{G})$ from $E_{\mathbf{A}}\{\ln p(\mathbf{R}|\mathcal{A}, \mathbf{G})\}$ which may not be tight, but is much easier to compute. From (17), the derivatives follow as

$$\frac{\partial \ln p(\mathbf{R}|\mathbf{G})}{\partial \mathbf{G}^T} = \frac{1}{\sigma^2}(\mathbf{R} - \mathcal{A}\tilde{\mathbf{\Psi}}\mathbf{G})^\dagger \mathcal{A}\tilde{\mathbf{\Psi}} \tag{19}$$

$$\frac{\partial^2 \ln p(\tilde{\mathbf{R}}|\mathbf{G})}{\partial \mathbf{G}^* \partial \mathbf{G}^T} = -\frac{1}{\sigma^2}\tilde{\mathbf{\Psi}}^\dagger \mathcal{A}^\dagger \mathcal{A}\tilde{\mathbf{\Psi}}. \tag{20}$$

Since the Alamouti's scheme imposes an orthogonal structure on the transmitted symbols $\mathcal{A}^\dagger\mathcal{A} = \mathbf{I}$ and using $\tilde{\mathbf{\Psi}}^\dagger\tilde{\mathbf{\Psi}} = \mathbf{I}$ and taking the expected values yields the simple form

$$\mathbf{J}(\mathbf{G}) = -E\left[\frac{\partial^2 \ln p(\tilde{\mathbf{R}}|\mathbf{G})}{\partial \mathbf{G}^* \partial \mathbf{G}^T}\right] = \frac{1}{\sigma^2}\mathbf{I}. \tag{21}$$

Petitioner Samsung Ex-1004, 0125

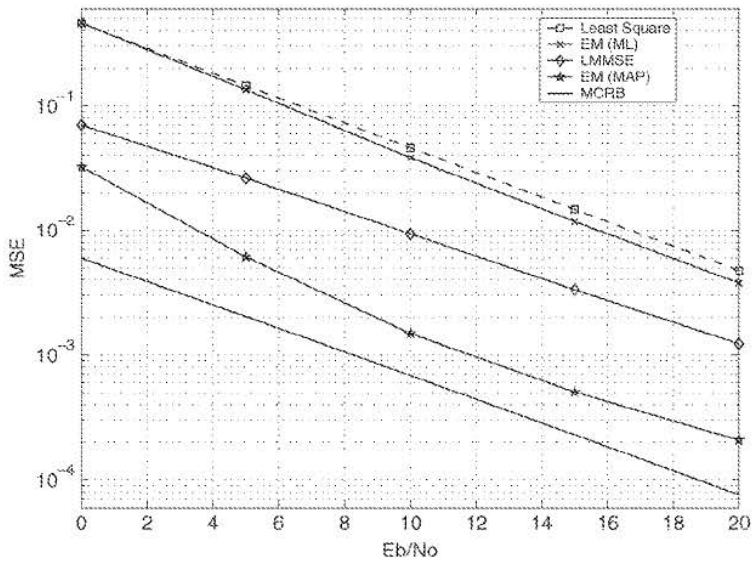


Fig. 2. Channel-estimation mse as a function of the average E_b/N_0.

The second term in (16) is easily obtained as follows. Consider the prior PDF $p(\mathbf{G}) \sim \exp[(-\mathbf{G}^\dagger \widetilde{\mathbf{\Lambda}}^{-1}\mathbf{G})]$. The respective derivatives are found as

$$\frac{\partial \ln p(\mathbf{G})}{\partial \mathbf{G}^T} = -\mathbf{G}^\dagger \mathbf{\Lambda}^{-1}, \qquad \frac{\partial^2 \ln p(\mathbf{G})}{\partial \mathbf{G}^* \partial \mathbf{G}^T} = -\mathbf{\Lambda}^{-1}. \tag{22}$$

Upon taking the negative expectations, the second term in (16) becomes $\mathbf{J}_P(\mathbf{G}) = \mathbf{\Lambda}^{-1}$. Substituting $\mathbf{J}(\mathbf{G})$ and $\mathbf{J}_P(\mathbf{G})$ in (16) produces the modified FIM as follows:

$$\begin{aligned}\mathbf{J}_M(\mathbf{G}) &= \mathbf{J}(\mathbf{G}) + \mathbf{J}_P(\mathbf{G}) \\ &= \frac{1}{\sigma^2}\mathbf{I} + \mathbf{\Lambda}^{-1}.\end{aligned} \tag{23}$$

Inverting the matrix $\mathbf{J}_M(\mathbf{G})$ yields $\mathrm{CRB}(\hat{\mathbf{G}}) = \mathbf{J}_M^{-1}(\mathbf{G})$. $\mathrm{CRB}(\hat{\mathbf{G}})$ is a diagonal matrix with the elements on the main diagonal equaling the reciprocal of that of the $\mathbf{J}(\mathbf{G})$ matrix. Because of the zero-valued off-diagonal entries in the FIM, the errors between the corresponding estimates are not independent.

V. Simulations

In this section, we present some simulation results in order to verify the performance of the channel estimation via the EM algorithm for SFBC-OFDM systems. The diversity scheme with two transmit and one receive antenna is considered. The channels between the transmitter and receiver are generated according to the doubly-selective fading channel model. In this model, $H_\mu(k)$'s are with an exponentially decaying power delay profile $\theta(\tau_\mu) = C\exp(-\tau_\mu/\tau_{\mathrm{rms}})$ and delays τ_μ that are uniformly and independently distributed over the length of the cyclic prefix. C is a normalizing constant. Note that the normalized discrete channel correlations for different subcarriers and blocks of this channel model were presented in [17] as follows:

$$r_1(k,k') = \frac{1 - \exp\left[-L\left[\frac{1}{\tau_{\mathrm{rms}}} + \frac{2\pi j(k-k')}{N_c}\right]\right]}{\tau_{\mathrm{rms}}\left(1 - \exp\left(\frac{-L}{\tau_{\mathrm{rms}}}\right)\right)\left(\frac{1}{\tau_{\mathrm{rms}}} + \frac{j2\pi(k-k')}{N_c}\right)}.$$

The scenario for the SFBC-OFDM simulation study consists of a wireless QPSK-OFDM system. The system has a 2.28-MHz bandwith (for the pulse roll-off factor $\alpha = 0.2$) and is divided into $N_c = 512$ tones with a total period Ts of 136 μs, of which 1.052 μs constitutes the cyclic prefix ($L = 4$). The uncoded data rate is 7.6 Mb/s. We assume that the rms width is $\tau_{\mathrm{rms}} = 1$ sample (0.263 μs) for the power-delay profile.

The proposed EM-based iterative channel estimator of (11) is implemented and compared with the previously reported SFBC-OFDM channel estimator [13] in terms of average mse for a wide range of signal-to-noise ratio (E_b/N_0) levels. The average mse is defined as the norm of the difference between the vectors $\mathbf{G} = [\mathbf{G}_1^T, \mathbf{G}_2^T]$ and $\widehat{\mathbf{G}}_{\mathrm{map}}$, representing the true and the estimated values of the channel parameters, respectively. Namely, $\mathrm{mse} = 1/2N_c\|\mathbf{G} - \widehat{\mathbf{G}}_{\mathrm{map}}\|^2$. In order to obtain good initial values for the unknown channel parameters, $N_{PS} = 64$ equally spaced pilot tones are inserted into the data symbols. Corresponding to the pilot symbols, we employed the LS estimate to obtain under-sampled channel parameters. Then, the complete initial channel gains are determined using a lowpass interpolation technique [16]. Finally, the initial values of $\mathbf{G}_\mu^{(0)}$ are used in the iterative EM algorithm to avoid divergence.

Fig. 2 compares the performance of the proposed EM-MAP channel-estimation approach with an EM-ML [13] which is the modified version of [12] and both used LS for initialization. The proposed EM-based approach is also compared to other widely

Petitioner Samsung Ex-1004, 0126

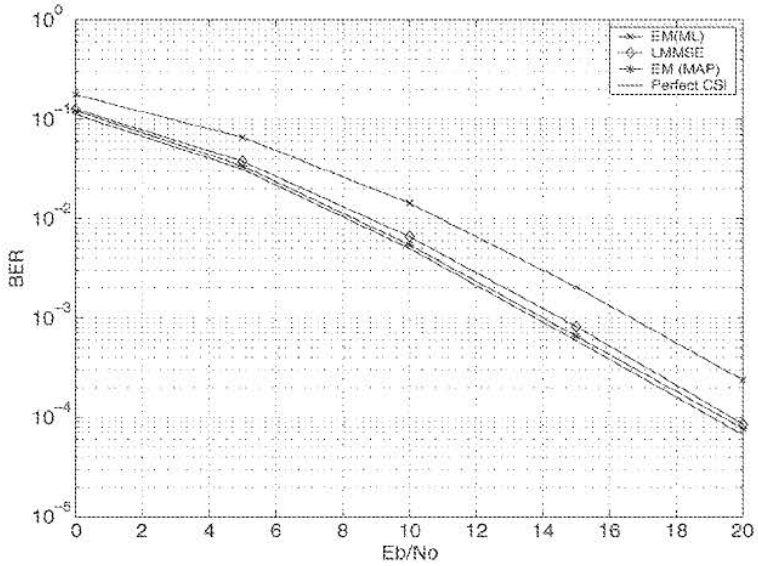


Fig. 3. BER performance of the EM algorithms as a function of the average E_b/N_0.

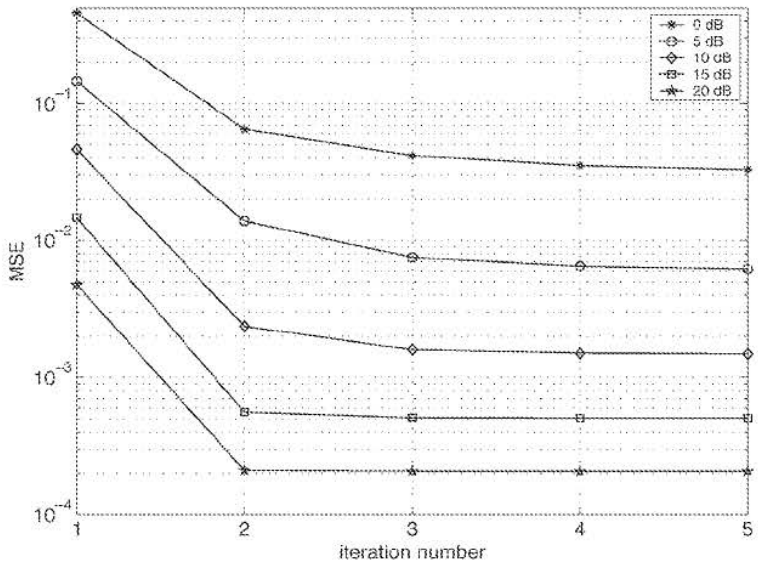


Fig. 4. Convergence of the mse with respect to the number of iterations.

used linear mmse (Lmmse) and LSE pilot symbol assisted modulation (PSAM) channel-estimation techniques [23]. It can be seen that the proposed EM-MAP significantly outperforms the EM ML as well as the PSAM techniques.

Assuming the channel parameters are estimated accurately, the SF block constructs the decision estimate vector in [14]. Therefore, we used channel estimates for symbol decoding and compared the bit error rate (BER) performance of the proposed iterative EM-MAP estimator with the EM-ML and the Lmmse ones. Fig. 3 shows the average results of 1000 Monte Carlo runs. We observe from the BER performance simulation results that the EM-MAP BER performance still outperforms the EM-ML and the Lmmse approaches, especially for high SNRs.

In Fig. 4, the average mse performance of the EM-MAP algorithm is presented as a function of the number of iterations. It is concluded from these curves that the mse performance of the EM-based algorithm converges within 2–4 iterations, depending on the average SNR.

Apart from the simulated BER performance, the truncated estimator performance is also studied as a function of the number of KL coefficients. Fig. 5 presents the mse result of the truncated EM-MAP estimator. If only a few expansion coefficients are employed to reduce the complexity of the proposed estimator, then the mse between channel parameters becomes large. However, if the number of parameters in the expansion is increased to include the dominant eigenvalues, we

Petitioner Samsung Ex-1004, 0127

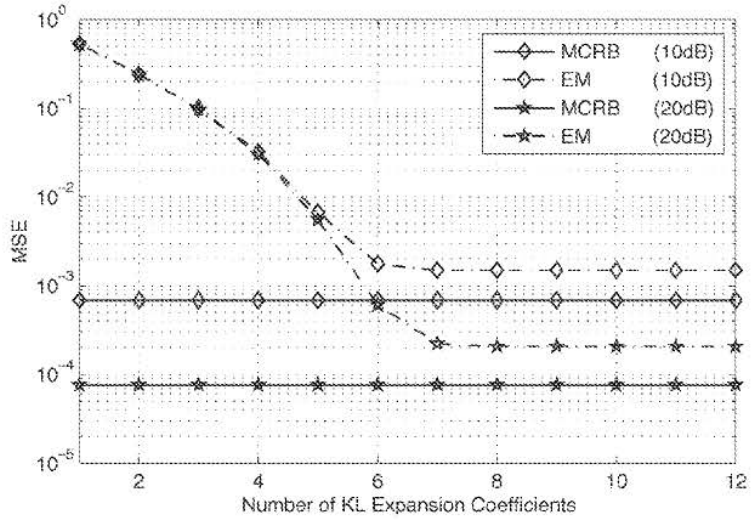


Fig. 5. Truncated EM algorithm mse performance.

are able to obtain a good approximation with a relatively small number of KL coefficients. For instance, by replacing 256×256 diagonal $\mathbf{\Lambda}$ in (11) with a 8×8 diagonal, $\mathbf{\Lambda}_r$ decreases the computational complexity enormously.

VI. Conclusion

In this paper, we proposed an efficient nondata-aided EM-based channel-estimation algorithm for SFBC-OFDM systems, which is crucial for the decoding of SF codes. This algorithm performs an iterative estimation of the channel according to the MAP criterion, using the EM algorithm employing the M-PSK modulation scheme with additive Gaussian noise. The likelihood ratio is properly averaged out over the data sequence so that the resulting algorithm does not need a training sequence to acquire the channel; thus, the throughput of the system improves substantially compared to the existing channel-estimation algorithms based on the data-aided schemes in literature. The performance of our channel-estimation algorithm is confirmed by corroborating simulations and is compared with existing EM-ML alternatives. It has been shown that the EM-MAP estimator performs well over the EM-ML. Moreover, the truncation property of the KL expansion significantly reduces the complexity of the EM-based algorithms.

Appendix I
Derivation of (11)

In (10), the term $\log p(\mathbf{R}, \mathcal{A}, \mathbf{G})$ can be expressed as

$$\log p(\mathbf{R}, \mathcal{A}, \mathbf{G}) \sim \log p(\mathcal{A}, \mathbf{G}) + \log p(\mathbf{R}|\mathcal{A}, \mathbf{G}) + \log p(\mathbf{G}). \tag{24}$$

The first term in (24) is constant, since the data sequences $\mathcal{A}$ have an equal *a priori* probability and $\mathcal{A}$ and $\mathbf{G}$ are independent of each other. Also, since the noise samples are independent, from (3) and (9), the second and third terms in (24) can be written as

$$\begin{aligned}\log p(\mathbf{R}|\mathcal{A}, \mathbf{G}) \sim & -\left[\mathbf{R}_e(n) - \mathbf{A}_e(n)\mathbf{H}_1 - \mathbf{A}_o(n)\mathbf{H}_2\right]^\dagger \\ & \times \mathbf{\Sigma}^{-1}\left[\mathbf{R}_e(n) - \mathbf{A}_e(n)\mathbf{H}_1 - \mathbf{A}_o(n)\mathbf{H}_2\right] \\ & - \left[\mathbf{R}_o(n) + \mathbf{A}_o^\dagger(n)\mathbf{H}_1 - \mathbf{A}_e^\dagger(n)\mathbf{H}_2\right]^\dagger \\ & \times \mathbf{\Sigma}^{-1}\left[\mathbf{R}_o(n) + \mathbf{A}_o^\dagger(n)\mathbf{H}_1 - \mathbf{A}_e^\dagger(n)\mathbf{H}_2\right] \\ \log p(\mathbf{G}) \sim & -\mathbf{G}_1^\dagger \mathbf{\Lambda}^{-1}\mathbf{G}_1 - \mathbf{G}_2^\dagger \mathbf{\Lambda}^{-1}\mathbf{G}_2. \end{aligned} \tag{25}$$

Taking the derivatives in (10) with respect to $\mathbf{G}_1$ and $\mathbf{G}_2$, along with the fact that $\|\mathbf{A}_e(n)\|^2 = |\mathbf{A}_o(n)|^2 = (1/2)\mathbf{I}$, and equating the resulting equations to zero, we have

$$\begin{aligned}\frac{\partial Q}{\partial \mathbf{G}_1} = & \sum_{\mathcal{A}} p\left(\mathbf{R}, \mathcal{A}, \mathbf{G}^{(i)}\right) \\ & \times \left[\mathbf{\Sigma}^{-1}\mathbf{\Psi}^\dagger\left(\mathbf{A}_e^\dagger(n)\mathbf{R}_e(n)\right.\right. \\ & \left.\left. - \mathbf{A}_o(n)\mathbf{R}_o(n) - \mathbf{H}_1\right) - \mathbf{\Lambda}^{-1}\mathbf{G}_1\right] = 0 \\ \frac{\partial Q}{\partial \mathbf{G}_1} = & \sum_{\mathcal{A}} p\left(\mathbf{R}, \mathcal{A}, \mathbf{G}^{(i)}\right) \\ & \times \left[\mathbf{\Sigma}^{-1}\mathbf{\Psi}^\dagger\left(\mathbf{A}_o^\dagger(n)\mathbf{R}_e(n)\right.\right. \\ & \left.\left. + \mathbf{A}_e(n)\mathbf{R}_o(n) - \mathbf{H}_2\right) - \mathbf{\Lambda}^{-1}\mathbf{G}_2\right] = 0. \end{aligned} \tag{26}$$

Since $p(\mathbf{R}, \mathcal{A}, \mathbf{G}^{(i)})$ may be replaced by $p(\mathcal{A}|\mathbf{R}, \mathbf{G}^{(i)})$ without violating the equalities in (26), defining the conditional probabilities as

$$\begin{aligned}\Gamma_\mu^{(i)}(k) = & \sum_{a_1} \sum_{a_2 \in S_k} a_\mu P \\ & \times \left(A_{2k}(n) = a_1, A_{2k+1}(n) = a_2|\mathbf{R}, \mathbf{G}^{(i)}\right) \end{aligned} \tag{27}$$

Petitioner Samsung Ex-1004, 0128

$$\Gamma_{\mu}^{(i)}(k) = \frac{\sum_{a_1,a_2\in S_k} a_{\mu} p\left(\mathbf{R}|A_{2k}(n)=a_1, A_{2k+1}(n)=a_2, \mathbf{G}^{(i)}\right) P\left(A_{2k}(n)=a_1, A_{2k+1}=a_2\right)}{\sum_{a_1,a_2\in S_k} p\left(\mathbf{R}|A_{2k}(n)=a_1, A_{2k+1}(n)=a_2, \mathbf{G}^{(i)}\right) P\left(A_{2k}(n)=a_1, A_{2k+1}=a_2\right)} \tag{30}$$

and the $N_c/2 \times N_c/2$ diagonal matrix

$$\mathbf{\Gamma}_{\mu}^{(i)} = \mathrm{diag}\left(\Gamma_{\mu}^{(i)}(0), \ldots, \Gamma_{\mu}^{(i)}\left(\frac{N_c}{2}-1\right)\right) \tag{28}$$

the equations in (26) can be expressed as

$$\begin{aligned}
\mathbf{\Sigma}^{-1}\mathbf{\Psi}^{\dagger}\left(\mathbf{\Gamma}_1^{(i)\dagger}\mathbf{R}_e(n) - \mathbf{\Gamma}_2^{(i)}\mathbf{R}_o(n) - \mathbf{H}_1\right) &= \mathbf{\Lambda}^{-1}\mathbf{G}_1 \\
\mathbf{\Sigma}^{-1}\mathbf{\Psi}^{\dagger}\left(\mathbf{\Gamma}_2^{(i)\dagger}\mathbf{R}_e(n) + \mathbf{\Gamma}_1^{(i)}\mathbf{R}_o(n) - \mathbf{H}_2\right) &= \mathbf{\Lambda}^{-1}\mathbf{G}_2
\end{aligned} \tag{29}$$

from which, the final expression for $\mathbf{G}_{\mu}^{(i+1)}$, $\mu = 1, 2$, given by (11) easily follows.

Appendix II
Exact Computation of $\Gamma_{\mu}^{(i)}(k)$ for QPSK Signaling

Let $a = (\pm 1 \pm j)/2$ represent the unit power and the independent and identically distributed data sequence modulating the QPSK carrier, $\Gamma_{\mu}^{(i)}(k)$ in (13) can be expressed (30), shown at the top of the page. From (9), it follows that

$$\Gamma_{\mu}^{(i)}(k) = \frac{\sum_{a_1,a_2\in S_k} a_{\mu} \exp\left(\frac{1}{\sigma^2}\mathrm{Re}\left[a_{\mu}^* Z_{\mu}^{(i)}(k)\right]\right)}{\sum_{a_1,a_2\in S_k} \exp\left(\frac{1}{\sigma^2}\mathrm{Re}\left[a^* Z_{\mu}^{(i)}(k)\right]\right)} \tag{31}$$

where

$$\begin{aligned}
Z_1^{(i)}(k) &= R_{e,k}\sum_m G_1^{(i)*}(m)\psi_m^*(k) \\
&\quad + R_{o,k}^*\sum_m G_2^{(i)}(m)\psi_m(k) \\
Z_2^{(i)}(k) &= R_{e,k}\sum_m G_2^{(i)*}(m)\psi_m^*(k) \\
&\quad - R_{o,k}^*\sum_m G_1^{(i)}(m)\psi_m(k)
\end{aligned}$$

Then, taking summations in the numerator and the denominator of (31) over the values of the QPSK symbols a, we have the final result as follows:

$$\begin{aligned}
\Gamma_{\mu}^{(i)}(k) = \frac{1}{2}\tanh\left[\frac{1}{\sigma^2}\mathrm{Re}\left(Z_{\mu}^{(i)}(k)\right)\right] \\
+ \frac{j}{2}\tanh\left[\frac{1}{\sigma^2}\mathrm{Im}\left(Z_{\mu}^{(i)}(k)\right)\right].
\end{aligned} \tag{32}$$

Acknowledgment

The authors would like to thank the anonymous reviewers for their insightful comments and suggestions that improved the quality of this paper.

References

[1] R. Van Nee and R. Prasad, *OFDM Wireless Multimedia Communications*. Boston, MA: Artech House, 2000.
[2] Z. Liu, Y. Xin, and G. B. Giannakis, "Space-time-frequency coded OFDM for frequency selective fading channels," *IEEE Trans. Signal Process.*, vol. 50, no. 10, pp. 2465–2476, Oct. 2002.
[3] S. M. Alamouti, "A simple transmitter diversity scheme for wireless communications," *IEEE J. Sel. Areas Commun.*, vol. 16, no. 8, pp. 1451–1458, Oct. 1998.
[4] V. Tarokh, N. Seshadri, and A. R. Calderbank, "Space-time codes for high data rate wireless communications: Performance analysis and code construction," *IEEE Trans. Inf. Theory*, vol. 44, no. 2, pp. 744–765, Mar. 1998.
[5] V. Tarokh, H. Jafarkhani, and A. R. Calderbank, "Space-time block codes from orthogonal designs," *IEEE Trans. Inf. Theory*, vol. 45, no. 5, pp. 1456–1467, Jul. 1999.
[6] Y. Li, L. J. Cimini, N. Seshadri, and S. Ariyavistakul, "Channel estimation for OFDM systems with transmitter diversity in mobile wireless channels," *IEEE J. Sel. Areas Commun.*, vol. 17, no. 3, pp. 461–471, Mar. 1999.
[7] Y. Li, "Simplified channel estimation for OFDM systems with multiple transmit antennas," *IEEE Trans. Wireless Commun.*, vol. 1, no. 1, pp. 67–75, Jan. 2002.
[8] Y. Li, C. N. Georghiades, and G. Huang, "Iterative maximum likelihood sequence estimation for space-time coded systems," *IEEE Trans. Commun.*, vol. 49, no. 6, pp. 948–951, Jun. 2001.
[9] C. Cozzo and B. L. Hughes, "Joint channel estimation and data detection in space-time communications," *IEEE Trans. Commun.*, vol. 51, no. 8, pp. 1266–1270, Aug. 2003.
[10] B. Lu, X. Wang, and Y. Li, "Iterative receivers for space-time block-coded ODFM systems in dispersive fading channels," *IEEE Trans. Wireless Commun.*, vol. 1, no. 2, pp. 213–225, Apr. 2002.
[11] B. Lu, X. Wang, and K. R. Narayanan, "LDPC-based space-time coded OFDM over correlated fading channels," *IEEE Trans. Commun.*, vol. 50, no. 1, pp. 74–88, Jan. 2002.
[12] X. Yongzhe and C. N. Georghiades, "Two EM-type channel estimation algorithms for OFDM with transmitter diversity," *IEEE Trans. Commun.*, vol. 51, no. 1, pp. 106–115, Jan. 2003.
[13] X. Ma, H. Kobayashi, and S. C. Schwarts, "An EM-based channel estimation for space-time and space-frequency block coded OFDM," in *Proc. IEEE Int. Conf. Acoustics, Speech, and Signal Processing (ICASSP)*, Hong Kong, Apr. 6–10, 2003, vol. 4, pp. IV-389–IV-392.
[14] K. F. Lee and D. B. Williams, "A space-frequency transmitter diversity technique for OFDM Systems," in *Proc. IEEE Global Telecommunications (GLOBECOM)*, San Francisco, CA, Nov. 2000, pp. 1473–1477.
[15] M. Feder and E. Weinstein, "Parameter estimation of superimposed signals using the EM algorithm," *IEEE Trans. Acoust., Speech, Signal Process.*, vol. 36, no. 4, pp. 477–489, Apr. 1988.
[16] S. Coleri, M. Ergen, A. Puri, and A. Bahai, "Channel estimation techniques based on pilot arrangement in OFDM systems," *IEEE Trans. Broadcast.*, vol. 48, no. 3, pp. 223–229, Sep. 2002.
[17] J.-J. van de Beek, O. Edfors, M. Sandell, S. K. Wilson, and P. O. Börjesson, "OFDM channel estimation by singular value decomposition," *IEEE Trans. Commun.*, vol. 46, no. 7, pp. 931–936, Jul. 1998.
[18] E. Panayirci and H. A. Cirpan, "Channel estimation for space-time block coded OFDM systems in the presence of multipath fading," in *Proc. IEEE Global Telecommunications (GLOBECOM)*, Taipei, Taiwan, R.O.C., Nov. 17–21, 2002, pp. 1157–1161.
[19] K. Yip and T. Ng, "Karhunen–Loeve expansion of the WSSUS channel

Petitioner Samsung Ex-1004, 0129

output and its application to efficient simulation," *IEEE J. Sel. Areas Commun.*, vol. 15, no. 4, pp. 640–646, May 1997.
[20] A. P. Dempster, N. M. Laird, and D. B. Rubin, "Maximum likelihood from incomplete data via the EM algorithm," *J. R. Stat. Soc.*, vol. 39, no. 1, pp. 1–17, 1977.
[21] G. K. Kaleh and R. Valet, "Joint parameter estimation and symbol detection for linear and nonlinear unknown channels," *IEEE Trans. Commun.*, vol. 42, no. 7, pp. 2406–2413, Jul. 1994.
[22] E. Panayirci and C. N. Georghiades, "Carrier phase synchronization of OFDM systems over frequency selective channels via EM algorithm," in *Proc. IEEE Vehicular Technology Conf. (VTC)*, Houston, TX, May 16–20, 1999, pp. 675–679.
[23] M. Morelli and U. Mengali, "A comparison of pilot-aided channel estimation methods for OFDM systems," *IEEE Trans. Signal Process.*, vol. 49, no. 12, pp. 3065–3073, Dec. 2001.
[24] H. L. Van Trees, *Detection, Estimation and Modulation Theory, Part I*. New York: Wiley, 1993.



Hakan A. Çırpan (M'97) received the B.S. degree from Uludag University, Bursa, Turkey, in 1989, the M.S. degree from the University of Istanbul, Istanbul, Turkey, in 1992, and the Ph.D. degree from Stevens Institute of Technology, Hoboken, NJ, in 1997, all in electrical engineering.

From 1995 to 1997, he was a Research Assistant at Stevens Institute of Technology, working on signal processing algorithms for wireless communication systems. In 1997, he joined the faculty of the Department of Electrical and Electronics Engineering, University of Istanbul. His general research interests cover wireless communications, statistical signal and array processing, system identification, and estimation theory. His current research activities are focused on signal processing and communication concepts with specific attention to channel estimation and equalization algorithms for space-time coding and multicarrier (orthogonal frequency-division multiplexing) systems.

Dr. Cirpan is a member of Sigma Xi. He received the Peskin Award from Stevens Institute of Technology as well as the Prof. Nazim Terzioglu Award from the Research Fund of the University of Istanbul.



Erdal Panayırcı (F'03) received the Diploma Engineering degree in electrical engineering from the Istanbul Technical University, Istanbul, Turkey, in 1964 and the Ph.D. degree in electrical engineering and system science from Michigan State University, East Lansing, in 1970.

From 1970 to 2000, he was with the Faculty of Electrical and Electronics Engineering, Istanbul Technical University, where he was a Professor and the Head of the Telecommunications Chair. He has also been a part-time Consultant to several leading companies in telecommunications in Turkey. From 1979 to 1981, he was with the Department of Computer Science, Michigan State University, as a Fulbright-Hays Fellow and a NATO Senior Scientist. Between 1983 and 1986, he served as a NATO Advisory Committee Member for the Special Panel on Sensory Systems for Robotic Control. From August 1990 to December 1991, he was a Visiting Professor at the Center for Communications and Signal Processing, New Jersey Institute of Technology, Newark, and took part in the research project on interference cancellation by array processing. Between 1998 and 2000, he was a Visiting Professor at the Department of Electrical Engineering, Texas A&M University, College Station, and took part in research on developing efficient synchronization algorithms for orthogonal frequency-division multiplexing (OFDM) systems. He is currently a Visiting Professor at the Department of Electrical and Electronics Engineering, Bilkent University, Ankara, Turkey. He is engaged in research and teaching in digital communications and wireless systems, equalization and channel estimation in multicarrier (OFDM) communication systems, and efficient modulation and coding techniques (TCM and turbo coding).

Prof. Panayırcı is a member of Sigma Xi. He was the Editor for the IEEE TRANSACTIONS ON COMMUNICATIONS in the fields of synchronization and equalizations from 1995 to 1999. He is currently the Head of the Turkish Scientific Commission on Signals, Systems, and Communications of the International Union of Radio Science.



Hakan Doğan (S'02) was born in Istanbul, Turkey, on 1979. He received the B.S. and M.S. degrees in electronics engineering from Istanbul University, Istanbul, Turkey, in 2001 and 2003, respectively, and is currently working toward the Ph.D. degree from the same university.

Since 2001, he has been a Research Assistant at the Department of Electrical and Electronics Engineering, Istanbul University. His general research interests cover communication theory, estimation theory, statistical signal processing, and information theory. His current research activities are focused on wireless communication concepts with specific attention to equalization and channel estimation for spread-spectrum and multicarrier (orthogonal frequency-division multiplexing) systems.

Petitioner Samsung Ex-1004, 0130

A Space-Frequency Transmitter Diversity Technique for OFDM Systems

King F. Lee [1,2] and Douglas B. Williams [2]

[1] Motorola Inc., Boynton Beach, Florida 33426

[2] School of Electrical and Computer Engineering
Georgia Institute of Technology, Atlanta, Georgia 30332

***Abstract*—A transmitter diversity technique for wireless communications over frequency selective fading channels is presented. The proposed technique utilizes orthogonal frequency division multiplexing (OFDM) to transform a frequency selective fading channel into multiple flat fading subchannels on which space-frequency processing is applied. Simulation results verify that in slow fading environments the proposed space-frequency OFDM (SF-OFDM) transmitter diversity technique has the same performance as a previously reported space-time OFDM (ST-OFDM) transmitter diversity system but shows better performance in the more difficult fast fading environments. Other implementation advantages of SF-OFDM over the ST-OFDM transmitter diversity technique are also discussed.**

I. Introduction

Spatial diversity is a well-known technique for combating the detrimental effects of multipath fading. Traditionally, spatial diversity has been implemented at the receiver end, requiring multiple antennas and RF front-end circuits at the receivers. This multiplicity of receiver hardware is a major drawback, especially for portable receivers where physical size and current drain are important constraints. In recent years, transmitter diversity has received strong interest. The main advantage of transmitter diversity is that diversity gain can be achieved by transmitting from multiple spatially separated antennas without significantly increasing the size or complexity of the receivers.

A number of orthogonal space-time transmitter diversity techniques have been proposed [1-3]. Unfortunately, the large delay spreads in frequency selective fading channels destroy the orthogonality of the received signals, which is critical to the operation of the diversity systems. Consequently, these techniques are often only effective over flat fading channels, such as indoor wireless networks or low data rate systems. Space-time coded OFDM (ST-OFDM) systems [4, 5] have been proposed recently for delay spread channels. In [5], it was shown that OFDM modulation with cyclic prefix can be used to transform frequency selective fading channels into multiple flat fading channels so that orthogonal space-time transmitter diversity can be applied, even for channels with large delay spreads. The use of OFDM also offers the possibility of coding in the frequency dimension in a form of space-frequency OFDM (SF-OFDM) transmitter diversity, which has also been suggested in [2]. This paper focusses on the implementation and performance evaluation of SF-OFDM transmitter diversity and its possible advantages over ST-OFDM transmitter diversity. Special considerations for the effective implementation of SF-OFDM transmitter diversity are also discussed.

II. OFDM Modulation with Cyclic Prefix

OFDM is a popular modulation scheme for high data rate digital communications, especially for channels with large delay spreads [6]. A block diagram of a conventional OFDM communication system is shown in Fig. 1. An OFDM communication system can be considered as a block or vector transmission system. Let $X(m)$ denote the input serial data symbols with symbol duration T_S. The serial to parallel converter collects N serial data symbols into a data vector $\mathbf{X}(n)=\left[X(nN)\ X(nN+1)\cdots X(nN+N-1)\right]^T$, which has a block duration of NT_S. An even block size N is assumed throughout the paper. In fact, N is often chosen to be powers of two to take advantage of the efficiency of the fast Fourier transform (FFT) in the modulation and demodulation processes. Let $X_k(n)$ denote the k-th forward polyphase component of the serial data symbols, i.e., $X_k(n)=X(nN+k)$ for $k=0,1,\cdots,N-1$. $X_k(n)$ can be viewed as the data symbol to be transmitted on the k-th subcarrier during the block instant n. The data vector $\mathbf{X}(n)$ can then be expressed in polyphase representation as $\mathbf{X}(n)=\left[X_0(n)\ X_1(n)\cdots X_{N-1}(n)\right]^T$. The data vector $\mathbf{X}(n)$ is modulated by an inverse discrete Fourier transform (IDFT) into an OFDM symbol vector $\mathbf{x}(n)$. A length G cyclic extension of the IDFT output is added to $\mathbf{x}(n)$ as a guard interval. The resulting vector with the cyclic prefix is given by $\mathbf{x}^s(n)=\left[x_{N-G}(n)\cdots x_{N-1}(n)\ x_0(n)\cdots x_{N-1}(n)\right]^T$. The vector $\mathbf{x}^s(n)$ is transmitted through a frequency selective fading channel of order L, i.e., the channel impulse response $h(m,\tau)\neq 0$ for $\tau=L$ and $h(m,\tau)=0$ for $\tau>L$.

0-7803-6451-1/00/$10.00 © 2000 IEEE

Petitioner Samsung Ex-1004, 0131

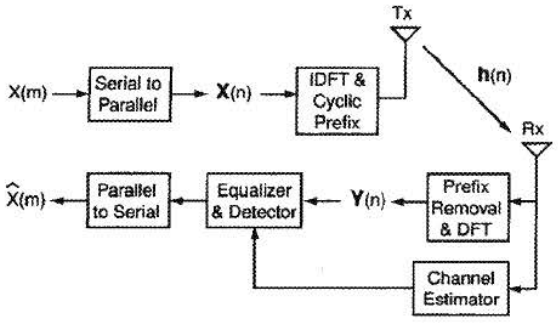


Fig. 1. Block diagram of a conventional OFDM system.

To avoid inter-block interference (IBI), the guard interval is chosen to satisfy $G \geq L$. Assuming the channel impulse response remains constant during the entire block interval, the received signal vector $\mathbf{y}^s(n)$ is simply the convolution of $\mathbf{x}^s(n)$ and the channel impulse response vector $\mathbf{h}(n)$, i.e., $\mathbf{y}^s(n) = \mathbf{x}^s(n) * \mathbf{h}(n)$. At the receiver, the guard interval is first removed from the received signal vector to form the vector $\mathbf{y}(n) = \left[y_G^s(n)\, y_{G+1}^s(n) \cdots y_{N+G-1}^s(n) \right]^T$. It can be shown that with $\mathbf{x}^s(n)$ constructed as the cyclic extension of $\mathbf{x}(n)$, the vector $\mathbf{y}(n)$ is the cyclic convolution of $\mathbf{x}(n)$ and $\mathbf{h}(n)$. The demodulator performs an $N-$point discrete Fourier transform (DFT) on the vector $\mathbf{y}(n)$ to yield the demodulated signal vector $\mathbf{Y}(n)$. A well-known property of the DFT is that cyclic convolution in the time domain results in multiplication in the frequency domain. Thus, the demodulated signal vector is given by $\mathbf{Y}(n) = \mathbf{\Lambda}(n)\mathbf{X}(n) + \mathbf{Z}(n)$, where $\mathbf{\Lambda}(n)$ is a diagonal matrix whose diagonal elements are the DFT of the channel impulse response $\mathbf{h}(n)$ and $\mathbf{Z}(n)$ is the DFT of the channel noise. Since $\mathbf{\Lambda}(n)$ is diagonal, the subchannels are completely decoupled from each other, and $\mathbf{\Lambda}_{k,k}(n)$ can be viewed as the complex channel gain of the k-th subcarrier. Thus, OFDM with cyclic prefix transforms a frequency selective fading channel into N perfectly flat fading subchannels on which orthogonal space-frequency transmitter diversity technique can be applied.

III. SF-OFDM Transmitter Diversity

The proposed two-branch SF-OFDM transmitter diversity system is an OFDM extension of the simple orthogonal transmitter diversity scheme first shown in [2]. The OFDM modulation with cyclic prefix allows the orthogonal transmitter diversity technique to work in frequency selective channels. A simplified block diagram for the proposed system is shown in Fig. 2.

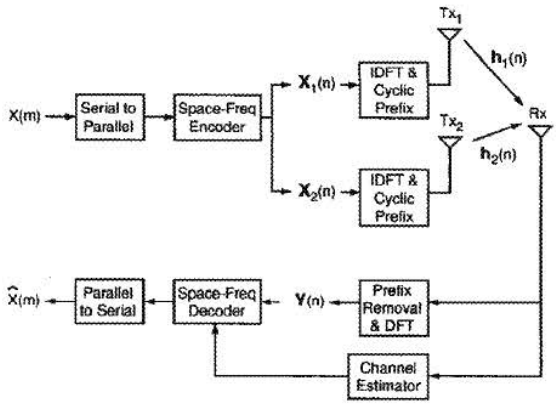


Fig. 2. Block diagram of the proposed two-branch space-frequency OFDM transmitter diversity system.

The data symbol vector $\mathbf{X}(n)$ is coded into two vectors $\mathbf{X}_1(n)$ and $\mathbf{X}_2(n)$ by the space-frequency encoder block as

$$\begin{aligned} \mathbf{X}_1(n) &= \left[X_0(n) \; -X_1^*(n) \cdots X_{N-2}(n) \; -X_{N-1}^*(n) \right]^T \\ \mathbf{X}_2(n) &= \left[X_1(n) \;\; X_0^*(n) \cdots X_{N-1}(n) \;\; X_{N-2}^*(n) \right]^T \end{aligned} \quad (1)$$

During the block instant n, $\mathbf{X}_1(n)$ is transmitted from the first base station Tx_1 while $\mathbf{X}_2(n)$ is transmitted simultaneously from the second base station Tx_2.

The operations of the space-frequency encoder and decoder can best be described in terms of even and odd polyphase component vectors. Let $\mathbf{X}_e(n)$ and $\mathbf{X}_o(n)$ be two length $N/2$ vectors denoting the even and odd component vectors of $\mathbf{X}(n)$, i.e.,

$$\begin{aligned} \mathbf{X}_e(n) &= \left[X_0(n) \;\; X_2(n) \cdots X_{N-4}(n) \;\; X_{N-2}(n) \right]^T \\ \mathbf{X}_o(n) &= \left[X_1(n) \;\; X_3(n) \cdots X_{N-3}(n) \;\; X_{N-1}(n) \right]^T \end{aligned}.$$

Similarly, $\mathbf{X}_{1,e}(n)$, $\mathbf{X}_{1,o}(n)$, $\mathbf{X}_{2,e}(n)$ and $\mathbf{X}_{2,o}(n)$ denote the even and odd component vectors of $\mathbf{X}_1(n)$ and $\mathbf{X}_2(n)$ respectively. Equation (1) can then be expressed in terms of the even and odd component vectors as

$$\begin{aligned} \mathbf{X}_{1,e}(n) &= \mathbf{X}_e(n) \quad , \quad \mathbf{X}_{1,o}(n) = -\mathbf{X}_o^*(n) \\ \mathbf{X}_{2,e}(n) &= \mathbf{X}_o(n) \quad , \quad \mathbf{X}_{2,o}(n) = \mathbf{X}_e^*(n) \end{aligned}. \quad (2)$$

The equivalent space-frequency block code transmission matrix [3] is given by

$$\mathcal{G}_2 = \begin{pmatrix} \mathbf{X}_e & \mathbf{X}_o \\ -\mathbf{X}_o^* & \mathbf{X}_e^* \end{pmatrix}.$$

Let $\mathbf{\Lambda}_1(n)$ and $\mathbf{\Lambda}_2(n)$ be two diagonal matrices whose elements are the DFTs of the respective channel impulse responses, $\mathbf{h}_1(n)$ and $\mathbf{h}_2(n)$. The demodulated signal at the receiver is given by

Petitioner Samsung Ex-1004, 0132

$$\mathbf{Y}(n) = \mathbf{\Lambda}_1(n)\mathbf{X}_1(n) + \mathbf{\Lambda}_2(n)\mathbf{X}_2(n) + \mathbf{Z}(n) \quad (3)$$

or, equivalently, as

$$\begin{aligned} \mathbf{Y}_e(n) &= \mathbf{\Lambda}_{1,e}(n)\mathbf{X}_{1,e}(n) + \mathbf{\Lambda}_{2,e}(n)\mathbf{X}_{2,e}(n) + \mathbf{Z}_e(n) \\ \mathbf{Y}_o(n) &= \mathbf{\Lambda}_{1,o}(n)\mathbf{X}_{1,o}(n) + \mathbf{\Lambda}_{2,o}(n)\mathbf{X}_{2,o}(n) + \mathbf{Z}_o(n) \end{aligned} \quad (4)$$

Assuming the channel responses are known or can be estimated accurately at the receiver, the space-frequency decoder block constructs the decision estimate vector $\hat{\mathbf{X}}(n)$ as

$$\begin{aligned} \hat{\mathbf{X}}_e(n) &= \mathbf{\Lambda}_{1,e}^*(n)\mathbf{Y}_e(n) + \mathbf{\Lambda}_{2,o}(n)\mathbf{Y}_o^*(n) \\ \hat{\mathbf{X}}_o(n) &= \mathbf{\Lambda}_{2,e}^*(n)\mathbf{Y}_e(n) - \mathbf{\Lambda}_{1,o}(n)\mathbf{Y}_o^*(n) \end{aligned} \quad (5)$$

The diversity performance of the proposed SF-OFDM transmitter diversity system can be analyzed by first substituting (2) into (4) to express the demodulated signal in terms of $\mathbf{X}_e(n)$ and $\mathbf{X}_o(n)$ as

$$\begin{aligned} \mathbf{Y}_e(n) &= \mathbf{\Lambda}_{1,e}(n)\mathbf{X}_e(n) + \mathbf{\Lambda}_{2,e}(n)\mathbf{X}_o(n) + \mathbf{Z}_e(n) \\ \mathbf{Y}_o(n) &= -\mathbf{\Lambda}_{1,o}(n)\mathbf{X}_o^*(n) + \mathbf{\Lambda}_{2,o}(n)\mathbf{X}_e^*(n) + \mathbf{Z}_o(n) \end{aligned} \quad (6)$$

Assuming the complex channel gains between adjacent subcarriers are approximately constant, i.e., $\mathbf{\Lambda}_{1,e}(n) \approx \mathbf{\Lambda}_{1,o}(n)$ and $\mathbf{\Lambda}_{2,e}(n) \approx \mathbf{\Lambda}_{2,o}(n)$, then substituting (6) into (5) results in

$$\begin{aligned} \hat{\mathbf{X}}_e &= \left(|\mathbf{\Lambda}_{1,e}|^2 + |\mathbf{\Lambda}_{2,e}|^2\right)\mathbf{X}_e + \mathbf{\Lambda}_{1,e}^*\mathbf{Z}_e + \mathbf{\Lambda}_{2,o}\mathbf{Z}_o^* \\ \hat{\mathbf{X}}_o &= \left(|\mathbf{\Lambda}_{1,o}|^2 + |\mathbf{\Lambda}_{2,o}|^2\right)\mathbf{X}_o + \mathbf{\Lambda}_{2,e}^*\mathbf{Z}_e - \mathbf{\Lambda}_{1,o}\mathbf{Z}_o^* \end{aligned} \quad (7)$$

where the implicit dependency on the block instant n has been omitted for briefness. Note that the decision variable equation (7) for the proposed SF-ODFM transmitter diversity scheme is similar in form to that of the optimal two-branch maximal ratio combining (MRC) receiver diversity system [7] and is exactly the same as that of the ST-OFDM transmitter diversity system in [5]. It is thus reasonable to expect the proposed SF-OFDM transmitter diversity system to have the same diversity performance as the previously reported ST-OFDM transmitter diversity system.

IV. Performance of SF-OFDM Transmitter Diversity

The bit error rate (BER) performance of the proposed two-branch SF-OFDM transmitter diversity system was verified by simulation. The simulation system used OFDM with cyclic prefix length set to the channel order L and 4-QAM on each subcarrier. The COST207 six-ray channel power delay profiles [8] were used throughout the simulations, and it was assumed that perfect channel estimation was available at the receiver. Simulation results for the SF-OFDM transmitter diversity system in a slow fading typical urban (TU) channel with maximum Doppler frequency $f_D = 10\text{Hz}$ are shown in Fig. 3.

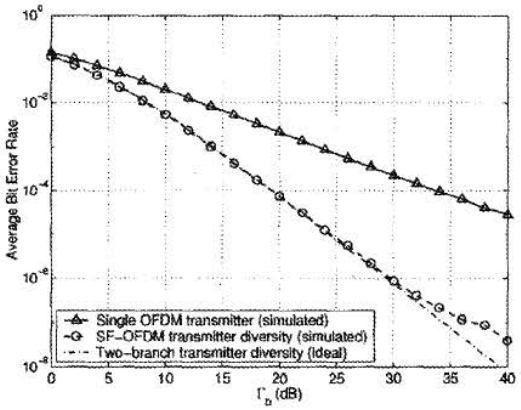


Fig. 3. SF-OFDM transmitter diversity in typical urban (TU) channel, $T_s = 2^{-20}$ Sec., $N = 512$ and $f_D = 10\text{Hz}$.

Simulation results show that the SF-OFDM transmitter diversity system significantly outperforms the conventional OFDM system. It provides about 5 dB of diversity gain at a bit error rate (BER) of 10^{-2} and about 15 dB of gain at a BER of 10^{-4}. Also shown in Fig. 3 is the theoretical performance curve of an ideal two-branch transmitter diversity system. The performance of the SF-OFDM transmitter diversity matches that of the ideal transmitter diversity system very well up to a signal to noise ratio (SNR) of 30 dB. At higher SNR, the SF-OFDM transmitter diversity curve starts to exhibit an error floor, which is a well-known characteristic of all OFDM systems in Doppler spread channels [9].

For conventional OFDM systems, the BER error floor is mainly a function of the normalized Doppler frequency $f_D NT_s$. The BER error floor will degrade as $f_D NT_s$ increases [9]. With transmitter diversity, complex channel gain variation between successive OFDM blocks (in the ST-OFDM case) or between subcarriers (in the SF-OFDM case) can degrade the error floor of the diversity systems. The decision variables for ST-OFDM transmitter diversity are computed over two OFDM blocks [5], so it relies on the channel response to remain constant for two block periods $2NT_s$. With SF-OFDM transmitter diversity, the decision variables are completely determined within a single OFDM block, so it is reasonable to expect SF-OFDM to perform better than ST-OFDM in fast fading environments where $f_D NT_s$ is large. In Fig. 4 (a), the performance of the proposed SF-OFDM transmitter diversity technique is compared to that of the previously reported ST-OFDM transmitter diversity technique [5]. Simulation results show that SF-OFDM transmitter diversity significantly outperforms ST-OFDM transmitter diversity when the normalized Doppler frequency is large.

Petitioner Samsung Ex-1004, 0133

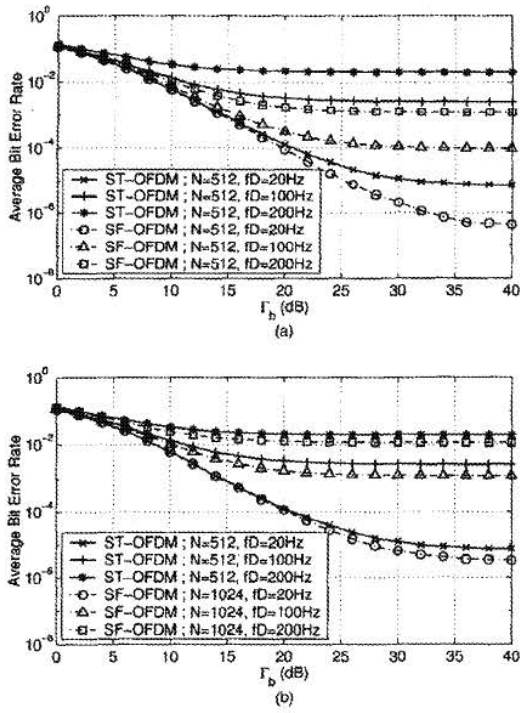


Fig. 4. Performance comparison of ST-OFDM and SF-OFDM transmitter diversity systems over the TU channel. (a) The same $f_D N T_s$ is used for both ST-OFDM and SF-OFDM. (b) $f_D N T_s$ is doubled for SF-OFDM.

To further illustrate the effectiveness of SF-OFDM in fast fading environments, the block size is doubled for the SF-OFDM system in Fig. 4 (b). Simulation results show that SF-OFDM still slightly outperforms ST-OFDM transmitter diversity even at twice the normalized Doppler frequency.

Besides its superior performance in fast fading environments, SF-OFDM transmitter diversity has other practical implementation advantages over the ST-OFDM approach, as well. Since the proposed SF-OFDM transmitter diversity scheme performs the decoding within one OFDM block, it only requires half of the decoder memory needed for the ST-OFDM system of the same block size. Similarly, the decoder latency for SF-OFDM is also half that of the ST-OFDM implementation.

Despite the number of advantages SF-OFDM transmitter diversity has over the ST-OFDM approach, there is one important parameter that requires careful consideration for SF-OFDM transmitter diversity systems. Recall the assumption used to derive (7) that the complex channel gain remains constant between adjacent subcarriers. Any significant

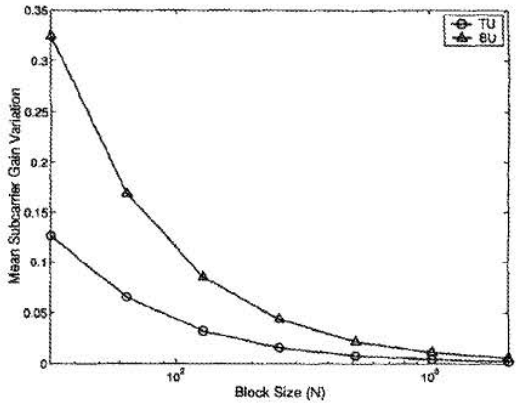


Fig. 5. Mean complex channel gain variation between adjacent subcarriers vs. block size N for typical urban (TU) and bad urban (BU) channel power delay profiles.

variation in complex channel gain between adjacent subcarriers will introduce error in the decoding process and will degrade the BER performance of the diversity system. The assumption of constant gain between subcarriers is, of course, only true for non-dispersive or flat channels. For frequency selective fading channels, the complex channel gain variation between subcarriers depends on the channel order L, the channel power delay profile, and the block size N. The gain variation between subcarriers will be worse for higher order channels and channels with larger root-mean-square (RMS) delay spreads. On the other hand, a larger block size reduces the gain variation between subcarriers because of the finer partitioning of the frequency selective channel.

Although an analytical expression for the subcarrier gain variation is not available, simulation of the complex channel gain of the subcarriers can provide a qualitative measure on how the gain variation is affected by the channel characteristics and block size. Fig. 5 shows the simulation results of the mean subcarrier gain variation as a function of the block size for the COST207 TU and bad urban (BU) channel power delay profiles. As expected, the gain variation between adjacent subcarriers is worse for small block sizes and for channels with poor power delay profiles, i.e., gain variation is worse for the BU channel because of its larger RMS delay spread. For $N = 32$, the mean gain variations are 0.13 for the TU channel and 0.33 for the BU channel. The gain variation becomes small quickly as N increases. For $N = 512$, the mean gain variations are reduced to 0.004 and 0.011 for the TU and BU channels, respectively.

Simulation results for an SF-OFDM transmitter diversity system with a block size of $N = 64$ in a slow fading BU channel is shown in Fig. 6. Although the normalized

Petitioner Samsung Ex-1004, 0134

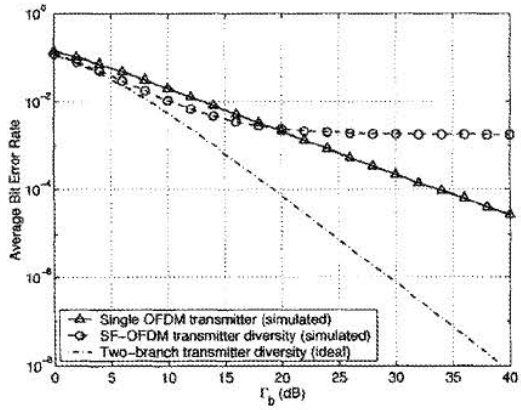


Fig. 6. SF-OFDM transmitter diversity over the bad urban (BU) channel with $T_s = 2^{-20}$ Sec., $N = 64$ and $f_D = 10$Hz.

Doppler frequency is very small in this case, the BER is severely degraded because of excessive gain variation between subcarriers. Based on the results in Fig. 5 and Fig. 6, it can be concluded that a sufficiently large block size is essential for the implementation of SF-OFDM transmitter diversity systems. However, an excessively large block size is not required for SF-OFDM transmitter diversity to work effectively. For the symbol rate and channel characteristics used in the simulations for this study, a moderate block size of 512 is quite adequate as apparent from the results in Fig. 4 (a).

V. Summary and Discussions

A simple two-branch SF-OFDM transmitter diversity technique for wireless communications over frequency selective fading channels has been presented. It has been shown that SF-OFDM is an efficient and effective transmitter diversity technique, especially for applications where the normalized Doppler frequency $f_D N T_s$ is large.

This paper has focused on two-branch diversity because of its simplicity and its unity coding rate. Higher order SF-OFDM transmitter diversity can be implemented in similar fashion along the frequency dimension. Unfortunately, higher order complex orthogonal block codes [3] all have less than unity coding rate, which results in a reduction in data throughput or an expansion in bandwidth in order to maintain the same data rate. Even if the coding rate loss is acceptable, it is not clear whether using higher order transmitter diversity directly or applying other error correction codes (ECC) on top of the second order transmitter diversity system will achieve better overall performance. The tradeoffs between higher order diversity and ECC is an interesting topic for further study. Also not addressed in this paper is the important issue of channel estimation in the SF-OFDM transmitter diversity setting. A channel parameter estimation technique has been proposed for the ST-OFDM transmitter diversity system in [10]. It would be interesting to investigate if similar or better channel estimation approaches can be developed for SF-OFDM transmitter diversity systems.

References

[1] A. Wittneben, "A new bandwidth efficient transmit antenna modulation diversity scheme for linear digital modulation," in *Proc. IEEE ICC*, Geneva, Switzerland, May 1993, vol. 3, pp. 1630-1634.

[2] S. M. Alamouti, "A simple transmitter diversity scheme for wireless communications," *IEEE J. Select. Areas Commun.*, vol. 16, no. 8, pp. 1451-1458, Oct. 1998.

[3] V. Tarokh, H. Jafarkhani, and A. R. Calderbank, "Space-time block coding for wireless communications: performance results," *IEEE J. Select. Areas Commun.*, vol. 17, no. 3, pp. 451-460, March 1999.

[4] D. Agrawal, V. Tarokh, A. Naguib, and N. Seshadri, "Space-time coded OFDM for high data-rate wireless communication over wideband," in *Proc. IEEE VTC*, Ottawa, Ont., Canada, May 1998, vol. 3, pp. 2232-2236.

[5] K. F. Lee and D. B. Williams, "A space-time coded transmitter diversity technique for frequency selective fading channels," in *Proc. IEEE Sensor Array and Multichannel Signal Processing Workshop*, Cambridge, MA, March 2000, pp. 149-152.

[6] L. J. Cimini, Jr., "Analysis and simulation of a digital mobile channel using orthogonal frequency division multiplexing," *IEEE Trans. Commun.*, vol. COM-33, no. 7, pp. 665-675, July 1985.

[7] T. Eng, N. Kong, and L. B. Milstein, "Comparison of diversity combining techniques for Rayleigh-fading channels," *IEEE Trans. Commun.*, vol. 44, no. 9, pp. 1117-1129, Sept. 1996.

[8] COST207 TD(86)51-REV 3 (WG1), "Proposal on channel transfer functions to be used in GSM tests late 1986,", Sept. 1986.

[9] D. T. Harvatin and R. E. Ziemer, "Orthogonal frequency division multiplexing performance in delay and Doppler spread channels," in *Proc. IEEE VTC*, Phoenix, AZ, May 1997, vol. 3, pp. 1644-1648.

[10] Y. Li, N. Seshadri, and S. Ariyavisitakul, "Channel estimation for OFDM systems with transmitter diversity in mobile wireless channels," *IEEE J. Select. Areas Commun.*, vol. 17, no. 3, pp. 461-471, March 1999.

Petitioner Samsung Ex-1004, 0135

Effects of Channel-Estimation Errors on Receiver Selection-Combining Schemes for Alamouti MIMO Systems With BPSK

Wenyu Li, *Student Member, IEEE,* and Norman C. Beaulieu, *Fellow, IEEE*

***Abstract*—The bit-error rate (BER) of binary phase-shift keying in Rayleigh fading, using the Alamouti transmission scheme and receiver selection diversity in the presence of channel-estimation error, is studied. Closed-form expressions for the BER of log-likelihood ratio selection, signal-to-noise ratio (SNR) selection, switch-and-stay combining selection, and maximum ratio combining are derived in terms of the SNR and the cross-correlation coefficient of the channel gain and its corrupted estimate. Two new selection schemes, space–time sum-of-squares combining selection diversity and space–time sum-of-magnitudes selection diversity, are proposed and proven to provide almost the same performance as SNR selection, but with much simpler implementations. The effects of channel-estimation errors on each selection scheme are examined.**

***Index Terms*—Alamouti multiple-input multiple-output (MIMO) systems, error analysis, estimation error, fading channels, pilot-symbol-assisted modulation (PSAM), selection diversity.**

I. Introduction

MULTIPLE-INPUT multiple-output (MIMO) systems have attracted great interest, since they can improve the channel capacity and reliability of wireless communication [1]. However, adopting a MIMO system increases the system complexity and the cost of implementation. A promising approach for reducing implementation complexity, while retaining a reasonably good performance, is to employ some form of antenna selection.

In general, MIMO antenna selection combining (SC) includes receiver (Rx) antenna selection, transmitter (Tx) antenna selection, and joint Tx/Rx selection. Both Tx/Rx selection and Tx selection require that channel estimation be fed back from the Rx to the Tx. In order to avoid the need for a feedback channel, and to keep the system simple, some systems will implement Rx selection diversity only. In MIMO Rx selection diversity, L_s out of L Rx antennas are selected, while the Tx uses all available antennas. Some past work has examined MIMO Rx selection diversity. In [2]–[4], the Rx selection criteria are based on achieving the maximum received signal-to-noise ratio (SNR). An approximation of pairwise error probability is given in [2]. An upper bound on pairwise error probability is presented in [3]. In [4], an upper bound on bit-error rate (BER) is derived.

Paper approved by Y. Li, the Editor for Wireless Communications Theory of the IEEE Communications Society. Manuscript received February 3, 2005; revised July 5, 2005. This paper was presented in part at the Vehicular Technology Conference, Dallas, TX, September 2005.

The authors are with the Department of Electrical and Computer Engineering, University of Alberta, Edmonton, AB T6G 2V4, Canada (e-mail: wendy@ece.ualberta.ca; beaulieu@ece.ualberta.ca).

Digital Object Identifier 10.1109/TCOMM.2005.861648

In this paper, we examine the effect of channel-estimation error on the BER performance of a MIMO system using binary phase-shift keying (BPSK) modulation and Rx selection diversity in a slow flat Rayleigh fading channel. The Alamouti space–time block code (STBC) [5] is used at the Tx. The "best" of L Rx antennas is chosen according to some selection criterion. Since all SC schemes require some knowledge of the complex channel gains for all the diversity branches, and the complex channel gains have to be estimated at the Rx, channel-estimation errors affect the performance of all practical SC schemes. Quantitative results for the effects of noisy channel estimation are derived.

Five different selection schemes are considered for Rx antenna selection. The first scheme is log-likelihood ratio (LLR) selection, which was proposed in [6] for a one Tx antenna and L Rx antennas system. In LLR selection, full knowledge of all the complex diversity branch gains is needed, and the branch providing the largest magnitude of LLR is chosen. This selection scheme was extended in [7] to include a two Tx antennas and N_R Rx antennas system using the Alamouti scheme. The BER for this scheme is given by an expression involving a single integral. However, perfect channel estimation is assumed in [7]. Here, we derive a closed-form BER expression for this LLR selection scheme, accounting for the presence of channel-estimation errors.

Traditional SC is the second scheme considered in this paper. The selection of the best antenna is based on the largest SNR among the diversity branches at the detector input. Unlike LLR selection, which requires full knowledge of the complex channel gains for all the diversity branches, SNR selection only requires ordering fading amplitudes on the diversity branches. In [8], SNR selection is applied to Tx selection. Two Tx antennas which provide the largest and the second largest SNR are used for transmitting an STBC. The performance of the system is assessed in terms of an outage capacity analysis, but exact BER results are not given. In [4] and [7], the BER of SNR selection at the Rx side is evaluated. In this paper, this result is extended to include the effects of channel-estimation errors.

Since both LLR selection and SNR selection schemes require channel knowledge, we propose a new selection scheme, which we will refer to as space–time sum-of-squares (STSoS) selection. The STSoS selection scheme does not require knowledge of the channel gains to make the Rx antenna selection. Furthermore, branch selection is done before the space–time decoding, so that channel estimation for the space–time decoding is only performed for the branch selected, achieving a significant complexity reduction. Compared with the two former schemes, this new scheme is much simpler to implement. Significantly, it is shown in the following that it provides essentially the same performance as the SNR selection scheme.

0090-6778/$20.00 © 2006 IEEE

Petitioner Samsung Ex-1004, 0136

The proposed STSoS SC scheme requires squaring the amplitudes of the received bit signals. In order to further simplify the hardware implementation, we propose another scheme, which only needs the amplitudes of the received bit signals. Similar to STSoS selection, this scheme, called space–time sum-of-magnitudes (STSoM) selection, does not require channel estimation. The simulation results in the following section show that STSoM selection has only slightly poorer BER performance than STSoS and SNR selection.

In order to implement all the former SC schemes, the Rx needs to monitor all the diversity branches to select the "best" branch. Furthermore, the Rx may switch frequently in order to use the best branches. It is desirable in some practical implementations to minimize switching in order to reduce switching transients. Therefore, SC is often implemented in the form of switched diversity [9], [10] in practical systems, in which rather than continuously picking the best branch, the Rx selects a particular branch until its SNR drops below a predetermined threshold. When this happens, the Rx switches to another branch. [11] and [12] investigate a switched diversity system with one Tx antenna and N_R Rx antennas. A performance analysis for this system without space–time coding was given in Rayleigh fading in [11], and in Nakagami fading in [12]. In [13], switched diversity is applied at the Tx side and the cumulative distribution function (cdf), the probability density function (pdf), and the moment-generating function (MFG) of the received signal power are derived, again without space–time coding. In this paper, we analyze a transmission system with an Alamouti code at the Tx and switched diversity at the Rx. The average BER accounting for the effects of channel-estimation error is derived, and the optimal switching threshold that minimizes the BER for this switched diversity scheme is determined.

The remainder of this paper is organized as follows. In Section II, we present the system model. In Section III, we consider a wireless system with two Tx antennas using the Alamouti scheme and L Rx antennas, and derive the BER for the four SC schemes with channel-estimation error considered. The analysis of a maximum ratio combining (MRC) Rx [14] is also recalled, and the performances of these four selection schemes are compared with the optimal MRC scheme. In Section IV, numerical results are presented and the relative performances of the four selection schemes are discussed. Conclusions are drawn in Section V.

II. System Model

In general, we consider a system where an Alamouti scheme [5] is applied with two Tx antennas and L Rx antennas. Reference [5, Fig. 3] shows the STBC system for the special case of two Rx antennas for illustration. We assume a BPSK modulation, so that the transmitted signal is either $+1$ or -1. Signals s_1 and s_2, corresponding to two information bits, are sent simultaneously during two consecutive bit intervals. The corresponding received signals in these two intervals on the ith branch can be expressed as [5]

$$r_{1,i} = g_{1,i}s_1 + g_{2,i}s_2 + n_{1,i} \tag{1a}$$

$$r_{2,i} = -g_{1,i}s_2 + g_{2,i}s_1 + n_{2,i} \tag{1b}$$

where $g_{j,i}$, $j = 1, 2$, $i = 1, \ldots, L$ is the complex gain between the jth Tx antenna and the ith Rx antenna, and $n_{j,i}$, $j = 1, 2$, $i = 1, \ldots, L$ represents additive channel noise. The variances of the real (or imaginary) components of $g_{j,i}$ and $n_{j,i}$ are denoted by σ_g^2 and σ_n^2, respectively. The average SNR of the received signal is defined here as $\bar{\gamma} = 2\sigma_g^2/\sigma_n^2$. The maximum-likelihood (ML) decoding of s_1 and s_2 is based on the combiner outputs [5]

$$y_{1,i} = \hat{g}_{1,i}^* r_{1,i} + \hat{g}_{2,i} r_{2,i}^* \tag{2a}$$

$$y_{2,i} = \hat{g}_{2,i}^* r_{1,i} - \hat{g}_{1,i} r_{2,i}^* \tag{2b}$$

where $\hat{g}_{j,i}$ is the estimate of $g_{j,i}$ with variance $\sigma_{\hat{g}}^2$, in the real and imaginary parts. The signal estimate is $\hat{s}_j = \mathrm{sgn}(\Re(y_{j,i}))$, $j = 1, 2$, where $\mathrm{sgn}(x) = \mathrm{signum}(x)$ is defined in [15, p. xlv].

The complex channel gains $g_{j,i}$ are estimated at the Rx prior to fading compensation. We assume identical statistics for the independent diversity branches, and that the correlation between $g_{j,i}$ and its estimate $\hat{g}_{j,i}$ is the same on each branch. Extending the results in [16] to include the case when the variances of the channel gain and its estimate are unequal, we define

$$g_{j,i} = \left(\frac{R_c}{\sigma_{\hat{g}}^2} + j\frac{R_{cs}}{\sigma_{\hat{g}}^2}\right)\hat{g}_{j,i} + (x_{j,i} + jy_{j,i}) \tag{3}$$

where $x_{j,i}$ and $y_{j,i}$ are uncorrelated with $\hat{g}_{j,i}$. The parameters R_c and R_{cs} are given by

$$R_c = E[g_I\hat{g}_I] = E[g_Q\hat{g}_Q] \tag{4a}$$

$$R_{cs} = E[g_I\hat{g}_Q] = -E[g_Q\hat{g}_I]. \tag{4b}$$

Under the Rayleigh fading assumption, $R_{cs} = 0$ [17], and we can simplify (3) to

$$g_{j,i} = k\hat{g}_{j,i} + d_{j,i} \tag{5}$$

where $k = R_c/\sigma_{\hat{g}}^2$ and $d_{j,i} = (x_{j,i} + jy_{j,i})$. The variance of the real (or imaginary) component of $d_{j,i}$ is $\sigma_d^2 = (1-\rho)\sigma_g^2$ [18], where ρ is the squared amplitude of the cross-correlation coefficient of the channel fading and its estimate

$$\rho = \frac{E^2[g\hat{g}^*]}{E[|g|^2]E[|\hat{g}|^2]} = \frac{R_c^2}{\sigma_g^2\sigma_{\hat{g}}^2} = \frac{\sigma_{\hat{g}}^2}{\sigma_g^2}k^2. \tag{6}$$

When pilot-symbol-assisted modulation (PSAM) is employed to estimate the fading channel gain, the cross-correlation coefficient of the channel fading and its estimate can be expressed as shown in (7) at the bottom of the page, where K is the size of the interpolator, h_k^n and h_m^n are the interpolator coefficients, f_D is the Doppler shift, T_s is the symbol interval, N

$$\rho = \frac{\left[\sum_{k=-\lfloor (K-1)/2\rfloor}^{\lfloor K/2\rfloor} h_k^n J_0(2\pi f_D|kN - 2n|T_s)\right]^2}{\sum_{k=-\lfloor (K-1)/2\rfloor}^{\lfloor K/2\rfloor}\sum_{m=-\lfloor (K-1)/2\rfloor}^{\lfloor K/2\rfloor} h_k^n h_m^n J_0(2\pi f_D|k-m|NT_s) + \frac{1}{\bar{\gamma}}\sum_{m=-\lfloor (K-1)/2\rfloor}^{\lfloor K/2\rfloor}(h_k^n)^2} \tag{7}$$

Petitioner Samsung Ex-1004, 0137

is the frame size, and $J_0(\cdot)$ is the zeroth-order Bessel function of the first kind. The detailed derivation of ρ is in Appendix A.

III. Bit-Error Rate Analysis

By symmetry, the BER is the same for s_1 and s_2, so the following analysis will consider s_1 only. The results for s_i, $i = 1, 2$ can be obtained by appropriately renaming the variables.

Using (1), (2a), and (5), the combiner output $y_{1,i}$ can be written as

$$y_{1,i} = k\left(|\hat{g}_{1,i}|^2 + |\hat{g}_{2,i}|^2\right)s_1 + \left(\hat{g}_{1,i}^* d_{1,i} + \hat{g}_{2,i} d_{2,i}^*\right)s_1 + \left(\hat{g}_{1,i}^* d_{2,i} - \hat{g}_{2,i} d_{1,i}^*\right)s_2 + \hat{g}_{1,i}^* n_{1,i} + \hat{g}_{2,i} n_{2,i}^*. \quad (8)$$

Since $s_2 = +s_1$ or $-s_1$, each with probability 1/2, we can calculate the BER as $P_b = 1/2(P_{b,s_2=s_1} + P_{b,s_2=-s_1}) = P_{b,s_2=s_1} = P_{b,s_2=s_1=1}$, where the last two equations follow from symmetry. For the case $s_2 = s_1 = 1$, from (8), we can write the decision variable for $y_{1,i}$ as

$$\Re(y_{1,i}) = k\left(|\hat{g}_{1,i}|^2 + |\hat{g}_{2,i}|^2\right) + \Re\left[\hat{g}_{1,i}^*(d_{1,i} + d_{2,i}) + \hat{g}_{2,i}(d_{2,i} - d_{1,i})^*\right] + \Re(\hat{g}_{1,i}^* n_{1,i}) + \Re(\hat{g}_{2,i} n_{2,i}^*). \quad (9)$$

Conditioning on $|\hat{g}_{1,i}|^2$ and $|\hat{g}_{2,i}|^2$, it can be shown that $\Re[\hat{g}_{1,i}^*(d_{1,i} + d_{2,i})]$, $\Re[\hat{g}_{2,i}^*(d_{2,i} - d_{1,i})]$, $\Re(\hat{g}_{1,i}^* n_{1,i})$ and $\Re(\hat{g}_{2,i} n_{2,i}^*)$ are independent, zero-mean Gaussian random variables with variance $2|\hat{g}_{1,i}|^2\sigma_d^2$, $2|\hat{g}_{2,i}|^2\sigma_d^2$, $|\hat{g}_{1,i}|^2\sigma_n^2$ and $|\hat{g}_{2,i}|^2\sigma_n^2$, respectively. Therefore, $\Re(y_{1,i})$, conditioned on $|\hat{g}_{1,i}|^2$ and $|\hat{g}_{2,i}|^2$, is a Gaussian random variable as well. It has mean $k(|\hat{g}_{1,i}|^2 + |\hat{g}_{2,i}|^2)$ and variance $(2\sigma_d^2 + \sigma_n^2)(|\hat{g}_{1,i}|^2 + |\hat{g}_{2,i}|^2)$.

To simplify the following BER calculation, we normalize the expression in (9) by dividing both sides of the equation with $2k\sigma_{\hat{g}}^2$. Then (9) can be written as

$$\Re(y'_{1,i}) = \frac{\Re(y_{1,i})}{2k\sigma_{\hat{g}}^2} = \frac{1}{2\sigma_{\hat{g}}^2}\left(|\hat{g}_{1,i}|^2 + |\hat{g}_{2,i}|^2\right) + \frac{1}{2k\sigma_{\hat{g}}^2}\left\{\Re\left[\hat{g}_{1,i}^*(d_{1,i} + d_{2,i}) + \hat{g}_{2,i}(d_{2,i} - d_{1,i})^*\right] + \Re(\hat{g}_{1,i}^* n_{1,i}) + \Re(\hat{g}_{2,i} n_{2,i}^*)\right\}. \quad (10)$$

Let $a_i = (|\hat{g}_{1,i}|^2 + |\hat{g}_{2,i}|^2)/2\sigma_{\hat{g}}^2$; conditioned on a_i, the new decision variable $\Re(y'_{1,i})$ has mean a_i and variance $((2\sigma_d^2 + \sigma_n^2)/2k^2\sigma_{\hat{g}}^2)a_i$. Using (6) and $\sigma_d^2 = (1-\rho)\sigma_g^2$, this variance is simplified to $(((1-\rho)\bar{\gamma} + 1)/\rho\bar{\gamma})a_i$. Define the effective SNR

$$\bar{\gamma}_c = \frac{\rho\bar{\gamma}}{(1-\rho)\bar{\gamma} + 1}. \quad (11)$$

Then the variance is $a_i/\bar{\gamma}_c$.

Since $\hat{g}_{1,i}$ and $\hat{g}_{2,i}$ are independent, zero-mean complex Gaussian random variables, a_i has a chi-square distribution with four degrees of freedom, and its pdf is given by [14]

$$f_A(a_i) = a_i \exp(-a_i). \quad (12)$$

A. LLR SC

The LLR Rx selection system model is described in [7]. With the Alamouti scheme and imperfect channel estimation, the LLR for data s_1, given $\hat{g}_{j,i}$, $j = 1, 2$ and $y_{1,i}$ is

$$\Lambda_i = \ln\frac{P(s_1 = +1|\hat{g}_{j,i}, y_{1,i})}{P(s_1 - 1|\hat{g}_{j,i}, y_{1,i})} = \ln\frac{p(y_{1,i}|\hat{g}_{j,i}, s_1 = +1)}{p(y_{1,i}|\hat{g}_{j,i}, s_1 = -1)}. \quad (13)$$

From (8), conditioning on $\hat{g}_{j,i}$, we can show that $y_{1,i}$ is a complex Gaussian random variable with mean $k(|\hat{g}_{1,i}|^2 + |\hat{g}_{2,i}|^2)s_1 = m_y s_1$ and real/imaginary part variance $\sigma_y^2 = (2\sigma_d^2 + \sigma_n^2)(|\hat{g}_{1,i}|^2 + |\hat{g}_{2,i}|^2)$. Then continuing (13), we have

$$\Lambda_i = \ln\frac{\exp\left[\frac{-|y_{1,i} - m_y|^2}{(2\sigma_y^2)}\right]}{\exp\left[\frac{-|y_{1,i} + m_y|^2}{(2\sigma_y^2)}\right]} = \frac{2m_y}{\sigma_y^2}\Re(y_{1,i}) = \frac{2k}{(2\sigma_d^2 + \sigma_n^2)}\Re(y_{1,i}) = \frac{2R_c}{(2\sigma_d^2 + \sigma_n^2)\sigma_{\hat{g}}^2}\Re(y_{1,i}). \quad (14)$$

Since R_c, σ_d^2, σ_n^2, and $\sigma_{\hat{g}}^2$ are the same across all the Rx branches, the LLR Rx SC is equivalent to selecting the branch providing the largest amplitude of $\Re(y_{1,i})$. Note, with perfect channel estimation, i.e., when $R_c = \sigma_{\hat{g}}^2 = \sigma_g^2$ and $\sigma_d^2 = 0$, $\Lambda_i = (4/N_0)\Re(y_{1,i})$, which matches the result in [7, eq. (37)], where N_0 is the noise power spectral density.

The final expression for the BER is derived in Appendix B. It is shown in (15) at the bottom of the next page, where $A - C$ and m_1-m_7 are given in (39b) and (40b), respectively.

A simpler suboptimum SC rule was also proposed by Kim and Kim in [6]. Instead of the amplitude of $\Re(y_{1,i})$, $|(y_{1,i})|$ is used for this envelope-LLR SC. Simulation results for the BER of this envelope-LLR selection scheme will be given together with results for the other SC schemes in Section IV.

$$P_b = L\sum_{n=0}^{L-1}\sum_{m=0}^{L-1-n}\sum_{p=0}^{n}\sum_{q=0}^{m}\sum_{i=0}^{1}\binom{L-1}{n}\binom{L-1-n}{m}\binom{n}{p}\binom{m}{q} \times AB^i m_1^{n-p} m_2^p m_4^{m-q} m_5^q m_7^{L-1-n-m}\frac{(-1)^{m+p}(p+q+i)!}{(m_3 n + m_6 m + B + C)^{p+q+i+1}} \quad (15)$$

Petitioner Samsung Ex-1004, 0138

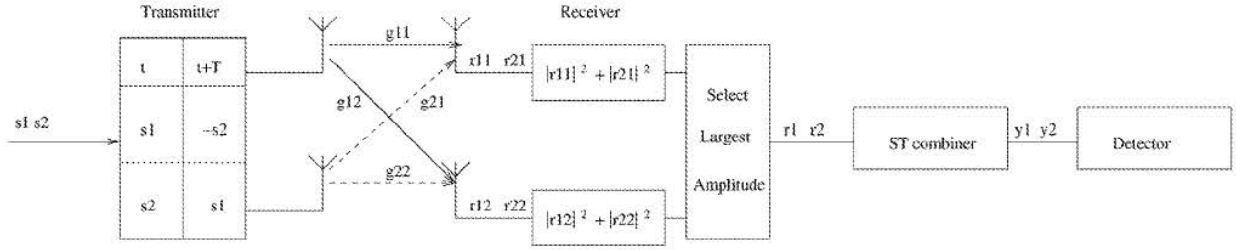


Fig. 1. STSoS Rx selection system model.

B. SNR SC

The Rx SC scheme model is same as the model in [4] and [7]. In SNR SC, the Rx antenna with the largest SNR will be chosen for space–time decoding. From (8), the SNR, given the ith Rx antenna selected, is $k^2(|\hat{g}_{1,i}|^2+|\hat{g}_{2,i}|^2)/2(2\sigma_d^2+\sigma_n^2) = \bar{\gamma}_c a_i/2$. Therefore, the antenna providing the largest SNR is the one providing the largest a_i. Let $A_{\max} = \max[(|\hat{g}_{1,i}|^2 + |\hat{g}_{2,i}|^2)/2\sigma_{\hat{g}}^2]$. Then, the expression of the BER can be rewritten as [7]

$$P_b = L \cdot \int_0^\infty \Pr\left(\Re(y_{1,i}) \le 0 | A_{\max} = a\right) f_{A_{\max}}(a) da = \int_0^\infty \mathrm{Q}\left(\sqrt{\bar{\gamma}_c a}\right) f_{A_{\max}}(a) da \quad (16a)$$

where the pdf of $A_{\max}$ is [19]

$$f_{A_{\max}}(a) = L\left[\int_0^a f_A(a_i) da_i\right]^{L-1} f_A(a) = L\left[1-(1+a)\exp(-a)\right]^{L-1} f_A(a) \quad (16b)$$

and $f_A(a)$ is given in (12).

Expanding $\left[\int_0^a f_A(a)da\right]^{L-1}$ in (16) using the binomial theorem gives

$$P_b = L \times \sum_{i=0}^{L-1}\sum_{j=0}^{i}\binom{L-1}{i}\binom{i}{j}(-1)^i \times \int_0^\infty \mathrm{Q}\left(\sqrt{\bar{\gamma}_c a}\right) a^{j+1}\exp[-(i+1)a] da. \quad (17)$$

Integrating (17) term-by-term, the final expression for the BER is derived as

$$P_b = L \times \sum_{i=0}^{L-1}\sum_{j=0}^{i}\sum_{m=0}^{j+1}(-1)^i \binom{L-1}{i}\binom{i}{j} \times \frac{(j+1+m)!}{m!(1+i)^{j+2}}\left(\frac{1-\mu_1}{2}\right)^{j+2}\left(\frac{1+\mu_1}{2}\right)^m \quad (18a)$$

$$\mu_1 = \sqrt{\frac{\bar{\gamma}_c}{\bar{\gamma}_c + 2i + 2}}. \quad (18b)$$

C. New SC Method 1: STSoS Selection

Both LLR-based and SNR-based SC schemes require knowledge of all the Rx branch fading gains in order to decide which branch to choose. This increases the Rx complexity. Here, we propose a new selection-diversity scheme that selects the branch providing the largest sum of the squared amplitudes of the two received bit signals, i.e., $|r_{1,i}|^2+|r_{2,i}|^2$ (see Fig. 1). This scheme is similar to square-law combining, although square-law combining is used for noncoherent modulation and we deal with coherent modulation here. To the best of the authors' knowledge, this SC diversity scheme as used in space–time coding here with coherent modulation is novel. We will call it STSoS selection. The advantage of this selection scheme is that it does not require channel estimation to perform the selection. Hence, the Rx implementation is simpler than other selection schemes. Moreover, this new scheme provides comparable performance to SNR-based selection, as is shown in Section IV.

The system model is shown in Fig. 1. Observe that

$$\begin{aligned} &2|r_{1,i}|^2+2|r_{2,i}|^2 \\ &\quad = |r_{1,i}+r_{2,i}|^2 + |r_{1,i}-r_{2,i}|^2 \\ &\quad = |g_{1,i}(s_1-s_2)+g_{2,i}(s_1+s_2)+n_{1,i}+n_{2,i}|^2 \\ &\qquad +|g_{1,i}(s_1+s_2)+g_{2,i}(s_2-s_1)+n_{1,i}-n_{2,i}|^2 \end{aligned} \quad (19a)$$

and, observe further that $s_1+s_2 = \pm 2$ and $s_1 - s_2 = 0$, or $s_1+s_2 = 0$ and $s_2 - s_1 = \pm 2$, so that

$$\begin{aligned} &|r_{1,i}+r_{2,i}|^2 + |r_{1,i}-r_{2,i}|^2 \\ &= \begin{cases} |\pm 2g_{1,i}+n_{1,i}+n_{2,i}|^2 + |\pm 2g_{2,i}+n_{1,i}-n_{2,i}|^2, & s_1 = -s_2 \\ |\pm 2g_{2,i}+n_{1,i}+n_{2,i}|^2 + |\pm 2g_{1,i}+n_{1,i}-n_{2,i}|^2, & s_1 = s_2. \end{cases} \end{aligned} \quad (19b)$$

Thus, selecting the branch having the maximum value of $|r_{1,i}|^2 + |r_{2,i}|^2$ is equivalent to selecting the branch with the maximum value of

$$|g_{1,i}+n_1^e|^2 + |g_{2,i}+n_2^e|^2 \quad (20)$$

where n_1^e and n_2^e are independent, complex noise samples, each of variance $\sigma_n^2/2$ in each of the real and imaginary components. Note that when the SNR becomes large, STSoS selection is equivalent to selecting the branch with the maximum value of $|g_{1,i}|^2 + |g_{2,i}|^2$, because the noise terms in (20) become small. On the other hand, in SNR SC, selecting the antenna providing the largest $a_i = (|\hat{g}_{1,i}|^2 + |\hat{g}_{2,i}|^2)/2\sigma_{\hat{g}}^2$ is equivalent to selecting the antenna providing the largest $|\hat{g}_{1,i}|^2+|\hat{g}_{2,i}|^2$, because the $\sigma_{\hat{g}}^2$ is the same over all the Rx branches. Since the channel gain estimate depends on the SNR, with a large SNR value, one has $\hat{g}_{j,i} \to g_{j,i}$, $j = 1, 2$. As a result, the SNR selection is equivalent to selecting the branch with the maximum value of $|g_{1,i}|^2+|g_{2,i}|^2$ as well when the SNR becomes large, and STSoS selection becomes equivalent to SNR-based selection in slow fading. Observe further that the noise affecting the branch selection is effectively reduced by 3 dB in the STSoS combiner.

Petitioner Samsung Ex-1004, 0139

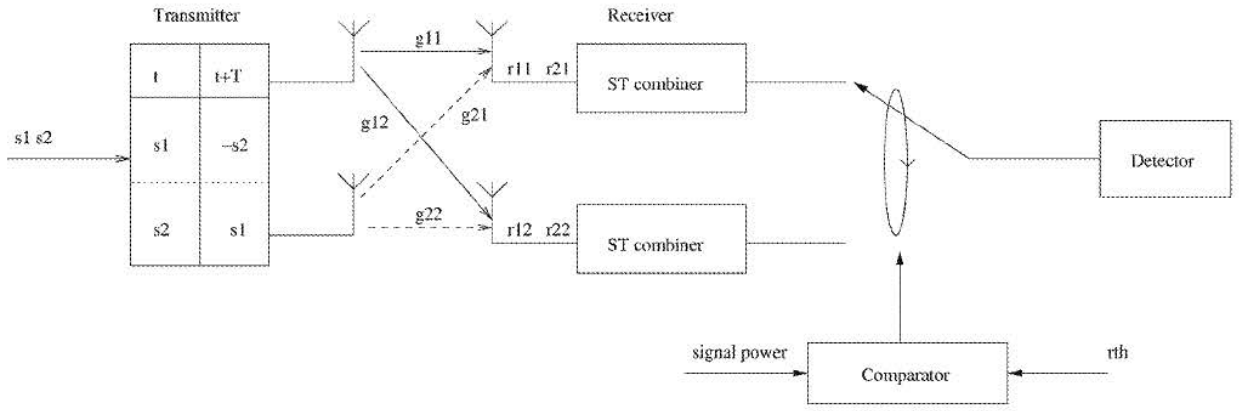


Fig. 2. SSC Rx selection system model.

Also note that when the SNR becomes small, both STSoS selection and SNR selection become dominated by noise terms, e.g., n_j^c, $j = 1, 2$ for STSoS selection and estimation error for SNR selection. Both these terms are Gaussian distributed, such that the BER performances of both selection methods approach 0.5. As a result, the BER difference between the two methods is indistinguishable.

The simulation results in the following section show that STSoS selection has essentially the same performance as SNR-based selection.

D. New SC Method 2: STSoM Selection

The proposed STSoS SC scheme, which selects the branch providing the largest sum of $|r_{1,i}|^2 + |r_{2,i}|^2$, requires squaring the amplitudes of the received bit signals before making the selection. In order to further simplify the hardware implementation, we propose another scheme which selects the branch with the largest sum, $|r_{1,i}| + |r_{2,i}|$. Similar to STSoS selection, this scheme, called STSoM selection, does not require channel estimation. It is simpler than STSoS selection because the Rx only needs to obtain the amplitudes of the two received signals $r_{1,i}$ and $r_{2,i}$, and then take the sum. The simulation results in the following section show that it has only slightly poorer BER performance than STSoS and SNR selection.

E. Switch-and-Stay Selection

Switch-and-stay SC (SSC) [11] functions in the following manner: assuming antenna 1 is being used, one switches to antenna 2 only if the instantaneous signal power in antenna 1 falls below a certain threshold, $\gamma_{\rm th}$, regardless of the value of the instantaneous signal power in antenna 2. The switching from antenna 2 to antenna 1 is performed in the same manner. The system model is shown in Fig. 2. The major advantage of this strategy is that only one envelope signal need be examined at any instant. Therefore, it is much simpler to implement than traditional SC, because it is not necessary to keep track of the signals from both antennas simultaneously. However, the performance of SSC is poorer than the performance of SC. Using the Alamouti scheme at the Tx antenna side, and assuming the fadings on the Rx antenna branches are independent and identically Rayleigh distributed, the number of branches at the Rx side does not affect the average BER performance [13]. Consequently, only the case of two Rx antennas is examined here.

In Rx SSC, with channel-estimation error, the BER is related to the instantaneous effective SNR of the selected ith branch $\gamma_{\rm c}$ in (8), where $\gamma_{\rm c} = k^2(|\hat{g}_{1,i}|^2 + |\hat{g}_{2,i}|^2)/2(2\sigma_d^2 + \sigma_n^2)$. Conditioning on the pdf of $\gamma_{\rm c}$, the BER is $\mathrm{Q}(\sqrt{2\gamma_{\rm c}})$. The final BER expression is derived in Appendix C. It is

$$P_b = K_1 - \left[K_1\left(\frac{2\gamma_{th}}{\bar{\gamma}_c} + 1\right) - \frac{2\gamma_{\rm th} + \bar{\gamma}_{\rm c}}{\bar{\gamma}_c}\mathrm{Q}(\sqrt{2\gamma_{\rm th}}) + \frac{\sqrt{\gamma_{\rm th}}}{\sqrt{\pi}(\bar{\gamma}_c + 2)}\exp(-\gamma_{\rm th})\right]\exp\left(-\frac{2\gamma_{\rm th}}{\bar{\gamma}_c}\right) - K_2\mathrm{Q}\left(\sqrt{\frac{2\gamma_{\rm th}(\bar{\gamma}_c + 2)}{\bar{\gamma}_c}}\right) \tag{21}$$

where K_1 and K_2 are given in (45b).

Note that the BER depends on the value of the switching threshold $\gamma_{\rm th}$. The optimal value, $\gamma_{\rm th}^*$, is a solution of the equation $(\partial P_e/\partial\gamma_{\rm th})|_{\gamma_{\rm th}=\gamma_{\rm th}^*} = 0$. Differentiating (21) with respect to $\gamma_{\rm th}$, we get

$$\gamma_{\rm th}^* = \frac{1}{2}\left[Q^{-1}(\alpha)\right]^2, \alpha = \frac{1}{2} - \frac{\bar{\gamma}_{\rm c}\sqrt{\bar{\gamma}_{\rm c}}}{2\sqrt{(\bar{\gamma}_{\rm c}+2)^3}} - \frac{3\sqrt{\bar{\gamma}_{\rm c}}}{2\sqrt{(\bar{\gamma}_{\rm c}+2)^3}} \tag{22}$$

where $Q^{-1}(\cdot)$ denotes the inverse Gaussian Q-function, and $\bar{\gamma}_{\rm c}$ is the effective SNR (11).

F. MRC Diversity

In MRC, all the combiner outputs are weighted and summed to form the decision variable as illustrated in [5, Fig. 1]. From (10), the combiner output is

$$\Re\left[\sum_{i=1}^{L} y'_{1,i}\right] = \frac{1}{2\sigma_{\hat{g}}^2}\sum_{i=1}^{L}\left(|\hat{g}_{1i}|^2 + |\hat{g}_{2i}|^2\right) + \frac{1}{2k\sigma_{\hat{g}}^2} \cdot \Re\sum_{i=1}^{L}\left[\hat{g}_{1,i}^*(d_{1,i} + d_{2,i}) + \hat{g}_{2,i}(d_{2,i} - d_{1,i})^* + \hat{g}_{1,i}^* n_{1,i} + \hat{g}_{2,i} n_{2,i}^*\right]. \tag{23}$$

Petitioner Samsung Ex-1004, 0140

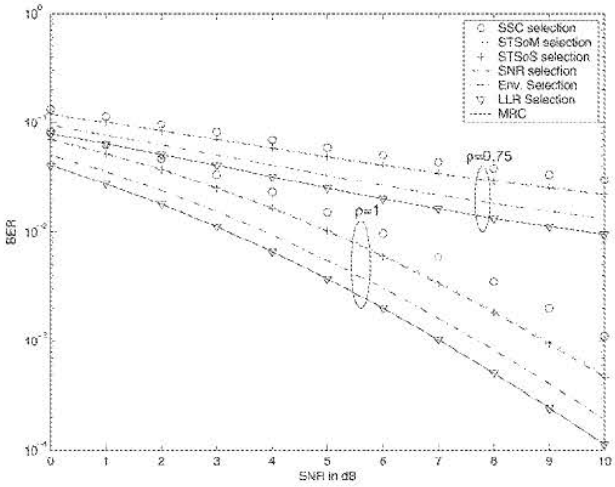


Fig. 3. BER versus SNR for the 2 TX and 2 Rx system using an Alamouti STBC.

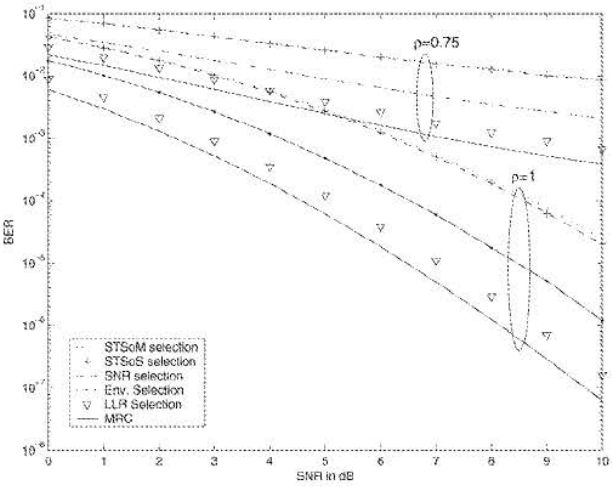


Fig. 4. BER versus SNR for the 2 TX and 4 Rx system using an Alamouti STBC.

Conditioned on $y = \sum_{i=1}^{L}(|\hat{g}_{1i}|^2 + |\hat{g}_{2i}|^2)/2\sigma_{\hat{g}}^2$, this decision variable is a Gaussian random variable with mean y and variance $y/\bar{\gamma}_c$. The pdf of y is chi-square distributed with $4L$ degrees of freedom [14]

$$f_Y(y) = \frac{1}{(2L-1)!} y^{2L-1} \exp(-y). \tag{24}$$

Following [14], the BER for MRC with Alamouti coding is obtained as

$$P_b = \int_0^\infty \mathrm{Q}\left(\sqrt{\bar{\gamma}_c y}\right) f_Y(y) dy \tag{25a}$$

$$= \left[\frac{1}{2}(1-\mu_2)\right]^{2L} \sum_{k=0}^{2L-1} \binom{2L-1+k}{k} \left[\frac{1}{2}(1+\mu_2)\right]^k$$

$$\mu_2 = \sqrt{\frac{\bar{\gamma}_c}{\bar{\gamma}_c + 2}}. \tag{25b}$$

IV. Numerical Results and Discussion

The BER results in this paper are functions of $\bar{\gamma}_c$, which is, in turn, a function of ρ and $\bar{\gamma}$. Figs. 3 and 4 show plots of the average BER versus SNR per bit for the different selection-diversity schemes in a flat Rayleigh fading channel with perfect channel estimation and cross-correlation 0.75, respectively. The envelope-LLR selection, STSoS selection, and STSoM selection schemes are evaluated by computer simulation. As expected, these results show that in all cases, the BER increases with increasing fading estimation error (decreasing value of ρ).

It is observed in Fig. 3 that the performances of LLR selection and MRC are the same for dual diversity. The performances are, indeed, identical, because for MRC, the sign of the combiner output $\Re(y_{1,1}) + \Re(y_{1,2})$ is determined by the maximum of $|\Re(y_{1,i})|$, which coincides with the LLR selection rule. It is also observed in Fig. 3 that the performances of STSoS selection and SNR selection are the same, at least to graphical accuracy. The STSoM selection scheme performs almost as well as the STSoS and SNR selection schemes, although it is simpler than both to implement. As does STSoS selection, STSoM selection choses the best branch without requiring any channel estimation. The envelope-LLR selection scheme, which does require channel estimation of all the channels, performs better than the STSoS, STSoM, and SNR selection schemes, but not as well as the LLR and MRC designs. The SSC selection offers the poorest performance, in exchange for its simplicity, as expected.

Fig. 4 shows the average BER as a function of SNR per bit for the various selection schemes used in four-fold diversity with perfect channel estimation and $\rho = 0.75$, respectively. There are a number of interesting observations. First, MRC and LLR are not the same, and MRC outperforms LLR, as expected. Second, the LLR selection outperforms envelope-LLR selection. Third, the envelope-LLR selection outperforms STSoS and STSoM. Fourth, the performances of SNR and STSoS selection are the same, as they were for the dual-branch case. This is a significant result. In order to implement SNR selection, the gains of all the diversity channels must be estimated. No channel estimation is required to implement STSoS selection. The demodulation will require channel estimation according to (2a), but in the case of STSoS, only two channel gains need to be estimated, while in the case of SNR selection, $2L$ channel gains must be estimated to implement the branch selection. We have also compared SNR and STSoS schemes for $L = 8$ and $L = 12$ [20]. In all cases, the performances are graphically the same.[1]

Figs. 5 and 6 show the average BER as a function of ρ for the various selection schemes with a SNR of 5 dB per bit for dual diversity and four-fold diversity, respectively. Observe from both figures that with poor channel estimation, i.e., $\rho \to 0$, all the BER curves converge to 0.5. At this point, the system is only affected by random noise and offers the worst BER performance. With the increase of ρ, there is a decrease of error rate for all the selection schemes. When $\rho = 1$, systems with various selection

[1]Extended simulation tests indicate that the STSoS scheme outperforms SNR selection in the fourth or higher significant figure.

Petitioner Samsung Ex-1004, 0141

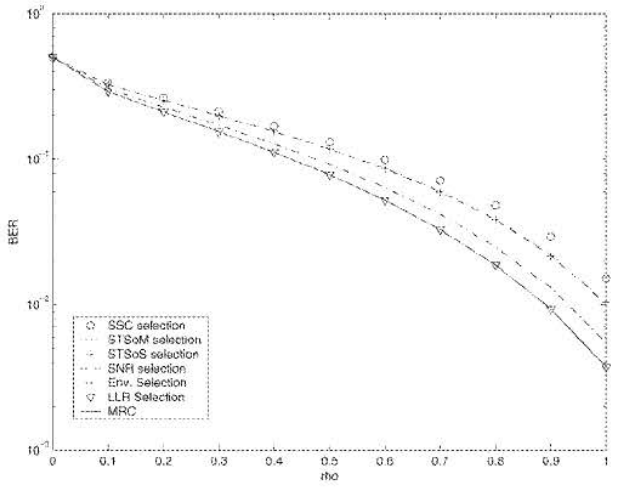


Fig. 5. BER versus ρ for the 2 TX and 2 Rx system using an Alamouti STBC with $\bar{\gamma}_b = 5$ dB.

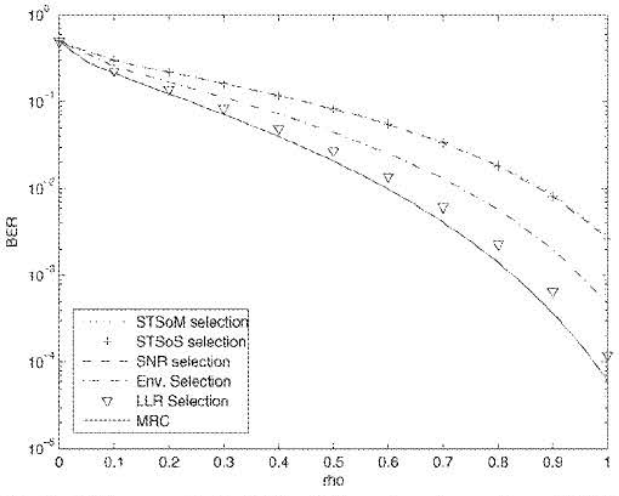


Fig. 6. BER versus ρ for the 2 TX and 4 Rx system using an Alamouti STBC with $\bar{\gamma}_b = 5$ dB.

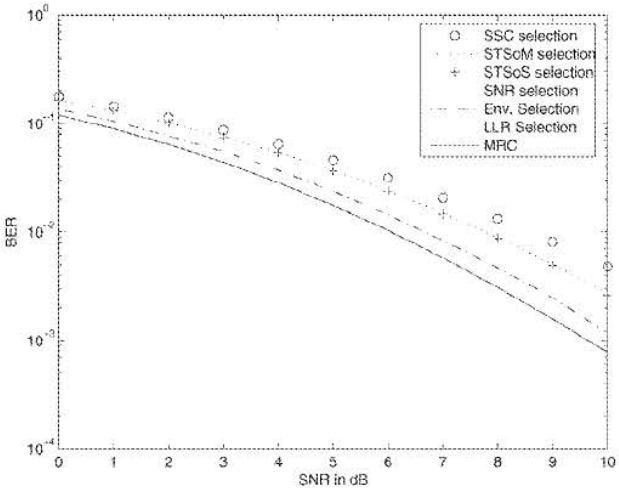


Fig. 7. PSAM BER versus SNR for the 2 TX and 2 Rx, STBC with Hamming windowing applied to a sinc interpolator for $K = 6$, $N = 14$, and $f_D T_s = 0.01$ with symbol location at $n = 3$.

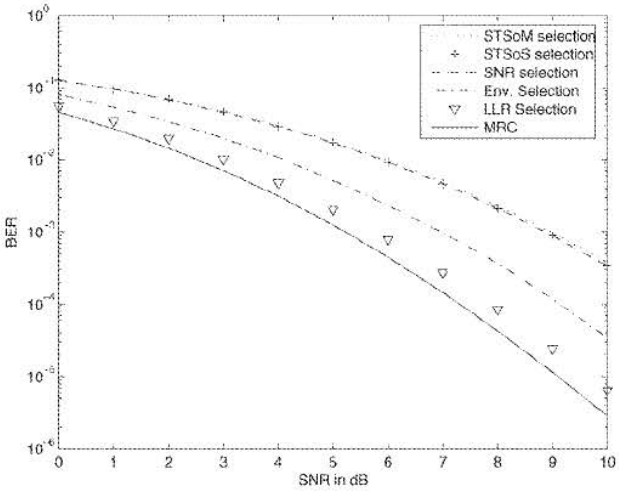


Fig. 8. PSAM BER versus SNR for the 2 TX and 4 Rx, STBC with Hamming windowing applied to a sinc interpolator for $K = 6$, $N = 14$, and $f_D T_s = 0.01$ with symbol location at $n = 3$.

schemes reach the best performance, where the BER values match the values in Figs. 3 and 4 at the $\rho = 1$ and $\bar{\gamma}_b = 5$ dB point.

Figs. 3–6 show the average BER versus SNR for specific, constant values of ρ. These results show clearly the performance differences between the selection schemes. They are also representative of a situation where the Rx electronics has reached a limit, and cannot provide a better estimate of the channel gain. On the the other hand, many practical estimators will show a dependence on SNR, i.e., give better estimates as the SNR increases. In these cases, a larger SNR value leads to a better channel estimate, which means a higher value of ρ. To show this effect on BER, we consider PSAM as an example. We assume that a sinc interpolator with a Hamming window is used to interpolate fading estimates, with a frame size of 14, and normalized Doppler shift of 0.01.[2] Fig. 7 shows the average BER versus SNR from 0 to 10 dB with $L = 2$. Since ρ is also a function of the symbol location, we give the BER of the third data symbol in a frame as an example. Computed from (33), the value of ρ for this PSAM system varies from 0.575 to 0.931 as the SNR varies from 0 to 10 dB. Similar to the results in Figs. 3 and 4, in Fig. 7, MRC and LLR selection still have the best performance, then envelope-LLR selection outperforms SNR and STSoS selection, which, in turn, slightly outperform STSoM selection. The simplest selection scheme, SSC selection, has the worst BER performance. Again, the performance of the SNR and STSoS schemes are indistinguishable. Fig. 8 shows similar results for four-fold diversity. In this case, MRC outperforms LLR selection, but SNR and STSoS selection again have the same performance, which is marginally better than STSoM selection.

[2]To simplify the analysis in this example, it is assumed that no branch switching occurs during a PSAM interpolation length. In the alternative, one can buffer the pilot symbols before the selection.

V. Conclusion

Analytical BER results were derived for LLR selection, SNR selection, SSC, and MRC with channel-estimation errors using Alamouti transmission systems. A new selection scheme,

Petitioner Samsung Ex-1004, 0142

STSoS selection, was proposed, with a much simpler hardware implementation. The results show that it has the same performance as SNR selection. A suboptimal selection scheme, STSoM, was also proposed with a still simpler implementation, but only slightly poorer performance than STSoS SC.

APPENDIX A
DERIVATION OF ρ

A. Fading Estimation in PSAM

We assume that PSAM is used for channel estimation. The PSAM frame format is similar to that considered in [21, Fig. 2], where pilot symbols are inserted periodically into the data sequence. Since there are two Tx antennas and an Alamouti scheme is employed, we consider two consecutive pilot symbols are transmitted together between data symbols. Under the assumption that the fading gain remains constant over two consecutive symbol intervals, $N/2$ clusters, each with two symbols, are formatted into one frame of N symbols, where N is an even number, with the first two pilot symbols ($n = 0$) followed by $N - 2$ data symbols ($1 \le n \le N/2 - 1$). The composite signal is transmitted over $2L$ flat, Rayleigh fading channels. At the Rx, after matched-filter detection, the pilot symbols are extracted and interpolated to form an estimate of the channel in the following manner.

Rewrite (1) to include the above assumptions as

$$r^n_{1,i,k} = g^n_{1,i,k}s^n_{1,i,k} + g^n_{2,i,k}s^n_{2,i,k} + n^n_{1,i,k} \tag{26a}$$

$$r^n_{2,i,k} = -g^n_{1,i,k}s^n_{2,i,k} + g^n_{2,i,k}s^n_{1,i,k} + n^n_{2,i,k} \tag{26b}$$

where $r^n_{1,i,k}$ denotes the first received symbol at the nth symbol cluster of the kth data frame in the ith Rx branch, and similarly for the fading gain g and noise n. Since the pilot symbols are known to the Rx, without loss of generality, we assume that the two pilot symbols at the first cluster ($n = 0$) of the frame have the values $+1$ and -1, respectively. Then for the two received pilot symbols, (26a) becomes

$$r^0_{1,i,k} = g^0_{1,i,k} - g^0_{2,i,k} + n^0_{1,i,k} \tag{27a}$$

$$r^0_{2,i,k} = g^0_{1,i,k} + g^0_{2,i,k} + n^0_{2,i,k}. \tag{27b}$$

Adding (27a) and (27b), we obtain the estimate of $g^0_{1,i,k}$ as

$$\hat{g}^0_{1,i,k} = g^0_{1,i,k} + \frac{n^0_{1,i,k} + n^0_{2,i,k}}{2}. \tag{28a}$$

Subtracting (27a) from (27b) generates

$$\hat{g}^0_{2,i,k} = g^0_{2,i,k} + \frac{n^0_{2,i,k} - n^0_{1,i,k}}{2}. \tag{28b}$$

The fading at the nth symbol ($1 \le n \le N/2 - 1$) in the kth frame of the ith branch is estimated from $2K$ pilot symbols of K adjacent frames, with pilot symbols from $k_1 = -\lfloor (K-1)/2 \rfloor$ previous frames and to $k_2 = \lfloor K/2 \rfloor$ subsequent frames. These estimates are given by

$$\hat{g}^n_{1,i,k} = \sum_{k=-k_1}^{k_2} h^n_k \hat{g}^0_{1,i,k} = \sum_{k=-k_1}^{k_2} h^n_k \left(g^0_{1,i,k} + \frac{n^0_{1,i,k} + n^0_{2,i,k}}{2} \right) \tag{29a}$$

$$\hat{g}^n_{2,i,k} = \sum_{k=-k_1}^{k_2} h^n_k \hat{g}^0_{2,i,k} = \sum_{k=-k_1}^{k_2} h^n_k \left(g^0_{2,i,k} + \frac{n^0_{2,i,k} - n^0_{1,i,k}}{2} \right), \quad n = 1, \ldots \frac{N}{2} - 1 \tag{29b}$$

where h^n_k is the interpolation coefficient for the nth data symbol in the kth frame.

B. Derivation of R_c

In an omnidirectional scattering Rayleigh fading channel, the autocorrelation of the real part of the fading gain is [21]

$$R(\tau) = \sigma_g^2 J_0(2\pi f_D \tau). \tag{30}$$

Since calculation of the correlations for the data symbols is the same at all branches, we drop the subscripts $\{1, i\}$ and $\{2, i\}$ in (28), (29). Then, combining (28), (29) with (4a), (30), we have

$$\begin{aligned} R_c = E\left[g^n_{Ik}\hat{g}^n_{Ik}\right] &= \sum_{k=-k_1}^{k_2} h^n_k E\left[g^n_{Ik}\left(g^0_{Ik} + \frac{n^0_{1,k} + n^0_{2,k}}{2} \right) \right] \\ &= \sum_{k=-k_1}^{k_2} \sigma_g^2 h^n_k J_0(2\pi f_D |kN - 2n| T_s). \end{aligned} \tag{31}$$

C. Derivation of $\sigma^2_{\hat{g}}$

From (28) and (29), the variance of $\hat{g}$ can be derived as

$$\begin{aligned} \sigma^2_{\hat{g}} = \frac{1}{2}E\left[\hat{g}^n_k \hat{g}^{n*}_k\right] &= \frac{1}{2}E\left[\sum_{k=-k_1}^{k_2} h^n_k \left(g^0_{1,i,k} + \frac{n^0_{1,i,k} + n^0_{2,i,k}}{2} \right) \right. \\ &\quad \left. \times \sum_{k=-k_1}^{k_2} h^n_k \left(g^{0,*}_{1,i,k} + \frac{n^{0,*}_{1,i,k} + n^{0,*}_{2,i,k}}{2} \right) \right] \\ &= \sum_{k=-k_1}^{k_2} \sum_{m=-k_1}^{k_2} h^n_k h^n_m \sigma_g^2 J_0(2\pi f_D |k-m| N T_s) \\ &\quad + \frac{\sigma_n^2}{2} \sum_{m=-k_1}^{k_2} (h^n_k)^2. \end{aligned} \tag{32}$$

D. Derivation of ρ

From (6), using (31) and (32), we have

$$\begin{aligned} \rho &= \frac{R_c^2}{\sigma_g^2 \sigma^2_{\hat{g}}} \\ &= \frac{\left[\sum_{k=-k_1}^{k_2} h^n_k J_0(2\pi f_D |kN - 2n| T_s) \right]^2}{\sum_{k=-k_1}^{k_2} \sum_{m=-k_1}^{k_2} h^n_k h^n_m J_0(2\pi f_D |k-m| N T_s) + \frac{1}{\bar{\gamma}} \sum_{m=-k_1}^{k_2} (h^n_k)^2}. \end{aligned} \tag{33}$$

Note that ρ is a function of the type of interpolator, the data symbol location, the Doppler shift, the data frame length, and the symbol interval. When a sinc interpolator [22] is used and a Hamming window is applied, the interpolation coefficients are given by

$$\begin{aligned} h^n_k &= \operatorname{sinc}\left(\frac{2n}{N} - k \right) \\ &\quad \times \left[0.54 - 0.46 \cos\left(\frac{2\pi(2n - kN)}{KN - 1} + \frac{2\pi \lfloor \frac{KN}{2} \rfloor}{KN - 1} \right) \right]. \end{aligned} \tag{34}$$

Petitioner Samsung Ex-1004, 0143

APPENDIX B
DERIVATION OF (15)

Similar to the analysis in [23], the BER for LLR Rx SC is

$$P_b = \sum_{i=1}^{L} \Pr(\Re(y_{1,i}) < 0, i\text{th branch selected}). \tag{35}$$

Since $\Re(y_{1,i})$ is proportional to $\Re(y'_{1,i})$, conditioning $\Re(y'_{1,i})$ in (10) on $\hat{g}_{1,i}$ and $\hat{g}_{2,i}$ yields

$$\begin{aligned} P_b &= \sum_{i=1}^{L} \Pr(\Re(y'_{1,i}) < 0, i\text{th branch selected}) \\ &= L \cdot \Pr\left(\Re(y'_{1,1}) < 0, 1\text{th branch selected}\right) \\ &= L \cdot \Pr\left(\Re(y'_{1,1}) < 0, \left|\Re(y'_{1,1})\right| > \left|\Re(y'_{1,i})\right|_{\forall i, i\neq 1}\right) \\ &= L \cdot \Pr\left(-\Re(y'_{1,1}) > \left|\Re(y'_{1,i})\right|_{\forall i, i\neq 1}\right). \end{aligned} \tag{36}$$

Let $r_i = \Re(y'_{1,i})$ and $r_1 = -\Re(y'_{1,1})$, then

$$\begin{aligned} &P_b \\ &= L \int_0^\infty \Pr\left(\left|r_i = \Re(y'_{1,i})\right|_{\forall i, i\neq 1} < r_1 \middle| r_1 = -\Re(y'_{1,1})\right) f_R(r_1) dr_1 \\ &= L \int_0^\infty \left[\Pr\left(-r_1 < r_i < r_1 | r_1\right)\right]^{L-1} f_R(r_1) dr_1 \end{aligned} \tag{37}$$

where $f_R(r_1)$ is the pdf of r_1. Since $r_1 = -\Re(y'_{1,1})$, $f_R(r_1)$ is equal to $f_{r_i}(-r_1)$, where $f_{r_i}(x)$ is the pdf of r_i. From (10), one has that $\Re(y'_{1,i})_{\forall i, i\neq 1}$ is Gaussian distributed with mean a_i and variance $a_i/\bar{\gamma}_c$, when conditioned on $a_i = (|\hat{g}_{1,i}|^2 + |\hat{g}_{2,i}|^2)/2\sigma_g^2$. Averaging over a_i, the pdf of r_i is given by

$$\begin{aligned} f_{r_i}(x) &= \int_0^\infty f_{r_i}(x|a_i) f_A(a_i) da_i \\ &= \int_0^\infty \sqrt{\frac{\bar{\gamma}_c}{2\pi a_i}} \exp\left[-\frac{\bar{\gamma}_c (x-a_i)^2}{2a_i}\right] a_i \exp(-a_i)\, da_i. \end{aligned} \tag{38}$$

Changing the variable of integration to $z = \sqrt{a_i}$, and using the result from [15, eq. (3.472)]

$$\begin{aligned} &\int_0^\infty b^2 \exp\left(-c_1 \frac{1}{b^2} - c_2 b^2\right) db \\ &\qquad = \frac{1}{4}\sqrt{\frac{\pi}{c_2^3}} (1 + 2\sqrt{c_1 c_2}) \exp(-2\sqrt{c_1 c_2}) \end{aligned}$$

(38) can be simplified as

$$f_{r_i}(x) = A(1 + B|x|) \exp(-B|x| + Cx) \tag{39a}$$

$$\text{where} \quad A = \frac{\sqrt{\bar{\gamma}_c(\bar{\gamma}_c + 2)}}{(\bar{\gamma}_c + 2)^2} \quad B = \sqrt{\bar{\gamma}_c(\bar{\gamma}_c + 2)} \quad C = \bar{\gamma}_c. \tag{39b}$$

Then, for the ith branch

$$\begin{aligned} \Pr(-r_1 < r_i < r_1 | r_1) &= \int_{-r_1}^{r_1} f_{r_i}(x) dx \\ &= m_7 + (m_1 - m_2 r_1) \exp(-m_3 r_1) \\ &\quad - (m_4 + m_5 r_1) \exp(-m_6 r_1) \end{aligned} \tag{40a}$$

$$\begin{aligned} \text{where} \quad m_1 &= \frac{AC - 2AB}{(C-B)^2} \quad m_2 = \frac{AB}{B-C} \\ m_3 &= B - C \quad m_4 = \frac{2AB + AC}{(B+C)^2} \\ m_5 &= \frac{AB}{B+C} \quad m_6 = B + C \quad m_7 = \frac{4AB^3}{(B^2 - C^2)^2}. \end{aligned} \tag{40b}$$

Combining (37), (38), and (40), the final expression for the BER is obtained as (41), shown at the bottom of the page.

APPENDIX C
DERIVATION OF (21)

Following [12], the cdf of γ_c can be written as

$$\begin{aligned} &F(\gamma_c) \\ &= \begin{cases} \Pr(\gamma_{c,1} \le \gamma_c) \Pr(\gamma_{c,2} \le \gamma_{\text{th}}), & \text{if } \gamma_c < \gamma_{\text{th}} \\ \Pr(\gamma_{\text{th}} \le \gamma_{c,1} \le \gamma_c) + \Pr(\gamma_{c,1} \le \gamma_c) & \\ \quad \Pr(\gamma_{c,2} \le \gamma_{\text{th}}), & \text{if } \gamma_c \ge \gamma_{\text{th}}. \end{cases} \end{aligned} \tag{42}$$

From (12), both $\gamma_{c,1}$ and $\gamma_{c,2}$ have a chi-squared distribution given by

$$f(\gamma_{c,i}) = \frac{4\gamma_{c,i}}{\bar{\gamma}_c^2} \exp\left(-\frac{2\gamma_{c,i}}{\bar{\gamma}_c}\right), \quad i = 1, 2. \tag{43}$$

The pdf is obtained by differentiating the cdf in (42) with respect to γ_c

$$\begin{aligned} &f(\gamma_c) \\ &= \begin{cases} \left[1 - \left(\frac{2\gamma_{\text{th}}}{\bar{\gamma}_c} + 1\right) \exp\left(-\frac{2\gamma_{\text{th}}}{\bar{\gamma}_c}\right)\right] \frac{4\gamma_c}{\bar{\gamma}_c^2} \exp\left(-\frac{2\gamma_c}{\bar{\gamma}_c}\right), & \gamma_c < \gamma_{\text{th}} \\ \left[2 - \left(\frac{2\gamma_{\text{th}}}{\bar{\gamma}_c} + 1\right) \exp\left(-\frac{2\gamma_{\text{th}}}{\bar{\gamma}_c}\right)\right] \frac{4\gamma_c}{\bar{\gamma}_c^2} \exp\left(-\frac{2\gamma_c}{\bar{\gamma}_c}\right), & \gamma_c \ge \gamma_{\text{th}}. \end{cases} \end{aligned} \tag{44}$$

$$\begin{aligned} P_b &= L \int_0^\infty \left[m_7 + (m_1 - m_2 r_1) \exp(-m_3 r_1) - (m_4 + m_5 r_1) \exp(-m_6 r_1)\right]^{L-1} \times A(1 + Br_1) \exp(-Br_1 - Cr_1) dr_1 \\ &= L \sum_{n=0}^{L-1} \sum_{m=0}^{L-1-n} \sum_{p=0}^{n} \sum_{q=0}^{m} \sum_{i=0}^{1} \binom{L-1}{n} \binom{L-1-n}{m} \binom{n}{p} \binom{m}{q} \times AB^i m_1^{n-p} m_2^p m_4^{m-q} m_5^q m_7^{L-1-n-m} \frac{(-1)^{m+p}(p+q+i)!}{(m_3 n + m_6 m + B + C)^{p+q+i+1}} \end{aligned} \tag{41}$$

Petitioner Samsung Ex-1004, 0144

Then, the BER is

$$\begin{aligned} P_b &= \int_0^\infty Q\left(\sqrt{2\gamma_c}\right) f(\gamma_c) d\gamma_c \\ &= K_3 \int_0^\infty Q(\sqrt{2\gamma_c}) \frac{4\gamma_c}{\bar{\gamma}_c^2} \exp\left(-\frac{2\gamma_c}{\bar{\gamma}_c}\right) d\gamma_c \\ &\quad + \int_{\gamma_{\rm th}}^\infty Q(\sqrt{2\gamma_c}) \frac{4\gamma_c}{\bar{\gamma}_c^2} \exp\left(-\frac{2\gamma_c}{\bar{\gamma}_c}\right) d\gamma_c \\ &= K_1 - \left[K_1\left(\frac{2\gamma_{\rm th}}{\bar{\gamma}_c}+1\right) - \frac{2\gamma_{\rm th}+\bar{\gamma}_c}{\bar{\gamma}_c} Q(\sqrt{2\gamma_{\rm th}}) \right. \\ &\quad \left. + \frac{\sqrt{\gamma_{\rm th}}}{\sqrt{\pi}(\bar{\gamma}_c+2)} \exp(-\gamma_{\rm th})\right] \exp\left(-\frac{2\gamma_{\rm th}}{\bar{\gamma}_c}\right) \\ &\quad - K_2 Q\left(\sqrt{\frac{2\gamma_{\rm th}(\bar{\gamma}_c+2)}{\bar{\gamma}_c}}\right) \end{aligned} \tag{45a}$$

where

$$K_1 = \frac{\sqrt{(\bar{\gamma}_c+2)^3} - \bar{\gamma}_c\sqrt{\bar{\gamma}_c} - 3\sqrt{\bar{\gamma}_c}}{2\sqrt{(\bar{\gamma}_c+2)^3}}$$

$$K_2 = \frac{\bar{\gamma}_c+3}{\bar{\gamma}_c+2}\sqrt{\frac{\bar{\gamma}_c}{\bar{\gamma}_c+2}}$$

$$K_3 = 1 - \left(\frac{2\gamma_{\rm th}}{\bar{\gamma}_c}+1\right)\exp\left(-\frac{2\gamma_{\rm th}}{\bar{\gamma}_c}\right). \tag{45b}$$

REFERENCES

[1] G. Foschini and M. Gans, "On the limits of wireless communications in a fading environment when using multiple antennas," *Wireless Pers. Commun.*, vol. 6, no. 3, pp. 311–335, Mar. 1998.

[2] A. Ghrayeb and T. M. Duman, "Performance analysis of MIMO systems with antenna selection over quasi-static fading channels," *IEEE Trans. Veh. Technol.*, vol. 52, no. 2, pp. 281–288, Mar. 2003.

[3] I. Bahceci, T. M. Duman, and Y. Altunbasak, "Antenna selection for multiple-antenna transmission systems: Performance analysis and code construction," *IEEE Trans. Inf. Theory*, vol. 49, no. 10, pp. 2669–2681, Oct. 2003.

[4] X. Zeng and A. Ghrayeb, "Performance bounds for space–time block codes with receive antenna selection," *IEEE Trans. Inf. Theory*, vol. 50, no. 9, pp. 2130–2137, Sep. 2004.

[5] S. M. Alamouti, "A simple transmit diversity technique for wireless communications," *IEEE J. Sel. Areas Commun.*, vol. 16, no. 10, pp. 1451–1458, Oct. 1998.

[6] S. W. Kim and E. Y. Kim, "Optimum selection diversity for BPSK signals in Rayleigh fading channels," *IEEE Trans. Commun.*, vol. 49, no. 10, pp. 1715–1718, Oct. 2001.

[7] ——, "Optimum receive antenna selection minimizing error probability," in *Proc. Wireless Commun. Netw. Conf.*, vol. 1, Mar. 2003, pp. 441–447.

[8] D. Gore and A. Paulraj, "Space–time block coding with optimal antenna selection," in *Proc. IEEE Int. Conf. Acoust., Speech, Signal Process.*, vol. 4, May 2001, pp. 2441–2444.

[9] W. C. Jakes, *Microwave Mobile Communications*. Piscataway, NJ: IEEE Press, 1993.

[10] W. Lee, *Mobile Communications Engineering*. New York: McGraw-Hill, 1982.

[11] M. A. Blanco and K. J. Zdunek, "Performance and optimization of switched diversity systems for the detection of signals with Rayleigh fading," *IEEE Trans. Commun.*, vol. COM-27, no. 12, pp. 1887–1895, Dec. 1979.

[12] A. A. Abu-Dayya and N. C. Beaulieu, "Analysis of switched diversity systems on generalized-fading channels," *IEEE Trans. Commun.*, vol. 42, no. 11, pp. 2959–2966, Nov. 1994.

[13] H. Yang and M. Alouini, "Performance analysis of multibranch switched diversity systems," *IEEE Trans. Commun.*, vol. 51, no. 5, pp. 782–794, May 2003.

[14] J. G. Proakis, *Digital Communications*. New York: McGraw-Hill, 1995.

[15] I. S. Gradshteyn and I. M. Ryzhik, *Table of Integral, Series, and Products*, 6th ed, A. Jeffrey and D. Zwillinger, Eds. New York: Academic, 2000.

[16] M. J. Gans, "The effect of Gaussian error in maximal ratio combiners," *IEEE Trans. Commun. Technol.*, vol. COM-19, no. 8, pp. 492–500, Aug. 1971.

[17] G. L. Stüber, *Principles of Mobile Communication*, 2nd ed. Norwell, MA: Kluwer, 2001.

[18] L. Cao and N. C. Beaulieu, "Exact error-rate analysis of diversity 16-QAM with channel estimation error," *IEEE Trans. Commun.*, vol. 52, no. 6, pp. 1019–1029, Jun. 2004.

[19] H. A. David, *Order Statistics*. New York: Wiley, 1981.

[20] W. Li, "Effects of channel estimation errors on receiver selection combining diversity for Alamouti MIMO systems," M.S. thesis, Univ. Alberta, Edmonton, AB, Canada, 2005.

[21] J. K. Cavers, "An analysis of pilot symbol assisted modulation for Rayleigh fading channels," *IEEE Trans. Veh. Technol.*, vol. 40, no. 6, pp. 686–693, Nov. 1991.

[22] Y.-S. Kim, C.-J. Kim, G.-Y. Jeong, Y.-J. Bang, H.-K. Park, and S. S. Choi, "New Rayleigh fading channel estimator based on PSAM channel sounding technique," in *Proc. IEEE Int. Conf. Commun.*, vol. 3, Jun. 1997, pp. 1518–1520.

[23] E. A. Neasmith and N. C. Beaulieu, "New results on selection diversity," *IEEE Trans. Commun.*, vol. 46, no. 5, pp. 695–703, May 1998.



Wenyu Li received the B.S.E.E. degree from Shanghai Jiaotong University, Shanghai, China, in 1993, and the M.S.E.E. degree from the University of Alberta, Edmonton, AB, Canada in 2005.

She was employed with China Telecom, Zhuhai, China, as a Telecommunications Engineer from July 1993 to August 1999, specializing in telephone network management and optimization. Her current research interests are in the area of wireless communications, with a focus on diversity, antenna selection, channel estimation, and space–time coding.



Norman C. Beaulieu (S'82–M'86–SM'89–F'99) received the B.A.Sc. (honors), M.A.Sc., and Ph.D. degrees in electrical engineering from the University of British Columbia, Vancouver, BC, Canada, in 1980, 1983, and 1986, respectively.

He was a Queen's National Scholar Assistant Professor with the Department of Electrical Engineering, Queen's University, Kingston, ON, Canada, from September 1986 to June 1988, an Associate Professor from July 1988 to June 1993, and a Professor from July 1993 to August 2000. In September 2000, he became the *i*CORE Research Chair in Broadband Wireless Communications at the University of Alberta, Edmonton, AB, Canada, and in January 2001, the Canada Research Chair in Broadband Wireless Communications. His current research interests include broadband digital communications systems, fading channel modeling and simulation, interference prediction and cancellation, decision-feedback equalization, and space–time coding.

Dr. Beaulieu is a Member of the IEEE Communication Theory Committee and served as its Representative to the Technical Program Committee of the 1991 International Conference on Communications and as Co-Representative to the Technical Program Committee of the 1993 International Conference on Communications and the 1996 International Conference on Communications. He was General Chair of the Sixth Communication Theory Mini-Conference in association with GLOBECOM '97 and Co-Chair of the Canadian Workshop on Information Theory 1999. He has been an Editor for Wireless Communication Theory of the IEEE TRANSACTIONS ON COMMUNICATIONS since January 1992, and was Editor-in-Chief from January 2000 to December 2003. He served as an Associate Editor for Wireless Communication Theory of the IEEE COMMUNICATIONS LETTERS from November 1996 to August 2003. He has also served on the Editorial Board of the PROCEEDINGS OF THE IEEE since November 2000. He received the Natural Science and Engineering Research Council of Canada (NSERC) E. W. R. Steacie Memorial Fellowship in 1999. He was awarded the University of British Columbia Special University Prize in Applied Science in 1980 as the highest standing graduate in the faculty of Applied Science. He is a Fellow of The Royal Society of Canada.

Petitioner Samsung Ex-1004, 0145

This full text paper was peer reviewed at the direction of IEEE Communications Society subject matter experts for publication in the WCNC 2008 proceedings.

Reduced-Complexity ICI Mitigation for Mobile SFBC-OFDM with Application to DVB-H

Sili Lu, Balachander Narasimhan and Naofal Al-Dhahir
University of Texas at Dallas
Email:{sxl059000, bxn062000, aldhahir}@utdallas.edu

***Abstract*— Effective Inter-carrier Interference (ICI) mitigation for MIMO-OFDM requires accurate channel estimation which is very challenging due to the large number and fast time-varying nature of the channel parameters to be estimated using scattered pilots. We present a novel SFBC-OFDM scheme for doubly-selective channels and a reduced complexity channel estimation algorithm which exploits the banded and sparse structure of the channel in the frequency and time-domains, respectively. Furthermore, we design an FIR-MMSE ICI cancellation algorithm for mobile SFBC-OFDM and demonstrate its effectiveness for Digital Video Broadcasting-Handheld (DVB-H) systems.**

I. Introduction

Orthogonal Frequency Division Multiplexing (OFDM) is very sensitive to time-selectivity which manifests itself as variations in the channel impulse response (CIR) within each OFDM symbol. This results in ICI, which is proportional to the Doppler frequency due to the mobility of the receiver, and is a significant performance-limiting impairment for OFDM receivers.

In most previous studies, a quasi-static channel is assumed where the channel response is assumed constant over each OFDM block and a conventional one-tap per subcarrier frequency-domain equalizer (FEQ) is used, which is highly suboptimal under severe Doppler. In [1], we proposed a Finite-Impulse-Response Minimum Mean Square Error (FIR-MMSE) FEQ which has few taps per subcarrier and utilizes the approximately banded structure of the channel matrix in the frequency-domain.

OFDM in a multiple-input multiple-output (MIMO) system, known as MIMO-OFDM, is an attractive multiple-antenna scheme for high-rate reliable broadband wireless transmission. The Alamouti space-time block code (STBC) [2] can be integrated with OFDM systems to achieve spatial and multipath diversity gains and reduce the error floor due to ICI. However, under high mobility, implementing the Alamouti STBC over adjacent OFDM blocks is not effective due to the significant channel time variations. Instead, space-frequency block coding (SFBC) was considered in [3] where the Alamouti scheme is implemented over adjacent subcarriers within the OFDM symbol [3], where the channel frequency response is approximately constant (especially for large FFT-size). However, the Alamouti structure is destroyed in the presence of ICI and the corresponding diversity gains are lost. In this paper, we design a novel *embedded* Alamouti SFBC-OFDM scheme and show how to efficiently integrate it with the low-complexity FIR-MMSE FEQ in [1]. To compute the MIMO FIR-MMSE FEQ coefficients, we develop a reduced-complexity hybrid time/frequency-domain channel estimation algorithm to estimate the Q main diagonals of the frequency-domain channel matrix. Simulation results show that our proposed scheme can effectively combat ICI under high mobility conditions.

This work was supported in part by Semiconductor Research Corporation under contract No. 2005-HJ-1328 and by a gift from Texas Instruments Inc.

This paper is organized as follows. In Section II, the OFDM system model is described and the FIR-MMSE FEQ design for the single-antenna case is briefly discussed. In Section III this design is generalized to the MIMO case and integrated with our new embedded SFBC-OFDM system. A reduced-complexity channel estimation algorithm to estimate the fast-varying channel is described in Section IV and a detailed complexity analysis is given in Section V. Simulation results are presented in Section VI, and finally conclusions are drawn in Section VII.

Notation: We use $(\cdot)^T$ to denote the transpose, $(\cdot)^*$ the complex-conjugate, $\lfloor \cdot \rfloor$ the floor operation and $(\cdot)_N$ the modulo-N operation. $G_{i,j}$ denotes the element in the i-th row and j-th column of matrix $\mathbf{G}$. The estimated value of a random variable a is denoted by $\hat{a}$. $\mathbf{I}_N$ denotes the $N \times N$ identity matrix and $\mathbf{G}(:, j)$ denotes the j-th column of $\mathbf{G}$.

II. System Model and Assumptions

A. Mobile OFDM

We consider an OFDM system with N subcarriers where each OFDM symbol, denoted by $\mathbf{X} = [X_0 \dots X_{N-1}]^T$, is converted into time-domain samples $\mathbf{x} = [x_0 \dots x_{N-1}]^T$ using the N-point Inverse Fast Fourier Transform (IFFT) operation $\mathbf{x} = \mathbf{F}^H \mathbf{X}$ where $\mathbf{F}^H$ is the N-point IFFT matrix. We assume that the cyclic prefix (CP) length is equal to or larger than the Channel Impulse Response (CIR) memory length denoted by ν. Then, the received OFDM symbol $\mathbf{y} = [y_0 \dots y_{N-1}]^T$ after CP removal is given by

$$\mathbf{y} = \mathbf{H}\mathbf{x} + \mathbf{v} \tag{1}$$

where $\mathbf{H}$ is an $N \times N$ time-domain channel matrix with elements $H_{n,l} = h_{n,(n-l)_N}$ where $h_{n,l}$ is the CIR at lag l for $0 \le l \le \nu - 1$ and time instant n for $0 \le n \le N-1$, and $\mathbf{v}$ is the time-domain noise vector with correlation matrix

1525-3511/08/$25.00 ©2008 IEEE

Petitioner Samsung Ex-1004, 0146

$\sigma^2\mathbf{I}_N$. Taking the FFT of (1), we obtain

$$\mathbf{Y} = \mathbf{F}\mathbf{y} = \mathbf{F}\mathbf{H}\mathbf{F}^H\mathbf{X} + \mathbf{F}\mathbf{v} = \mathbf{G}\mathbf{X} + \mathbf{V} \tag{2}$$

where $\mathbf{G} \triangleq \mathbf{F}\mathbf{H}\mathbf{F}^H$ is the frequency-domain channel matrix and $\mathbf{V}$ is the frequency-domain noise vector. For a quasi-static fading channel, $\mathbf{H}$ is a circulant matrix and hence transforms into a diagonal $\mathbf{G}$ matrix in (2). In this case, the OFDM subcarriers are decoupled, and a one-tap FEQ is optimal. For example, with a linear zero-forcing (ZF) FEQ, the data estimate for the k-th subcarrier $\hat{X}_k$ in this case is simply $\hat{X}_k = G_{k,k}^{-1}Y_k$. For the time-varying channel, however, $\mathbf{H}$ is not circulant, and hence $\mathbf{G}$ is no longer diagonal. In this case, the input-output relation for the k-th subcarrier is given by

$$Y_k = G_{k,k}X_k + \sum_{n=0,n\neq k}^{N-1} G_{k,n}X_n + V_k \tag{3}$$

The first term on the right hand side of (3) is the desired signal term while the second one is the ICI term which can be characterized by the normalized Doppler frequency $F_d = f_dT$ where f_d is the Doppler frequency and T is the time duration of the useful part of one OFDM block.

For the case of a MIMO system with M_r receive and M_t transmit antennas, we can generalize the model in (2) as follows. The frequency-domain channel matrix is $\mathbf{G} \in \mathbb{C}^{NM_t \times NM_t}$ whose (i,j)th block is the $N \times N$ frequency-domain channel matrix between the i-th receiver and j-th transmitter, denoted by $\mathbf{G}^{(i,j)} = \mathbf{F}\mathbf{H}^{(i,j)}\mathbf{F}^H$ and $\mathbf{H}^{(i,j)}$ is the corresponding time-domain channel matrix. $\mathbf{Y} = [(\mathbf{Y}^{(1)})^T \ \ldots (\mathbf{Y}^{(M_r)})^T]^T \in \mathbb{C}^{NM_r}$ and $\mathbf{X} = [(\mathbf{X}^{(1)})^T \ \ldots (\mathbf{X}^{(M_t)})^T]^T \in \mathbb{C}^{NM_t}$ are the receive and transmit blocks, respectively, where $\mathbf{Y}^{(i)} = [Y_0^{(i)} \ \ldots \ Y_{N-1}^{(i)}]^T$ and $\mathbf{X}^{(j)} = [X_0^{(j)} \ \ldots \ X_{N-1}^{(j)}]^T$ for $1 \le i \le M_r$ and $1 \le j \le M_t$.

B. FIR-MMSE FEQ for SISO-OFDM

Noting that $\mathbf{G}$ has most of its energy concentrated along the main diagonal, we can approximate it by a banded matrix, which has non-zero elements only along $(2D+1)$ main diagonals and two $D \times D$ triangular matrices in the top-right and bottom-left corners. Based on this banded structure, we proposed in [1] a reduced-tap MMSE FEQ algorithm which computes for each subcarrier an FIR FEQ by applying the MMSE criterion based only on the following $(2D+1) \times (4D+1)$ submatrix of $\mathbf{G}$:

$$\mathbf{G}_m = \begin{bmatrix} G_{(m-D)_N,(m-2D)_N} & \cdots & G_{(m-D)_N,(m+2D)_N} \\ \vdots & \vdots & \vdots \\ G_{m,(m-2D)_N} & \cdots & G_{m,(m+2D)_N} \\ \vdots & \vdots & \vdots \\ G_{(m+D)_N,(m-2D)_N} & \cdots & G_{(m+D)_N,(m+2D)_N} \end{bmatrix} \tag{4}$$

The Q-tap (where $Q = 2D+1$) FIR-MMSE FEQ is

$$\mathbf{w}_m = \mathbf{g}_m^H(\mathbf{G}_m\mathbf{G}_m^H + \sigma^2\mathbf{I}_Q)^{-1} \tag{5}$$

where $\mathbf{g}_m = \mathbf{G}_m(:, 2D+1)$ is the middle column of $\mathbf{G}_m$.

Hence, the FIR-MMSE FEQ output for the m-th subcarrier is given by

$$\hat{X}_m = \mathbf{w}_m\mathbf{Y}_m \tag{6}$$

where $\mathbf{Y}_m = [Y_{(m-D)_N}, \ldots, Y_{(m+D)_N}]^T$.

This FIR-MMSE FEQ has $\mathcal{O}(NQ^2)$ complexity, significantly less than the conventional N-tap FEQ. In [1], we showed that the choice of a 3-tap FEQ ($Q = 2D+1 = 3$) achieves a good performance-complexity tradeoff.

III. FIR-MMSE FEQ for MIMO-OFDM

In this section, we generalize our FIR-MMSE FEQ design to the MIMO case and propose a new embedded Alamouti SFBC-OFDM scheme which can be readily integrated with the FIR-MMSE FEQ. Here, we consider pilot-symbol-assisted estimation where the pilot tones are embedded in the data subcarriers in the frequency-domain.

A. Embedded Alamouti SFBC-OFDM Model

We consider a MIMO-OFDM system with $M_t = 2$ transmit and M_r receive antennas. In order to guarantee the spatial diversity gain (by preserving the Alamouti structure) in the presence of severe ICI, we design our SFBC encoding scheme as shown in Fig. 1. Each OFDM symbol of size N is divided into data blocks each consisting of L subcarriers separated by D pilot subcarriers where D is equal to the number of significant superdiagonals in $\mathbf{G}$ (see Section II-B). Two information symbols are grouped into pairs and form an Alamouti codeword which is implemented over the k-th ($1 \le k \le L$) subcarriers of two adjacent data blocks which are separated by $B = L + D$ subcarriers. As shown in Fig. 1, two adjacent data blocks and two pilot blocks form one *superblock*; hence, each superblock spans $2B$ subcarriers and contains L Alamouti codewords. For each non-edge codeword (i.e. $k \neq 1$ or L), ignoring noise and considering (for simplicity) ICI only from the adjacent subcarrier (i.e. $D = 1$) at the i-th receive antenna, we have

$$\begin{aligned} \mathbf{Y}_k^{(i)}(l) =& \mathbf{G}_{k,k-1}^{(i)}(l)\mathbf{X}_{k-1}(l) \\ &+ \mathbf{G}_{k,k}^{(i)}(l)\mathbf{X}_k(l) + \mathbf{G}_{k,k+1}^{(i)}(l)\mathbf{X}_{k+1}(l) \end{aligned} \tag{7}$$

where $\mathbf{Y}_k^{(i)}(l) = [Y_{2lB+k}^{(i)} \ (Y_{2lB+k+B}^{(i)})^*]^T$ and $\mathbf{X}_k(l) = [X_{2lB+2k-1} \ X_{2lB+2k}]^T$ correspond to the receive and transmit pair for the k-th Alamouti codeword in the l-th superblock, respectively, for $2 \le k \le L-1$. $\mathbf{G}_{k,m}^{(i)}(l)$ is the channel frequency response for the k-th Alamouti codeword given by

$$\mathbf{G}_{k,m}^{(i)}(l) = \begin{bmatrix} G_{2lB+k,2lB+m}^{(i,1)} & G_{2lB+k,2lB+m}^{(i,2)} \\ (G_{2lB+k+B,2lB+m+B}^{(i,2)})^* & -(G_{2lB+k+B,2lB+m+B}^{(i,1)})^* \end{bmatrix} \tag{8}$$

It is clear that $\mathbf{G}_{k,k}^{(i)}(l)$ is at the main diagonal of $\mathbf{G}$, hence the second term on the right-hand side of (7) is the desired term while the other two are ICI terms. Using this form, we can easily extend the FIR-MMSE FEQ for the SISO case

Petitioner Samsung Ex-1004, 0147

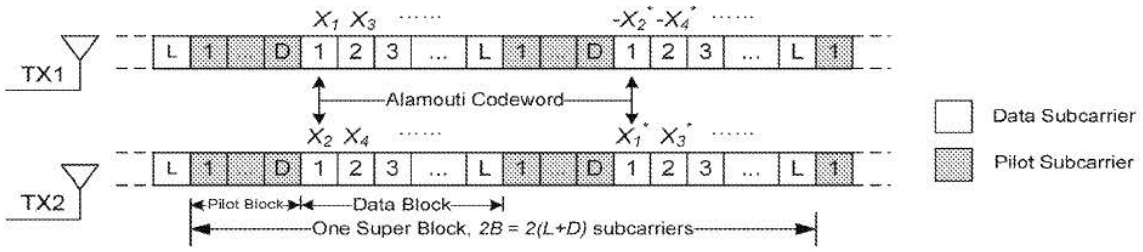


Fig. 1. Alamouti SFBC structure for FIR-MMSE FEQ

in Section II-B to the Alamouti SFBC case which will be discussed in the next subsection.

We insert two blocks of pilots, each with D subcarriers as shown in Fig. 1. Since the pilot tones are known to the receiver, their interference to the edge codewords in each data block can be computed and subtracted from the received signal to facilitate equalization. For a $Q = (2D+1)$ tap FEQ, we need D pilot subcarriers for each pilot block.

We emphasize that this scheme is different from STBC-OFDM [2] where the Alamouti scheme is implemented over the kth subcarriers of two adjacent OFDM symbols which is not suitable for the fast time-varying channel conditions considered in this paper. It is also different from conventional SFBC-OFDM [3] where the Alamouti scheme is implemented over adjacent subcarriers which also fails in the presence of severe ICI between adjacent subcarriers. In both of these schemes, the Alamouti structure is destroyed and hence spatial diversity gains can not be realized. Our proposed scheme solves this problem. To achieve full spatial diversity, $\mathbf{G}_{k,m}^{(i)}(l)$ must be as close to the Alamouti matrix as possible. This requires $G_{k,m}^{(i,j)} \approx G_{k+B,m+B}^{(i,j)}, j = 1,2$, or equivalently, the channel coherence bandwidth must be significantly larger than the width of B subcarriers. For the TU06 channel model we use in this paper for the DVB environment, the channel coherence bandwidth is around 200 KHz while the subcarrier width is 1 KHz for the 8K mode. Hence, the channel frequency response can be approximated as fixed over tens of subcarriers.

The choice of the design parameter L entails a performance/data-rate trade-off. Choosing a larger L results in higher data-rate but less diversity gain (since the channel frequency response fluctuates more within each Alamouti codeword). On the other hand, a smaller L results in a smaller data rate but approximating (8) as an Alamouti matrix becomes more accurate resulting in higher diversity gain. Fortunately, for the DVB-H 8K system, choosing a relatively large L still achieves a good performance as shown in Section VI.

B. FIR-MMSE FEQ for Alamouti SFBC-OFDM

In this section, we integrate the FIR-MMSE FEQ in Section II-B with our Alamouti SFBC-OFDM scheme in Section III-A. For the m-th Alamouti codeword of the l-th superblock, we omit the superblock index l, and construct a matrix $\mathbf{G}_m = [(\mathbf{G}_m^{(1)})^T \ \ldots \ (\mathbf{G}_m^{(M_t)})^T]^T$ as a stack of M_r matrices, each of which has a similar structure to (4) for the SISO case, i.e.

$$\mathbf{G}_m^{(i)} = \begin{bmatrix} \mathbf{G}^{(i)}_{(m-D)_N,(m-2D)_N} & \cdots & \mathbf{G}^{(i)}_{(m-D)_N,(m+2D)_N} \\ \vdots & \vdots & \vdots \\ \mathbf{G}^{(i)}_{m,(m-2D)_N} & \cdots & \mathbf{G}^{(i)}_{m,(m+2D)_N} \\ \vdots & \vdots & \vdots \\ \mathbf{G}^{(i)}_{(m+D)_N,(m-2D)_N} & \cdots & \mathbf{G}^{(i)}_{(m+D)_N,(m+2D)_N} \end{bmatrix} \tag{9}$$

where each element is a 2×2 matrix of the form given in (8) (setting $l = 0$ to omit the superblock index). Hence, similar to (5), the FIR-MMSE FEQ coefficients are given by

$$\mathbf{w}_m = \mathbf{g}_m{}^H(\mathbf{G}_m\mathbf{G}_m{}^H + \sigma^2\mathbf{I}_{2QM_r})^{-1} \tag{10}$$

where $\mathbf{g}_m \in \mathbb{C}^{2QM_r\times 2}$ contains the middle two columns of $\mathbf{G}_m$ and $\mathbf{w}_m \in \mathbb{C}^{2\times 2QM_r}$ is the FIR-MMSE FEQ coefficient matrix. Finally, the FEQ output for the m-th codeword is $\hat{\mathbf{X}}_m = \mathbf{w}_m\mathbf{Y}_m$ where $\mathbf{Y}_m = [(\tilde{\mathbf{Y}}_m^{(1)})^T \ \ldots (\tilde{\mathbf{Y}}_m^{(M_r)})^T]^T$, $\tilde{\mathbf{Y}}_m^{(i)} = [Y^{(i)}_{(m-D)_N} \ (Y^{(i)}_{(m-D+B)_N})^* \ \cdots \ Y^{(i)}_{(m+D)_N} \ (Y^{(i)}_{(m+D+B)_N})^*]^T$ and $\hat{\mathbf{X}}_m = [\hat{X}_{2m-1} \ \hat{X}_{2m}]^T$.

IV. Simplified Hybrid Frequency/time Channel Estimation

To estimate the channel at pilot locations, we need to place pilots in pairs of subcarriers, i.e. $D = 2$ in Fig. 1. Assuming we have $P = N/d$ pilot subcarriers equally spaced at $X_{p(0)}, X_{p(0)+1}, \cdots, X_{p(P)}, X_{p(P)+1}$ where $p(l) = l \times d$ and each pilot codeword contains two adjacent pilot subcarriers, we have $2P$ pilot subcarriers. Assuming the channels fixed over two adjacent subcarriers (i.e.$G_{k,k}^{(i,j)} \approx G_{k+1,k+1}^{(i,j)}, j = 1,2$ and $1 \le i \le M_r$) and ignoring ICI and noise, we obtain the input-output relation for subcarriers k and $(k+1)$ for the i-th receive antenna as

$$\begin{bmatrix} Y^{(i)}_{p(l)} \\ Y^{(i)}_{p(l)+1} \end{bmatrix} = \begin{bmatrix} X_{p(l)} & X_{p(l)+1} \\ -X^*_{p(l)+1} & X^*_{p(l)} \end{bmatrix} \begin{bmatrix} G^{i,1}_{p(l),p(l)} \\ G^{i,2}_{p(l),p(l)} \end{bmatrix} \tag{11}$$

which can be used to obtain the least squares (LS) estimate for the channel frequency response at pilot subcarriers.

To estimate the Q main diagonals of $\mathbf{G}^{(i,j)}$, we use the hybrid frequency/time-domain channel estimation algorithm

Petitioner Samsung Ex-1004, 0148

in [4]. This algorithm is based on the fact that for normalized Doppler of up to 20%, the channel time-variations can be approximated by a piece-wise linear model with a constant slope over each OFDM symbol duration.

We summarize the algorithm in [4] and extend it to the MIMO case as follows.

Step 1 Ignoring ICI, for each receive antenna i, we obtain the frequency response at pilot codeword locations using (11) and compute $\hat{G}^{(i,j)}_{p(l),p(l)}$ for $j = 1, 2$ and $1 \leq i \leq M_r$. For each pair of transmit-receive antennas, we omit the i, j indices to simplify the notation, since we are estimating each of the $2M_r$ frequency-domain channel matrices *independently*. Performing a linear or Wiener filtering interpolation on $\hat{G}_{p(l),p(l)}$, we obtain an estimate of the diagonal of $\mathbf{G}$, denoted by $\hat{\mathbf{g}}$, followed by a P-point IFFT to get an estimate of the average CIR (i.e. the middle row of $\mathbf{H}$) denoted by $\hat{\mathbf{h}}^{\text{avg}}_{t-1}$ where we assume that the current OFDM block index is $t-1$.

Step 2 Repeat Step 1 for the next two OFDM symbols so that we have the middle rows for three consecutive OFDM symbols, denoted by $\hat{\mathbf{h}}^{\text{avg}}_{t-1}$, $\hat{\mathbf{h}}^{\text{avg}}_{t}$ and $\hat{\mathbf{h}}^{\text{avg}}_{t+1}$.

Step 3 For the current OFDM symbol, we denote by $\hat{\boldsymbol{\alpha}}_1$ and $\hat{\boldsymbol{\alpha}}_2$ the estimated slope vectors for the first and second halves of the OFDM symbol, respectively. Hence

$$\hat{\boldsymbol{\alpha}}_1 = (\hat{\mathbf{h}}^{\text{avg}}_{t} - \hat{\mathbf{h}}^{\text{avg}}_{t-1})/N; \hat{\boldsymbol{\alpha}}_2 = (\hat{\mathbf{h}}^{\text{avg}}_{t+1} - \hat{\mathbf{h}}^{\text{avg}}_{t})/N \qquad (12)$$

Step 4 Using the CIR slope vectors, we can compute the estimated off-diagonal elements of $\mathbf{G}$ (see [5]). Combined with the estimated main diagonal obtained from Step 1, we now have an estimate of the full $\mathbf{G}$ matrix which we denote by $\hat{\mathbf{G}}$. This matrix is an $N \times N$ full matrix and we can use its Q main diagonals to compute the FEQ according to (10).

To reduce the complexity of this hybrid channel estimation algorithm, we exploit the *sparseness* of time-domain CIR and the *banded* structure of frequency-domain channel matrix $\mathbf{G}$. In practice, the CIR is usually sparse and the number of active channel taps is much less than L. In this case, many channel taps can be zeroed out to reduce the processing complexity with negligible performance loss. To do this, we choose the M taps from $\hat{\mathbf{h}}^{\text{avg}}$ with the largest absolute value, and zero out all the remaining taps. Therefore, we only need to estimate M instead of L slopes when calculating $\hat{\boldsymbol{\alpha}}_1$ and $\hat{\boldsymbol{\alpha}}_2$ in (12). Choosing the value of M entails a complexity-performance tradeoff.

The banded structure of $\mathbf{G}$ can also be exploited to reduce channel estimation complexity. Simulation results in Subsection VI show that a 3-tap FEQ [1] performs well even at a relatively high Doppler of 10% which requires an estimate of only the three main diagonals of $\mathbf{G}$. Since the main diagonal of $\mathbf{G}$ is estimated in Step 1, we only need to compute one sub-diagonal and one super-diagonal of $\hat{\mathbf{G}}$ in Step 4 instead of the full matrix. Furthermore, we proved in [5] that the elements of the sub-diagonals are approximately the negatives of the corresponding elements of the super-diagonals for large N; hence, we only need to compute one super-diagonal of $\hat{\mathbf{G}}$.

TABLE I
COMPLEXITY FOR HYBRID CHANNEL ESTIMATION ALGORITHM

	# of multiplications ($N_{multi.}$)		
System	single antenna	2-Tx 1-Rx	2-Tx 2-Rx
M=10, D=1	13850	27700	55400
M=10, D=2	15898	31796	63592
M=10, D=N-1	6.2×10^6	1.2×10^7	2.4×10^7
M=64, D=1	20253	40506	81012
M=64, D=2	22400	44800	89600
M=64, D=N-1	6.2×10^6	1.2×10^7	2.4×10^8

V. COMPLEXITY ANALYSIS

For the SISO case, Steps 1-3 have significantly less complexity than Step 4 in Section IV. In Step 4, a closed-form expression to compute the off-diagonal elements of $\mathbf{G}$ from $\hat{\boldsymbol{\alpha}}_1$ and $\hat{\boldsymbol{\alpha}}_2$ was given in [5]. We first need to calculate two N-point IFFT of an L-sample vector (namely $\hat{\boldsymbol{\alpha}}_1 + \hat{\boldsymbol{\alpha}}_2$ and $\hat{\boldsymbol{\alpha}}_1 - \hat{\boldsymbol{\alpha}}_2$), which has a complexity of $[\log_2 L + 2(1 - \frac{L}{N})] \cdot \frac{N}{2}$ complex multiplications each [6]. In [7], a generic FFT pruning algorithm is proposed which does not require the sparse input data to be grouped together (as in our case where the M active taps are dispersed among the entire L taps). This algorithm has a complexity saving ratio of β; Hence, we need approximately $(1-\beta)[\log_2 L + 2(1 - \frac{L}{N})]N$ complex multiplications for 2 IFFT operations, where β is given in [7] for different scenarios. Furthermore, to compute 1 off-diagonal element of $\hat{\mathbf{G}}$, we need 2 complex multiplications for odd-indexed diagonals and 1 for even-indexed diagonals [5]. We estimate D subdiagonals for a Q-tap FEQ (where $Q = 2D + 1$), which requires $(3\lfloor \frac{D}{2} \rfloor + 2(D)_2)N$ complex multiplications. Denoting the total number of multiplications by $N_{multi.}$, we have

$$N_{multi.} = (1-\beta)(\log_2 L + 2(1 - \frac{L}{N}))N + (3\lfloor \frac{D}{2} \rfloor + 2(D)_2)N \qquad (13)$$

For the MIMO case, we repeat the same procedure for all $M_t \times M_r$ channels; hence the complexity will increase by a factor of $M_t \times M_r$. Table I lists the total number of multiplications used by the hybrid channel estimation algorithm assuming $L = 64$ tap channel and $N = 2048$ for different M, D. By using $M = 10$ instead of 64, the IFFT complexity is reduced by approximately 40% (i.e. $\beta \approx 0.4$) [7]. In addition, by exploiting the banded structure of $\mathbf{G}$ (i.e. assuming a tri-diagonal $\mathbf{G}$ with $D = 1$ instead of a full $\mathbf{G}$ with $D = N - 1$), the number of required multipliers is reduced significantly.

VI. SIMULATION RESULTS

We choose the DVB-H standard as our case study, which is required to support high mobility. We evaluated the DVB-H receiver performance in the 8K mode with $N = 8192$ since the 8K mode suffers more from ICI than the 2K or 4K modes. We assumed the typical urban TU-06 channel delay profile defined by the COST 207 project with 6 taps in the continuous-time domain, 8 MHz channel bandwidth, and a carrier frequency of 800 MHz. After sampling, we get a long discrete-time CIR with approximately 50 taps. Each discrete channel tap is generated by an independent complex

Petitioner Samsung Ex-1004, 0149

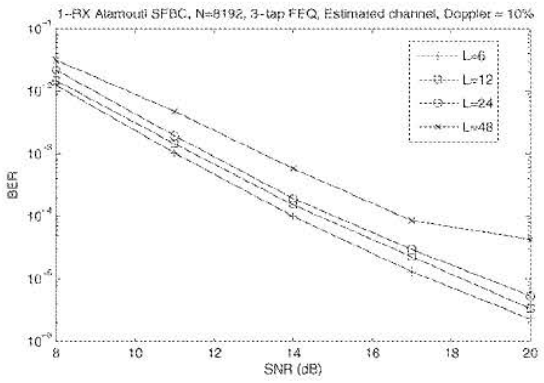


Fig. 2. 1-RX Alamouti SFBC-OFDM with different L, 10% Doppler

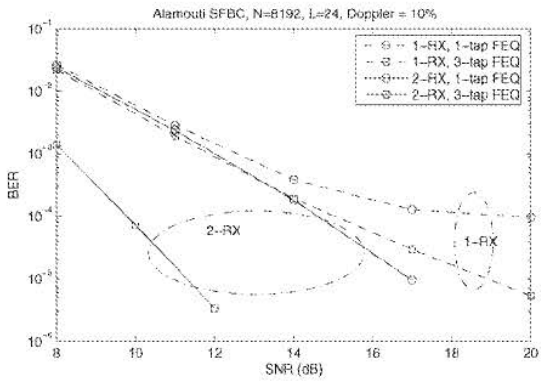


Fig. 4. Alamouti SFBC-OFDM with estimated channel, 10% Doppler

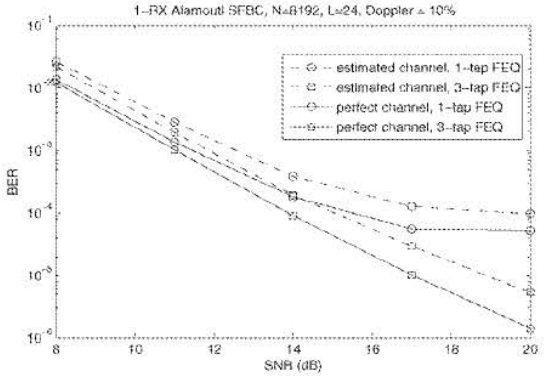


Fig. 3. 1-RX Alamouti SFBC-OFDM, 10% Doppler

Gaussian random variable with time correlation based on Jake's model. A 64-state rate-1/2 convolutional code is employed. The coded bits are interleaved and mapped into QPSK constellation points.

The performance for the 8K mode system is evaluated with a relatively high Doppler of 10% corresponding to a highway speed of approximately 100 Km/h in this simulation. Fig. 2 shows the BER performance for a two-transmit and one-receive antenna system implementing our proposed embedded Alamouti SFBC scheme with different L. We observe that as L increases, the BER performance becomes worse (due to less accurate assumption of Alamouti matrix in (8) and increased difficulty in channel interpolation between pilot subcarriers), but the pilot overhead is reduced.

Keeping the same 1/12 pilot overhead rate of the DVB standard, we insert a pair of pilots at every 24 subcarriers ($L = 24$) and Fig. 3 shows the performance for this scenario. Since there is significant ICI, error floors are observed with a 1-tap FEQ with either perfect or estimated channel. To combat this ICI, we implemented our 3-tap FEQ design as described in Section III which improves performance significantly. To estimate the 3 main diagonals of $\mathbf{G}$, we implemented the reduced-complexity hybrid channel estimation algorithm in Section IV and it results in only 2 dB performance loss from the case of perfect channel knowledge.

Finally, to realize additional spatial diversity gains, we increase the number of receive antennas to 2. Fig. 4 compares the performances of the 1-RX and 2-RX systems (with estimated channel) where the increased slope of the BER curves for 2-Rx is evident and results in additional ICI mitigation.

VII. Conclusion

High mobility causes performance-limiting ICI in MIMO-OFDM receivers. We designed a novel SFBC-OFDM scheme and showed how to integrate it with FIR ICI-mitigating equalization. To compute the equalizer coefficients, we showed how to estimate the fast time-varying MIMO channel matrix efficiently by exploiting its sparse and banded structure in the time and frequency-domains, respectively. Simulation results for the DVB-H system demonstrate the effectiveness of the proposed scheme.

References

[1] S. Lu, R. Kalbasi, and N. Al-Dhahir, "OFDM interference mitigation algorithms for doubly-selective channels," *In Proc. of IEEE Vihicular Tenology Conference*, Sep 2006.

[2] S. M. Alamouti, "A simple transmit diversity technique for wireless communications," *IEEE J. Select. Areas Commun.*, vol. 16, pp. 1451–1458, Oct 1998.

[3] K. F. Lee and D. B. Williams, "A space-frequency transmitter diversity technique for OFDM systems," in *Proc. of IEEE Global Telecommunication Conference*, vol. 3, Nov 2000, pp. 1473–1477.

[4] Y. Mostofi and D. Cox, "ICI mitigation for pilot-aided ofdm mobile systems," *IEEE Trans. Wireless Commun.*, vol. 4, pp. 765–774, Mar 2005.

[5] S. Lu and N. Al-Dhahir, "Reduced-complexity hybrid time/frequency channel estimation for DVB-H," in *Proc. of IEEE Sarnoff Symposium*, May 2007. Available at http://www.utdallas.edu/~aldhahir/sarnoff_best.pdf.

[6] J. Markel, "FFT pruning," *IEEE Trans. Audio Electroacoust.*, vol. 19, pp. 305–311, Dec 1971.

[7] Z. Hu and H. Wan, "A novel generic fast Fourier transform pruning technique and complexity analysis," *IEEE Trans. Signal Processing*, vol. 53, pp. 274–282, Jan 2005.

Petitioner Samsung Ex-1004, 0150

MISO JOINT SYNCHRONIZATION-PILOT DESIGN FOR OFDM SYSTEMS

John E. Kleider[†‡], *Xiaoli Ma*[‡], *Robert J. Baxley*[‡] *and G. Tong Zhou*[‡]

[†]General Dynamics C4 Systems, Scottsdale, AZ, USA
[‡]School of Electrical and Computer Engineering, Georgia Institute of Technology, Atlanta, GA, USA

ABSTRACT

In this paper we apply a new joint synchronization-pilot sequence (JSPS) optimization design technique to multiple transmitter OFDM systems. One objective in the design of the JSPS for MISO transmissions is to eliminate the requirement for the different preamble fields used for coarse and fine synchronization and channel training. In this work, independent JSPSs are designed for each transmitter in a multiple antenna system, but are transmitted simultaneously from each antenna. Consequently, JSPSs can potentially reduce the overhead of multiple antenna preamble transmissions (improving bandwidth efficiency). The objective of this paper is to determine the performance advantages of joint carrier frequency offset (CFO) and channel estimation using only the pilot portion of the JSPS. By jointly optimizing the position and power of each pilot across the transmitter antennas in Rayleigh fading channels with CFO, we show > 15 dB SNR improvement in the performance of the channel estimator.

Index Terms—Orthogonal frequency division multiplexing (OFDM), pilot symbol assisted modulation (PSAM), pilot design, MISO systems

1. INTRODUCTION

Orthogonal frequency division multiplexing (OFDM) is an attractive technique for high data rate transmission in multipath channels [1], while multiple transmit antennas can be utilized to improve diversity performance and thus reduce the receiver demodulation bit error rate (BER) [2]. In many wireless applications it is desirable to minimize transmitter power in multiple antenna OFDM systems and thus coherent modulation is commonly utilized for this purpose (as compared to differential modulation which requires 2-3 dB additional power)[3]. Coherent OFDM, however, requires accurate synchronization and channel estimation; otherwise the power savings of coherent modulation is diminished and becomes less attractive as a preference over differential OFDM [4]. Because of coherent OFDM's sensitivity to synchronization error, information packets are typically preceded by coarse/fine synchronization and channel estimation preambles, which are commonly separated into two fields, each field with a different sequence [5]. OFDM systems have been shown to be particularly sensitive to carrier frequency offset (CFO), which causes inter-carrier interference (ICI) and if left uncorrected can result in severe BER degradation at the receiver [6]. In addition, unresolved CFO will also degrade channel estimation and equalization due to ICI and uncorrected phase rotation over time.

In this work, we develop a single sequence preamble (as opposed to two separate sequences) for preamble-based OFDM systems, where this sequence can be used for coarse synchronization (timing- and frequency-acquisition), fine synchronization (fine timing and frequency estimation) and channel estimation. We denote this sequence as a joint synchronization-pilot sequence (JSPS). JSPSs have been shown to be effective for frequency and timing acquisition [7] and sampling offset can be estimated jointly during the channel estimation phase [8]. We assume that the preambles for each antenna are transmitted simultaneously in one time slot (to minimize preamble transmission overhead) and thus will interfere with each other. The pilot part of the JSPSs used for channel training is designed to be orthogonal in frequency across all transmitter antennas. This characteristic enables robust and low complexity CFO and channel estimation at the single antenna receiver.

A number of joint detection methods have been proposed in the literature for OFDM single-input single-output (SISO) systems [9] [10] and for OFDM transmit diversity systems [11] with CFO. Similar to the idea in [11], the preamble JSPS does not assume any specific space-time code as opposed to the space-time block-code (STBC) based iterative detection method in [12]. The JSPS is designed to enable decoupling of the CFO and channel estimation from the symbol decoding, which is attractive for low receiver complexity, compared to blind and semi-blind approaches [13][6]. The scope of this paper is to show that, within each JSPS, optimized pilot positions and power can yield improved CFO and channel estimation performance in multiple OFDM transmitter systems.

This paper is organized as follows. Section 2 describes the OFDM MISO model, the multiple antenna preamble JSPS sequence is developed in Section 3, while the pilot design part of the JSPS is described in Section 4. A robust performance CFO estimation algorithm, with low complexity, is detailed in Section 5, with performance results presented in Section 6. Section 7 concludes the paper.

2. SYSTEM MODEL

Figure 1 illustrates the basic structure of our OFDM system. We encode the data symbols using rate-1 space-frequency block-codes (SFBC), which can be transmitted in one OFDM block duration as contrasted to a STBC OFDM system, which requires two OFDM blocks. We denote N as the total number of OFDM subcarriers. The baseband time-domain transmission signal, $\boldsymbol{x}$, is structured such that preamble, $\boldsymbol{x}_p$, precedes information symbols, $\boldsymbol{x}_d$, and thus

This work was supported in part by the U. S. Army Research Laboratory under the Collaborative Technology Alliance Program, Cooperative Agreement DAAD19-01-2-0011.

Petitioner Samsung Ex-1004, 0151

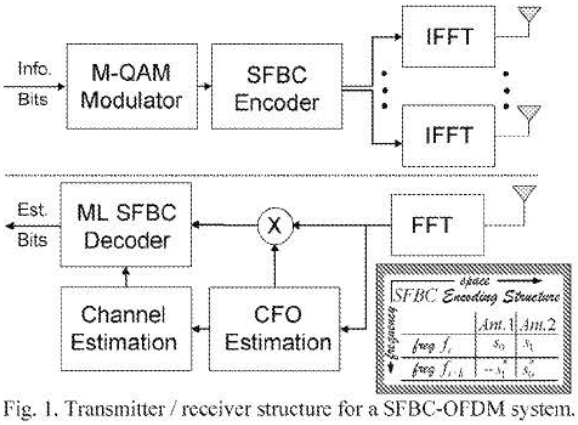


Fig. 1. Transmitter / receiver structure for a SFBC-OFDM system.

$$\boldsymbol{x} = [\boldsymbol{x}_p \ \boldsymbol{x}_d]^T. \tag{1}$$

The preamble part, $\boldsymbol{x}_p$, is not a SFBC, but is designed specifically to enable course / fine synchronization and channel estimation with low complexity at the receiver. $\boldsymbol{x}_p$ is the composite baseband transmitted preamble signal from both antennas and is denoted as

$$\boldsymbol{x}_p = \sum_{i=1}^{A} \mathbf{x}_p^i , \tag{2}$$

where $\mathbf{x}_p^i$ is the JSPS from the ith transmit antenna and A is the number of transmit antennas. The data part, $\boldsymbol{x}_d$, is encoded according to a SFBC. For example if $A = 2$, the SFBC encoding of two symbols s_0 and s_1 is performed across two OFDM subcarriers f_i and f_{i+k} using the Alamouti code [2] as denoted in the lower right-hand corner of Figure 1, where $(\cdot)^*$ is the complex conjugate operator. This process is continued until all $|K_{si}|$ of the N OFDM subcarriers are assigned, where K_{si} denotes the data subcarrier indexes and $|K_{si}|$ is the cardinality of K_{si}. Since the fine CFO and channel can be estimated using the preamble part, $\boldsymbol{x}_p$, and if the channel is approximately constant over the packet burst, then $|K_{si}| = N - |K_n|$, where K_n denotes the null (unused) subcarrier indexes and $|K_n|$ is the number of null subcarriers.

The composite transmitted data signal, $\boldsymbol{x}_d$, can be written as

$$\boldsymbol{x}_d = \sum_{i=1}^{A} \mathbf{x}_d^i , \tag{3}$$

where $\mathbf{x}_d^i$ is the SFBC vector data sequence from the ith transmit antenna. If $\tilde{\boldsymbol{x}}$ is the same as $\boldsymbol{x}$, but with the cyclic extension removed, then prior to the cyclic extension, the baseband signal for antenna i is

$$\tilde{\mathbf{x}}^i[n] = \frac{1}{\sqrt{N}} \sum_{k=0}^{N-1} X_k e^{j2\pi nk/N} , \tag{4}$$

where $n \in \{0, 1, \ldots, N\text{-}1\}$, $\{X_k\}_{k\in K_{si}}$, $\{X_k\}_{k\in K_{spi}}$, and $\{X_k\}_{k\in K_n}$ are the non-zero SFBC encoded symbols during the data part, the non-zero part of the JSPS during the preamble part and a zero vector for the null subcarriers at indexes, K_n, for both the data and preamble parts.

The received baseband signal after multipath and CFO is

$$y[n] = (x[n] * h[n]) e^{-j2\pi\varepsilon n/N} + w[n], \tag{5}$$

where $h[n]$ is a length-L vector of the channel impulse response, with Rayleigh distributed amplitude and each channel tap is i.i.d. complex Gaussian with zero mean and variance such that $E[|h|^2] = 1$. $\varepsilon = \Delta f T_s$ is the normalized CFO with respect to the subcarrier spacing $1/T_s$, where $T_s = TN$, T is the sample period, and $w[n]$ is zero-mean additive white Gaussian noise with variance σ_w^2 and "*" is the convolution operator. We note that $x[n]$ is the same as $\boldsymbol{x}$ in (1), with the index n representing the nth element of vector $\boldsymbol{x}$. In this paper, we assume coarse frame and frequency synchronization are achieved via acquisition of the JSPS [14]. Next we present algorithms to find the fine CFO and channel frequency response. Both CFO and channel estimators use the preamble JSPS, but because of the orthogonality of the transmitter pilot parts of the JSPS, the estimators are completely decoupled processes and are thus of low complexity.

3. MULTI-ANTENNA PREAMBLE JSPS DESIGN

Design of JSPS is described in [14] for SISO OFDM systems, where synchronization and pilot information are superimposed with the OFDM data. The pilot part of the JSPS in [14] uses a parametric pilot optimization process to improve symbol estimation from the least-squares (LS) channel estimates [15][16]. In this work, we extend the JSPS design introduced in [14] to multiple antennas. The pilot part of the JSPS is utilized for fine CFO estimation and also for channel estimation. In [15][16] it is shown that uniformly-spaced and constant-power (USCP) pilots are suboptimal. Accordingly, those authors propose a non-USCP solution for LS channel estimation that provides dramatic improvements over the USCP pilot schemes commonly used in OFDM. An alternative pilot design for OFDM systems with null subcarriers was proposed in [17], but was shown in [16] to perform worse than the USCP scheme for certain channel orders. Thus we choose to extend the scheme in [15][16] for the multiple antenna pilot portion of our JSPSs rather than the one proposed in [17].

In this paper, we use $N = 256$ and $|K_n| = 64$, where there are 32 null subcarriers on each band edge. Given we have chosen the null subcarrier locations, the next step of the JSPS design is to determine the pilot positions and power loading for each antenna. The pilot positions and powers for each antenna, respectively, are denoted as $K_{p1}, K_{p2}, \ldots K_{pA}$ and $P_{p1}, P_{p2}, \ldots P_{pA}$, where $|K_{p1}| = |K_{p2}| = \ldots = |K_{pA}|$ and $\sum_{i=1}^{K_{p1}} P_{p1}[i] = \sum_{i=1}^{K_{p2}} P_{p2}[i] = \ldots = \sum_{i=1}^{K_{pA}} P_{pA}[i]$. Once these pilot parameters are determined for each antenna, the leftover positions are used for coarse synchronization information denoted as $K_{s1}, K_{s2}, \ldots K_{sA}$, all exhibiting a flat power profile in the frequency domain, with equal total power P_s on each $K_{s1}, K_{s2}, \ldots K_{sA}$ for each transmit antenna. We note that to provide frequency orthogonal pilots across transmitter antennas, if $K_{sp1}, K_{sp2}, \ldots, K_{spA}$ represents all possible subcarrier positions, excluding $K_{n1} = K_{n2} = \ldots = K_{nA}$, then the ith transmit antenna power,

$$P_{spi} = \begin{cases} P_{pi} \ for \ K_{pi} \\ P_s \ \ for \ K_{si} \\ 0 \ \ for \ K_{pj}, j \neq i \end{cases} \tag{6}$$

Once the pilot positions and power are determined, the method in [7] is used to fill in the remaining subcarriers for each antenna with synchronization information.

Petitioner Samsung Ex-1004, 0152

For the data part of the transmission, symbols are encoded using the SFBC method described in the first part of Section 2. If no pilots are required during data transmission, $K_{s1} = K_{s2} = \ldots = K_{sA}$ $= K_{sp1} = K_{sp2} = \ldots = K_{spA}$ and $|K_{si}| = |K_{spi}|$. If pilots are required due to dynamic channel conditions and CFO drift, where $|K_{pi}|$ pilots are inserted every OFDM symbol for each transmitter antenna, then $|K_{si}| = |K_{spi}| - A\cdot|K_{pi}|$. Next we describe the pilot parameter optimization for multiple antennas.

4. MULTI-ANTENNA PILOT OPTIMIZATION

In [15][16] a parametric pilot optimization process is proposed for SISO OFDM systems. The parameterization is accomplished using a segmented optimization technique by applying boundary constraints to an un-tractable non-linear discontinuous optimization. We extend this technique to multiple-antenna OFDM systems. We will show from simulation that this extension provides near optimal performance when compared to the perfect channel knowledge case with no CFO.

Candidate K_{pi} indexes for each antenna can be formulated as

$$K_{pi} = \{\text{int}(f^{-1} \circ g_i(\tau)) \mid \tau \in \{0, 1, 2, \ldots, |K_{pi}| - 1\}, \quad (7)$$

until the minimizing set is found for each transmit antenna. The domain of f is restricted to $[1, N]$, where f is a one-to-one mapping such that $K_{pi} = f^{-1}(S)$ and S is a circularly shifted version of K_{pi}. Following the procedure in [16], a cubic function is used to parameterize the pilot subcarrier positions according to

$$g_i(\tau) = a_{3i}\tau^3 + a_{2i}\tau^2 + a_{1i}\tau + a_{0i}. \quad (8)$$

Given that the number of non-null subcarriers for the ith antenna is denoted as N_i and denoting the middle of the non-null subcarriers as ½, the constraint equations become

$$g_i\left(\frac{|K_{pi}|-1}{2}\right) = 1/2 \quad (9)$$

$$g_i(0) = -(N_i - 1)/2 + \delta_i \quad (10)$$

$$g_i(|K_{pi}|-1) = (N_i + 1)/2 - \delta_i \quad (11)$$

$$g_i'(0) > 0, \quad (12)$$

where δ_i represents the distance the edge pilots are from the signal band edges. Using the constraint equations in (9)-(12) and the fact that the edge pilot placement should be no further from the signal band edge than the average pilot spacing, three of the five variables can be eliminated and thus the optimization problem in (7) is greatly simplified. We note that once K_{pi} is found starting with antenna i, then K_{pi} are excluded from the set for the next antenna pilot positions and so on until K_{pA} are determined for all antennas. The composite pilot sequence from all antennas can be positioned in any non-null subcarriers and are placed symmetrically about the center of the signal band. Without loss of generality, the pilots are placed sequentially from left to right giving $g_i(\tau)$ a positive slope. If $\hat{K}_{pi}$ represents the ith antenna candidate set of pilot subcarrier positions and extending the single antenna optimization [16], the pilot powers are found by solving

$$\arg\min_{\mathbf{u}} \quad \|\mathbf{A}\mathbf{u}\|_{\infty}, \text{ subject to } \sum_{k=1}^{|K_{pi}|} \frac{1}{[\mathbf{u}]_k} = E_p, \quad (13)$$

$$\hat{K}_{pi} = K_{pi}, \ [\mathbf{u}]_k > 0 \forall k,$$

where E_p is the power allocated to the pilots, $\mathbf{A}$ is the element-wise magnitude square of the matrix $\mathbf{Q}_{si}\mathbf{Q}_{pi}^{+}$, where $\mathbf{Q}_{pi} = [\mathbf{Q}]_{K_{pi},\{1,2,\ldots,L\}}$, $\mathbf{Q}_{si} = [\mathbf{Q}]_{K_{si},\{1,2,\ldots,L\}}$, $\mathbf{Q}_{k,n} = N^{-1/2}\exp(-j2\pi(n-1)(k-1)/N), 1 \le k, n \le N$, and the LS channel estimator is $\hat{H}_i = \mathbf{Q}_{si}\mathbf{Q}_{pi}^{+}Y_{ki}^{p}[X_{ki}^{p}]^{-1}$ (CFO = 0). The LS estimator data subcarrier MSE of the channel estimate is approximated by $z_i = \text{diag}\left\{\frac{\sigma_w^2}{E_p}\mathbf{Q}_{si}\mathbf{Q}_{pi}^{+}\mathbf{D}_{|K_{pi}|}\mathbf{Q}_{pi}^{H^T}\mathbf{Q}_{si}^{H}\right\}$, where $\mathbf{X}_i^p$ are the ith antenna modulated pilot values, $\mathbf{D}_{\mathbf{u}}$ is a diagonal matrix with diagonal elements from vector $\mathbf{u}$, $\mathbf{Q}^{+}$ and $\mathbf{Q}^{H}$ denote the pseudo inverse and Hermitian transpose of $\mathbf{Q}$, respectively. The transmitter pilot optimization does not require channel knowledge. At the receiver, CFO estimation is performed prior to channel estimation.

5. CFO ESTIMATION

The CFO is estimated prior to channel estimation. The preamble part for each antenna is comprised of one JSPS followed by another JSPS (i.e., [JSPS JSPS]) [6]. The CFO is estimated by measuring the phase change from JSPS-to-JSPS along each pilot subcarrier k. We can write the received version of preamble JSPS part of (1) as $\mathbf{y}_p$, which can be separated into two parts such that $\mathbf{y}_p = [\mathbf{y}_{p1}\ \mathbf{y}_{p2}]^T$. The frequency domain pilot part of the $\mathbf{y}_{p1}$ and $\mathbf{y}_{p2}$ signals for the ith transmit antenna (ignoring receiver noise, assuming $L <$ cyclic prefix length and the CFO ICI is part of the channel frequency response, H_i) can be approximated as $Y_{ki1}^{p} = X_{ki1}^{p}H_{ki1}^{p}e^{-j2\pi\varepsilon_1'/N}$ and $Y_{ki2}^{p} = X_{ki2}^{p}H_{ki2}^{p}e^{-j2\pi\varepsilon_2'/N}$, respectively. If the phases ϕ_{ki1} and ϕ_{ki2}, are computed as $\angle Y_{ki1}^{p}$ and $\angle Y_{ki2}^{p}$, respectively, then the CFO is estimated according to

$$CFO_i = \frac{1}{2\pi T_s}\sum_{k=0}^{|K_{pi}|-1}(\phi_{ki1} - \phi_{ki2})\cdot v_{ki}, \quad (14)$$

where v_{ki} is a weighting vector of size $|K_{pi}|$ based on the received pilot power. If $P_{ki1} = Y_{ki1}^{p}\cdot(Y_{ki1}^{p})^{*}$, then v_k can be written as

$$v_{ki} = \frac{(P_{ki1} + P_{ki2})/2}{\sum_{k=0}^{|K_{pi}|-1}(P_{ki1} + P_{ki2})/2}. \quad (15)$$

This CFO estimator has low complexity and is decoupled between transmitters. This *decoupling* between each antenna means that we can exploit both estimates for reduced estimation variance.

6. PERFORMANCE RESULTS

Unless otherwise specified, the SNR is defined as E_s/N_0, where E_s is the energy in a single constellation symbol s and $N_0 = 2\sigma_w^2$ is the noise spectral density. The left plot in Figure 2 shows the MSE profile for antenna 1 of a 2-transmitter system using the optimization procedure outlined in Section 4 for two values of a_{3i}. The USCP pilot design occurs when $a_{3i} = 0.0$ and $a_{3i} = -0.057$ provides a flat maximum MSE profile, which we denote as the "*optimized*" pilot design in subsequent plots. The MSE profile for antenna 2 is nearly identical to that of antenna 1, so it is not shown. The right plot in Figure 2 compares the channel estimate maximum MSE in an $L = 16$ tap multipath channel as described in Section 2. The optimized scheme performs greater than 15 dB better than the USCP scheme.

Simulated MSE performance of CFO_i in (14) for $|K_{pi}|=L=16$ tap Rayleigh channel and CFO, $\varepsilon_1 = \varepsilon_2 = 0.25$, is shown in Figure 3 for both pilot schemes. SNR in Figure 3 is defined as the JSPS, x_p,

Petitioner Samsung Ex-1004, 0153

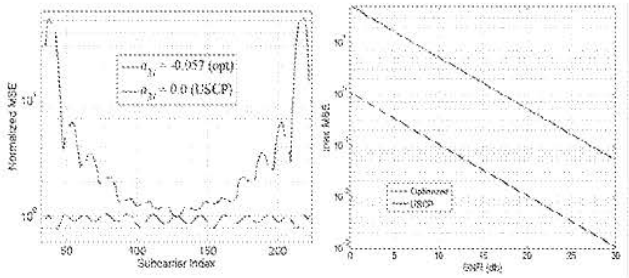


Fig. 2. Normalized MSE profile (left), LS $\hat{H}$, maximum MSE (right).

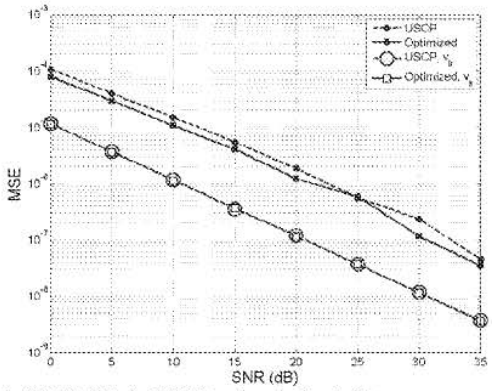


Fig. 3. *CFO*, MSE for USCP and optimized pilots.

signal-to-noise power, $\sigma_{v_p}^2 / \sigma_w^2$. The MSE is measured according to $E[|CFO_i - \Delta f|^2]$. For CFO estimation, the optimized pilot design works slightly better than USCP pilots without weighting. Once weighting is utilized according to (15), a factor of 10 reduction in MSE performance is found. In the weighting case both pilot schemes perform equally well.

Demodulated BER performance is measured for A=2 transmit antennas and one receiver antenna SFBC-OFDM system. BER performance is compared in Figure 4 for channel estimation with and without CFO correction. Without CFO correction, the induced CFO is, $\varepsilon_1 = \varepsilon_2 = 0.05$ (0.2 kHz), while for the case with CFO correction, $\varepsilon_1 = \varepsilon_2 = 0.25$ (1 kHz). A maximum likelihood decoder is utilized, as defined in [2]. When the CFO is not corrected, both the USCP and optimized pilot schemes degrade severely. When the CFO is estimated and corrected (denoted as the "w/C" curves) prior to channel estimation, the optimized design performs nearly 4 dB better than USCP and within ~0.5 dB of the perfect channel state information (PCSI) curve.

7. CONCLUSIONS

A new parametric pilot optimization scheme was developed for multi-antenna OFDM transmission systems. The optimized scheme provides >15 dB improvement in maximum MSE LS channel estimation performance compared to uniformly-spaced constant-power (USCP) pilots. The optimized pilot scheme MSE performance was shown to be equal or better than USCP pilots for carrier frequency offset (CFO) estimation. For demodulation BER performance of SFBC-OFDM, the optimized pilot scheme performs at least 3 dB better than USCP.

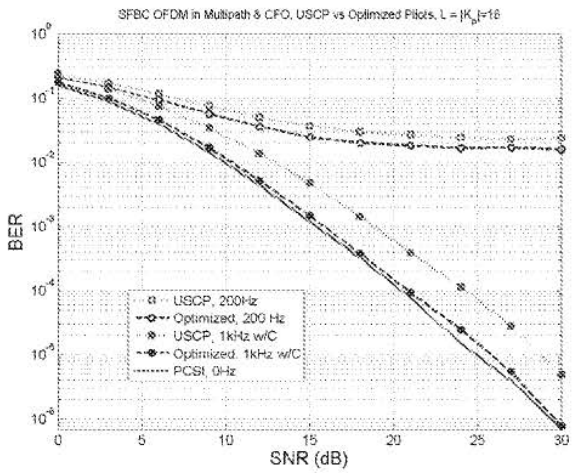


Fig. 4. BER for SFBC-OFDM, USCP and optimized pilots in multipath and CFO (with and without CFO correction).

8. REFERENCES[1]

[1] Z. Wang and G. Giannakis, "Wireless multicarrier communications," *IEEE Signal Processing Magazine*, vol. 17, pp. 29--48, June 2000.

[2] S. Alamouti, "A simple transmit diversity technique for wireless communications," IEEE JSAC, vol. 16, no 8., Oct. 1998, pp. 1451-1458.

[3] G. Giannakis, Z. Liu, X. Ma, and S. Zhou, *Space-Time Coding for Broadband Wireless Communications*, John Wiley and Sons, 2007.

[4] Q. Ma, C. Tepedelenlioglu, and Z. Liu, "Differential space-time-frequency coded OFDM with maximum multipath diversity," *IEEE Trans. Wireless Commun.*, vol. 4, no. 5, pp. 2232 -- 2243, Sept. 2005.

[5] A. van Zelst and T. Schenk, "Implementation of a MIMO-OFDM-based wireless LAN system," *IEEE Trans. Signal Proc.*, vol. 52, no. 2, pp. 483 – 494, Febr. 2004.

[6] T.M. Schmidl and D.C. Cox, "Robust frequency and timing synchronization for OFDM," *IEEE Trans. On Commun.*, vol. 45, no. 12, pp. 1613 - 1621, Dec. 1997.

[7] R.J. Baxley and J.E. Kleider, "Embedded synchronization/pilot sequence creation using POCS," *in Proc. ICASSP*, vol. 4, pp. 14 – 19, May 2006.

[8] S. Gault, W. Hachem, and P. Ciblat, "Joint sampling clock offset and channel estimation for OFDM Signals: Cramér-Rao bound and algorithms," *IEEE Trans. Signal Proc.*, vol. 54, no. 5, pp. 1875 -1885, May 2006.

[9] T. Cui and C. Tellambura, "Joint frequency offset and channel estimation for OFDM systems using pilot symbols and virtual carriers," *IEEE Trans. On Wireless Commun.*, vol. 6, no. 4, pp. 1193 - 1202, April 2007.

[10] X. Ma, H. Kobayashi, and S.C Schwartz, "Joint frequency offset and channel estimation for OFDM," *in Proc. Globecom*, vol. 1, pp. 15 - 19, Dec. 2006.

[11] X. Ma, M.-K. Oh, and G. Giannakis, "Hopping pilots for estimation of frequency offset and multiantenna channels in MIMO-OFDM," *IEEE Trans. On Wireless Commun.*, vol. 1, no. 2, pp. 213 - 225, April 2002.

[12] B. Lu, X. Wang, and Y. Li, "Iterative receivers for space-time block-coded OFDM systems in dispersive fading channels," *IEEE Trans. On Commun.*, vol. 53, no. 1, pp. 162 - 172, Jan. 2005.

[13] M. Ghogho and A. Swami, "Semi-blind frequency offset synchronization for OFDM," *in Proc. ICASSP*, vol. 3, pp. 2333 - 2336, May 2002.

[14] R.J. Baxley, J. Kleider, and G.T Zhou, "A method for joint peak-to-average power radio reduction and synchronization in OFDM," accepted *MILCOM*, Orlando. FL, Oct. 2007.

[15] R.J. Baxley, J.E Kleider, and G.T Zhou, "Pilot design for IEEE 802.16 OFDM and OFDMA," *in Proc. ICASSP*, vol. 2, pp. 321 - 324, April 2007.

[16] R.J. Baxley, J.E Kleider, and G.T Zhou, "Pilot design for OFDM with null edge subcarriers," *submitted to IEEE Trans. On Signal Proc.*, 2007.

[17] S. Ohno, "Preamble and pilot symbol design for channel estimation in OFDM," *in Proc. ICASSP*, vol. 3, pp. 281 - 284, April 2007.

[1]The views and conclusions contained in this document are those of the authors and should not be interpreted as representing the official policies, either expressed or implied, of the Army Research Laboratory or the U.S. Government.

Petitioner Samsung Ex-1004, 0154

Intercarrier Interference in MIMO OFDM

Anastasios Stamoulis, Suhas N. Diggavi, and Naofal Al-Dhahir, *Senior Member, IEEE*

***Abstract*—In this paper, we examine multicarrier transmission over time-varying channels. We first develop a model for such a transmission scheme and focus particularly on multiple-input multiple output (MIMO) orthogonal frequency division multiplexing (OFDM). Using this method, we analyze the impact of time variation within a transmission block (time variation could arise both from Doppler spread of the channel and from synchronization errors). To mitigate the effects of such time variations, we propose a time-domain approach. We design ICI-mitigating block linear filters, and we examine how they are modified in the context of space-time block-coded transmissions. Our approach reduces to the familiar single-tap frequency-domain equalizer when the channel is block time invariant. Channel estimation in rapidly time-varying scenarios becomes critical, and we propose a scheme for estimating channel parameters varying within a transmission block. Along with the channel estimation scheme, we also examine the issue of pilot tone placement and show that in time-varying channels, it may be better to group pilot tones together into clumps that are equispaced onto the FFT grid; this placement technique is in contrast to the common wisdom for time-invariant channels. Finally, we provide numerical results illustrating the performance of these schemes, both for uncoded and space-time block-coded systems.**

***Index Terms*—Channel estimation, Doppler, fast fading channels, intercarrier interference, MIMO, multicarrier transmission, pilot tones, wireless transmission.**

I. Introduction

THE explosive growth of wireless communications is creating the demand for high-speed, reliable, and spectrally efficient communication over the wireless medium. There are several challenges in attempts to provide high-quality service in this dynamic environment. These pertain to channel time-variation and the limited spectral bandwidth available for transmission. In this paper, we are concerned with the role of time variation in transmission of multicarrier modulated signals and the design of schemes to handle such variations.

Multicarrier transmission for wireline channels has been well studied [1]. The main advantage of orthogonal frequency division multiplexing (OFDM[1]) transmission stems from the fact that the Fourier basis forms an eigenbasis for time-invariant (DMT) channels. This simplifies the receiver and leads to inexpensive hardware implementations, as the equalizer is just a single-tap filter in the frequency domain (under the assumption that the channel is time-invariant within a transmission block). Furthermore, combined with multiple antennas [2], [3], OFDM modems are attractive for high data rate wireless networks (wireless LANs and home networking). However, the block time-invariance assumption may not be valid at high mobile speeds or when there are impairments such as synchronization errors (e.g., frequency offsets). In such situations, the Fourier basis need not be the eigenbasis, and the loss of orthogonality (of the carriers) at the receiver results in intercarrier interference (ICI). Depending on the Doppler spread in the channel and the block length chosen for transmission, ICI can potentially cause a severe deterioration of quality of service (QoS) in OFDM systems. Essentially, ICI arises from "time-selectivity" of the channel and, therefore, is the frequency-domain dual of the intersymbol interference (ISI) seen in single-carrier transmission over frequency-selective channels.

Given the direct relationship between achievable data rate and the signal-to-inter-carrier-interference-plus-noise ratio (SINR) at every subcarrier (see, e.g., [1]), ICI has a negative impact on the data throughput as it effectively decreases the SINR. Starting from an analysis of the ICI impact on system performance, we develop herein an ICI mitigation scheme for both single-input single-output (SISO) and multiple-input multiple-output (MIMO) OFDM systems. Founded on optimum block linear filters and practically realizable channel estimation techniques, our proposed scheme significantly improves the SINR (which serves as a figure of merit for the system performance) over a wide range of channel and system configurations.

In SISO OFDM, carrier frequency errors induce a structured ICI pattern that can be eliminated using either training-based or blind techniques (see, e.g., [4] and references therein). The frequency offset manifests itself as a multiplicative factor in the frequency channel response (at each subcarrier of the FFT grid), and once the frequency offset has been estimated, it can be removed rather easily. Without estimating the carrier offset, transmit precoding can be employed to suppress its impact on ICI (see, e.g., [5] and references therein). On the other hand, Doppler-induced ICI appears to be more challenging. In SISO OFDM, previous studies have quantified the effects of ICI on the system performance. In [6], a central limit theorem argument is used to model ICI as a Gaussian random process and quantify its impact on bit error rate (BER), whereas [7] presents results for a number of different Doppler spectra. In [8], the focus is on the wide-sense stationary uncorrelated scattering (WSSUS) [9] channel to show that if the OFDM block duration is greater than 8% of the channel coherence time, then the SINR (due to ICI) is less than 20 dB (see also [10] and references therein).

Similar to SISO OFDM, MIMO OFDM is sensitive to Doppler and carrier frequency errors that destroy the subcarrierorthogonality and give rise to ICI. MIMO OFDM may be

Manuscript received June 10, 2001; revised May 9, 2002. Parts of this paper appeared in WCNC'02 and ICC'02. The associate editor coordinating the review of this paper and approving it for publication was Prof. Brian L. Hughes.

The authors are with the AT&T Shannon Laboratory, Florham Park, NJ 07932 USA (e-mail: naofal@research.att.com).

Publisher Item Identifier 10.1109/TSP.2002.803347.

[1]For wireline transmissions, OFDM is commonly referred to as discrete multitone [1].

1053-587X/02$17.00 © 2002 IEEE

Petitioner Samsung Ex-1004, 0155

equipped with transmit and/or receive diversity (see, e.g., [2] and [11]) and may build on beamforming, space-time coding, and interference cancellation (to name just a few techniques) to increase the achievable data rates over the wireless medium. Our ICI-mitigating designs encompass generic MIMO OFDM systems. In particular, for space-time-coded transmissions, we illustrate through simulations the significant SINR gains by our approach.

Compensation for Doppler-induced ICI hinges on the estimation of the time-varying channel. When the OFDM block duration is less than 10% of the channel coherence time, [12] argues that the channel can be assumed to vary in a linear fashion (and as a result, it can be obtained by linear interpolation between two channel estimates acquired from training blocks). When the OFDM block duration is much smaller than the channel coherence time (relatively mild Doppler), the channel can be assumed approximately constant (over an OFDM block), and its estimation has been thoroughly studied (see [10] and references therein). For rapidly time-varying environments and for the cases where the channel obeys a parsimonious model, techniques in [13] and [14] can be used for channel estimation and tracking. In this work, we look at *severe* Doppler cases, where the channel can no longer be assumed constant within a transmission block: for such rapidly time-varying channels, we develop a novel estimation method.

Our contributions in this paper can be summarized as follows.

- We develop a model for intercarrier interference applicable to MIMO channels.
- We present an ICI analysis for MIMO OFDM.
- We propose a time-domain filtering scheme for mitigating ICI.
- We propose a channel estimation and tracking scheme for estimating the time-varying (within transmission block) channel parameters.
- We propose a pilot tone placement scheme (which works in conjunction with the channel estimation scheme).

The following is an overview of the paper organization. In Section II, we present the model and the notation used in the paper. We present an ICI analysis for MIMO OFDM in Section III, and in Section IV, we develop optimum block linear filters that suppress ICI and yield significant SINR improvement. In Section V, we address the problem of estimating a rapidly time-varying channel, and in Section VI, we present illustrative simulations. Finally, in Section VII, we conclude with some discussion.

II. Data Model

The input data $\{x(k)\}$ is passed through the filter $g(t)$ to produce the transmitted signal $s(t)$. The received signal can be written as

$$y_c(t) = \int h_c(t;\tau)s(t-\tau)d\tau + z(t) \tag{1}$$

where $h_c(t;\tau)$ is the impulse response of the time-varying channel, and $z(t)$ is the additive Gaussian noise. We collect sufficient statistics through Nyquist sampling. The basic idea is that if we sample at a rate larger than $2(W_I + W_s)$, where W_I is the input bandwidth and W_s is the bandwidth of the channel time-variation [15], then we get Nyquist sampling. A careful argument about the sampling rate required for time-varying channels can be found in [16]. In this paper, we assume that this criterion is met, and therefore, we have the discrete-time model

$$y(k) = y_c(kT_s) = \sum_{l=0}^{\nu-1} h(k;l)x(k-l) + z(k) \tag{2}$$

where $h(k;l)$ represents the sampled time-varying channel impulse response (which combines the transmit filter $g(t)$ with the physical channel $h_c(t;\tau)$). The approximation of having a finite impulse response in (2) can be made as good as we need by choosing ν [16]. In this paper, we focus on the discrete-time model given in (2). For the case of multiple transmitter and receiver diversity channel with M_r receive and M_t transmit antennas, we can easily generalize this model to

$$\mathbf{y}(k) = \sum_{l=0}^{\nu-1} \mathbf{H}(k;l)\mathbf{x}(k-l) + \mathbf{z}(k) \tag{3}$$

where $\mathbf{H}(k;l) \in \mathbb{C}^{M_r \times M_t}$ is the lth tap of the matrix response with

- $\mathbf{x}(k) \in \mathbb{C}^{M_t}$ input;
- $\mathbf{y}(k) \in \mathbb{C}^{M_r}$ output;
- $\mathbf{z}(k) \in \mathbb{C}^{M_r}$ complex additive temporally-white circularly-symmetric Gaussian noise with $\mathbf{z}(k) \sim \mathbb{CN}(0, \mathbf{R}_{zz})$, i.e., a complex Gaussian vector with mean 0 and covariance $\mathbf{R}_{zz}$.

The noise is assumed independent of the input. Throughout this paper, we impose an average power constraint on the input that is assumed to be zero mean, i.e., $\mathbb{E}[\|\mathbf{x}(k)\|^2] \leq P$. The specific structure of $\{\mathbf{H}(k;l)\}$ could be constructed by assigning a special structure to $\mathbf{H}_c(t;\tau)$ (for example a discrete multipath channel).

Over a time block of N symbol durations, (3) can be expressed in matrix notation as

$$\mathbf{y} = \mathbf{H}\mathbf{x} + \mathbf{z} \tag{4}$$

where $\mathbf{y}, \mathbf{z} \in \mathbb{C}^{N,M_r}$, $\mathbf{x} \in \mathbb{C}^{N,M_t}$, and $\mathbf{H} \in \mathbb{C}^{N,M_r \times N,M_t}$. We assume that a cyclic prefix of length equal to channel memory is inserted in each input block to eliminate interblock interference (IBI). This prefix serves just as a guard interval between blocks when we have channel time variation within a transmission block. However, when the channel impulse response (CIR) is time invariant over the block, the cyclic prefix serves the role played in OFDM, i.e., $\mathbf{H}$ becomes a *block-circulant* matrix.

Now, let us consider OFDM transmission, where each of the M_t time-domain N-dimensional input vectors in $\mathbf{x}$ is generated by taking IDFT of an information-bearing vector, i.e.,

$$\mathbf{x} = \mathbf{Q}^{(\mathrm{Tx})H}\mathbf{X} \tag{5}$$

where[2] $\mathbf{Q}^{(\mathrm{Tx})} = \tilde{\mathbf{Q}} \otimes \mathbf{I}_{M_t}$ ($\otimes$ denotes the Kronecker product [17]), $\mathbf{I}_{M_t}$ is the identity matrix of dimension M_t, and $\tilde{\mathbf{Q}}(l,k) = 1/\sqrt{N}e^{-j(2\pi/N)lk}$ for $0 \leq l, k \leq N-1$ is the standard N-dimensional DFT matrix. We will first develop more detailed notation for the case $M_r = M_t = 1$, and then, the generalization would not be difficult.

[2]We denote complex matrix transpose with superscript H, complex conjugation by superscript $*$, and matrix transpose by superscript T.

Petitioner Samsung Ex-1004, 0156

We can write the output of the DFT at the receiver for a time-block $[-(\nu-1),\ldots,N-1]$ (where N is the number of carriers) as

$$Y(p) = G(p,p)X(p) + \sum_{\substack{q=0 \\ p\neq q}}^{N-1} G(p,q)X(q) + Z(p) \quad (6)$$

for $p = 0,\ldots,N-1$, where $Y(p)$, $X(p)$, and $Z(p)$ are the DFTs of $\{y(k)\}$, $\{x(k)\}$ and $\{z(k)\}$, respectively. We have also defined $G(p,q)$ as the (p,q)th element of $\mathbf{G} = \tilde{\mathbf{Q}}\bar{\mathbf{H}}^{(N)}\tilde{\mathbf{Q}}^H/N$. Here, $\tilde{\mathbf{Q}}$ is the DFT matrix defined as $\tilde{\mathbf{Q}}^H = [\mathbf{q}_0,\ldots\mathbf{q}_{N-1}]$ and $\mathbf{q}_s = 1/\sqrt{N}[1,\ldots,\exp(j2\pi s(N-1)/N)]^T$, and $\bar{\mathbf{H}}^{(N)}$ is the equivalent channel matrix including the effects of the cyclic prefix (used in OFDM) defined as (7), shown at the bottom of the page. We can easily evaluate $G(m,s)$ as

$$G(m,s) = \frac{1}{N}\sum_{r=0}^{N-1}\sum_{l=0}^{\nu-1} h(r;l)e^{j2\pi r(s-m)/N}e^{-j2\pi sl/N}. \quad (8)$$

Note that the form of the model in (6) is applicable to more general transmission scenarios than using OFDM. We can replace $\tilde{\mathbf{Q}}$ by any arbitrary matrix $\mathbf{B}$, and for a given structure of the guard interval (prefix), we can find the specific structure of $\mathbf{G}$ [as in (8) for OFDM] for that case.

In the case when we have transmit and receive diversities, we can modify (6) to

$$\mathbf{Y}(p) = \mathbf{G}(p,p)\mathbf{X}(p) + \sum_{\substack{q=0 \\ q\neq p}}^{N-1} \mathbf{G}(p,q)\mathbf{X}(q) + \mathbf{Z}(p) \quad (9)$$

where $[\mathbf{G}(p,q)]_{i,j} = [\tilde{\mathbf{Q}}\mathbf{H}^{(i,j)}\tilde{\mathbf{Q}}^H/N]_{p,q}$, $1 \le i \le M_r$, $1 \le j \le M_t$, $0 \le p \le N-1$, $0 \le q \le N-1$, and $\mathbf{H}^{(i,j)}$ is the equivalent channel matrix [as in (7)] for the time-varying ISI channel between the ith receiver and the jth transmitter, which is denoted by $\{h^{(i,j)}(k;l)\}$. In addition, the received vector for the pth frequency bin is $\mathbf{Y}(p) = [Y^{(1)}(p),\ldots,Y^{(M_r)}(p)]^T$, $\mathbf{X}(p) = [X^{(1)}(p),\ldots,X^{(M_t)}(p)]^T$ is the transmitted vector for the pth frequency bin, and $\mathbf{Z}(p) = [Z^{(1)}(p),\ldots,Z^{(M_r)}(p)]^T$ is the noise vector. We can rewrite (9) in compact form as

$$\mathbf{Y} = \mathbf{G}\mathbf{X} + \mathbf{Z} \quad (10)$$

where the (p,q)th block of $\mathbf{G}$ is given by $\mathbf{G}(p,q)$, $\mathbf{Y} = [\mathbf{Y}(0),\ldots,\mathbf{Y}(N-1)]^T \in \mathbb{C}^{N.M_r}$, $\mathbf{X} = [\mathbf{X}(0),\ldots,\mathbf{X}(N-1)]^T \in \mathbb{C}^{N.M_t}$, and $\mathbf{Z} = [\mathbf{Z}(0),\ldots,\mathbf{Z}(N-1)]^T \in \mathbb{C}^{N.M_r}$. We can also write the matrix $\mathbf{G}$ in more compact notation as

$$\mathbf{G} = \mathbf{Q}^{(\mathrm{Rx})}\mathbf{H}\mathbf{Q}^{(\mathrm{Tx})H} \quad (11)$$

where $\mathbf{Q}^{(\mathrm{Rx})} = \tilde{\mathbf{Q}}\otimes\mathbf{I}_{M_r}$, $\mathbf{Q}^{(\mathrm{Tx})} = \tilde{\mathbf{Q}}\otimes\mathbf{I}_{M_t}$, and $\mathbf{H}$ is obtained from (4).

III. ICI Analysis

We start with the data model given in (9)

$$\mathbf{Y}(m) = \mathbf{G}(m,m)\mathbf{X}(m) + \sum_{\substack{n=0 \\ n\neq m}}^{N-1} \mathbf{G}(m,n)\mathbf{X}(n) + \mathbf{Z}(m). \quad (12)$$

We are interested in finding the covariance matrix of the ICI (with noise) $\ddot{\mathbf{Z}}(m) = \mathbf{Z}_{\mathrm{ICI}}(m) + \mathbf{Z}(m)$, where $\mathbf{Z}_{\mathrm{ICI}}(n) = \sum_{\substack{m=0 \\ m\neq n}}^{N-1} \mathbf{G}(m,n)\mathbf{X}(n)$. In order to find the covariance of $\mathbf{Z}_{\mathrm{ICI}}(n)$, we need to make a few simplifying assumptions.

- Each channel $\{h^{(i,j)}(k;l)\}$ is modeled as a WSSUS channel, i.e., $\mathbb{E}[h^{(i,j)}(k;l)h^{(i,j)*}(k;n)] = \mathbb{E}[|h^{(i,j)}(k;l)|^2]\delta_{l-n}$. Moreover, the channel is modeled as a complex Gaussian stochastic process.
- The channel between the ith receiver and the jth transmitter is uncorrelated with the channel between the kth receiver and the lth transmitter when $i \neq k$ or $j \neq l$. That is, elements of $\mathbf{H}^{(i,j)}$ are uncorrelated with the elements of $\mathbf{H}^{(k,l)}$. Moreover, we assume that the channels $\{h^{(i,j)}(k;l)\}$ are identically distributed over $\{(i,j)\}$.

These statistical assumptions on the channel are *not* crucial, and the analysis can be accomplished without these assumptions. However, they do simplify the algebra and expose the important issues that we need to point out. Given these assumptions, we can make the following observation.

Fact III.1: The elements of the matrix $\mathbf{G}(m,n)$ are independent and identically distributed (i.i.d.) Gaussian random variables.

Proof: As $[\mathbf{G}(m,n)]_{i,j} = [\tilde{\mathbf{Q}}\mathbf{H}^{(i,j)}\tilde{\mathbf{Q}}^H/N]_{m,n}$, the elements of $\mathbf{G}(m,n)$ are i.i.d. complex Gaussian because the channels $\mathbf{H}^{(i,j)}$ are modeled as complex Gaussian and independent across the transmit and receive antennas. □

Given these statistical assumptions, we can now proceed to evaluate the covariance of $\mathbf{Z}_{\mathrm{ICI}}(n)$

$$\begin{aligned}\mathbb{E}[\mathbf{Z}_{\mathrm{ICI}}(n)\mathbf{Z}_{\mathrm{ICI}}^H(n)] &= \mathbb{E}\left[\sum_{\substack{p=0 \\ p\neq m}}^{N-1}\sum_{\substack{n=0 \\ n\neq m}}^{N-1} \mathbf{G}(m,p)\mathbf{X}(p)\mathbf{X}^H(n)\mathbf{G}^H(m,n)\right] \\ &= \sum_{\substack{p=0 \\ p\neq m}}^{N-1}\sum_{\substack{n=0 \\ n\neq m}}^{N-1} \mathbb{E}[\mathbf{G}(m,p)\mathbf{R}_{XX}(p,n)\mathbf{G}^H(m,n)] \quad (13)\end{aligned}$$

$$\bar{\mathbf{H}}^{(N)} = \begin{bmatrix} h(0;0) & 0 & \ldots & h(0;2) & h(0;1) \\ h(1;1) & h(1;0) & \ldots & h(1;3) & h(1;2) \\ \vdots & \vdots & \vdots & \vdots & \vdots \\ h(\nu-1;\nu-1) & h(\nu-1;\nu-2) & \vdots & 0 & 0 \\ \vdots & \vdots & \vdots & \vdots & \vdots \\ \vdots & \vdots & \vdots & h(N-2;0) & 0 \\ 0 & 0 & \ldots & h(N-1;1) & h(N-1;0) \end{bmatrix}. \quad (7)$$

Petitioner Samsung Ex-1004, 0157

where we have defined $\mathbf{R}_{XX}(p,n) = \mathbb{E}[\mathbf{X}(p)\mathbf{X}^H(n)]$. Equation (13) indicates that the basic component of the calculation is $\mathbb{E}[\mathbf{G}(m,p)\mathbf{R}_{XX}(p,n)\mathbf{G}^H(m,n)]$; this is what we focus on next.

We start from the observation that we can do an eigendecomposition of the signal covariance matrix as $\mathbf{R}_{XX}(p,n) = \mathbf{U}(p,n)\mathbf{\Lambda}_X(p,n)\mathbf{U}^H(p,n)$, where $\mathbf{U}(p,n)$ is a unitary matrix. From Fact III.1), the matrix $\mathbf{G}(m,p)$ has i.i.d. Gaussian elements (i.e., $\mathbf{G}(m,p)$ is isotropically distributed), which implies that the matrix $\mathbf{G}(m,p)\mathbf{U}(p,n)$ is distributionally equivalent to $\mathbf{G}(m,p)$ (note that if we apply a unitary transformation on an i.i.d. Gaussian matrix, the resultant matrix is also an i.i.d. Gaussian matrix with the same distribution). Hence, we can rewrite $\mathbb{E}[\mathbf{G}(m,p)\mathbf{R}_{XX}(p,n)\mathbf{G}^H(m,n)]$ in the following way:

$$\mathbb{E}[\mathbf{G}(m,p)\mathbf{R}_{XX}(p,n)\mathbf{G}^H(m,n)] = \mathbb{E}[\mathbf{G}(m,p)\mathbf{\Lambda}_X(p,n)\mathbf{G}^H(m,n)] \quad (14)$$

where $\mathbf{\Lambda}_X(p,n) = \mathrm{diag}(\lambda_1(p,n),\ldots,\lambda_{M_t}(p,n))$ is a diagonal matrix of the eigenvalues of $\mathbf{R}_{XX}(p,n)$.

Now, let us examine the elements of the matrix given in (14). The (r,s)th element is

$$\begin{aligned}\left\{\mathbb{E}[\mathbf{G}(m,p)\mathbf{\Lambda}_X(p,n)\mathbf{G}^H(m,n)]\right\}_{r,s} &= \sum_{k=1}^{M_t}\lambda_k(p,n)\mathbb{E}\left[\left\{\mathbf{G}(m,p)\right\}_{r,k}\left\{\mathbf{G}^H(m,n)\right\}_{k,s}\right] \\ &\overset{(a)}{=} \sum_{k=1}^{M_t}\lambda_k(p,n)\mathbb{E} \\ &\quad\times\left[\left\{\mathbf{G}(m,p)\right\}_{r,k}\left\{\mathbf{G}^H(m,n)\right\}_{k,r}\right]\delta_{r-s} \end{aligned} \quad (15)$$

where (a) is due to the assumption that the channels on different links are uncorrelated[3]. Hence, the component matrices $\mathbb{E}[\mathbf{G}(m,p)\mathbf{R}_{XX}(p,n)\mathbf{G}^H(m,n)]$ are diagonal (a direct result of the fact that the channels are modeled as being spatially white).

Using the WSSUS modeling assumption and using the Fourier basis, we can write

$$\begin{aligned}\mathbb{E}\left[\left\{\mathbf{G}(m,p)\right\}_{r,k}\left\{\mathbf{G}^H(m,n)\right\}_{k,r}\right] &= \frac{1}{N^2}\left(\sum_{l=0}^{\nu-1}e^{-j2\pi l(p-n)/N}\right) \\ &\quad\times\sum_{r_1=0}^{N-1}\sum_{r_2=0}^{N-1}r_{hh}(r_1-r_2)e^{j2\pi r_1(p-m)/N}e^{-j2\pi r_2(n-m)/N}\end{aligned} \quad (16)$$

where we have defined $r_{hh}(r_1-r_2) = \mathbb{E}[h^{(k,r)}(r_1;l)\,h^{(k,r)*}(r_2;l)]$.

[3]This can be seen from the fact that $[\mathbf{G}(m,p)]_{r,k} = [\tilde{\mathbf{Q}}\mathbf{H}^{(r,k)}\tilde{\mathbf{Q}}^H/N]_{m,p}$ and $[\mathbf{G}^H(m,n)]_{k,s} = [\tilde{\mathbf{Q}}\mathbf{H}^{(s,k)H}\tilde{\mathbf{Q}}^H/N]_{m,n}$, which shows that if $r \neq s$, then $[\mathbf{G}(m,p)]_{r,k}$ and $[\mathbf{G}^H(m,n)]_{k,s}$ are uncorrelated.

Consequently, as the channels are spatially independent, we can write the covariance matrix of the ICI as

$$\begin{aligned}\mathbb{E}\left[\mathbf{Z}_{\mathrm{ICI}}(n)\mathbf{Z}_{\mathrm{ICI}}^H(n)\right] &= \sum_{\substack{p=0\\p\neq n}}^{N-1}\sum_{\substack{m=0\\m\neq n}}^{N-1}\frac{\mathrm{tr}(\mathbf{\Lambda}_X(p,n))}{N^2}\left(\sum_{l=0}^{\nu-1}e^{-j2\pi l(p-n)/N}\right) \\ &\quad\times\left(\sum_{r_1=0}^{N-1}\sum_{r_2=0}^{N-1}r_{hh}(r_1-r_2)\right. \\ &\quad\left.\times e^{j2\pi r_1(p-m/N)}e^{-j2\pi r_2(n-m/N)}\right)\mathbf{I}\end{aligned}$$

where tr(.) denotes the trace of a matrix.

This analysis points to a few issues worth noting.

- The ICI is accentuated with the presence of multiple transmit antennas (i.e., $M_t > 1$).
- The covariance of the ICI is spatially white in (17) due to the assumption that the channel matrices $\mathbf{H}^{(i,j)}$ were assumed to be so. We can analyze spatial correlation with similar techniques, but the expressions turn out to be a little more complicated without adding much more insight.
- Multiple-receive antennas could be used to mitigate the ICI. For example, the ICI term in (12) can be seen as interference, and hence, using multiple receive-antennas, we can do either zero-forcing or MMSE interference suppression purely in the spatial domain [18]. However, this might require many receive antennas, depending on the amount of dominant ICI. In order to also utilize the additional available degrees of freedom (dimensions) in the time domain, we examine next a combined time and spatial domain approach.

IV. Time-Domain ICI Mitigation Technique

Henceforth, we focus on the case $M_t = M_r = M$ as it brings out the essential ideas without unduly complicating the algebra. Extending the analysis to the general case is straightforward. Therefore, as $M_r = M_t = M$, for notational convenience using (11), we write $\mathbf{Q} = \mathbf{Q}^{(\mathrm{Rx})} = \mathbf{Q}^{(\mathrm{Tx})}$.

To combat ICI, the length-NM received vector $\mathbf{y}$ is multiplied by an $NM \times NM$ matrix (corresponding to an NM-tap time-varying filter) $\mathbf{W}$ resulting in

$$\tilde{\mathbf{y}} = \mathbf{W}\mathbf{y} = \mathbf{W}(\mathbf{H}\mathbf{x}+\mathbf{z}) = \mathbf{W}\mathbf{H}\mathbf{x}+\tilde{\mathbf{z}} \quad (17)$$

where the colored noise vector $\tilde{\mathbf{z}}$ has auto-correlation matrix $\mathbf{R}_{\tilde{z}\tilde{z}} = \sigma_z^2\mathbf{W}\mathbf{W}^H$. Taking the DFT of both sides of (17), we get

$$\begin{aligned}\tilde{\mathbf{Y}} &\overset{\mathrm{def}}{=} \mathbf{Q}\tilde{\mathbf{y}} = \mathbf{Q}\mathbf{W}\mathbf{H}\mathbf{Q}^H\mathbf{X}+\mathbf{Q}\tilde{\mathbf{z}} \\ &\overset{\mathrm{def}}{=} \tilde{\mathbf{G}}\mathbf{X}+\tilde{\mathbf{Z}}.\end{aligned} \quad (18)$$

Note here that $\tilde{\mathbf{G}}$ captures the effect of filtering with $\mathbf{W}$. In contrast, in (10), $\mathbf{G}$ captures the effects of ICI before the filtering operation. Next, we show how to design linear ICI-cancellation

Petitioner Samsung Ex-1004, 0158

filters for OFDM. We start with the SISO case ($M = 1$) and then extend the design to the MIMO case.

A. Optimum Linear ICI-Cancellation Filter for SISO OFDM

Using (18), we can express the SINR at the mth frequency bin ($1 \leq m \leq N$) as follows [19]:

$$\text{SINR}_m = \frac{E_{x,m}|\bar{\mathbf{G}}(m,m)|^2}{\frac{1}{N}\text{tr}(\mathbf{R}_{\tilde{z}\tilde{z}}) + \sum_{n\neq m} E_{x,n}|\bar{\mathbf{G}}(m,n)|^2} \tag{19}$$

where $E_{x,n}$ is the input energy allocated to the nth frequency bin. We assume that the channel is unknown at the transmitter. Therefore, the total input energy $E_{x,\text{tot}}$ is divided equally across all frequency bins, i.e., $E_{x,n} = (E_{x,\text{tot}}/N) \stackrel{\text{def}}{=} E_x$. Under this assumption and defining $\mathbf{e}_i$ to be the ith unit vector, (19) becomes

$$\begin{aligned}
&\text{SINR}_m \\
&= \frac{E_x \left|\mathbf{e}_m^H \bar{\mathbf{G}} \mathbf{e}_m\right|^2}{\frac{\sigma_z^2}{N}\text{tr}(\mathbf{W}\mathbf{W}^H) + E_x \sum_{n\neq m} \left|\mathbf{e}_m^H \bar{\mathbf{G}} \mathbf{e}_n\right|^2} \\
&= \frac{\mathbf{e}_m^H \mathbf{Q}\mathbf{W}\mathbf{H}\mathbf{Q}^H \mathbf{e}_m \mathbf{e}_m^H \mathbf{Q}\mathbf{H}^H \mathbf{W}^H \mathbf{Q}^H \mathbf{e}_m}{\frac{1}{\text{SNR}} + \mathbf{e}_m^H \mathbf{Q}\mathbf{W}\mathbf{H}\mathbf{Q}^H \left(\sum_{n\neq m} \mathbf{e}_n \mathbf{e}_n^H\right) \mathbf{Q}\mathbf{H}^H \mathbf{W}^H \mathbf{Q}^H \mathbf{e}_m} \\
&= \frac{\mathbf{q}_m^H \mathbf{W}\mathbf{h}_m \mathbf{h}_m^H \mathbf{W}^H \mathbf{q}_m}{\frac{1}{\text{SNR}} + \mathbf{q}_m^H \mathbf{W}\mathbf{H}\left(\mathbf{I}_N - \mathbf{q}_m\mathbf{q}_m^H\right)\mathbf{H}^H \mathbf{W}^H \mathbf{q}_m} \\
&= \frac{\mathbf{w}_m^H \mathbf{h}_m \mathbf{h}_m^H \mathbf{w}_m}{\mathbf{w}_m^H \left(\frac{1}{\text{SNR}}\mathbf{I}_N + \mathbf{R}_m\right)\mathbf{w}_m}
\end{aligned} \tag{20}$$

where we have defined $\text{SNR} = E_x/\sigma_z^2$, $\mathbf{q}_m \stackrel{\text{def}}{=} \mathbf{Q}^H \mathbf{e}_m$, $\mathbf{h}_m = \mathbf{H}\mathbf{q}_m$, $\mathbf{w}_m = \mathbf{W}^H \mathbf{q}_m$, and $\mathbf{R}_m = \mathbf{H}\mathbf{Q}^H(\mathbf{I}_N - \mathbf{e}_m\mathbf{e}_m^H)\mathbf{Q}\mathbf{H}^H = \mathbf{H}\mathbf{H}^H - \mathbf{h}_m\mathbf{h}_m^H$. Furthermore, we assumed that $\mathbf{w}_m^H\mathbf{w}_m = 1$ for $1 \leq m \leq N$, which implies that $\text{tr}(\mathbf{W}\mathbf{W}^H) = \sum_{m=1}^N \mathbf{w}_m^H\mathbf{w}_m = N$.

The achievable bit rate in an OFDM system is (approximately) given by [19]

$$\text{Rate} = \left[\sum_{m=1}^{N} \log_2\left(1 + \frac{\text{SINR}_m}{\Gamma}\right)\right] \tag{21}$$

where $\Gamma \approx (\gamma_m/3\gamma_c)(Q^{-1}(P_e/N_e))^2$ is the *SNR gap* (assumed the same for all frequency bins), the Q-function is defined by $Q(x) = \int_x^\infty e^{-x^2/2}dx$, and γ_m and γ_c denote the desired performance margin and overall coding gain, respectively. Furthermore, P_e and N_e are the target probability of error and the number of nearest neighbors in the used signal constellation, respectively. It is clear from (21) that optimizing $\mathbf{w}_m$ (and hence $\mathbf{W}$) in (20) to maximize SINR_m also maximizes the bit rate in (21).

We have the following optimization problem:

$$\begin{aligned}
&\max_{\mathbf{w}_m} \mathbf{w}_m^H \mathbf{h}_m \mathbf{h}_m^H \mathbf{w}_m \\
&\quad \text{subject to } \mathbf{w}_m^H \left(\frac{1}{\text{SNR}}\mathbf{I} + \mathbf{R}_m\right)\mathbf{w}_m = 1 \\
&\quad \text{and } \mathbf{w}_m^H \mathbf{w}_m = 1.
\end{aligned}$$

This is a standard *generalized eigenvalue problem* whose solution is determined as follows.

1) Define the Cholesky factorization $\tilde{\mathbf{R}}_m \stackrel{\text{def}}{=} (1/SNR)\mathbf{I} + \mathbf{R}_m \stackrel{\text{def}}{=} \mathbf{L}\mathbf{L}^H$.
2) Compute the *dominant* eigenvector (call it $\mathbf{v}_1$) of the matrix $\mathbf{L}^{-1}\mathbf{h}_m\mathbf{h}_m^H\mathbf{L}^{-H}$. Now, since the matrix $\mathbf{h}_m\mathbf{h}_m^H$ is rank-1, it can be shown that $\mathbf{v}_1 = \alpha\mathbf{L}^{-1}\mathbf{h}_m$, where α is a constant that makes $\mathbf{v}_1$ a unit-norm vector.
3) Compute $\mathbf{w}_{m,\text{opt}} = \mathbf{L}^{-H}\mathbf{v}_1 = \beta\tilde{\mathbf{R}}_m^{-1}\mathbf{h}_m$, where the constant β is chosen to make $\mathbf{w}_{m,\text{opt}}$ a unit-norm vector.
4) The corresponding optimum SINR for the mth frequency bin is

$$\text{SINR}_{m,\text{opt}} = \mathbf{h}_m^H \tilde{\mathbf{R}}_m^{-1} \mathbf{h}_m. \tag{22}$$

B. Alternative Form

We can avoid the need to compute $\tilde{\mathbf{R}}_m^{-1}$ for each m as follows. Using the matrix inversion lemma, we can write

$$\begin{aligned}
\tilde{\mathbf{R}}_m &= \frac{1}{\text{SNR}}\mathbf{I} + \mathbf{R}_m = \frac{1}{\text{SNR}}\mathbf{I} + \mathbf{H}\mathbf{H}^H - \mathbf{h}_m\mathbf{h}_m^H \\
&\stackrel{\text{def}}{=} \mathbf{R}_{yy} - \mathbf{h}_m\mathbf{h}_m^H \\
\Rightarrow \tilde{\mathbf{R}}_m^{-1} &= \left(\frac{1}{\text{SNR}}\mathbf{I} + \mathbf{R}_m\right)^{-1} \\
&= \mathbf{R}_{yy}^{-1}\left(\mathbf{I} + \frac{\mathbf{h}_m\mathbf{h}_m^H\mathbf{R}_{yy}^{-1}}{\left(1 - \mathbf{h}_m^H\mathbf{R}_{yy}^{-1}\mathbf{h}_m\right)}\right).
\end{aligned}$$

Therefore, only one inverse, namely, that of the output autocorrelation matrix $\mathbf{R}_{yy}$, needs to be computed. In summary, the optimum filters $\mathbf{w}_{m,\text{opt}}$ are computed as follows.

1) Compute $\mathbf{R}_{yy}^{-1}$ (using channel estimates obtained with pilot tones and interpolation or using an ensemble average from several received vectors $\mathbf{y}$).
2) For each frequency bin $1 \leq m \leq N$, compute the following.
   a) $\tilde{\mathbf{w}}_m = \mathbf{R}_{yy}^{-1}\mathbf{h}_m$.
   b) $\mathbf{w}_{m,\text{opt}} = \tilde{\mathbf{w}}_m/|\tilde{\mathbf{w}}_m|$.
   c) The corresponding optimum SINR for mth frequency bin is

$$\text{SINR}_{m,\text{opt}} = \frac{\mathbf{h}_m^H\mathbf{R}_{yy}^{-1}\mathbf{h}_m}{\left(1 - \mathbf{h}_m^H\mathbf{R}_{yy}^{-1}\mathbf{h}_m\right)}. \tag{23}$$

Finally, we note that computational complexity can be further reduced using a low-rank approximation of $\mathbf{R}_{yy}$ (this technique has been used in [20] as part of the channel estimation process).

C. ICI Cancellation Filter for MIMO OFDM

We can express the SINR for the jth transmit antenna and the kth frequency bin, which is denoted by SINR_k^j, in MIMO OFDM as in (24), shown at the bottom of the next page.[4] Assuming that $\mathbf{w}_l^H\mathbf{w}_l = 1$ for $1 \leq l \leq MN$, we have $\sum_{r=1}^M \mathbf{w}_{kM+r}^H\mathbf{w}_{kM+r} = M$, and hence, $\text{tr}(\mathbf{W}\mathbf{W}^H) = NM$.

[4]Note that in the MIMO case, we define intercarrier interference to include interference from all other frequency bins for the same antenna and interference from all frequency bins (including kth) for other antennas.

Petitioner Samsung Ex-1004, 0159

Therefore, (24) becomes [using (18)] the second equation at the bottom of the page, where we have defined $\mathbf{q}_i = \mathbf{Q}^H\mathbf{e}_i$, $\mathbf{h}_i = \mathbf{H}\mathbf{q}_i$, and $\mathbf{w}_i = \mathbf{W}^H\mathbf{q}_i$. If we further define $\tilde{\mathbf{R}}_{kj} = (1/M.\text{SNR})\mathbf{I}_{NM} + \mathbf{H}\mathbf{H}^H - \mathbf{h}_{kM+j}\mathbf{h}_{kM+j}^H$ and $\bar{\mathbf{R}}_{kj} = \mathbf{h}_{kM+j}\mathbf{h}_{kM+j}^H$, we get

$$\begin{aligned}\text{SINR}_k^j &= \frac{\sum_{r=1}^{M}\mathbf{w}_{kM+r}^H\bar{\mathbf{R}}_{kj}\mathbf{w}_{kM+r}}{\sum_{r=1}^{M}\mathbf{w}_{kM+r}^H\tilde{\mathbf{R}}_{kj}\mathbf{w}_k} \\ &= \frac{\tilde{\mathbf{w}}_k^H\bar{\mathbf{R}}_{kj}\tilde{\mathbf{w}}_k}{\tilde{\mathbf{w}}_k^H\tilde{\mathbf{R}}_{kj}\tilde{\mathbf{w}}_k}\end{aligned}$$

where we have made the definitions $\bar{\mathbf{R}} = \text{diag}(\underbrace{\bar{\mathbf{R}}_{kj},\ldots,\bar{\mathbf{R}}_{kj}}_{M})$, $\tilde{\mathbf{R}} = \text{diag}(\underbrace{\tilde{\mathbf{R}}_{kj},\ldots,\tilde{\mathbf{R}}_{kj}}_{M})$, and $\tilde{\mathbf{w}}_k^H = \underbrace{\begin{bmatrix}\mathbf{w}_{kM+1}^H & \mathbf{w}_{kM+2}^H & \cdots & \mathbf{w}_{(k+1)M}^H\end{bmatrix}}_{M}$. It can be shown that SINR_k^j is maximized by the filters

$$\begin{aligned}\mathbf{w}_{kM+r,\text{opt}} &= \alpha\mathbf{R}_{yy}^{-1}\mathbf{h}_{kM+r}\text{: for } 0 \le k \le N-1 \\ &\quad 1 \le r \le M\end{aligned} \tag{25}$$

where α is a normalizing constant, and $\mathbf{R}_{yy} = (1/M.SNR)\mathbf{I}_{NM} + \mathbf{H}\mathbf{H}^H$. Finally, the optimum filter $\mathbf{W}_{\text{opt}}$ is given by

$$\mathbf{W}_{\text{opt}} = \mathbf{Q}^H\begin{bmatrix}\mathbf{w}_{1,\text{opt}}^H \\ \mathbf{w}_{2,\text{opt}}^H \\ \vdots \\ \mathbf{w}_{NM,\text{opt}}^H\end{bmatrix}.$$

It is worth emphasizing that the filter $\mathbf{W}_{\text{opt}}$ calculated above performs joint intercarrier and interantenna interference suppression. With zero Doppler, the matrix $\mathbf{H}$ will be *block circulant*; hence, the matrix $\mathbf{QHQ}^H$ will be *block diagonal* (i.e., interantenna interference is still present). However, the matrix $\mathbf{QW}_{\text{opt}}\mathbf{HQ}^H$ will be (approximately) *diagonal*, indicating that the matrix filter $\mathbf{W}_{\text{opt}}$ in this case acts also as a linear "multiuser" detector that suppresses interantenna interference.

D. Space-Time-Coded OFDM

In this section, we will explore a special case of coded MIMO OFDM, namely, a space-time block-coded OFDM with two transmit and one receive antennas, i.e., $M_t = 2$ and $M_r = 1$ (the analysis can be extended to the case $M_t > 2$ and $M_r > 1$). We study a space-time block-coded OFDM system based on

$$\begin{aligned}\text{SINR}_k^j &= \frac{E_x\sum_{r=1}^{M}|\bar{\mathbf{G}}(kM+r,kM+j)|^2}{\frac{1}{NM}\text{tr}(\mathbf{R}_{\tilde{z}\tilde{z}}) + E_x\sum_{r=1}^{M}\sum_{i=1,i\neq kM+j}^{MN}|\bar{\mathbf{G}}(kM+r,i)|^2} \\ &= \frac{\sum_{r=1}^{M}\left|\mathbf{e}_{kM+r}^H\bar{\mathbf{G}}\mathbf{e}_{kM+j}\right|^2}{\left(\frac{1}{\text{SNR}}\right)\left(\frac{1}{NM}\right)\text{tr}(\mathbf{W}\mathbf{W}^H) + \sum_{r=1}^{M}\sum_{i=1,i\neq kM+j}^{MN}\left|\mathbf{e}_{kM+r}^H\bar{\mathbf{G}}\mathbf{e}_i\right|^2}.\end{aligned} \tag{24}$$

$$\begin{aligned}\text{SINR}_k^j &= \frac{\sum_{r=1}^{M}\mathbf{e}_{kM+r}^H\mathbf{QWHQ}^H\mathbf{e}_{kM+j}\mathbf{e}_{kM+j}^H\mathbf{QH}^H\mathbf{W}^H\mathbf{Q}^H\mathbf{e}_{kM+r}}{\frac{1}{\text{SNR}} + \sum_{r=1}^{M}\mathbf{e}_{kM+r}^H\mathbf{QWHQ}^H\left(\sum_{i=1,i\neq kM+j}^{MN}\mathbf{e}_i\mathbf{e}_i^H\right)\mathbf{QH}^H\mathbf{W}^H\mathbf{Q}^H\mathbf{e}_{kM+r}} \\ &= \frac{\sum_{r=1}^{M}\mathbf{q}_{kM+r}^H\mathbf{W}\mathbf{h}_{kM+j}\mathbf{h}_{kM+j}^H\mathbf{W}^H\mathbf{q}_{kM+r}}{\frac{1}{\text{SNR}} + \sum_{r=1}^{M}\mathbf{q}_{kM+r}^H\mathbf{WH}\left(\mathbf{I}_N - \mathbf{q}_{kM+j}\mathbf{q}_{kM+j}^H\right)\mathbf{H}^H\mathbf{W}^H\mathbf{q}_{kM+r}} \\ &= \frac{\sum_{r=1}^{M}\mathbf{w}_{kM+r}^H\mathbf{h}_{kM+j}\mathbf{h}_{kM+j}^H\mathbf{w}_{kM+r}}{\frac{1}{SNR} + \sum_{r=1}^{M}\mathbf{w}_{kM+r}^H\left(\mathbf{H}\mathbf{H}^H - \mathbf{h}_{kM+j}\mathbf{h}_{kM+j}^H\right)\mathbf{w}_{kM+r}} \\ &= \frac{\sum_{r=1}^{M}\mathbf{w}_{kM+r}^H\mathbf{h}_{kM+j}\mathbf{h}_{kM+j}^H\mathbf{w}_{kM+r}}{\sum_{r=1}^{M}\mathbf{w}_{kM+r}^H\left(\frac{1}{M.SNR}\mathbf{I}_{NM} + \mathbf{H}\mathbf{H}^H - \mathbf{h}_{kM+j}\mathbf{h}_{kM+j}^H\right)\mathbf{w}_{kM+r}},\end{aligned}$$

Petitioner Samsung Ex-1004, 0160

the the Alamouti code [21] (as first proposed in [22]); although details can be found in [22], the basic mechanism is as follows. We consider two source symbols $c_1(m)$ and $c_2(m)$, which, in a conventional OFDM system, would be transmitted over two consecutive OFDM blocks on the same subcarrier m. Similar to the Alamouti code, the two source symbols are mapped as

$$\begin{aligned}\mathbf{X}_{(1)}(m) &= [c_1(m), c_2(m)]^T \\ \mathbf{X}_{(2)}(m) &= [-c_2^*(m), c_1^*(m)]^T \end{aligned} \tag{26}$$

where $\mathbf{X}_{(1)}$ represents the information-bearing vector for the first OFDM block, and $\mathbf{X}_{(2)}$ corresponds to the second OFDM block[5].

Our goal is to understand the effect of channel time-variation over such a transmission scheme and the performance of optimal MMSE receiver structures. Using (12), we can write the output of two consecutive OFDM blocks as

$$\begin{aligned}\mathbf{Y}_{(1)}(m) &= \mathbf{G}_{(1)}(m,m)\mathbf{X}_{(1)}(m) \\ &\quad + \sum_{\substack{n=0 \\ n\neq m}}^{N-1} \mathbf{G}_{(1)}(m,n)\mathbf{X}_{(1)}(n) + \mathbf{Z}_{(1)}(m) \quad (27a) \\ \mathbf{Y}_{(2)}(m) &= \mathbf{G}_{(2)}(m,m)\mathbf{X}_{(2)}(m) \\ &\quad + \sum_{\substack{n=0 \\ n\neq m}}^{N-1} \mathbf{G}_{(2)}(m,n)\mathbf{X}_{(2)}(n) + \mathbf{Z}_{(2)}(m) \quad (27b)\end{aligned}$$

and, with the aid of (26), obtain

$$\begin{aligned}\begin{bmatrix} \mathbf{Y}_{(1)}(m) \\ \mathbf{Y}_{(2)}{}^*(m) \end{bmatrix} &= \begin{bmatrix} [\mathbf{G}_{(1)}(m,m)]_{1,1} & [\mathbf{G}_{(1)}(m,m)]_{1,2} \\ [\mathbf{G}_{(2)}(m,m)]_{1,2}^* & -[\mathbf{G}_{(2)}(m,m)]_{1,1}^* \end{bmatrix} \\ &\quad \times \begin{bmatrix} c_1(m) \\ c_2(m) \end{bmatrix} \\ &\quad + \sum_{\substack{n=0 \\ n\neq m}}^{N-1} \begin{bmatrix} [\mathbf{G}_{(1)}(m,n)]_{1,1} & [\mathbf{G}_{(1)}(m,n)]_{1,2} \\ [\mathbf{G}_{(2)}(m,n)]_{1,2}^* & -[\mathbf{G}_{(2)}(m,n)]_{1,1}^* \end{bmatrix} \\ &\quad \times \begin{bmatrix} c_1(n) \\ c_2(n) \end{bmatrix} + \begin{bmatrix} \mathbf{Z}_{(1)}(m) \\ \mathbf{Z}_{(2)}^*(m) \end{bmatrix} \end{aligned} \tag{28}$$

which can be written as

$$\mathbf{Y}(m) \stackrel{\text{def}}{=} \mathbf{G}(m,m)\mathbf{c}(m) + \sum_{n=0, n\neq m}^{N-1} \mathbf{G}(m,n)\mathbf{c}(n) + \mathbf{Z}(m).$$

Now, it can be seen that the mathematical structure of the Alamouti-coded OFDM is identical to that of the MIMO OFDM (with ICI) structure defined in (12), and therefore, the MMSE analysis done in Section IV-C carries through with the appropriate interpretations of notation. Furthermore, the derivation of the optimum linear MIMO ICI cancellation filter $\mathbf{W}$ is straightforward (by applying the results of Section IV-C). In this case, $\mathbf{W}$ is a $2N \times 2N$ matrix as it processes $2N$ tones over $2N$ symbol durations.

[5]Intuitively, each OFDM subcarrier can be thought of as a flat-fading channel, and the Alamouti code is applied to each of the OFDM subcarriers. As a result, the Alamouti code yields diversity gains at every subcarrier.

Computational complexity can be reduced by defining a per-tone 2×2 filter $\mathbf{W}_m$ that suboptimally attempts to minimize ICI by processing only $\mathbf{Y}_{(1)}(m)$ and $\mathbf{Y}_{(2)}(m)$. With time-invariant channels, and in the absence of noise, it can be seen that $\mathbf{W}_m$ reduces to

$$\mathbf{W}_m = \begin{bmatrix} [\mathbf{G}_{(1)}(m,m)]_{1,1} & [\mathbf{G}_{(1)}(m,m)]_{1,2} \\ [\mathbf{G}_{(2)}(m,m)]_{1,2}^* & -[\mathbf{G}_{(2)}(m,m)]_{1,1}^* \end{bmatrix}^*$$

which coincides with the Alamouti-decoding matrix. Note that with time-invariant channels, in (28), all "off-diagonal" terms become zero, $[\mathbf{G}_{(1)}(m,m)]_{1,1} = [\mathbf{G}_{(2)}(m,m)]_{1,1}$, and $[\mathbf{G}_{(1)}(m,m)]_{1,2} = [\mathbf{G}_{(2)}(m,m)]_{1,2}$.

V. Channel Estimation and Tracking

In this section, we address the challenging problem of channel estimation in an OFDM system with severe Doppler and we propose a promising technique based on channel interpolation and judiciously-placed pilot tones. Throughout this section, we assume $M_r = M_t = 1$.

In a time-varying environment, estimation of $\mathbf{H}$ amounts to estimating N channels $\mathbf{h}_n := [h(n;0), \ldots, h(n;\nu-1)]^T$, $0 \leq n \leq N-1$ that comprise the rows of $\mathbf{H}$; in other words, we need to estimate $N\nu$ parameters. This number of parameters can be significantly reduced if *a priori* knowledge about the channel dynamics is available (see, e.g., [23]), or if it is assumed that the channel is quasistatic (i.e., constant within an OFDM block, but varying from block to block). Although it has been shown that the aforementioned methods have provided promising results, both of them rely on assumptions that do not necessarily hold true in the OFDM environment considered in this work. On the one hand, we have made no assumptions about the underlying channel structure; on the other hand, our work addresses scenarios where there is significant ICI, and as a result, the channel cannot be assumed quasistatic.

Given the minimal set of assumptions on the structure of the underlying channel, the estimation of $\mathbf{H}$ appears, at first sight, to be a daunting task. Even when a full training block is used (in other words, all OFDM subcarriers are pilot tones), we have available only N values for the estimation of $N\nu$ parameters. To reduce the number of parameters needed for channel estimation from $N\nu$ to less than N, we make the reasonable assumption that some of the channels $\mathbf{h}_n$ can be obtained by linear interpolation. Such an assumption holds true if there is not significant variation between channels $\mathbf{h}_n$ and $\mathbf{h}_{n+1}$, $0 \leq n \leq (N-2)$, and as we illustrate later on, channel interpolation does not have a significant negative impact on the achievable performance of our methods. Furthermore, channel interpolation transforms a seemingly very difficult problem to a tractable one, as we will shortly see.

The basic idea of using interpolation to reduce the number of parameters is as follows. We parameterize the matrix $\mathbf{H}$ by using a small number of its rows. We then express the entire matrix as a function of these rows, therefore reducing the number of parameters to be estimated. Physically, this puts "markers" in time where the channel is estimated, and the estimates at other times are interpolated using these estimates. Let us consider M channels $\mathbf{h}_{n(1)}, \ldots, \mathbf{h}_{n(M)}$, which form M rows of the channel

Petitioner Samsung Ex-1004, 0161

Suppose $N = 3$, $\nu = 2$, $\mathcal{M} = \{0, 2\}$, $\mathbf{a}_2 = (0.3, 0.7)^T$. Then, $\tilde{\mathbf{H}}$ is given by

$$\begin{bmatrix} h(0;0) & 0 & h(0;1) \\ .3h(0;1)+.7h(2;1) & .3h(0;0)+.7h(2;0) & 0 \\ 0 & h(2;1) & h(2;0) \end{bmatrix} = \begin{bmatrix} 1 & 0 & 0 \\ 0 & .3 & 0 \\ 0 & 0 & 0 \end{bmatrix} \begin{bmatrix} h(0;0) & 0 & h(0;1) \\ h(0;1) & h(0;0) & 0 \\ 0 & h(0;1) & h(0;0) \end{bmatrix} + \begin{bmatrix} 0 & 0 & 0 \\ 0 & .7 & 0 \\ 0 & 0 & 1 \end{bmatrix} \begin{bmatrix} h(2;0) & 0 & h(2;1) \\ h(2;1) & h(2;0) & 0 \\ 0 & h(2;1) & h(2;0) \end{bmatrix}$$

and $\mathbf{H}$, $\tilde{\mathbf{H}}$ differ only in the second "interpolated" row.

Fig. 1. Example of interpolated matrix.

matrix $\mathbf{H}$; let us denote by $\mathcal{M} := \{m(1), \ldots, m(M)\}$ the set of these rows. Our method is based on the assumption that each channel $\mathbf{h}_n$, $n \notin \mathcal{M}$ can be expressed as a linear combination of the M channels $\mathbf{h}_{m(1)}, \ldots, \mathbf{h}_{m(M)}$, i.e.,

$$h(n;l) = \mathbf{a}_n^T [h(m(1);l), \ldots, h(m(M);l)]^T \quad 0 \le l \le \nu - 1. \tag{29}$$

For example, when the channel process $\{\mathbf{h}_n\}$ is Gaussian, then such a linear interpolation is optimal in the MMSE sense. Note that in (29), we have used the same $M \times 1$ weight vector $\mathbf{a}_n$ for all of the ν-channel taps of $\mathbf{h}_n$. Using the same weight vector is a direct consequence of the assumption that $h(n;0), \ldots, h(n;\nu-1)$ are i.i.d. processes for every n (but there is correlation between $h(n;l)$ and $h(m;l)$ for $n \neq m$).

In Section V-C , we present guidelines on the choice of the weight vectors $\mathbf{a}_n$s. In Section V-A , we study how channel estimation can be accomplished using pilot tones.

A. Channel Estimation Using Pilot Tones

Let us denote by $H_C(\mathbf{h}_m)$ the $N \times N$ circulant matrix that we would have in the OFDM system if the underlying channel was fixed and equal to $\mathbf{h}_m$, i.e., we have (30), shown at the bottom of the page. Using (29), we can see that the channel matrix $\tilde{\mathbf{H}}$ obtained by the interpolation of the channels $\mathbf{h}_m(1), \ldots, \mathbf{h}_m(M)$ is

$$\tilde{\mathbf{H}} = \sum_{1 \le i \le M} \mathbf{A}_{m(i)} H_C(\mathbf{h}_{m(i)}) \tag{31}$$

where $\mathbf{A}_{m(i)}$ is an $N \times N$ diagonal matrix with entries

$$[\mathbf{A}_{m(i)}]_{n,n} = \begin{cases} 1, & n = m(i) \\ 0, & n \in \mathcal{M} \text{ and } n \neq m(i) \\ a_n(m(i)), & \text{otherwise.} \end{cases} \tag{32}$$

An example of this formulation is given in Fig. 1.

Given the structured form of $\tilde{\mathbf{H}}$, its estimation amounts to estimating $M\nu$ parameters grouped in the $M\nu \times 1$ vector

$$\tilde{\mathbf{h}} := \left[\mathbf{h}_{m(1)}^T, \ldots, \mathbf{h}_{m(M)}^T\right]^T. \tag{33}$$

To perform channel estimation using pilot tones, we need to express $\tilde{G}(m,s) := [\mathbf{Q}\tilde{\mathbf{H}}\mathbf{Q}^H]_{m,s}$ as a function of $\tilde{\mathbf{h}}$. From (31), we can express $\tilde{G}(m,s)$ as

$$\tilde{G}(m,s) = \sum_{1 \le i \le M} \left[\mathbf{Q}\mathbf{A}_{m(i)} H_C(\mathbf{h}_{m(i)}) \mathbf{Q}^H\right]_{m,s}. \tag{34}$$

We can easily evaluate

$$[\mathbf{Q}\mathbf{A}_{m(i)} H_C(\mathbf{h}_{m(i)}) \mathbf{Q}^H]_{m,s} = \frac{1}{N} \sum_{r=0}^{N-1} \sum_{l=0}^{\nu-1} [\mathbf{A}_{m(i)}]_{r,r} h(m(i);l) \times e^{j(2\pi r(s-m)/N)} e^{-j(2\pi s l/N)} \tag{35}$$

which implies that $h(m(i);l)$ is scaled by

$$b_{m(i)}^{m,s}(l) := e^{-j(2\pi s l/N)} \frac{1}{N} \sum_{r=0}^{N-1} [\mathbf{A}_{m(i)}]_{r,r} e^{j(2\pi r(s-m)/N)}. \tag{36}$$

$$H_C(\mathbf{h}_m) := \begin{bmatrix} h(m;0) & 0 & \ldots & h(m;2) & h(m;1) \\ h(m;1) & h(m;0) & \ldots & h(m;3) & h(m;2) \\ \vdots & \vdots & \vdots & \vdots & \vdots \\ h(m;\nu-1) & h(m;\nu-2) & \vdots & 0 & 0 \\ \vdots & \vdots & \vdots & \vdots & \vdots \\ \vdots & \vdots & \vdots & h(m;0) & 0 \\ 0 & 0 & \ldots & h(m;1) & h(m;0) \end{bmatrix}. \tag{30}$$

Petitioner Samsung Ex-1004, 0162

Hence, by defining the $1 \times \nu$ row vector

$$\mathbf{b}_{m(i)}^{m,s} := \left[b_{m(i)}^{m,s}(0), \ldots, b_{m(i)}^{m,s}(\nu-1)\right] \tag{37}$$

we can write

$$[\mathbf{Q}\mathbf{A}_{m(i)}H_C(\mathbf{h}_{m(i)})\mathbf{Q}^H]_{m,s} = \mathbf{b}_{m(i)}^{m,s}\mathbf{h}_{m(i)}. \tag{38}$$

By defining the $1 \times M\nu$ row vector $\mathbf{b}^{m,s} := \left(\mathbf{b}_{m(1)}^{m,s}, \ldots, \mathbf{b}_{m(M)}^{m,s}\right)$, it follows from (34) and (38) that

$$\tilde{G}(m,s) = \mathbf{b}^{m,s}\tilde{\mathbf{h}}. \tag{39}$$

If the channel matrix was $\tilde{\mathbf{H}}$ (instead of $\mathbf{H}$), then the received tone $Y(m)$ would be

$$Y(m) = \tilde{G}(m,m)X(m) + \underbrace{\sum_{n \neq m} \tilde{G}(m,n)X(n)}_{\text{ICI}} + \text{noise}. \tag{40}$$

Inspired by how pilot-based channel estimation is done in OFDM systems, one could proceed as follows.

1) Ignore the ICI term, and assume that $Y(p) = \tilde{G}(p,p)X(p) + \text{noise} \overset{(39)}{=} X(p)\mathbf{b}^{p,p}\tilde{\mathbf{h}} + \text{noise}$.
2) Assuming that there are P pilot tones, which are placed at subcarriers $p(1), \ldots, p(P)$, form the $P \times M\nu$ system of linear equations

$$\begin{bmatrix} Y(p(1)) \\ \vdots \\ Y(p(P)) \end{bmatrix} = \begin{bmatrix} X(p(1))\mathbf{b}^{p(1),p(1)} \\ \vdots \\ X(p(P))\mathbf{b}^{p(P),p(P)} \end{bmatrix} \tilde{\mathbf{h}} + \text{noise}$$

or $\mathbf{Y}_{(P)} = \mathbf{B}_{(P)}\tilde{\mathbf{h}} + \text{noise}$.
3) With P chosen such that $P \geq M\nu$, obtain $\tilde{\mathbf{h}}$ as the least-squares solution of the aforementioned system of linear equations, i.e., $\hat{\tilde{\mathbf{h}}} = \mathbf{B}_{(P)}^{\dagger}\mathbf{Y}_{(P)}$, where $\mathbf{B}_{(P)}^{\dagger}$ is the pseudoinverse of $\mathbf{B}_{(P)}$.

Unfortunately, this approach does not produce reliable channel estimates because $\mathbf{B}_{(P)}$ is not full column rank. As we prove in the Appendix, $\mathbf{B}_{(P)}$ has rank ν, irrespective of the choice of interpolation coefficients $\{\mathbf{a}_n\}_{n \notin \mathcal{M}}$. Consequently, channel estimation is not possible if we look only at "isolated" pilot tones. Intuitively, this is not a surprising result as we study a system where ICI is not negligible; hence, we should account for the ICI in the channel estimation process. The important *practical implication* of this fact is that in OFDM systems with severe ICI, pilot tones should not be placed far apart from each other, but rather, they should be grouped together. Before we explore the reasons for this grouping of pilot tones, let us note the contrast with OFDM in time-invariant or slowly time-varying environments, where it has been shown that the pilot tones should be equispaced [24], [25].

Revisiting (40) for a pilot tone p, we obtain

$$Y(p) = \tilde{G}(p,p)X(p) + \sum_{\substack{q \text{ pilot} \\ q \neq p}} \tilde{G}(m,q)(q) + \sum_{n \text{ not pilot}} \tilde{G}(m,n)X(n) + \text{noise} \tag{41}$$

which yields

$$Y(p) = \tilde{\mathbf{b}}^p\tilde{\mathbf{h}} + \sum_{n \text{ not pilot}} \tilde{G}(m,n)X(n) + \text{noise}$$

$$\tilde{\mathbf{b}}^p := \left(\sum_{q \text{ pilot}} X(q)\mathbf{b}^{p,q}\right). \tag{42}$$

Equation (42) is the basis of the following channel estimation method.

1) Assume that for every pilot tone p

$$Y(p) = \tilde{\mathbf{b}}^p\tilde{\mathbf{h}} + e(p)$$

$$e(p) := \left(\sum_{q \text{ not pilot}} X(q)\mathbf{b}^{p,q}\right)\tilde{\mathbf{h}} + Z(p). \tag{43}$$

2) Form the $P \times M\nu$ system of linear equations

$$\begin{bmatrix} Y(p(1)) \\ \vdots \\ Y(p(P)) \end{bmatrix} = \begin{bmatrix} \tilde{\mathbf{b}}^{p(1),p(1)} \\ \vdots \\ \tilde{\mathbf{b}}^{p(P),p(P)} \end{bmatrix} \tilde{\mathbf{h}} + \begin{bmatrix} e(p(1)) \\ \vdots \\ e(p(P)) \end{bmatrix}$$

or $\mathbf{Y}_{(P)} = \tilde{\mathbf{B}}_{(P)}\tilde{\mathbf{h}} + \mathbf{e}_{(P)}$.
3) Obtain $\tilde{\mathbf{h}}$ as the least squares solution of the aforementioned system of linear equations $\hat{\tilde{\mathbf{h}}} = \tilde{\mathbf{B}}_{(P)}^{\dagger}\mathbf{Y}_{(P)}$. Extension of this technique to MIMO OFDM is straightforward.

B. Placement of Pilot Tones

Unlike time-invariant or slowly-time varying OFDM systems where pilot tones should be equispaced [24], [25], our proposed channel estimation method implies that pilot tones should be grouped together (but in more than one group). In this section, we quantify this observation and propose a pilot tone placement scheme. For analytical tractability, we start from the case $\nu = 1$, which corresponds to channels that are time-varying but not frequency-selective. Work on pilot symbol assisted modulation (PSAM) [26] has suggested that for Rayleigh flat-fading channels, pilot symbols should be placed periodically in the time domain to produce channel estimates; the coherent detection of the transmitted symbols is based on the interpolation of these channel estimates. The periodic transmission of pilot symbols in the time domain suggests a grouping of pilot tones in the frequency domain, which is an intuitive idea explored by the ensuing discussion.

We adopt as figure of merit the approximation error $e(p)$ in (43), and we seek the pilot tone placement scheme that minimizes $\mathbf{E}[\|e(p)\|^2]$ for a specific pilot tone p. Assuming that the transmitted symbols are i.i.d. with $\mathbf{E}[\|X(q)\|^2] = 1$, we obtain

$$\mathbf{E}\{\|e(p)\|^2\} = \left(\sum_{q \text{ not pilot}} \mathbf{b}^{p,q}\mathbf{R}_{\tilde{h}\tilde{h}}(\mathbf{b}^{p,q})^H\right) + \sigma^2 \tag{44}$$

where $\mathbf{R}_{\tilde{h}\tilde{h}} := \mathbf{E}[\tilde{\mathbf{h}}\tilde{\mathbf{h}}^H]$, and $\sigma^2 = \mathbf{E}[\|Z(p)\|^2]$ is the variance of the AWGN (which is the same across all subcarriers). In the Appendix, we show that $\mathbf{b}^{p,q}\mathbf{R}_{\tilde{h}\tilde{h}}(\mathbf{b}^{p,q})^H$ is a decreasing function of $((p-q) \bmod N)$. Consequently, $\mathbf{E}[\|e(p)\|^2]$ is minimized if we place all pilot tones $q \neq p$ as close to p as possible. It is implied that for time-selective channels, pilot tones should

Petitioner Samsung Ex-1004, 0163

be grouped together. On the other hand, in frequency-selective time-invariant channels, placing the pilot tones equispaced on the FFT grid is the optimal scheme [24], [25]. Intuitively, for frequency-selective time-varying channels, the pilot tones should be grouped together *but* in more than one group. As we discuss in the simulations section, we have found that our channel estimation method indeed produces the best results when the *pilot tones are partitioned into equispaced groups on the FFT grid.*

C. Selection of the Interpolation Weight Vectors $\mathbf{a}_n$

Without imposing any assumptions on the underlying channel variations, linear interpolation appears to be the simplest method for choosing the weight vectors $\mathbf{a}_n$. On the other hand, if *a priori* knowledge about the underlying channel model is available, more sophisticated channel interpolation schemes can be devised. Let us suppose that the channels follow the Jakes model [27]: $\mathbf{E}[(h(m;l)h^H(n;l))] = J_o(2\pi f_d(m-n)T)$, with f_d denoting the Doppler frequency, and T denoting the symbol period. Then, the calculation of the interpolation weights is straightforward. For example, if we fix rows $\mathbf{h}_0, \mathbf{h}_{N/2-1}, \mathbf{h}_{N-1}$, the set of weights $\mathbf{a}_n = [a_n(1), a_n(N/2-1), a_n(N-1)]^T$ that minimizes the error $\mathbf{E}[|h(n;l) - \mathbf{a}_n^H\tilde{\mathbf{h}}(l)|^2]$ with $\tilde{\mathbf{h}}(l) := [h(1;l), h(N/2-1;l), h(N-1;l)]^T$ can be obtained using the the orthogonality principle

$$\mathbf{a}_n^H = \mathbf{R}_{h_n\tilde{h}}\mathbf{R}_{\tilde{h}\tilde{h}}^{-1}$$

where $\mathbf{R}_{h_n\tilde{h}} = \mathbf{E}[h(n;l)\tilde{\mathbf{h}}^H(l)]$, and $\mathbf{R}_{\tilde{h}\tilde{h}} = \mathbf{E}[\tilde{\mathbf{h}}(l)\tilde{\mathbf{h}}^H(l)]$. With $J_o[n] := J_o(2\pi f_d nT)$, it can be seen that

$$\mathbf{R}_{h_n\tilde{h}} = \left[J_o[n], J_o\left[\left|\frac{N}{2}-1-n\right|\right], J_o[N-1-n]\right]$$
$$\mathbf{R}_{\tilde{h}\tilde{h}} = \begin{bmatrix} 1 & J_o\left[\frac{N}{2}-1\right] & J_o[N-1] \\ J_o\left[\frac{N}{2}-1\right] & 1 & J_o\left[\frac{N}{2}\right] \\ J_o[N-1] & J_o\left[\frac{N}{2}\right] & 1 \end{bmatrix}. \quad (45)$$

As we demonstrate in the simulations section, for Doppler values of practical importance (i.e., less than 200 Hz), there is little to be gained by adopting the Jakes-based estimator in place of the linear interpolator. Hence, from an implementation point of view, the linear estimator appears to be an attractive solution as it dispenses with the estimation of the Doppler frequency without sacrificing performance.

D. Channel Tracking

Under relatively mild Doppler, the quality of the channel estimates (and, consequently, the SINR gains of our ICI mitigating methods) can be improved by channel tracking. A simple tracking scheme is the following: An initial channel estimate $\hat{\mathbf{H}}_{(0)}$ can be obtained by transmitting a full training block; subsequent blocks contain pilot tones that are used to acquire new estimates $\mathbf{H}'_{(n)}$. The channel estimate for the nth OFDM block is obtained using a forgetting factor α as follows: $\hat{\mathbf{H}}_{(n)} = \alpha\hat{\mathbf{H}}_{(n-1)} + (1-\alpha)\mathbf{H}'_{(n)}$ (see, e.g., [24] for a similar method in SISO OFDM). Frequent retraining can further improve the quality of the channel estimates at the expense of the overhead of the training symbols. As we illustrate in the simulations section, the aforementioned tracking technique results in higher SINR gains (as channel estimates become more accurate).

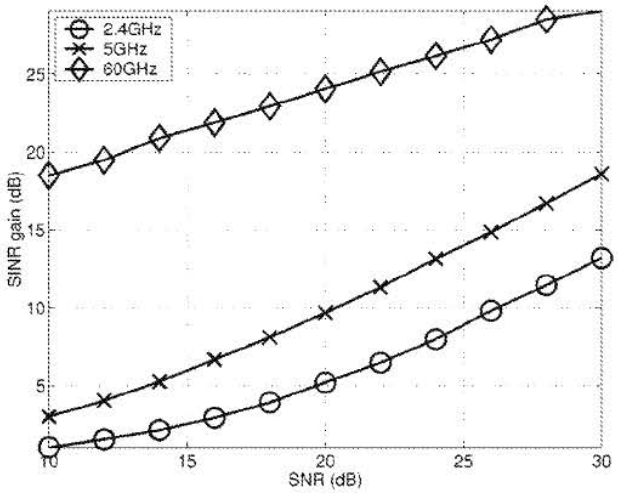


Fig. 2. Gains with known channel.

VI. Numerical Results

In this section, we present numerical examples that illustrate the SINR improvement due to the $\mathbf{W}$ filter in both SISO and MIMO OFDM systems. As the design of $\mathbf{W}$ depends on channel knowledge, we also study the accuracy of our channel estimation method and the penalty it incurs on the SINR. Throughout our simulation experiments, we investigate an OFDM system with $N = 64$ subcarriers, a total bandwidth of 200 KHz, carrier frequency $f_c = 2.4$ GHz, and the velocity of the mobile is set to 60 mi/h (the corresponding Doppler frequency is 214 Hz). In all simulations, we have chosen as figure of merit the average *SINR* gain, which is defined as

$$\text{SINR} = \left(\frac{\prod_{m=0}^{N-1}\text{SINR}_m^W}{\prod_{m=0}^{N-1}\text{SINR}_m}\right)^{1/N}$$

with SINR_m^W (SINR_m) being the SINR at subcarrier m with (or without) the filter $\mathbf{W}$. The *SINR* metric expresses the SINR improvement over all subcarriers, and since it depends on the channel realization, in all figures, we depict the average SINR over 1000 random channel matrices $\mathbf{H}$. The entries of $\mathbf{H}$ were generated using the Jakes model, with $\nu = 4$, and each channel tap modeled as a complex Gaussian random variable $\mathcal{N}(0,1)$.

SINR Improvements With Known Channel: First, we look at the SINR improvement due to the $\mathbf{W}$ filter in SISO OFDM with perfect channel knowledge. Fig. 2 depicts, for various values of SNR, the SINR gain achieved with perfect channel knowledge for the carrier frequencies of $f_c = 2.4$ GHz and $f_c = 60$ GHz. For smaller values of the SNR, the SINR improvement is smaller, as $\mathbf{W}$ attempts to suppress both ICI and additive noise. As the SNR increases, the SINR improvement increases because $\mathbf{W}$ attempts to suppress (essentially) only the ICI. It is also evident that at $f_c = 60$ GHz, the ICI is much more

Petitioner Samsung Ex-1004, 0164

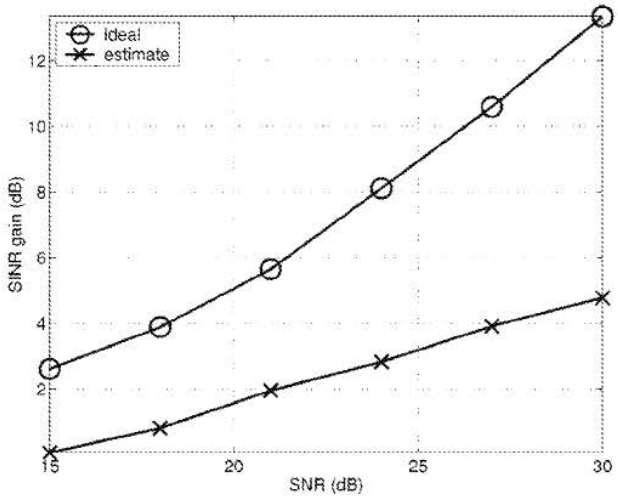


Fig. 3. Gains with estimated channel.

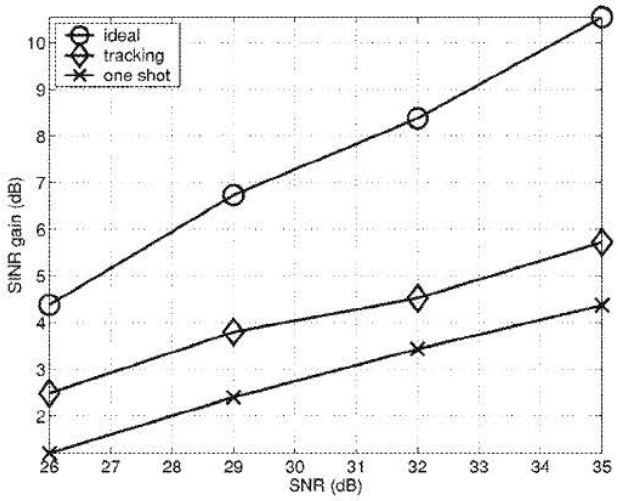


Fig. 4. Channel tracking.

severe and, consequently, $\mathbf{W}$ results in higher SINR improvements over a wider range of SNR. In both cases, the substantial SINR gains illustrate the merits of our ICI mitigation technique.

SINR Improvements With Estimated Channel: Fig. 3 illustrates the performance penalty due to channel estimation ($f_c = 2.4$ GHz). The channel estimates are obtained using the method described in Section V with $M = 2$ (the top and the bottom row of $\mathbf{H}$ are estimated, and the rest of the rows are obtained with linear interpolation). We have used 4ν pilot tones grouped into ν groups that are equispaced onto the FFT grid (i.e., subcarriers $\{6, 7, 8, 9, 22, 23, 24, 25, 38, 39, 40, 41, 54, 55, 56, 57\}$ are pilot tones). From Fig. 3, we observe that even with imperfect channel estimation, significant SINR gains can be achieved; this observation serves as testament to the effectiveness of our channel estimation technique. Additionally, under relatively mild Doppler (90 Hz), 2–3 dB of SNR can be gained by using frequent retraining and channel tracking, as Fig. 4 illustrates.

Pilot Tone Placement Scheme: Fig. 5 depicts the average SINR gains when $\mathbf{W}$ is based on channel estimation, and a

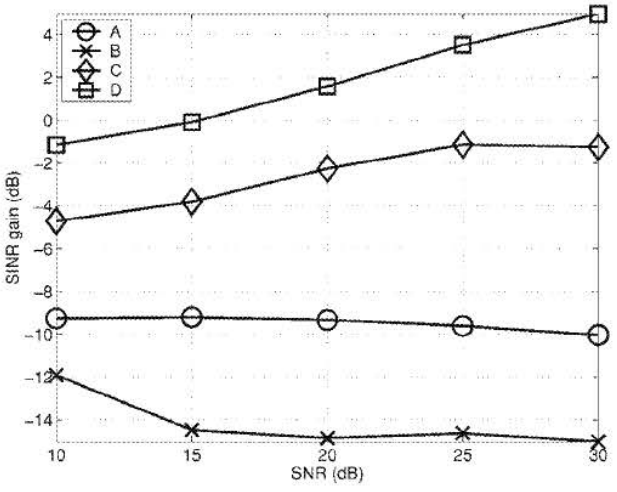


Fig. 5. Pilot tone placement.

total of 4ν pilot tones are placed on the FFT grid according to a number of different schemes.

- In scheme "A", the pilot tones $\{1, 5, 9, 13, 17, 21, 25, 29, 33, 37, 41, 45, 49, 53, 57, 61\}$ are placed equispaced on the FFT grid.
- In scheme "B", the pilot tones $\{24, 25, 26, 27, 28, 29, 30, 31, 32, 33, 34, 35, 36, 37, 38, 39\}$ are placed into a big group of subcarriers centered on the FFT grid.
- In scheme "C", the pilot tones $\{13, 14, 15, 16, 17, 18, 19, 20, 45, 46, 47, 48, 49, 50, 51, 52\}$ are placed into $M = 2$ groups of 2ν tones.
- In scheme "D", the pilot tones $\{6, 7, 8, 9, 22, 23, 24, 25, 38, 39, 40, 41, 54, 55, 56, 57\}$ are placed into ν groups of $2M$ tones.

It is clear from Fig. 5 that the placement of pilot tones has a significant impact on the quality of the channel estimates and the resulting SINR gains. It is worth noting that placing the pilot tones equispaced on the FFT grid results in very poor performance, unlike the time-invariant case [24], [25].

Interpolation Technique: Although pilot placement does have a significant impact on the achievable SINR gains, this does not seem to be necessarily the case with the choice of interpolation weights. To illustrate this observation, let us look at the case $\mathcal{M} = \{0, N/2, N-1\}$ (i.e., the top, middle, and bottom rows are to be estimated, and the rest of the rows are obtained using interpolation). We compare the SINR gains obtained with linear interpolation weights and the performance obtained using the weights of Section V-C. To isolate the effects of the choice of the interpolation weights, we let all subcarriers be pilot tones (which amounts to having a full training OFDM block utilized for channel estimation), and Fig. 6 depicts the performance of the two interpolation methods. We observe that linear interpolation achieves the same performance as the "Jakes-based" interpolation, which, intuitively, is a not a surprising result: For Doppler frequency values of practical interest, the variation of the rows of $\mathbf{H}$ is not very large, and as a result, linear interpolation performs adequately. On the other hand, for significant variation, the Jakes-based estimator

Petitioner Samsung Ex-1004, 0165

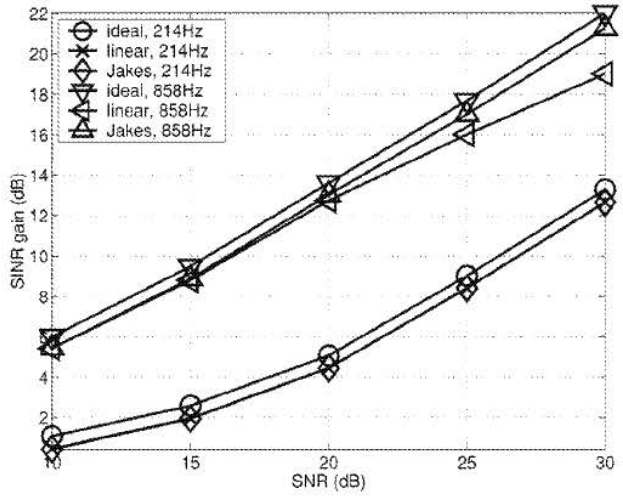


Fig. 6. Interpolation scheme.

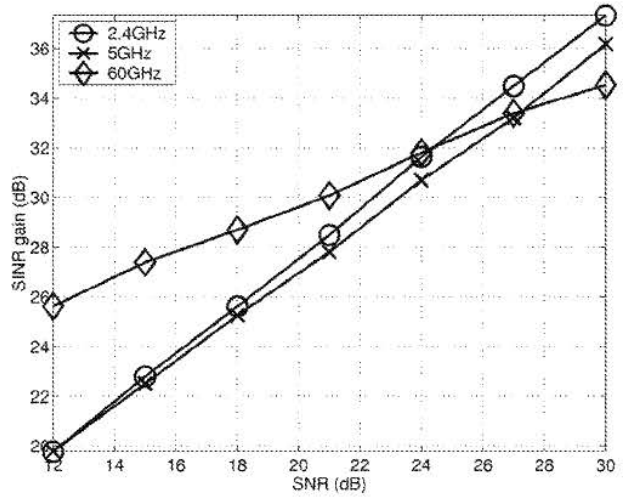


Fig. 7. SINR gains in space-time-coded OFDM.

outperforms the linear interpolator. For illustration purposes only, we look at the case of 858-Hz Doppler. Fig. 6 depicts the achieved performance at this extremely high Doppler, and it is evident that the Jakes based-estimator outperforms the linear interpolator. In addition, it can be deduced from Fig. 6 that even at high SNRs, where high quality of the channel estimate is expected (with a full training block), there is significant difference between the performance achieved with perfect channel knowledge and channel estimates. This is due to the large variation across the channel matrix rows that invalidates the assumption that some channel rows can be expressed as a function of as few as three channel rows.

SINR Improvements in MIMO OFDM: Finally, Fig. 7 illustrates the SINR gains achieved in space-time block-coded OFDM transmissions where the channel is perfectly known at the receiver. As described in Section IV-D, the filter $\mathbf{W}$ of Section IV-C operates on two consecutive transmission blocks, and we define the *SINR* as the geometric average of the gains achieved over the tones of the two blocks, i.e.,

$$\text{SINR} = \sqrt{\text{SINR}_{(1)}\text{SINR}_{(2)}}.$$

Similar to Fig. 2, we can clearly see the SNR improvements that the MIMO filter $\mathbf{W}$ yields.

VII. Conclusions

In this paper, we have analyzed the effect of intercarrier interference on MIMO-OFDM. The cause of such an impairment is time-variation within a transmission block and occurs in practice due to both Doppler spread of the transmission channel and synchronization errors. We proposed time-domain filtering-based ICI mitigation techniques that cascade the time-varying channel with a receive filter so that the overall channel is approximately (in the appropriate mean-square-error metric) time invariant. The associated problem of estimating such a rapidly varying channel was addressed, and a novel estimation scheme was proposed. Coupled to the proposed channel estimation scheme is the issue of pilot tone placement. Examination of this issue showed that nonuniform placement of pilot tones and in particular grouping of tones into clumps equispaced on the FFT grid is effective for these situations. Numerical results illustrating these techniques were also presented.

Appendix A

$\mathbf{B}_{(P)}$ has Rank ν

From (36), we obtain

$$\begin{aligned} b^{p,p}_{m(i)}(l) &= e^{-j(2\pi pl/N)}\frac{1}{N}\sum_{r=0}^{N-1}[A_{m(i)}]_{r,r} \\ &= \frac{\frac{1}{N}\sum_{r=0}^{N-1}[A_{m(i)}]_{r,r}}{\frac{1}{N}\sum_{r=0}^{N-1}[A_{m(1)}]_{r,r}} b^{p,p}_{m(1)} \\ &= c_{m(i)} b^{p,p}_{m(1)}(l), \quad c_{m(i)} := \frac{\frac{1}{N}\sum_{r=0}^{N-1}[A_{m(i)}]_{r,r}}{\frac{1}{N}\sum_{r=0}^{N-1}[A_{m(1)}]_{r,r}}. \end{aligned}$$

Hence, with the aid of (37), we obtain $\mathbf{b}^{p,p}_{m(i)} = c_{m(i)}\mathbf{b}^{p,p}_{m(1)}$, which readily yields that

$$\mathbf{B}_{(P)} = \begin{pmatrix} \mathbf{b}^{p(1),p(1)}_{m(1)} & \cdots & \mathbf{b}^{p(1),p(1)}_{m(i)} & \cdots & \mathbf{b}^{p(1),p(1)}_{m(M)} \\ \vdots & \vdots & \vdots & \vdots & \vdots \\ \mathbf{b}^{p(P),p(P)}_{m(1)} & \cdots & \mathbf{b}^{p(P),p(P)}_{m(i)} & \cdots & \mathbf{b}^{p(P),p(P)}_{m(M)} \end{pmatrix}$$

has rank ν. □

Petitioner Samsung Ex-1004, 0166

APPENDIX B

$\mathbf{b}^{p,q}\mathbf{R}_{\tilde{h}\tilde{h}}(\mathbf{b}^{p,q})^*$ AS A FUNCTION OF $(p-q)$

For analytical tractability, let us focus on the case $\nu = 1$ and $\mathcal{M} = \{0, N-1\}$. From (33), we have $\tilde{\mathbf{h}} := (h_0(0), h_{N-1}(0))^T$, and $\mathbf{R}_{\tilde{h}\tilde{h}}$ can be evaluated as

$$\mathbf{R}_{\tilde{h}\tilde{h}} = \begin{bmatrix} 1 & \gamma \\ \gamma & 1 \end{bmatrix}, \quad 0 < \gamma < 1.$$

Then, the term $\beta^{p,q} := \mathbf{b}^{p,q}\mathbf{R}_{\tilde{h}\tilde{h}}(\mathbf{b}^{p,q})^*$ is written as (cf. (37))

$$\begin{aligned}\beta^{p,q} &= \begin{pmatrix} b_0^{p,q}(0) & b_{N-1}^{p,q}(0) \end{pmatrix} \begin{bmatrix} 1 & \gamma \\ \gamma & 1 \end{bmatrix} \begin{bmatrix} \left(b_0^{p,q}(0)\right)^* \\ \left(b_{N-1}^{p,q}(0)\right)^* \end{bmatrix} \\ &= \left|b_0^{p,q}(0)\right|^2 + \left|b_{N-1}^{p,q}(0)\right|^2 \\ &\quad + \gamma\left(\left(b_0^{p,q}(0)\right)^* b_{N-1}^{p,q}(0) \right. \\ &\quad \left. + \left(b_0^{p,q}(0)\right)\left(b_{N-1}^{p,q}(0)\right)^*\right). \end{aligned} \tag{46}$$

Without any assumptions on the underlying physical channels, we adopt the linear interpolation scheme for the selection of the weights $\mathbf{a}_n$ of (29); hence, we set

$$a_n = \begin{pmatrix} \frac{N-1-n}{N-1} & \frac{n}{N-1} \end{pmatrix}^T, \quad 1 \le n \le N-2. \tag{47}$$

With the aid of (32) and (36), we can write $b_0^{p,q}(0)$, $b_{N-1}^{p,q}(0)$ in closed-form as

$$\begin{aligned} b_0^{p,q}(0) &= \frac{1}{N}\sum_{r=0}^{N-1}[\mathbf{A}_0]_{r,r}e^{j(2\pi r(p-q)/N)} \\ &\overset{(32),(47)}{=} \frac{1}{N}\sum_{r=0}^{N-1}\left(1 - \frac{r}{N-1}\right)e^{j(2\pi r(p-q)/N)} \\ &= \frac{(-1)}{N(N-1)}\sum_{r=0}^{N-1} re^{j(2\pi r(p-q)/N)}, \text{ because} \\ &\quad \times \sum_{r=0}^{N-1} e^{j(2\pi r(p-q)/N)} = 0 \text{ for } p \neq q \\ &= \frac{(-1)}{N(N-1)}\sum_{r=0}^{N-1} r\omega^r, \text{ with } \omega := e^{j(2\pi(p-q)/N)} \\ &= \frac{(-1)}{N(N-1)}\frac{\omega^N(N(\omega-1)-\omega)+\omega}{(\omega-1)^2} \\ &= \frac{(-1)}{(N-1)(\omega-1)} \text{ since } \omega^N = 1 \end{aligned}$$

which finally yields

$$b_0^{p,q}(0) = \frac{(-1)}{(N-1)(e^{j(2\pi(p-q)/N)}-1)}, \text{ for } p \neq q. \tag{48}$$

Similarly, we can verify that $b_{N-1}^{p,q}(0) = -b_0^{p,q}(0)$ for $p \neq q$. Hence, we obtain $\beta^{p,q} = 2(1-\gamma)|b_0^{p,q}(0)|^2$, which, with the aid of (48), finally yields

$$\beta^{p,q} = \frac{2(1-\gamma)}{(N-1)^2\left(1-\cos\left(\frac{2\pi(p-q)}{N}\right)\right)}, \text{ for } p \neq q. \tag{49}$$

Equation (49) constitutes an intuitive result: The further a tone q is from p, the less its interference on tone p is.

REFERENCES

[1] J. M. Cioffi, A multicarrier primer, presented at ANSI T1E1.4 Comm. Contribution. [Online]. Available: http://www-isl.stanford.edu/people/cioffi/papers.html

[2] G. G. Raleigh and J. M. Cioffi, "Spatio-temporal coding for wireless communication," *IEEE Trans. Commun.*, vol. 46, pp. 357–366, Mar. 1998.

[3] L. J. Cimini, B. Daneshrad, and N. R. Sollenberger, "Clustered OFDM with transmitter diversity and coding," in *Proc. GLOBECOM*, 1996, pp. 703–707.

[4] U. Tureli, D. Kivanc, and H. Liu, "Experimental and analytical studies on a high-resolution OFDM carrier frequency offset estimator," *IEEE Trans. Veh. Technol.*, vol. 50, pp. 629–643, Mar. 2001.

[5] J. Armstrong, "Analysis of new and existing methods of reducing intercarrier interference due to carrier frequency offset in OFDM," *IEEE Trans. Commun.*, pp. 365–369, Mar. 1999.

[6] M. Russell and G. Stuber, "Interchannel interference analysis of OFDM in a mobile environment," in *Proc. Veh. Technol. Conf.*, 1995, pp. 820–824.

[7] P. Robertson and S. Kaiser, "Analysis of the loss of orthogonality through doppler spread in OFDM systems," in *Proc. GLOBECOM*, 1999, pp. 701–706.

[8] J. Li and M. Kavehrad, "Effects of time selective multipath fading on OFDM systems for broadband mobile applications," *IEEE Commun. Lett.*, pp. 332–334, Dec. 1999.

[9] W. C. Jakes, *Microwave Mobile Communications*. New York: Wiley, 1974.

[10] Y. Li and L. J. Cimini, "Bounds on the interchannel interference of OFDM in time-varying impairments," *IEEE Trans. Commun.*, vol. 49, pp. 401–404, Mar. 2001.

[11] D. Agrawal, V. Tarokh, A. Naguib, and N. Seshadri, "Space-time coded OFDM for high data-rate wireless communication over wideband channels," in *Proc. 48th IEEE Veh. Technol. Conf.*, vol. 3, 1998, pp. 2232–6.

[12] W. Jeon, K. Chang, and Y. Cho, "An equalization technique for orthogonal frequency-division multiplexing systems in time-variant multipath channels," *IEEE Trans. Commun.*, pp. 27–32, Jan. 1999.

[13] M. K. Tsatsanis and Z. Xu, "Pilot symbol assisted modulation in frequency selective fading wireless channels," *IEEE Trans. Signal Processing*, vol. 48, pp. 2353–2365, Aug. 2000.

[14] C. Tepedelenlioglu and G. B. Giannakis, "Transmitter redundancy for blind estimation and equalization of time- and frequency-selective channels," *IEEE Trans. Signal Processing*, vol. 48, pp. 2029–2043, July 2000.

[15] T. Kailath, "Channel characterization: Time-variant dispersive channels," in *Lectures on Communcation System Theory*, E. J. Baghdady, Ed. New York: McGraw-Hill, 1961, pp. 95–123.

[16] M. Medard, "Capacity of time-varying multiple user channels in wireless communications," Ph.D. dissertation, Mass. Inst. Technol., Cambridge, MA, 1995.

[17] R. A. Horn and C. R. Johnson, *Matrix Analysis*, U.K.: Cambridge Univ. Press, 1990.

[18] J. H. Winters, J. Salz, and R. Gitlin, "The impact of antenna diversity on the capacity of wireless communication systems," *IEEE Trans. Commun.*, vol. 42, no. 2–4, pp. 1740–1751, Feb/Mar/Apr 1994.

[19] S. Diggavi, "Analysis of multicarrier transmission in time-varying channels," in *Proc. Int. Contr. Conf.*, 1997, pp. 1191–1195.

[20] Y.-S. Choi, P. J. Voltz, and F. A. Cassara, "On channel estimation and detection for multicarrier signals in fast and selective Rayleigh fading channels," *IEEE Trans. Commun.*, vol. 49, pp. 1375–1387, Aug. 2001.

[21] S. M. Alamouti, "A simple transmit diversity technique for wireless communications," *IEEE J. Select. Areas Commun.*, vol. 16, pp. 1451–1458, Oct. 1998.

[22] Z. Liu, G. B. Giannakis, A. Scaglione, and S. Barbarossa, "Decoding and equalization of unknown multipath channels based on block precoding and transmit-antenna diversity," in *Proc. Asilomar Conf. Signals, Syst. Comput.*, 1999, pp. 1557–1561.

[23] G. B. Giannakis and C. Tepedelenlioglu, "Basis expansion models and diversity techniques for blind equalization of time-varying channels," *Proc. IEEE*, vol. 86, pp. 1969–1986, Oct. 1998.

[24] R. Negi and J. Cioffi, "Pilot tone selection for channel estimation in a mobile OFDM system," *IEEE Trans. Consum. Electron.*, vol. 44, pp. 1122–8, Aug. 1998.

[25] S. Ohno and G. B. Giannakis, "Capacity maximizing pilots and precoders for wireless OFDM over rapidly fading channels," IEEE Trans. Inform. Theory, May 2001, submitted for publication.

Petitioner Samsung Ex-1004, 0167

[26] J. K. Cavers, "An analysis of pilot symbol assisted modulation for Rayleigh fading channels (mobile radio)," *IEEE Trans. Veh. Technol.*, vol. 40, pp. 686–693, Nov. 1991.
[27] W. C. Jakes, *Microwave Mobile Communications*. New York: Wiley, 1994.

Anastasios Stamoulis received the Diploma degree in computer engineering from University of Patras, Patras, Greece, in July 1995, the M.Sc. degree in computer science from the University of Virginia, Charlottesville in May 1997, and the Ph.D. degree in electrical engineering from the University of Minnesota, Minneapolis, in December 2000.

In January 2001, he joined the AT&T Shannon Laboratory, Florham Park, NJ, as a Senior Technical Staff Member. His research interests include wireless networking, QoS networks, digital communications, and digital signal processing.

Suhas N. Diggavi received the B.Tech degree in electrical engineering from the Indian Institute of Technology, Delhi, India, and the Ph.D. degree in electrical engineering from Stanford University, Stanford, CA, in 1998.

Currently, he is a Principal Member Technical Staff with the Information Sciences Center, AT&T Shannon Laboratories, Florham Park, NJ. His research interests include wireless networks, information theory, source coding, and signal processing.



Naofal Al-Dhahir (SM'98) received the M.S. and Ph.D. degrees in electrical engineering from Stanford University, Stanford, CA, in 1990 and 1994, respectively.

He was an Instructor at Stanford University during the Winter of 1993. From August 1994 to July 1999, he was a Member of Technical Staff at the Communications Program at GE Corporate R&D Center, Schenectady, NY, where he worked on various aspects of satellite communication systems design and antijam GPS receivers. Since August 1999, he has been a Principal Member of Technical Staff at AT&T Shannon Laboratory, Florham Park, NJ. His current research interests include equalization schemes, space-time coding and signal processing, OFDM, and digital subscriber line technology. He has authored 45 journal papers and holds seven U.S. patents in the areas of satellite communications, digital television, and space-time processing.

Dr. Al-Dhahir is a member of the IEEE SP4COM Technical Committee. He is an Associate Editor for the IEEE TRANSACTION ON SIGNAL PROCESSING, IEEE COMMUNICATIONS LETTERS, and the IEEE TRANSACTIONS ON COMMUNICATIONS. He is co-author of the book *Doppler Applications for LEO Satellite Systems* (Boston, MA: Kluwer, 2001).

Petitioner Samsung Ex-1004, 0168

EM-Based Iterative Receiver Design With Carrier-Frequency Offset Estimation for MIMO OFDM Systems

Yong Sun, Zixiang Xiong, *Senior Member, IEEE*, and Xiaodong Wang, *Member, IEEE*

***Abstract*—In this letter, we study the design of expectation-maximization (EM)-based iterative receivers for multiple-input multiple-output (MIMO) orthogonal frequency-division multiplexing systems with the presence of carrier-frequency offset (CFO). Motivated by the spirit of maximum-likelihood estimation in the EM algorithm, we first present a pilot-aided CFO estimation scheme that allows fast Fourier transform-based fast implementation. Then this CFO estimation is incorporated into the initialization step of the iterative receiver. Experimental results show the effectiveness of our receiver design in combating CFO.**

***Index Terms*—Carrier-frequency offset (CFO), expectation-maximization (EM) algorithm, multiple-input multiple-output (MIMO), orthogonal frequency-division multiplexing (OFDM).**

I. Introduction

NEXT-GENERATION wireless communication systems are required to support high-data-rate applications. The multiple-input multiple-output (MIMO) technique has been shown to be capable of achieving extraordinary throughput without additional power consumption or bandwidth expansion [1]. MIMO systems rely on antenna diversity to mitigate the effect of multipath fading. To combat multipath delay spread in high-rate wireless systems, one efficient method is orthogonal frequency-division multiplexing (OFDM), which transforms a multipath channel to parallel independent flat-fading subchannels [2]–[4].

Iterative techniques for receiver design have attracted considerable attention lately [5]–[8]. The turbo principle has been successfully applied to detection/decoding problems such as serial concatenated decoding [9], equalization [10], coded modulation [11], and joint source-channel decoding [12]. Compared with noniterative receivers, iterative ones can successively improve the performance in typical wireless channels, but at the cost of high computational complexity. In [8], Lu *et al.* designed an iterative receiver based on the expectation-maximization (EM) algorithm [13], [14] for space–time block-coded (STBC) OFDM systems with reduced complexity.

Aiming at improving the receiver design in [8], we take into account the carrier-frequency offset (CFO), because CFO estimation/compensation was not addressed in that work. It is well known that OFDM systems suffer severe performance degradation due to CFO [15]. Many existing frequency-estimation techniques (with the exception of [16]) rely on transmission of reference symbols (e.g., repeated data symbol [15] or pilot-symbol sequences periodically inserted in the OFDM codeword [17]). However, most of them are designed for single-antenna OFDM systems instead of MIMO systems. One work on MIMO OFDM systems was recently reported in [18], where carefully designed training symbols are inserted in the information symbol block for both CFO estimation and MIMO channel estimation.

In this letter, based on the fact that the iterative receiver in [8] also requires pilot slots to obtain a good initialization, we target at designing a *pilot-aided* CFO estimator which can work well with the EM-based iterative receiver for MIMO OFDM systems. Following the spirit of maximum-likelihood (ML) estimation in the EM algorithm, we devise a scheme for ML estimation of the CFO. This scheme is incorporated into the initialization step of the iterative receiver and implemented via fast Fourier transform (FFT). We hence arrive at an EM-based iterative receiver for MIMO OFDM systems subject to CFO. We also take advantage of the available multiple frames of received symbols in previous pilot slots to refine the estimation of CFO. Experimental results confirm the effectiveness of our new receiver design.

II. EM-Based Iterative Receiver With CFO Estimation for MIMO OFDM Systems

MIMO systems have been well studied in conjunction with STBC [19], [20] with multiple receive antennas. An efficient EM-based iterative receiver for the STBC OFDM system was introduced in [8]. Since OFDM systems are very sensitive to CFO [15], it is challenging to take the CFO into account in the receiver design.

In this letter, we devise a new ML scheme to estimate the CFO in MIMO OFDM systems with $M_T = 2$ transmit antennas and $M_R = 2$ receive antennas. For practical reasons, we assume that the absolute value of the CFO is bounded by half of the OFDM subcarrier spacing, since larger CFOs can be compensated by an automatic frequency-control circuit [21] and what remains is the residual CFO. The same CFO is assumed for all the transmit and receive antenna pairs. For the multipath frequency-selective fading channel, the channel responses of different taps and from different transmit antennas are uncorrelated. Note that the above assumptions are made for the sake of simplicity. Some more general cases (e.g., MIMO systems with $N_T > 2$ transmit antennas) are currently under investigation.

A. MIMO OFDM Systems Subject to CFO

In the following, we consider an STBC-OFDM system with N subcarriers, $M_T = 2$ transmit antennas, and $M_R = 2$ receive antennas, signalling through an L-tap frequency-selective

Paper approved by A. Anastasopoulos, the Editor for Wireless Communications of the IEEE Communications Society. Manuscript received March 12, 2004; revised August 29, 2004.

Y. Sun and Z. Xiong are with the Department of Electrical Engineering, Texas A&M University, College Station, TX 77843 USA (e-mail: sunny@ee.tamu.edu; zx@ee.tamu.edu).

X. Wang is with the Department of Electrical Engineering, Columbia University, New York, NY 10027 USA (e-mail: wangx@ee.columbia.edu).

Digital Object Identifier 10.1109/TCOMM.2005.844920

0090-6778/$20.00 © 2005 IEEE

Petitioner Samsung Ex-1004, 0169

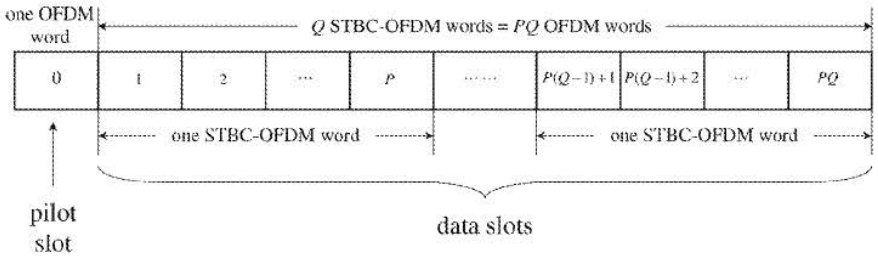


Fig. 1. One data-burst structure in STBC-OFDM system.

fading channel. We also assume that the fading channel coefficients remain constant within the interval of one STBC word, namely $P = 2$ consecutive OFDM words.

From [8], pilot symbols are required to initialize the EM algorithm. For practical data transmission, as shown in Fig. 1, a data burst spans $PQ + 1$ OFDM words, with the first OFDM word containing the pilot symbols. The remaining PQ OFDM words are composed of Q STBC codewords.

Our idea is to simultaneously make use of these pilot symbols for EM initialization and for CFO estimation. We modify the traditional transmission model as follows. First, the normalized CFO ε is included in the model. Second, at each transmitter, K out of the total of N OFDM subcarriers are used to transmit symbols. Note that this is different from inserting a guard interval in OFDM systems, because nothing is transmitted from the remaining $(N-K)$ subcarriers. As will be seen shortly, this truncated observation window of subcarriers is needed for good estimation of the CFO. Third, we treat the optimal pilot-symbol matrix $\boldsymbol{X}_P$ as inputs. In order to improve the spectral efficiency, we only transmit one pilot OFDM word at time slot $p = 0$, as illustrated in Fig. 1. According to [22], a carefully designed optimal training sequence for STBC-OFDM systems can achieve the minimum mean square error (MSE) and avoid matrix inversion. For a system with M_T transmit antennas, the optimal pilot symbol at the nth subcarrier of the ith transmitter, $X_{Pi}[n]$, is designed as $X_{Pi}[n] = X_{P0}[n]e^{-j(2\pi\breve{L}/N)in}$, $n = 0, 1, \ldots, N-1$, $i = 0, 1, \ldots, M_T - 1$, with $\breve{L} \triangleq \lfloor N/M_T \rfloor \geq L$. Usually, we set the pilot-symbol sequence at the zeroth transmit antenna to be $X_{P0}[n] = 1/\sqrt{2}, \forall\, n$, where the factor $1/\sqrt{2}$ is used to normalize the energy of the transmitted symbols since two transmit antennas are considered here.

Accordingly, the MIMO OFDM system model subject to CFO is given as

$$\boldsymbol{Y}_j = \underbrace{\boldsymbol{W}_N \boldsymbol{F}(\varepsilon) \boldsymbol{W}_K^I \boldsymbol{X}_P \boldsymbol{W}_{KL}}_{\triangleq \boldsymbol{W}_F(\varepsilon)} \boldsymbol{h}_j + \boldsymbol{Z}_j, \quad j = 0, 1, \ldots, M_R - 1 \tag{1}$$

with

$$\begin{aligned}
\boldsymbol{Y}_j &\triangleq [Y_j(0), Y_j(1), \ldots, Y_j(N-1)]^T_{(N\times 1)} \\
\boldsymbol{F}(\varepsilon) &\triangleq \mathrm{diag}(1, e^{j(2\pi\varepsilon/N)}, \ldots, e^{j(2\pi\varepsilon(N-1)/N)}) \\
\boldsymbol{X}_P &\triangleq (\boldsymbol{X}_{P0}, \boldsymbol{X}_{P1})_{(K\times 2K)} \\
\boldsymbol{X}_{P0} &= \mathrm{diag}(X_{P0}[0], X_{P0}[1], \ldots, X_{P0}[K-1])_{(K\times K)} \\
\boldsymbol{X}_{P1} &= \mathrm{diag}(X_{P1}[0], X_{P1}[1], \ldots, X_{P1}[K-1])_{(K\times K)} \\
[\boldsymbol{W}_N]_{r,s} &\triangleq \frac{1}{\sqrt{N}} e^{j(2\pi/N)rs}, \\
& r = 0, 1, \ldots, N-1; \;\; s = 0, 1, \ldots, N-1 \\
[\boldsymbol{W}_K^I]_{r,s} &\triangleq \frac{1}{\sqrt{N}} e^{j(2\pi/N)rs}, \\
& r = 0, 1, \ldots, N-1; \;\; s = 0, 1, \ldots, K-1 \\
\boldsymbol{W}_{KL} &\triangleq \mathrm{diag}(\boldsymbol{w}_{KL}, \boldsymbol{w}_{KL})_{(2K\times 2L)} \\
[\boldsymbol{w}_{KL}]_{r,s} &\triangleq e^{-j(2\pi/N)rs}, \\
& r = 0, 1, \ldots, K-1; \;\; s = 0, 1, \ldots, L-1 \\
\boldsymbol{h}_j &\triangleq \left[\boldsymbol{h}_{0,j}^T, \boldsymbol{h}_{1,j}^T\right]^T_{(2L\times 1)} \\
\boldsymbol{h}_{i,j} &\triangleq \left[h_{i,j}^0, h_{i,j}^1, \ldots, h_{i,j}^{L-1}\right]^T
\end{aligned}$$

where $Y_j(n)$ is the frequency-domain received symbol of the nth subcarrier at the jth receive antenna; $h_{i,j}^l, l = 0, 1, \ldots, L-1$ is the fading coefficient of the lth tap associated with the ith transmit antenna and the jth receive antenna, which is independent of other pairs of antennas and is modeled as a complex Gaussian variable of variance $\sigma_{i,j,l}^2$ with Jakes' correlation structure [23]. The additive white Gaussian noise (AWGN) vector $\boldsymbol{Z}_j$ contains independent zero-mean complex Gaussian random variables with power σ_z^2. The normalized CFO ε is introduced through the matrix $\boldsymbol{F}(\varepsilon)$ in (1). Since $\boldsymbol{F}(\varepsilon) \neq \boldsymbol{I}_N$ (the $N \times N$ identity matrix) for $\varepsilon \neq 0$, orthogonality among all N subcarriers is destroyed. Due to this loss of subcarrier orthogonality, the interchannel interferences (ICIs) from other subcarriers will impact the transmitted symbol at the desired subcarrier.

B. ML Estimation of CFO

The transmission model in (1) contains two unknown parameters: the CFO ε and the complex Gaussian distributed vector $\boldsymbol{h}_j$. The ML detection problem for ε is formulated as

$$\hat{\varepsilon} = \arg\max_{\varepsilon} Q(\varepsilon) = \arg\max_{\varepsilon} \sum_{j=0}^{M_R-1} \log p(\boldsymbol{Y}_j | \boldsymbol{F}(\varepsilon)). \tag{2}$$

Using the same strategy as the E-step in [8, eq. (17)], we can compute the cost function as

$$\begin{aligned}
Q(\varepsilon) &= -\sum_{j=0}^{M_R-1} \left\{ E_{\boldsymbol{h}_j|(\boldsymbol{Y}_j,\varepsilon)} \left\{ \|\boldsymbol{Y}_j - \boldsymbol{W}_F(\varepsilon)\boldsymbol{h}_j\|^2 \right\} \right\} + \text{const.} \\
&= -\sum_{j=0}^{M_R-1} \left\{ \left\| \boldsymbol{Y}_j - \boldsymbol{W}_F(\varepsilon)\hat{\boldsymbol{h}}_j \right\|^2 \right. \\
&\qquad \left. + \mathrm{trace}\left(\boldsymbol{W}_F(\varepsilon) \hat{\Sigma}_{\tilde{h}_j} \boldsymbol{W}_F^H(\varepsilon) \right) \right\} \\
&\quad + \text{const.},
\end{aligned} \tag{3}$$

Petitioner Samsung Ex-1004, 0170

with $\hat{\Sigma}_{h_j} \triangleq \left(\boldsymbol{W}_F^H(\varepsilon)\Sigma_{Z_j}^{-1}\boldsymbol{W}_F(\varepsilon) + \Sigma_{h_j}^{-1}\right)^{-1}$

$$\hat{\boldsymbol{h}}_j \triangleq \hat{\Sigma}_{h_j}\boldsymbol{W}_F^H(\varepsilon)\Sigma_{Z_j}^{-1}\boldsymbol{Y}_j. \tag{4}$$

It is easy to show that $\Sigma_{Z_j} = \sigma_z^2\boldsymbol{I}_N$. By assuming that the fading channels of different paths and from different transmit antennas are uncorrelated, we can show $\Sigma_{h_j} = \text{diag}\left(\sigma_{0,j,0}^2, \sigma_{0,j,1}^2, \ldots, \sigma_{0,j,L-1}^2, \sigma_{1,j,0}^2, \sigma_{1,j,1}^2, \ldots, \sigma_{1,j,L-1}^2\right)$. Note that $\boldsymbol{W}_F^H(\varepsilon)\boldsymbol{W}_F(\varepsilon)$ is not a scaled identity matrix due to truncation of $(N-K)$ subcarriers. However, if K is sufficiently close to N (e.g., $K = 120$ and $N = 128$), the off-diagonal elements are negligible, and $\boldsymbol{W}_F^H(\varepsilon)\boldsymbol{W}_F(\varepsilon)$ can be approximated as $K/2 \cdot \boldsymbol{I}_{2L}$. Then $\hat{\Sigma}_{h_j}$ can be simplified to $\hat{\Sigma}_{h_j} = \text{diag}\left(\hat{\sigma}_{0,j,0}^2, \hat{\sigma}_{0,j,1}^2, \ldots, \hat{\sigma}_{0,j,L-1}^2, \hat{\sigma}_{1,j,0}^2, \hat{\sigma}_{1,j,1}^2, \ldots, \hat{\sigma}_{1,j,L-1}^2\right)$ with

$$\hat{\sigma}_{i,j,l}^2 = \left(\sigma_z^2/\left(K/2 + \sigma_z^2/\sigma_{i,j,l}^2\right)\right).$$

Further simplification is achieved by assuming $K/2$ is much larger than $\sigma_z^2/\sigma_{i,j,l}^2$, since the latter is inversely proportional to the signal-to-noise ratio (SNR) of the fading channel and much smaller than $K/2$ when SNR ≥ 0 dB.

Based on the above approximations, we have $\hat{\Sigma}_{h_j} \approx \left(2\sigma_z^2/K\right)\boldsymbol{I}_{2L}$, $\hat{\boldsymbol{h}}_j \approx (2/K)\boldsymbol{W}_F^H(\varepsilon)\boldsymbol{Y}_j$ and $Q(\varepsilon)$ in (3) reduces to

$$\begin{aligned} Q(\varepsilon) &= -\sum_{j=0}^{M_R-1}\left\{\left\|\boldsymbol{Y}_j - \frac{2}{K}\boldsymbol{W}_F(\varepsilon)\boldsymbol{W}_F^H(\varepsilon)\boldsymbol{Y}_j\right\|^2 \right. \\ &\qquad \left. + \text{trace}\left(\frac{2\sigma_z^2}{K}\boldsymbol{W}_F(\varepsilon)\boldsymbol{W}_F^H(\varepsilon)\right)\right\} \\ &= -\sum_{j=0}^{M_R-1}\left\{\left\|\boldsymbol{S}\boldsymbol{F}^H(\varepsilon)\underbrace{\boldsymbol{W}_N^H\boldsymbol{Y}_j}_{\boldsymbol{y}_j}\right\|^2 \right. \\ &\qquad \left. + \text{trace}\left(\frac{2\sigma_z^2}{K}\boldsymbol{W}_{KL}^H\boldsymbol{X}_P^H\boldsymbol{X}_P\boldsymbol{W}_{KL}\right)\right\} \end{aligned} \tag{5}$$

where $\boldsymbol{S} = \left(\boldsymbol{I} - (2/K)\boldsymbol{W}_K^I\boldsymbol{X}_P\boldsymbol{W}_{KL}\boldsymbol{W}_{KL}^H\boldsymbol{X}_P^H\boldsymbol{W}_K^{IH}\right)$, and $\boldsymbol{y}_j$ is the time-domain received symbol sequence at the jth receiver. The second term is independent of ε, and hence has no contribution to the detector.

Based on (2) and (5), we form a new ML estimator for the CFO. Details of the search algorithm and subsequent discussions follow.

- **FFT-Based Search Algorithm:** It is possible to simplify (5) to

$$\begin{aligned} Q(\varepsilon) &= -\sum_{j=0}^{M_R-1}\left\{\boldsymbol{y}_j^H\boldsymbol{F}(\varepsilon)\underbrace{\boldsymbol{S}^H\boldsymbol{S}}_{\boldsymbol{T}}\boldsymbol{F}^H(\varepsilon)\boldsymbol{y}_j\right\} \\ &= -\sum_{j=0}^{M_R-1}\left\{\sum_{n=0}^{N-1}[\boldsymbol{T}]_{n,n}|y_j(n)|^2 \right. \\ &\qquad \left. + 2\Re\left(\sum_{m=0}^{N-2}\sum_{n=m+1}^{N-1}[\boldsymbol{T}]_{m,n}y_j^*(m)y_j(n) \right.\right. \\ &\qquad \left.\left. \times e^{-j(2\pi\varepsilon/N)(n-m)}\right)\right\} \end{aligned} \tag{6}$$

where $y_j(n)$ denotes the time-domain received symbol at the nth subcarrier associated with the jth receive antenna. $\Re(\cdot)$ is the real part of a quantity. Note that the first term in (6) is a constant. And the second term is due to the Hermitian symmetry of $\boldsymbol{T}$.

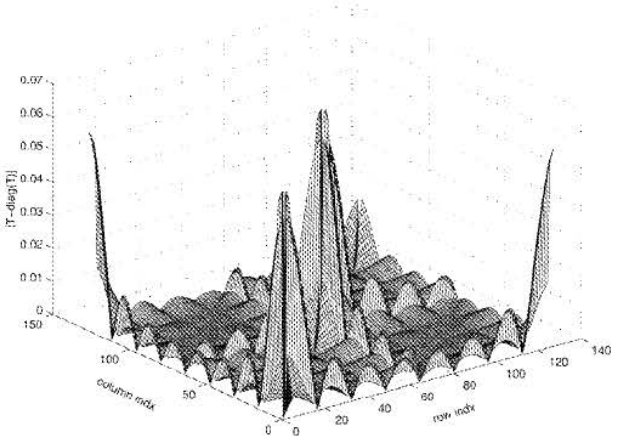


Fig. 2. Absolute values of the off-diagonal elements of matrix $\boldsymbol{T}$, as defined in (6), with $K = 120$, $N = 128$. The pilot-symbol sequence from the zeroth transmit antenna is set to $X_0[n] = 1/\sqrt{2}, \forall\, n$.

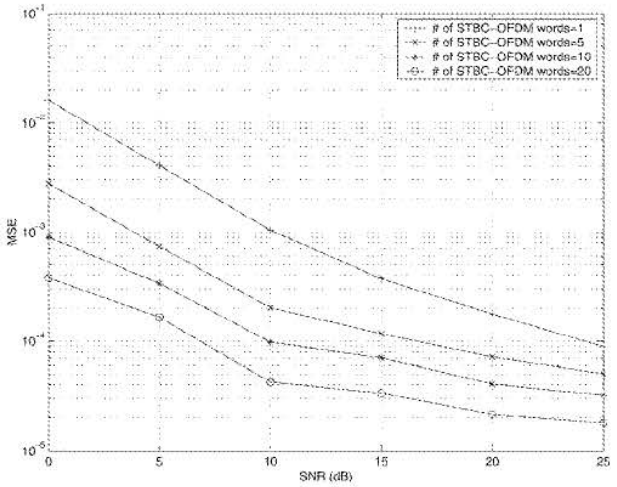


Fig. 3. MSE of the CFO estimate $\hat{\varepsilon}$. Various numbers of STBC-OFDM codewords are considered. We set the true ε to 0.1 and the length of symbol sequence as 1024 when performing FFT in (7).

By denoting $n' = n - m$, we can further simplify (6) to

$$\begin{aligned} Q(\varepsilon) &= -2\Re\left(\sum_{j=0}^{M_R-1}\left\{\sum_{n'=1}^{N-1}r_j(n')e^{-j(2\pi\varepsilon/N)n'}\right\}\right) + \text{const.} \\ &= -2\Re\left(\sum_{j=0}^{M_R-1}R_j(\varepsilon)\right) + \text{const.} \end{aligned} \tag{7}$$

where $r_j(n') = \sum_{m=0}^{N-1-n'}[\boldsymbol{T}]_{m,m+n'} \cdot y_j^*(m)y_j(m+n')$, and $R_j(\varepsilon) = \sum_{n'=1}^{N-1}r_j(n')e^{-j(2\pi\varepsilon/N)n'}$ can be easily computed using the FFT algorithm. Better frequency resolution can be achieved by zero-padding to effectively increase the length of the symbol sequence. We also assume a small ε (i.e., $|\varepsilon| < 0.5$, since larger CFOs

Petitioner Samsung Ex-1004, 0171

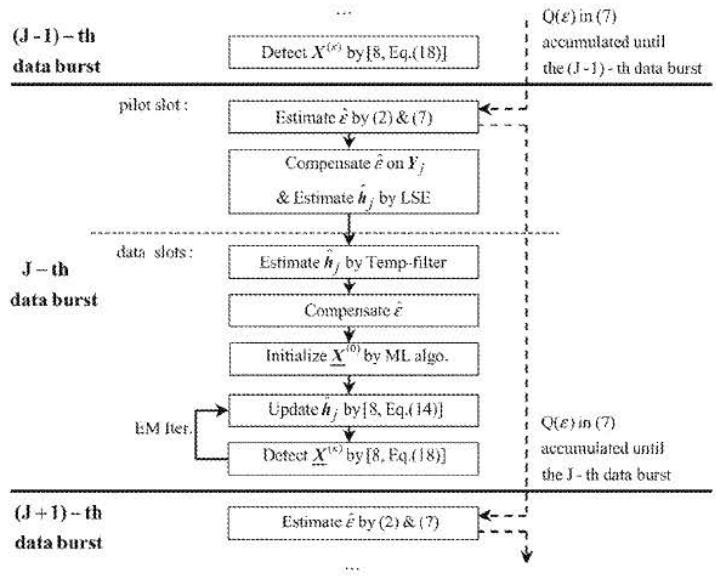


Fig. 4. Overview of our EM-based iterative receiver for MIMO OFDM systems subject to CFO.

can be compensated by an automatic frequency-control circuit [21] and what remains is the residual CFO) between any pair of the transmit and receive oscillators. This assumption, together with the FFT-based implementation, will significantly accelerate the search algorithm for $\hat{\varepsilon}$ in (2).

- **Truncated Observation Window of Subcarriers:** We now explain the reason why not all N OFDM subcarriers are required for symbol transmission. Since the first term in (6) is independent of ε, the diagonal elements in matrix $\boldsymbol{T}$ are useless for the detection. So we only examine the off-diagonal elements.

  After careful computation, we show that the off-diagonal elements of matrix $\boldsymbol{S}$ in (5) are in (8), shown at the bottom of the next page.

  When $K = N$, based on the fact that $\sum_{n=0}^{N-1} e^{j(2\pi/N)nm} = 0$ for $\forall\, m \neq 0$, we see that at least one term in the (A_1, A_2) or (B_1, B_2) pair is zero if $r \neq s$. Hence, when $K = N$, all the off-diagonal elements of $\boldsymbol{S}$ and $\boldsymbol{T} = \boldsymbol{S}^H\boldsymbol{S}$ in (6) are equal to zero. However, this does not hold when $K < N$. For example, Fig. 2 shows the nonzero absolute values of the off-diagonal elements in $\boldsymbol{T}$ with $K = 120$, $N = 128$. Thus, in order to perform good detection, it is necessary to reserve some redundant OFDM subcarriers.

- **Multiple-Symbol Estimation Scheme:** Another observation is that the MSE of the CFO estimate is reduced with the increase of the number of STBC-OFDM codewords, as shown in Fig. 3. Note that the floor of MSE at high SNRs is due to the limited frequency resolution when performing FFT, which is determined by the length of symbol sequence after zero padding. In the example of Fig. 3, the length of symbol sequence is set at 1024.

C. Integration of CFO Estimation and EM-Based Iterative Receiver Design

We have introduced a new ML estimator for CFO in Section II-B. We now combine it with our low-complexity EM-based iterative receiver, since both the CFO estimation and initialization steps of the EM algorithm are pilot-aided. We also discuss the overall design of an EM-based iterative receiver with CFO estimation for MIMO OFDM systems.

The performance of the EM algorithm depends on the initial estimation of transmitted symbols, which are computed by the traditional ML algorithm. Thus, good estimation of the fading coefficients is necessary in the initialization step of the EM algorithm. One simple solution involves pilot symbols, as shown in the data-burst structure in Fig. 1.

In the pilot slot, we estimate the normalized CFO ε with the aid of pilot symbols by (2) and (7). After compen-

$$[\boldsymbol{S}]_{r,s} = -\frac{1}{KN} \times \sum_{l=0}^{L-1} \left(\underbrace{\sum_{n_1=0}^{K-1} e^{j(2\pi/N)n_1(r-l)}}_{A_1} \underbrace{\sum_{n_2=0}^{K-1} e^{-j(2\pi/N)n_2(s-l)}}_{A_2} + \underbrace{\sum_{n_1=0}^{K-1} e^{j(2\pi/N)n_1(r-\tilde{L}-l)}}_{B_1} \underbrace{\sum_{n_2=0}^{K-1} e^{-j(2\pi/N)n_2(s-\tilde{L}-l)}}_{B_2} \right), \quad r, s = 0, 1, \ldots, N-1;\ r \neq s \tag{8}$$

Petitioner Samsung Ex-1004, 0172

sating the estimated $\hat{\varepsilon}$, the fading coefficients during the pilot slot are computed by the ML algorithm based on (1), i.e., $\hat{\boldsymbol{h}}_j = \mathrm{LSE}(\boldsymbol{Y}_j, \boldsymbol{W}_F(\hat{\varepsilon}))$ with LSE $(\cdot,\cdot)$ meaning the least-square estimator.

In the following data slots, a temporal filter is first applied to exploit the time correlation of channel responses (i.e., the Jakes' correlation structure), as introduced in [24] and [25].

Based on this channel estimation, after compensating the normalized CFO $\hat{\varepsilon}$ on the received symbols, an initial estimate of the transmitted symbols (denoted by $\underline{\boldsymbol{X}}^{(0)}$) is obtained by the traditional ML algorithm.

Then in the following EM iterations, $\hat{\boldsymbol{h}}_j$ is updated by [8, eq. (14)] and $\underline{\boldsymbol{X}}^{(\kappa)}$, the estimated transmitted matrix after κ iterations, is detected by [8, eq. (18)].

The overall EM-based iterative receiver design with CFO estimation is illustrated in the block diagram in Fig. 4. Note that in estimating ε in the pilot slot, the cost function $Q(\varepsilon)$ keeps increasing with the arrival of data bursts and will help improve the estimation, since multiple-codeword schemes can effectively reduce the MSE, as indicated in Fig. 3.

III. Simulation Results

In this section, we present simulation results to validate our proposed EM-based iterative receiver design for quadrature phase-shift keying (QPSK)-modulated MIMO OFDM systems subject to CFO. The available bandwidth is 800 KHz and is divided into $N = 128$ subcarriers. For the fading channel, we assume the $L = 4$ resolvable taps with various powers as $\sigma^2_{i,j,0} = \sigma^2_{i,j,1} = 0.3$, $\sigma^2_{i,j,2} = \sigma^2_{i,j,3} = 0.2$, $\forall\, i, j$. The OFDM system transmits in a bursty manner, i.e., each data burst includes $PQ + 1 = 11$ OFDM codewords; the first OFDM codeword contains optimal pilot symbols and the remaining 10 codewords have $Q = 5$ STBC-OFDM codewords.

Fig. 5(a) gives the BER performance of the iterative receiver for a MIMO OFDM system with the CFO $\varepsilon = 0.1$ and the Doppler frequency $f_D = 200$ Hz. The curve of the lowest BER is the performance of an ML receiver with perfect knowledge of ε and coherent detection (CD), which is computed by the analysis in [26]. Obviously, it becomes flat for high SNR. This error floor is due to the time variance of the fading channel, which we neglected in the model of (1). To study the effect of CFO, we also plot the BER curves without compensating a small $\varepsilon = 0.1$ in dash lines. It is not surprising to see the significant performance loss due to ICI.

The BER performance for the case with a slow-fading channel, e.g., $f_D = 50$ Hz, is illustrated in Fig. 5(b). Similar observations can be made except that the error floor is imperceptible when SNR < 20 dB. In other words, in the low-SNR range, the effect of temporal correlation due to fading is much less pronounced.

Besides the lower and upper bounds in Fig. 5, three other curves are plotted as the BER results of the EM-based iterative receiver after four iterations with perfect CFO information, with CFO estimation using single data burst and with CFO estimation using five successive data bursts, denoted by "EM#4 w/ perfect ε," "EM#4 w/ 1-burst est. ε," and "EM#4 w/ 5-burst est. ε," respectively. Note that for a fair comparison to the case of coherent detection, the rate loss by inserting pilot symbols for the EM-based receiver has been compensated, i.e., (SNR after compensation) $= (PQ/PQ+1)\cdot$ (SNR before compensation).

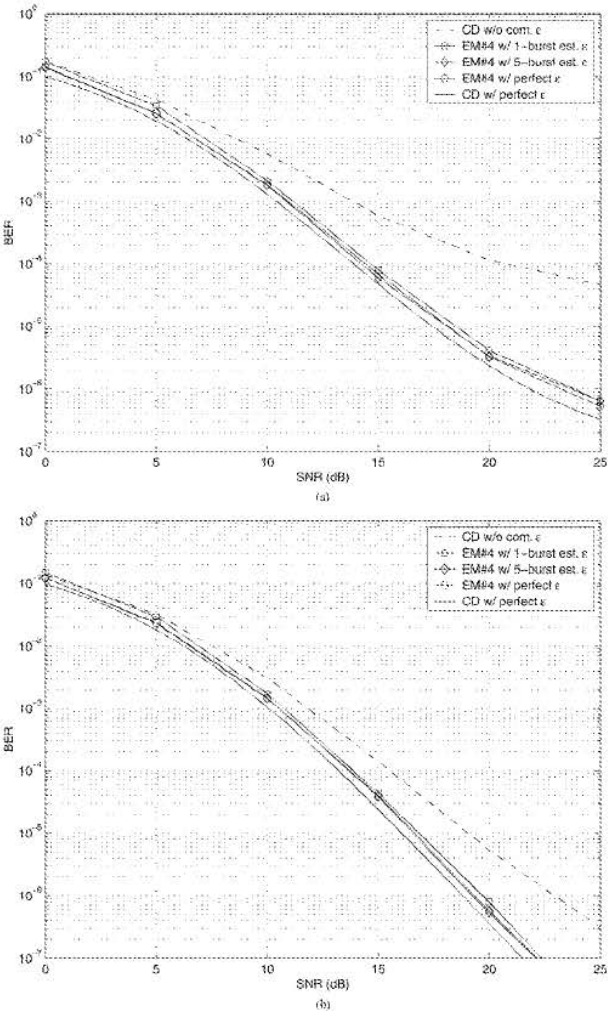


Fig. 5. BER performance of a ($N_T = 2$, $N_R = 2$) QPSK-modulated MIMO OFDM system with the true CFO $\varepsilon = 0.1$. Both coherent detection (with/without compensation of ε) and the EM-based iterative receiver (with perfect knowledge of ε, with single-burst estimation of ε and with five-burst estimation of ε) are considered. The Doppler frequency is set to (a) $f_D = 200$ Hz and (b) $f_D = 50$ Hz.

From Fig. 5, we observe that at low SNR, the EM result with perfect ε after several iterations is about 0.5 dB away from the ML outcome with coherent detection. Moreover, the performance loss from using the five-burst CFO estimation rather than the perfect knowledge of ε is imperceptible. This shows the effectiveness of our receiver in combating CFO in MIMO fading channels.

Another observation from Fig. 5 is that the EM-based receiver with multiple-symbol CFO detection (i.e., five-burst estimation of ε) outperforms the case of single-burst estimation. The gap is less than 0.4 dB, and becomes smaller with the increase of SNR, since better MSE estimation is obtained at high SNR. This small performance gain indicates that quite good BER performance

Petitioner Samsung Ex-1004, 0173

can be achieved via burst-by-burst CFO estimation, which is more practical without the assumption that the CFO remains constant within the interval of many data bursts.

REFERENCES

[1] H. Bolcskei, D. Gesbert, and A. Paulraj, "On the capacity of OFDM-based spatial multiplexing systems," *IEEE Trans. Commun.*, vol. 50, pp. 225–234, Feb. 2002.

[2] M. Uysal, N. Al-Dhahir, and C. N. Georghiades, "A space–time block-coded OFDM scheme for unknown frequency-selective fading channels," *IEEE Commun. Lett.*, vol. 5, pp. 393–395, Oct. 2001.

[3] R. A. Stirling-Gallacher and Z. Wang, "Improving performance of coherent coded OFDM systems using space–time transmit diversity," *Electron. Lett.*, vol. 37, pp. 457–458, Mar. 2001.

[4] S. N. Diggavi, N. Al-Dhahir, A. Stamoulis, and A. R. Calderbank, "Differential space–time coding for frequency-selective channels," *IEEE Commun. Lett.*, vol. 6, pp. 253–255, Jun. 2002.

[5] X. Wang and H. Poor, "Iterative (turbo) soft interference cancellation and decoding for coded CDMA," *IEEE Trans. Commun.*, vol. 47, pp. 1046–1061, Jul. 1999.

[6] B. Lu and X. Wang, "Iterative receivers for multiuser space–time coding systems," *IEEE J. Sel. Areas Commun.*, vol. 18, pp. 2322–2335, Nov. 2000.

[7] ——, "Bayesian blind turbo receiver for coded OFDM systems with frequency offset and frequency-selective fading," *IEEE J. Sel. Areas Commun.*, vol. 19, pp. 2516–2527, Dec. 2001.

[8] B. Lu, X. Wang, and Y. Li, "Iterative receivers for space–time block coded OFDM systems in dispersive fading channels," *IEEE Trans. Wireless Commun.*, vol. 1, pp. 213–225, Apr. 2002.

[9] K. R. Narayanan and G. L. Stuber, "A serial concatenation approach to iterative demodulation and decoding," *IEEE Trans. Commun.*, vol. 47, pp. 956–961, Jul. 1999.

[10] C. Douillard, M. Jzquel, C. Berrou, A. Picart, P. Didier, and A. Glavieux, "Iterative correction of intersymbol interference: Turbo equalization," *Eur. Trans. Telecommun.*, vol. 6, pp. 507–511, Sep.–Oct. 1995.

[11] S. Benedetto, D. Divsalar, G. Montorsi, and F. Pollara, "Parallel concatenated trellis coded modulation," in *Proc. Int. Conf. Commun.*, vol. 2, Jun. 1996, pp. 974–978.

[12] Y. Sun, Z. Xiong, and X. Wang, "Iterative decoding of differentially space–time coded multiple descriptions of images," *IEEE Signal Process. Lett.*, vol. 11, pp. 686–689, Aug. 2004.

[13] G. J. McLachlan and T. Krishnan, *The EM Algorithm and Extensions*. New York: Wiley, 1997.

[14] C. N. Georghiades and J. Han, "Sequence estimation in the presence of random parameters via the EM algorithm," *IEEE Trans. Commun.*, vol. 45, pp. 300–308, Mar. 1997.

[15] P. H. Moose, "A technique for orthogonal frequency division multiplexing frequency offset correction," *IEEE Trans. Commun.*, vol. 42, pp. 2908–2914, Oct. 1994.

[16] H. Ge and K. Wang, "Efficient method for carrier offset correction in OFDM system," in *Proc. Int. Conf. Acoust., Speech, Signal Process.*, vol. 5, Mar. 1999, pp. 2467–2470.

[17] M. Luise and R. Reggiannini, "Carrier frequency acquisition and tracking for OFDM systems," *IEEE Trans. Commun.*, vol. 44, pp. 1590–1598, Nov. 1996.

[18] M.-K. Oh, X. Ma, G. B. Giannakis, and D.-J. Park, "Hopping pilots for estimating of frequency-offset and multi-antenna channels in MIMO OFDM," in *Proc. IEEE GLOBECOM*, vol. 2, Dec. 2003, pp. 1084–1088.

[19] S. M. Alamouti, "A simple transmit diversity technique for wireless communications," *IEEE J. Sel. Areas Commun.*, vol. 16, pp. 1451–1458, Oct. 1998.

[20] V. Tarokh, H. Jafarkhani, and A. R. Calderbank, "Space–time block coding for wireless communications: Performance results," *IEEE J. Sel. Areas Commun.*, vol. 17, pp. 451–460, Mar. 1999.

[21] S. A. Fechtel, "OFDM carrier and sampling frequency synchoronization and its performance on stationary and mobile channels," *IEEE Trans. Consum. Electron.*, vol. 46, pp. 438–441, Aug. 2000.

[22] Y. Li, "Simplified channel estimation for OFDM systems with multiple transmit antennas," *IEEE Trans. Wireless Commun.*, vol. 1, pp. 67–75, Jan. 2002.

[23] W. Jakes, *Microwave Mobile Communications*. New York: IEEE Press, 1974.

[24] Y. Li, L. J. Cimini, Jr., and N. R. Sollenberger, "Robust channel estimation for OFDM systems with rapid dispersive fading channels," *IEEE Trans. Commun.*, vol. 46, pp. 902–915, Jul. 1998.

[25] Y. Li, N. Seshadri, and S. Ariyavisitakul, "Channel estimation for OFDM systems with transmitter diversity in mobile wireless channels," *IEEE J. Sel. Areas Commun.*, vol. 17, pp. 461–471, Mar. 1999.

[26] Y. Sun and Z. Xiong, "Progressive image transmission over space–time coded OFDM systems with adaptive modulation," *IEEE Trans. Multimedia*, submitted for publication.

Petitioner Samsung Ex-1004, 0174

AN EM-BASED CHANNEL ESTIMATION ALGORITHM FOR SPACE-TIME AND SPACE-FREQUENCY BLOCK CODED OFDM

Xiaoqiang Ma, Hisashi Kobayashi, and Stuart C. Schwartz

Electrical Engineering Department, Princeton University
Princeton, New Jersey 08544-5263
Email: xma, hisashi, stuart@ee.princeton.edu

ABSTRACT

The combination of multiple-antenna and orthogonal frequency division multiplexing (OFDM) provides reliable communications over frequency selective fading channels. We investigate this approach and focus on the application of space-time block codes (STBC) and space-frequency block codes (SFBC) in OFDM systems. We compare the performance of maximum likelihood (ML), zero forcing (ZF) and conventional detection algorithms. We show that ZF provides a good trade-off between computational complexity and performance. The problem of channel estimation in STBC-OFDM and SFBC-OFDM system is also studied, including the derivation of the Cramer-Rao lower bound (CRLB). Since knowledge of the channel is required to coherently decode STBC-OFDM and SFBC-OFDM, we propose an iterative channel estimation algorithm based on the EM algorithm that requires very few pilot symbols. The CRLB can be achieved by the channel estimation algorithm.

1. INTRODUCTION

The combination of MIMO and OFDM is a strong candidate for the fourth-generation wireless communications [8]. It can provide very high spectrum efficiency and high data rate with reasonable complexity. In this paper we will investigate the combination of STBC and SFBC with OFDM. In particular, we will focus on the Alamouti STBC [1] with one receive antenna as an example. The same idea can be extended to STBC-OFDM or SFBC-OFDM with more transmit or receive antennas. Lee and Williams [6][7], studied STBC-OFDM and SFBC-OFDM. But their study was based on the the conventional decoding scheme, which assumed the channel response during one codeword is constant. We will investigate the effect of time or frequency variation on the performance using different decoding schemes. The channel estimation problem for MIMO-OFDM was first studied by Li [3]. A corresponding simplified algorithm was proposed in [4]. The main drawback of the above algorithm is that it is not suitable in a system with channel variation from frame to frame. Lee and Williams [5] proposed a multirate pilot-symbol-assisted channel estimator for OFDM with multiple transmit antennas. However, the percentage of pilot symbols is quite high, which decreases the spectrum efficiency. Another shortcoming is the delay caused by the time domain filtering. We propose an EM-based channel estimation algorithm for STBC-OFDM and SFBC-OFDM, which is a modified version of [2]. It is a frame based algorithm, which means that time domain filtering is not necessary. Therefore, the detection delay is minimized.

The rest of the paper is organized as follows. In Section 2 we will describe the baseband OFDM system model with transmit antenna diversity. In Section 3 we will discus several STBC decoding algorithms. The CRLB and modified CRLB (MCRB) for channel estimation in MIMO-OFDM will be derived in Section 4. An EM-based channel estimation algorithm is discussed in Section 5. Finally, we draw some conclusions in Section 6.

2. SYSTEM MODEL

The schematic diagram of Fig. 1 is a baseband equivalent representation of an OFDM system with two transmit antennas and one receive antenna.

2.1. STBC-OFDM

STBC-OFDM encoding scheme involves two OFDM frames. At the m^{th} subcarrier, symbol $X_1(m)$ is transmitted from antenna 1 and symbol $X_2(m)$ is transmitted from antenna 2 at time instant 1. At time instant 2, $-X_2^*(m)$ and $X_1^*(m)$ are transmitted from antenna 1 and antenna 2, respectively. Denote the frequency response from transmit antenna 1 to the receive antenna as $H_{11}(m)$ and $H_{12}(m)$ at time instant 1 and 2, respectively, and the frequency response from transmit antenna 2 to the receive antenna as $H_{21}(m)$ and $H_{22}(m)$ at time instant 1 and 2, respectively. The received signals are given as

$$Y_1(m) = H_{11}(m)X_1(m) + H_{21}(m)X_2(m) + N_1(m),$$

Petitioner Samsung Ex-1004, 0175

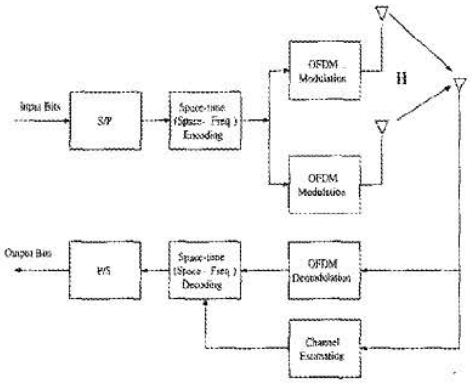


Fig. 1. Baseband OFDM system model with transmit diversity

$$Y_2(m) = -H_{12}(m)X_2^*(m) + H_{22}(m)X_1^*(m) + N_2(m).$$

2.2. SFBC-OFDM

The rationale for the use of SFBC in OFDM is that the channel frequency response of adjacent subcarriers remains almost constant in such a system. It only involves one OFDM frame. In the $2m^{th}$ subcarrier, symbol $X_1(2m)$ is transmitted from antenna 1 and symbol $X_2(2m)$ is transmitted from antenna 2. At the same time, $-X_2^*(2m)$ and $X_1^*(2m)$ are transmitted from antenna 1 and antenna 2 respectively in the $(2m+1)^{th}$ subcarrier. Denote the frequency response from transmit antenna 1 to the receive antenna as $H_1(2m)$ and $H_1(2m+1)$ of the $2m^{th}$ and the $(2m+1)^{th}$ subcarriers, respectively, and the frequency response from transmit antenna 2 to the receive antenna as $H_2(2m)$ and $H_2(2m+1)$ of the $2m^{th}$ and the $(2m+1)^{th}$ subcarriers, respectively. The received signals can be expressed in a similar way.

3. STBC DECODING SCHEMES

STBC decoding is discussed in [1]. It assumes the channel is constant during one codeword. We call it the conventional decoding method in this paper. For the case of STBC with changing channels and SFBC in OFDM, the assumption no longer holds. The channel coefficient matrix is not a scaled unitary matrix in general. Therefore, the conventional decoding method is not optimal. The optimal decoding method in this case is the maximum likelihood (ML) algorithm. The main shortcoming of the optimal decoding algorithm is the high computation burden that grows exponentially as the number of constellation points increases.

A suboptimal decoding approach is the so called zero-forcing (ZF) approach. It is less computationally complex and in the case of two transmit antennas, the matrix inversion is quite simple.

Simulation results (omitted due to limited space) show that the performance of the ZF approach is only slightly worse than the performance of the optimal ML approach. Therefore, the ZF approach is a good tradeoff between performance and complexity.

4. CRAMER-RAO LOWER BOUND

In this section we will derive the CRLB and MCRB for the channel estimate in general MIMO-OFMDM systems. In particular, we will focus on MIMO-OFDM systems with two transmit antennas and one receive antenna.

The MIMO-OFDM system model with two transmit antennas and one receive antenna can be written in vector form

$$\underline{Y} = \mathbf{X}_1\mathbf{W}_L\underline{h}_1 + \mathbf{X}_2\mathbf{W}_L\underline{h}_2 + \underline{N}. \quad (1)$$

where $\underline{Y}$ is the received signal, $\mathbf{X}_1$ and $\mathbf{X}_2$ are transmitted signals from antennas 1 and 2 in diagonal matrix form, $\underline{h}_1$ and $\underline{h}_2$ are CIRs from transmit antenna 1 and 2 to the receive antenna, respectively. $\underline{N}$ is the Gaussian noise vector and each element is zero mean and variance $\sigma^2/2$ for each dimension. $\mathbf{W}_L$ is the submatrix of the FFT matrix with first L columns.

The parameter vector here is obviously $\underline{\theta} = [\underline{h}_1^T \quad \underline{h}_2^T]^T$. The CRLB gives a lower bound for the variance of an unbiased estimate

$$CRLB(\underline{\theta}_i) = I^{-1}(\underline{\theta})_{ii}, \quad 1 \le i \le 2L, \quad (2)$$

where L is the channel delay spread and $I(\theta)$ is Fisher information matrix

$$I(\underline{\theta}) = \mathrm{E}\left\{\frac{\partial}{\partial\underline{\theta}}\log f(\underline{Y}|\underline{\theta})\left(\frac{\partial}{\partial\underline{\theta}}\log f(\underline{Y}|\underline{\theta})\right)^H\right\} \quad (3)$$

Following (1) we have the pdf of $\underline{Y}$ given $\underline{\theta}$

$$f(\underline{Y}|\underline{\theta}) = \frac{1}{(\pi\sigma^2)^M}\exp\left\{-\frac{1}{\sigma^2}\|\underline{Y} - \sum_{k=1}^{2}\mathbf{X}_k\mathbf{W}_L\underline{h}_k\|^2\right\}, \quad (4)$$

where we assume the data matrices $\mathbf{X}_1$ and $\mathbf{X}_2$ are known so that they do not appear as conditioned variables.

The Fisher information matrix can be partitioned into four small blocks $I(\underline{\theta}) = \begin{bmatrix} I_1 & I_2 \\ I_3 & I_4 \end{bmatrix}$, where

$$I_1 = \frac{1}{\sigma^2}\mathbf{W}_L^H\mathbf{X}_1^H\mathbf{X}_1\mathbf{W}_L, I_2 = \frac{1}{\sigma^2}\mathbf{W}_L^H\mathbf{X}_2^H\mathbf{X}_1\mathbf{W}_L$$

$$I_3 = \frac{1}{\sigma^2}\mathbf{W}_L^H\mathbf{X}_1^H\mathbf{X}_2\mathbf{W}_L, I_4 = \frac{1}{\sigma^2}\mathbf{W}_L^H\mathbf{X}_2^H\mathbf{X}_2\mathbf{W}_L$$

Petitioner Samsung Ex-1004, 0176

We define the CRLB of $\underline{h}_1$ and $\underline{h}_2$ as

$$CRLB(\underline{h}_1) = \sum_{i=1}^{L} I^{-1}(\underline{\theta})_{ii}, \quad (5)$$

$$CRLB(\underline{h}_2) = \sum_{i=L+1}^{2L} I^{-1}(\underline{\theta})_{ii}. \quad (6)$$

These CRLBs are obviously signal dependent since the transmitted signals $\mathbf{X}_1$ and $\mathbf{X}_2$ appear in the Fisher information matrix. In order to eliminate the dependency of the transmitted signals, we take expectations of I_i with respect to $\mathbf{X}_1$ and $\mathbf{X}_2$. We also make an additional assumption that transmitted signals from different antennas are independent, i.e., $\mathsf{E}\{X_1(m)X_2^*(m)\} = 0$. And, we also assume $\mathsf{E}\{|X(m)|^2\} = A$. This assumption is valid for general MIMO-OFDM systems with independent transmitted signals from different transmit antennas as well as STBC-OFDM and SFBC-OFDM. Therefore, we have the following expectations $\mathsf{E}\{I_1\} = \mathsf{E}\{I_4\} = \frac{MA}{\sigma^2} I_L$ and $\mathsf{E}\{I_2\}\mathsf{E}\{I_3\} = 0$. The CRLBs becomes modified CRLB (MCRB) after taking the above expectations. The MCRBs can easily be calculated as

$$MCRB(\underline{h}_1) = MCRB(\underline{h}_2) = \frac{L\sigma^2}{MA}, \quad (7)$$

where M is the number of subcarriers. The above derivation can easily be extended to the case of using D frames of data, assuming the channel is constant during these D frames. The result becomes

$$MCRB(\underline{h}_1) = MCRB(\underline{h}_2) = \frac{L\sigma^2}{MDA}, \quad (8)$$

which is D times smaller than the case that only one frame of data are observed. Further extensions to arbitrary number of transmit or receive antenna is straightforward.

5. AN EM-BASED CHANNEL ESTIMATION ALGORITHM FOR STBC-OFDM AND SFBC-OFDM

If the system is perfectly time and frequency synchronized for STBC-OFDM and SFBC-OFDM, channel estimation error is the main source of performance degradation. In this section, we propose an EM-based channel estimation algorithm for STBC-OFDM and SFBC-OFDM, which is a modified version of [2].

First we give the EM-based channel estimation algorithm for SFBC-OFDM which only involves one OFDM frame. The SFBC-OFDM system model is given by 1 with $X_1(2m+1) = -X_2^*(2m)$ and $X_2(2m+1) = X_1^*(2m)$.

Following [9], a natural choice for "complete" data $\underline{Z}_1$ and $\underline{Z}_2$ is obtained by decomposing the observed data $\underline{Y}$ into 2 components, i.e.,

$$\underline{Z}_i = \mathbf{X}_i \mathbf{W}_L \underline{h}_i + \underline{N}_i, \quad i = 1, 2, \quad (9)$$

where $\underline{N}_i, i = 1, 2$ are obtained by arbitrarily decomposing the total noise $\underline{N}$ into 2 components such that $\underline{N}_1 + \underline{N}_2 = \underline{N}$. Thus, the relation between the "complete" data $(\underline{Z}_1, \underline{Z}_2)$ and "incomplete" data $\underline{Y}$ is given by $\underline{Y} = \underline{Z}_1 + \underline{Z}_2$.

It is easy to show the above described EM-base channel estimation algorithm takes the following form:

$$\underline{h}_i^{(p+1)} = \mathbf{W}_L^H \mathbf{X}_i^{-1} \underline{\hat{Z}}_i^{(p)}, \quad i = 1, 2, \quad (10)$$

where

$$\underline{\hat{Z}}_i^{(p)} = \underline{Z}_i^{(p)} + \beta_i \left(\underline{Y} - \sum_{j=1}^{2} \underline{Z}_j^{(p)} \right), \quad (11)$$

$$\underline{Z}_i^{(p)} = \mathbf{X}_i \mathbf{W}_L \underline{h}_i^{(p)}. \quad (12)$$

Observe that β_i can be arbitrarily selected due to the arbitrarily decomposition of the independent noise components $\underline{N}_i$. The only constraint is $\beta_1 + \beta_2 = 1$. A typical value is $\beta_1 = \beta_2 = 0.5$ for the case of two transmit antennas.

Note that the above result can only be applied for pilot frames, i.e, the transmitted signals $\underline{X}_1$ and $\underline{X}_2$ are known at the receiver, which is exactly the case in [2]. However, in the case of signal transmission, we don't know all the transmitted signals in these OFDM frames except for some pilot symbols. Thus, to make it feasible we adopt the p^{th} estimates $\underline{X}_1^{(p)}$ and $\underline{X}_2^{(p)}$ instead of the actual values in the algorithm. In SFBC-OFDM systems, we propose to use the ZF detection approach to obtain the estimates of transmit signals. Consequently, the algorithm is actually decision-directed and (10) and (12) become

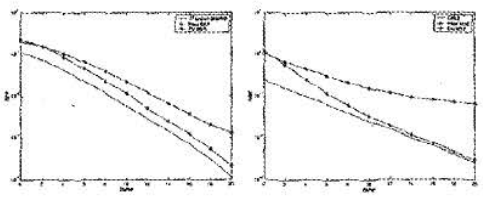
$$\underline{h}_i^{(p+1)} = \mathbf{W}_L^H (\mathbf{X}_i^{(p)})^{-1} \underline{\hat{Z}}_i^{(p)}, \quad i = 1, 2, \quad (13)$$

$$\underline{Z}_i^{(p)} = \mathbf{X}_i^{(p)} \mathbf{W}_L \underline{h}_i^{(p)}. \quad (14)$$

The above algorithm can easily be applied to STBC-OFDM systems. The only difference is that in STBC-OFDM systems the algorithm involves two OFDM frames and only one OFDM frame is involved in SFBC-OFDM systems. Thus, the algorithm should be carried out twice in each iteration for those two OFDM frames. The ZF detection approach is also used to detect the transmitted signals in these two frames.

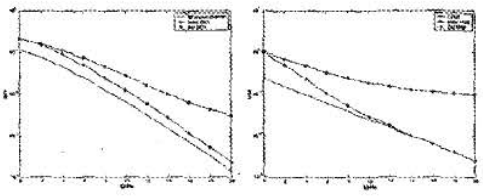
From Figs. 2 and 3 we can observe that the EM-based channel estimation algorithm can reduce the BER and MSE. Furthermore, it can achieve a BER performance close to the case where the channel characteristic is completely known at the receiver in the high SNR region. However, there is still a BER gap between the lower bound and the BER of the EM-based algorithm. The MSE also is very close to the MCRB when the SNR increases. Comparing Figure 2(b) with 3(b) we find that the MCRB can be achieved by increasing the SNR in a SFBC-OFDM system, while this is not the case in a STBC-OFDM system. It turns out that the

Petitioner Samsung Ex-1004, 0177



(a) BER (b) MSE

Fig. 2. BER and MSE of the EM-based channel estimation algorithm for STBC-OFDM systems.



(a) BER (b) MSE

Fig. 3. BER and MSE of the EM-based channel estimation algorithm for SFBC-OFDM systems.

number of iterations per frame of STBC-OFDM systems is slightly larger than that of SFBC-OFDM systems. This is observed from Fig. 4. In general, the proposed EM-based channel estimation algorithm works both for STBC-OFDM and SFBC-OFDM systems. Similar performance, including BER and MSE, can be achieved by the algorithm. However, it is more suitable for SFBC-OFDM systems due to the lower MSE and smaller iterations per frame.

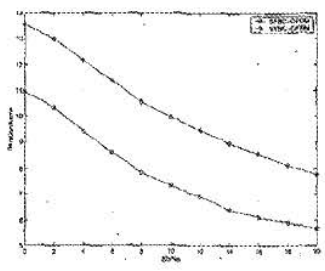


Fig. 4. Iterations per OFDM frame of the EM-based channel estimation algorithm for STBC-OFDM and SFBC-OFDM systems.

6. CONCLUSION

In this paper we investigated applications of STBC and SFBC in OFDM systems. Channel estimation in STBC-OFDM and SFBC-OFDM is studied, including the derivation of the CRLB and MCRB. We proposed an iterative channel estimation algorithm based on the EM algorithm with only a few pilot symbols required. Simulation results show that it is a very promising channel estimation technique, which can achieve near optimum BER and the CRLB when the SNR becomes large. Furthermore, it appears to be more suitable for SFBC-OFDM in terms of lower MSE and smaller required iterations.

Note: Additional details in a longer paper and larger figures can be found at http://www.ee.princeton.edu/~xma/mimo.pdf.

7. REFERENCES

[1] S. Alamouti, "A simple transmit diversity technique for wireless communications," *IEEE JSACs*, vol. 16, no. 8, pp. 1451-1458, Oct. 1998.

[2] Y. Xie and C. N. Georghiades, "An EM-based channel estimation algorithm for OFDM with transmitter diversity," in *Proc. of Globecom 2001*, pp. 871-875.

[3] Ye(Geoffrey) Li, N. Seshadri, and S. Ariyavisitakul, "Channel estimation for OFDM systems with transmitter diversity in mobile wireless channels," *IEEE JSAC*, vol. 17, no. 3, pp. 451-460, Mar. 1999.

[4] Ye(Geoffrey) Li, "Simplified channel estimation for OFDM systems with multiple transmit antennas," *IEEE Trans. on Wireless Comm.*, vol. 1, no. 1, pp. 67-75, Jan. 2002.

[5] K. F. Lee and D. B. Williams, "A multirate pilot-symbol-assisted channel estimator for OFDM transmitter diversity systems," in *Proc. of ICASSP 2001*, vol. 4, pp. 2409 -2412, 2001.

[6] K. F. Lee and D. B. Williams, "A space-time coded transmitter diversity technique for frequency selective fading channels," in *Proc. of 2000 IEEE Sensor Array and Multichannel Signal Processing Workshop*, pp. 149 -152, 2000.

[7] K. F. Lee and D. B. Williams, "A space-frequency transmitter diversity technique for OFDM systems," in *Proc. of Globlecom 2000*, vol. 3, pp. 1473 -1477, 2000.

[8] H. Sampath, S. Talwar, J. Tellado, V. Erceg and A. Paulraj, "A fourth-generation MIMO-OFDM broadband wireless systems: design, performance, and field trial results," *IEEE Comm. Mag.*, vol. 40, no. 9, pp. 143-149, Sep. 2002.

[9] Meir Feder and Ehud Weinstein, "Parameter estimation of superimposed signals using the EM algorithm," *IEEE Trans. on Acoustic, Speech, and Signal Processing*, Vol. 36, No. 4, pp. 477-489, Apr. 1989.

Petitioner Samsung Ex-1004, 0178

A Road to Future Broadband Wireless Access: MIMO-OFDM-Based Air Interface

Hongwei Yang, Alcatel Shanghai Bell Co., Ltd.

ABSTRACT

Orthogonal frequency-division multiplexing is a popular method for high-data-rate wireless transmission. OFDM may be combined with multiple antennas at both the access point and mobile terminal to increase diversity gain and/or enhance system capacity on a time-varying multipath fading channel, resulting in a multiple-input multiple-output OFDM system. In this article we give a brief technical overview of MIMO-OFDM system design. We focus on various research topics for the MIMO-OFDM-based air interface, including spatial channel modeling, MIMO-OFDM transceiver design, MIMO-OFDM channel estimation, space-time techniques for MIMO-OFDM, and error correction code. The corresponding link-level simulation results are encouraging, and show that MIMO-OFDM is a promising road to future broadband wireless access.

INTRODUCTION

The first-generation (1G) radio systems use analog communication techniques to transmit voice over radio, such as Advanced Mobile Phone Services (AMPS), the Nordic Mobile Telephone (NMT) system, and the Total Access Communication System (TACS), which were developed in the 1970s and 1980s. The 2G systems were built in the 1980s and 1990s, and featured the implementation of digital technology, such as Global System for Mobile Communications (GSM), Digital-AMPS (D-AMPS), code-division multiple access (CDMA), and personal digital cellular (PDC); among them GSM is the most successful and widely used 2G system. 3G mobile technologies provide users with high-data-rate mobile access, which developed rapidly in the 1990s and is still developing today. The three major radio air interface standards for 3G are wideband CDMA (WCDMA), time-division synchronous CDMA (TD-SCDMA), and cdma2000. The transmitted data rate of 3G is up to 144 kb/s for high-mobility traffic, 384 kb/s for low-mobility traffic, and 2 Mb/s in good conditions. However, there are two limitations with 3G. One is the difficult extension to very high data rates such as 100 Mb/s with CDMA due to excessive interference between services. The other is the difficulty of providing a full range of multirate services, all with different quality of service (QoS) and performance requirements, due to the restrictions imposed on the core network by the air interference standard. Therefore, the future mobile communication system with features of high-data-rate transmission and open network architecture, called 4G, is desired to satisfy the increasing demand for broadband wireless access. Hence, 4G refers to a collection of technologies and standards that will find their way into a range of new ubiquitous computing and communication systems. The key objectives of 4G are to provide reliable transmission with high peak data rates ranging from 100 Mb/s for high-mobility applications to 1 Gb/s for low-mobility applications, high spectrum efficiency up to 10 b/s/Hz, and ubiquitous services that can accommodate various radio accesses.

To take international technology leadership and reserve competitiveness in the growing mobile communication market, Alcatel Research and Innovation Center has been carrying out research and innovation toward 4G for a long time. Their research topics cover MIMO and OFDM related technologies including turbo product code, channel modeling, channel estimation, adaptive modulation and coding (AMC), hybrid automatic repeat request (H-ARQ), dynamic resource allocation (DRA), and so on. They have also participated in a program sponsored by the Chinese government, Future Technologies for Universal Radio Environment (FuTURE), since 2001.

This article focuses on 4G air interface technologies, especially MIMO-OFDM-based air interface to provide reliable communications with high data rates and bandwidth efficiency.

OFDM AND MIMO

OFDM

OFDM has become a popular technique for transmission of signals over wireless channels. It converts a frequency-selective channel into a parallel collection of frequency flat subchannels, which makes the receiver simpler. The time

 0163-6804/05/$20.00 © 2005 IEEE

Petitioner Samsung Ex-1004, 0179

Because of the sensitivity of MIMO algorithms with respect to the channel matrix properties, channel modeling is particularly critical to assess the relative performance of MIMO-OFDM systems.

domain waveforms of the subcarriers are orthogonal, yet the signal spectra corresponding to the different subcarriers overlap in frequency. Hence, the available bandwidth is used very efficiently. Using adaptive bit loading techniques based on the estimated dynamic properties of the channel, the OFDM transmitter can adapt its signaling to match channel conditions, and approach the ideal water pouring capacity of a frequency-selective channel.

Advantages of OFDM systems are:

- High spectral efficiency
- Simple implementation by fast Fourier transform (FFT)
- Low receiver complexity
- Suitability for high-data-rate transmission over a multipath fading channel
- High flexibility in terms of link adaptation
- Low-complexity multiple access schemes such as orthogonal frequency-division multiple access (OFDMA)

Disadvantages of OFDM systems are:

- Higher peak-to-average power ratio (PAPR) compared to single-carrier modulation
- Sensitivity to time and frequency synchronization errors

OFDM has been adopted in several wireless standards such as digital audio broadcasting (DAB), terrestrial digital video broadcasting (DVB-T), the IEEE 802.11a wireless local area network (WLAN) standard, and IEEE 802.16a. Undoubtedly, OFDM could be a potential air interface candidate for future-generation mobile wireless systems.

MIMO

Multiple antennas can be used at the transmitter and receiver, now widely termed a MIMO system. A MIMO system takes advantage of the spatial diversity obtained by spatially separated antennas in a dense multipath scattering environment. MIMO systems may be implemented in a number of different ways to obtain either a diversity gain to combat signal fading or to obtain a capacity gain. Generally, there are three categories of MIMO techniques. The first one aims to improve the power efficiency by maximizing spatial diversity. Such techniques include delay diversity, space-time block codes (STBC) [1], and space-time trellis codes (STTC) [2]. The second type uses a layered approach to increase capacity [3]. One popular example of such a system is the vertical-Bell Laboratories layered space-time (V-BLAST) architecture, where independent data signals are transmitted over antennas to increase the data rate, but full spatial diversity is usually not achieved. The third type exploits knowledge of the channel at the transmitter. It decomposes the channel matrix using singular value decomposition (SVD) and uses these decomposed unitary matrices as pre- and post-filters at the transmitter and receiver to achieve capacity gain [4].

MIMO opens a new dimension, space, to offer the advantage of diversity, and therefore has been adopted in various standards. For instance, MIMO may be implemented in the high-speed downlink packet access (HSDPA) channel, which is a part of the Universal Mobile Telecommunications System (UMTS) standard. Preliminary efforts are also underway to define a MIMO overlay for the IEEE 802.11 standard for WLAN under the newly formed Wireless Next Generation (WNG) group.

MIMO-OFDM

MIMO is known to boost capacity. For high-data-rate transmission, the multipath characteristic of the environment causes the MIMO channel to be frequency-selective. OFDM can transform such a frequency-selective MIMO channel into a set of parallel frequency-flat MIMO channels, and therefore decrease receiver complexity. The combination of the two powerful techniques, MIMO and OFDM, is very attractive, and has become a most promising broadband wireless access scheme.

MIMO-OFDM Key Techniques

The Spatial Channel Model

Because of the sensitivity of MIMO algorithms with respect to the channel matrix properties, channel modeling is particularly critical to assess the relative performance of MIMO-OFDM systems. This section briefly describes the key channel characteristics that influence air interface design, such as time selectivity, frequency selectivity, and spatial selectivity.

Time Selectivity — We define the coherence time as the time difference at which the magnitude or envelope correlation coefficient between two signals at the same frequency falls below 0.5. Thus, a signal experiences slow or time-nonselective fading if its symbol period is much smaller than the channel coherence time, and fast or time-selective fading if its symbol period is more than the coherence time. When a signal is slow fading, we can assume that the channel impulse response (CIR) is time-invariant during a block transmission. When the coherence time is in the order of a symbol block interval, we say that the channel is quasi-static fading, which means that the channel fading is assumed to be constant over each block, and changes independently from block to block.

Frequency Selectivity — The coherence bandwidth captures the analogous notion for two signals of different frequencies transmitted at the same time. A signal experiences flat or frequency-nonselective fading if its bandwidth is much smaller than the channel coherence bandwidth, and frequency-selective fading if its bandwidth is more than the channel coherence bandwidth.

Spatial Selectivity — When using multiple-element antennas, the coherence distance represents the minimum distance in space separating two antenna elements such that they experience independent fading. Due to scattering environments, the channel exhibits independent or spatially selective fading. Spatially correlated fading results in lower achievable capacity of MIMO.

K-Factor — The fading signal magnitude follows a Rice distribution, and the ratio of the line-of-sight (LOS) component power to the diffraction component power is defined as the Ricean *K*-

Petitioner Samsung Ex-1004, 0180

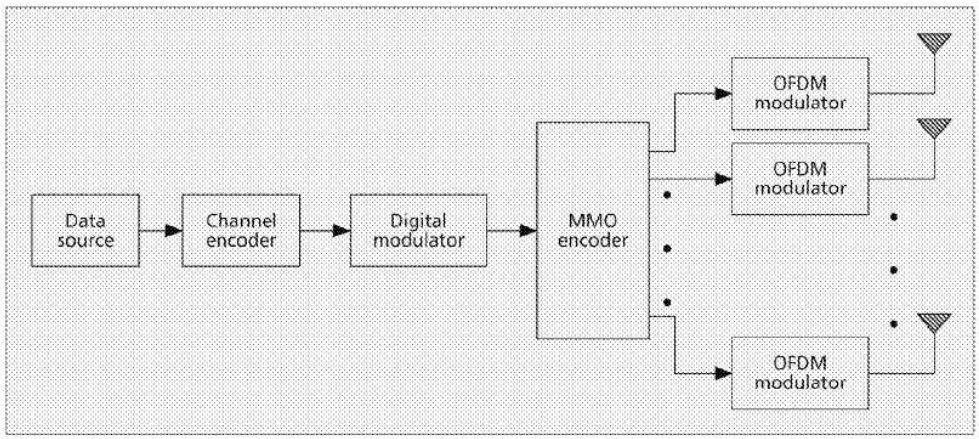


Figure 1. *A simplified block diagram of a MIMO-OFDM transmitter.*

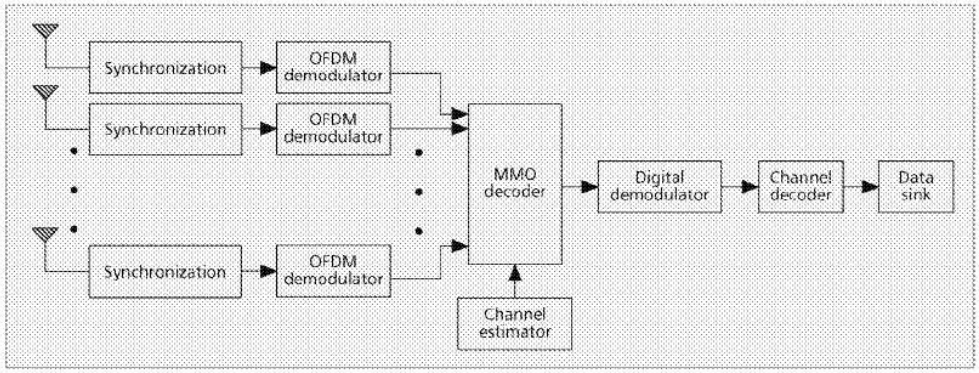


Figure 2. *A simplified block diagram of a MIMO-OFDM receiver.*

factor. The worst case fading occurs when the power of the LOS component is zero and the fading signal magnitude is regarded as Rayleigh distribution. Spatial channel often becomes more and more correlated as K-factor increases, and therefore lower multiplexing gain of MIMO system can be obtained.

MIMO-OFDM System Model

Transmitter — Figure 1 shows a simplified block diagram of a MIMO -OFDM transmitter. The source bitstream is encoded by a forward error correction (FEC) encoder. After that, the coded bitstream is mapped to a constellation by the digital modulator, and encoded by a MIMO encoder. Then each of the parallel output symbol streams corresponding to a certain transmit antenna follows the same transmission process. First, pilot symbols are inserted according to the pilot patterns. Then the symbol sequence in frequency is modulated by inverse FFT (IFFT) to an OFDM symbol sequence. A cycle prefix (CP) is attached to every OFDM symbol to mitigate the effect of channel delay spread, and a preamble is inserted in every slot for timing. Finally, the constructed data frame is transferred to IF/RF components for transmission.

Receiver — Figure 2 shows a simplified block diagram of a MIMO-OFDM receiver. The received symbol stream from IF/RF components over the receive antennas are first synchronized, including coarse frequency synchronization and timing aided by the preamble. After that, the preambles and CP are extracted from the received symbol stream, and the remaining OFDM symbol is demodulated by FFT. Frequency pilots are extracted from the demodulated OFDM symbol in the frequency domain, and fine frequency synchronization and timing are carried out to extract pilots and data symbols accurately for the following processing. The refined frequency pilots from all the receive antennas are used for channel estimation (CE). The estimated channel matrix aids the MIMO decoder in decoding the refined OFDM symbols. The estimated transmit symbols are then demodulated and decoded. Finally, the decoded source bitstreams are transmitted to the sink.

Frame Structure — Figure 3 shows an example for the frame format of the MIMO-OFDM system. In the time domain, a frame is a minimum transmission unit that includes 10 slots. Each slot consists of one slot preamble and eight OFDM symbols. The preamble is used for time synchronization. Each OFDM in a slot is attached to a CP that is used to reduce ISI, and therefore the design of channel equalizer is simplified. A scattered pilot pattern is used for CE at high mobility.

The frame is structured such that data and pilot symbols are transmitted over sub-carries, which allows the estimation of the above parameters. Once synchronization is obtained, fine timing estimates can be computed from the pilot symbols.

Petitioner Samsung Ex-1004, 0181

For OFDM systems with multiple transmit antennas, different signals are transmitted from different antennas simultaneously, and consequently, the received signal is the superposition of these signals, which gives rise to challenges for CE.

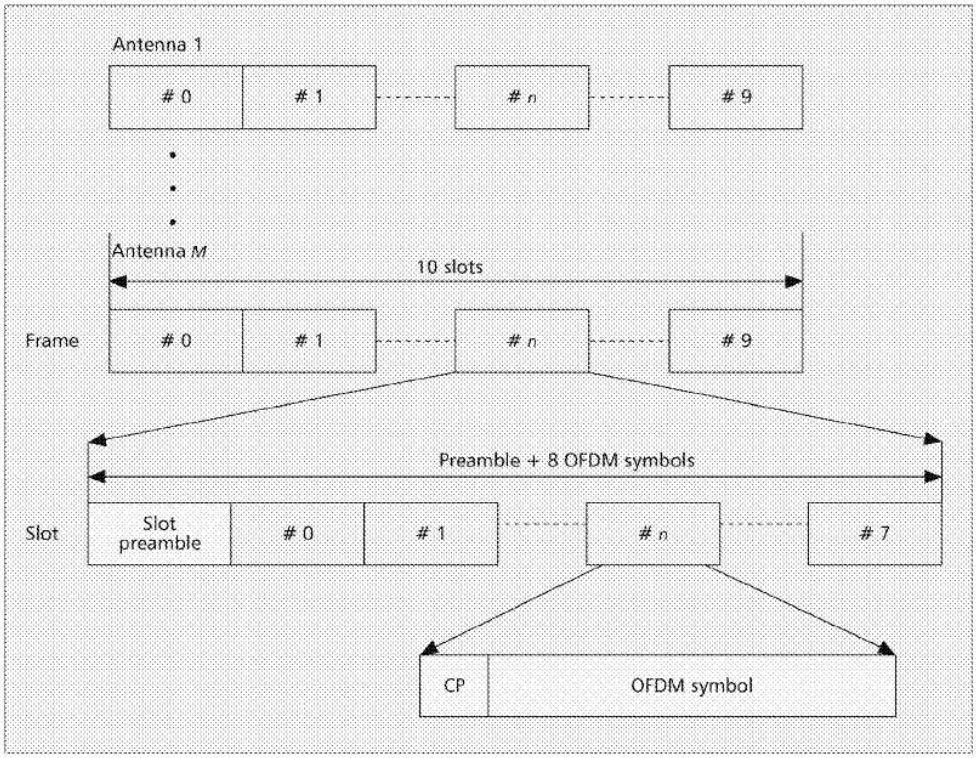


Figure 3. *The frame structure of a MIMO-OFDM system.*

SYNCHRONIZATION

Timing phase, timing frequency, and frequency offset estimation are carried out aided by the preamble of each slot and the pilot symbols in the frequency domain [5]. The frame is structured such that data and pilot symbols are transmitted over subcarries, which allows estimation of the above parameters. Once synchronization is obtained, fine timing estimates can be computed from the pilot symbols.

CE

MIMO-OFDM is a promising scheme for achieving high data rates and large system capacity over wireless links. To obtain the promised increase in data rate, accurate channel state information is required in the receiver. However, for OFDM systems with multiple transmit antennas, different signals are transmitted from different antennas simultaneously, and consequently, the received signal is the superposition of these signals, which gives rise to challenges for CE. As for pilot patterns, there are three kinds of CE algorithms for MIMO-OFDM system, respectively, based on scattered pilots, orthogonal pilots, and block pilots [6, 7]. Comparatively, the first one adapts to wide applications over fast fading and frequency selective channel. Therefore, we focus on it in the following.

Pilot Pattern — The scattered pilot pattern of transmit antennas is designed as follows. The pilot spacing in the time domain is designed to satisfy the sampling theorem, and the channel frequency response (CFR) of the OFDM symbols without pilots can be estimated through time domain interpolation according to the CE results of the adjacent OFDM symbols with pilots. Pilot spacing in the frequency domain should be designed such that the following inequality is satisfied, which is required by the MIMO-OFDM CE algorithm described here:

$$\frac{FFTsize}{PSF \cdot M} > Maximum\ Delay$$

where *PSF* denotes the pilot spacing in the frequency domain, and *Maximum Delay* is the maximum excess delay of the multipath channels between transmitter and receiver in units of sampling time. Figure 4 shows the pilot pattern over a transmit antenna. All the transmit antennas have the same pilot pattern.

MIMO-OFDM CE — We just focus on the processing in frequency domain. The time domain interpolation processing is omitted. The algorithm to estimate CFR of the multi-path channel between one transmit/receive antenna pair is the same as the following steps.

1) Multiply the received pilot sequence with the conjugate sequence of the pilot sequence of the transmit antenna and get the sequence of CFRs over pilots.

2) Make the *FFTsize*/*PSF*-point IFFT for the sequence of CFRs over pilots and get the sequence of CIRs.

3) Divide the sequence of CIRs into *M* segments of the same segment length, where *M* is the number of transmit antennas. Then the *i*th

Petitioner Samsung Ex-1004, 0182

segment ($i = 1, 2, \ldots, M$) will be the estimated CIR of the transmit/receive antenna pair. Hence, after making the *FFTsize*-point FFT for each segment with zero padding, we get the estimation of all the channels.

Simulation Result — A 3.2 GHz spatially uncorrelated UMTS vehicular A channel with speed of 60 km/h is used [8]. FFT size is 1024, OFDM sampling rate is 11.52 MHz, the pilot interval in the frequency domain is 8, pilots in the time domain are inserted in every OFDM symbol. The number of transmit/receive antennas is (2,2) and (4,4).

Mean square error (MSE) of the developed CE algorithm is shown in Fig. 5. From the figure we can observe that the MSE of the designed MIMO-OFDM estimator has a floor resulting from inter-subcarrier and inter-antenna interference. Related techniques to interference cancellation are desired for MIMO-OFDM system.

Space-Time Processing Techniques for MIMO

Current space-time processing techniques for MIMO typically fall into two categories, data rate maximization and diversity maximization schemes, although there has been some effort toward unification recently.

Spatial Multiplexing — Spatial multiplexing multiplexes multiple spatial channels to send as many independent data as we can over different antennas for a specific error rate. There are four spatial multiplexing schemes: diagonal BLAST, horizontal BLAST, V-BLAST, and turbo BLAST. Of them, V-BLAST is the most promising for its implementation simplicity [3].

The method to detect the transmitted signals consists of three main steps:

1). Estimate the channel matrix. This is often done through training sequence

2). Determinate the optimal detecting order and the nulling vectors

3). Detect the received signals based on the optimal detecting order and successive interference cancellation.

- Zero-forced (ZF) or minimum mean square error (MMSE) nulling: ZF or MMSE estimation of the strongest transmit signal is obtained via nulling out the weaker transmit signals.
- Detecting: The actual value of the strongest signal is detected by slicing to the nearest value in the signal constellations.
- Symbol interference cancellation: The effect of the strongest transmitted signal on the other weaker transmitted signal to be detected is removed from the vector of the received signals, after which we return to nulling in the first step.

Since the spatial multiplexing detector uses some form of channel matrix inversion, a unique solution is only possible if the number of receive antennas is greater than or equal to the number of independent transmit signals. Moreover, spatial multiplexing has poor detection performance over a spatially correlated channel.

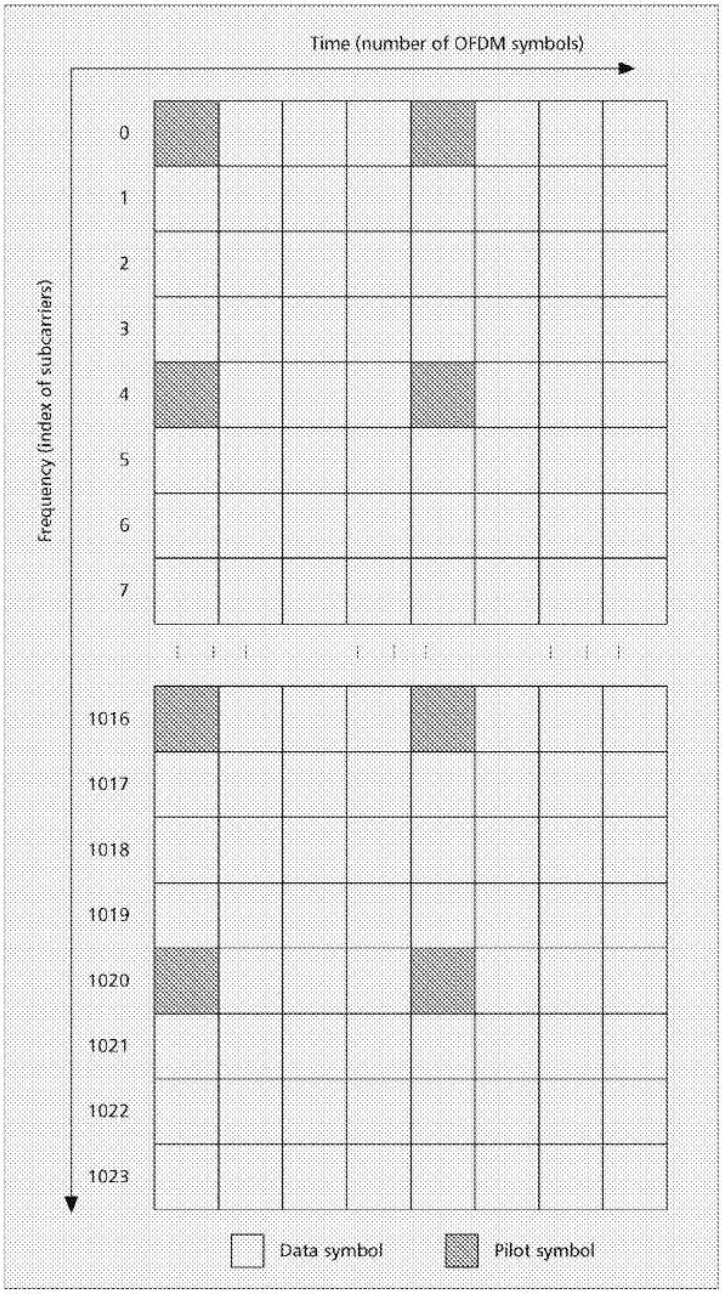


Figure 4. *An example of the pilot pattern over a transmit antenna.*

Space-Time Coding — Space-time coding jointly encodes the data streams over different antennas, and therefore aims to maximize diversity gain. Two main space-time coding schemes, STBC [1] and STTC [2], are mentioned here. STTC obtains coding and diversity gains due to coding in space-time dimension. But its decoding complexity increases greatly as the size of modulation constellations, state number, and code length increase. STBC based on orthogonal design obtains full diversity gain with low decoding complexity, and therefore has been widely

Petitioner Samsung Ex-1004, 0183

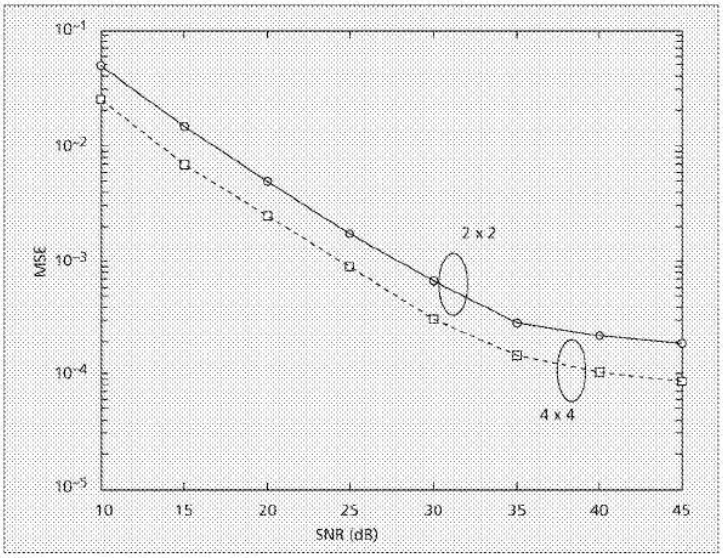


Figure 5. *MSE of the CE.*

MIMO candidates	SFBC/STBC	Spatial multiplexing
Data rate	U → High S → Low	S → High U → Low
Diversity gain	S	U
Spatial correlated channel	S	S → Low U → High
Frequency selective channel	S → MIMO-STBC	S
Fast fading channel	S → MIMO-SFBC	S
Channel estimation error	Insensitive	Insensitive → Low Sensitive → High
LOS	S	U
Antenna configuration	S → 2 Tx	S → Tx ≥ Rx

S: Suitable
U: Unsuitable

Table 1. *Comparisons of STC and spatial multiplexing.*

used. The well-known Alamouti code is just a special case of STBC with double transmit antennas [9]. Space-frequency block code (SFBC) is based directly on space-time codes (with time reinterpreted as frequency).

STBC is optimally designed under the assumption that the fading channel is quasi-static. Therefore, the time or frequency selectivity degrades the performance of STBC and SFBC. Between SFBC and STBC, one is selected based on the selectivity of the channel in the time or frequency domain. Whatever the delay spread of the channel, STBC is chosen only if the channel is slowly varying in the time domain when the terminal moves slowly. Similarly, at whatever speed the terminal moves, SFBC is chosen only if the channel is slowly varying in the frequency domain when the delay spread of the channel is small.

Comparisons of STC and Spatial Multiplexing — Based on the algorithms above, STC and spatial multiplexing are compared by analysis and simulations here. Advantages and disadvantages of STC and spatial multiplexing are listed in Table 1.

Data rate: SFBC/STBC is only suitable for low-data-rate service. Here, low data rate is just relative to the very high data rate achieved by spatial multiplexing. Thus, in order to achieve very high bandwidth efficiency up to the future 10 b/s/Hz, spatial multiplexing is a better choice.

Diversity gain: There is no coding in the time or space domain for spatial multiplexing, and it is not suitable for achieving diversity gain. If a system is designed to achieve better QoS for average data rate, STBC/SFBC is a better choice.

Spatially correlated channel: Over a weak spatially correlated channel, both SFBC/STBC and spatial multiplexing can work well. Over a spatially correlated channel, STBC/SFBC is preferred because spatial correlation leads to much less performance degradation for STBC/SFBC than spatial multiplexing.

Frequency-selective channel: Spatial multiplexing and STBC can work well in a frequency-selective channel at low mobility. At high mobility, only MIMO spatial multiplexing or SFBC can work well.

Fading channel: Both spatial multiplexing and SFBC can work well in a fast fading channel only if the channel is not frequency-selective. Over a frequency-selective channel such as UMTS vehicular B channel, spatial multiplexing is better.

Channel estimation technique: SFBC/STBC is not as sensitive to channel estimation error as spatial multiplexing. Thus, if a CE technique with low accuracy is used for low channel resource cost and low implementation complexity, SFBC/STBC is a better choice.

Channel with LOS: A channel with LOS is spatially correlated, and the receiver often has higher received SNR. Therefore, SFBC/STBC can work well due to high received SNR, while spatial multiplexing fails to work in the LOS case due to spatial correlation.

Antenna configuration: For a configuration with more than two transmit antennas, either two of the transmit antennas are chosen for SFBC/STBC, or spatial multiplexing is used. For more than two transmit antennas, full or higher rate SFBC/STBC are desired.

Iterative Decoding

Channel coding undoubtedly plays an important role in modern digital communications. A reasonable coding scheme is always related to the requirements of a particular communication system. GSM supplies low-bit-rate speech service and some data service; a combination of block coding and convolutional coding is used on important bits. 3G mobile communications are expected to provide a wide range of user services spanning from voice to high-rate data, so besides convolutional code, turbo code is used for the first time.

For the limit of transmit power according to the consideration of 4G, decoders will work at

Petitioner Samsung Ex-1004, 0184

low SNR. To improve the decoding performance, all the features known to decoder should be used, such as interleaving, soft decisions, channel state information, and concatenation. On the other hand, the dramatic increase of integrated circuit capacity makes sophisticated error control methods possible. Two kinds of codes, turbo code and low density parity check (LDPC) code, which have very good error correction performance, are promising candidates for an FEC scheme in 4G.

Turbo Code — In 1993, decoding of two or more concatenated codes was proposed using soft iterative decoding. The basic concept of this new coding scheme is to use a parallel concatenation of at least two codes with an interleaver between the component encoders. Decoding is based on alternately decoding the component codes and passing the extrinsic information to the next decoding stage. Even though very simple component codes are used, the turbo coding scheme is able to achieve performance close to Shannon's capacity bound, at least for a large interleaver and at BER of approximately 10^{-5}. Long latency due to large interleaver size and the performance floor at high SNR are two disadvantages related to turbo code.

Another near-optimum turbo code, turbo product code (TPC), is built on 2D or 3D arrays of extended Hamming codes, and works with hard decision or soft decision. The iteration is made between row and column. The advantages of TPC are summarized as followed:

- A single low-cost TPC encoder/decoder can support code rates from 1/5 to 19/20 with excellent performance at high code rates.
- Near zero latency can be attained, and no tailing bits are required.
- Any packet size is supported.
- There is no error floor for TPC.

LDPC — LDPC, proposed by Gallager in 1962, is a linear block code whose parity check matrix is composed of 0 elements dominantly. LDPC code shows good error correction capacity with soft iterative decoding by the sum-product algorithm or belief propagation (BP) algorithm. LDPC codes possess several advantages over turbo codes:

- BP decoding for LDPC codes can be implemented fully parallel and can potentially be implemented at a significantly faster speed.
- LDPC codes have better block error performance.
- There is no error floor for LDPC codes.

Recently, some researchers have investigated the performance of LDPC applied to OFDM systems. The good error rate performance obtained makes it a candidate access method for 4G.

Adaptive Modulation and Coding

Time-varying wireless channel conditions and therefore time-varying system capacity are two important features of wireless and mobile communication systems. Accordingly, future systems should have a high degree of adaptivity on many levels in order to achieve desired performance. Examples of such adaptivity are information rate adaption, power control, code adaptation, bandwidth adaptation, antenna adaptation, and protocol adaptation. AMC is a kind of information rate adaptation, and is used presently in HSDPA and IEEE 802.16.

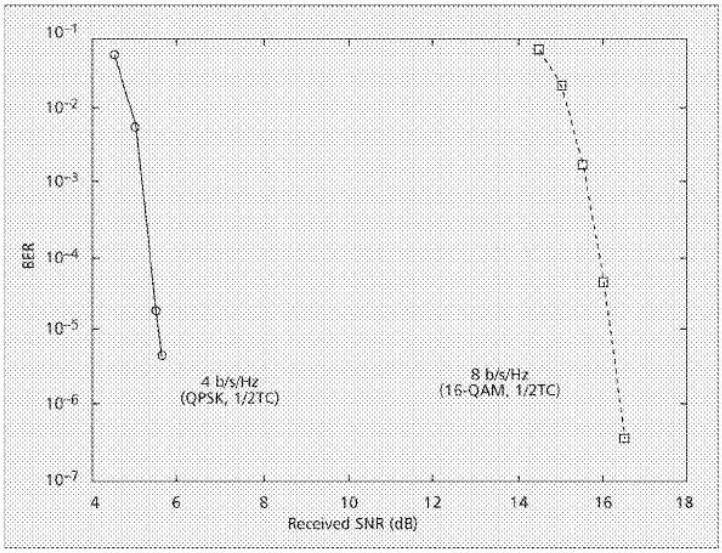


Figure 6. *BER performance of a MIMO-OFDM spatial multiplexing system with bandwidth efficiency of 4 b/s/Hz and 8 b/s/Hz.*

The principle of AMC is to change the modulation and coding format in accordance with instantaneous fluctuation in channel conditions, subject to system restrictions. Channel conditions should be estimated based on feedback from the receiver. For a system with AMC, users close to the cell site are typically assigned higher-order modulation with higher code rates. On the other hand, users close to the cell boundary are assigned lower-order modulation with lower code rates.

The implementation of AMC offers several challenges. First, AMC is sensitive to channel measurement error and delay. In order to select appropriate modulation schemes, the scheduler must be aware of the channel quality. Errors in the channel estimate will cause the scheduler to select the wrong data rate, and transmit at either too high power, wasting system capacity, or too low power, raising the block error rate. Delay in reporting channel measurements also reduces the reliability of the channel quality estimate. Furthermore, changes in interference also increase measurement errors.

One objective of AMC is to greatly improve the MIMO channel capacity with the help of turbo-like codes.

Intercarrier Interference Cancellation

For a traditional OFDM communication system, the frequency offset caused by oscillator inaccuracies or Doppler shift results in ICI that degrades the BER performance of the system greatly. Although frequency synchronization is used, the residential frequency offset causes a number of impairments including attenuation and rotation of each of the subcarriers and ICI

Petitioner Samsung Ex-1004, 0185

Parameter	Value
Sampling factor (MHz)	11.52
FFT size	1024
Carrier frequency (GHz)	3.2
Mobile speed (km/h)	250
Antenna configuration	4 × 4
Spatial correlation model	Independent Identical Distribution
Multipath fading channel	UMTS Vehicular A
Mobile speed (km/h)	60
Spatial multiplexing detector	MMSE
Turbo code length (bits)	5000
Turbo code rate	0.5
Modulation type	QPSK, 16-QAM
Random interleaving length (ms)	40
Synchronization and CE	Perfect
Spatial channel model	Link level channel model C [8]

Table 2. *Simulation parameters.*

between subcarriers. Similarly, MIMO-OFDM is also sensitive to Doppler shift and carrier frequency offset that destroy orthogonality of subcarriers and give rise to ICI. ICI mitigation (e.g., a time-domain filtering scheme [10]) is needed to increase the achievable data rates over the wireless medium.

PAPR

The main limitation of OFDM-based transmission systems is the high PAPR of the transmitted signals, and large peaks will occasionally reach the amplifier saturation region and result in signal distortion. Several PAPR reduction schemes have been proposed and investigated; of them, the partial transmit sequence (PTS) scheme is an efficient approach and a distortionless scheme for PAPR reduction by optimally combining signal subblocks. Selective mapping (SLM) is also a good approach, in which some statistically independent sequences are generated from the same information and the sequence with the lowest PAPR is transmitted. Both techniques provide improved PAPR statistics at the cost of additional complexity.

Simulation Results

In Fig. 6 we show the BER performance of a MIMO-OFDM spatial multiplexing system with bandwidth efficiency of 4 b/s/Hz and 8 b/s/Hz. The simulation parameters are listed in Table 2. The results show that for BER of 10^{-5}, bandwidth efficiency of 4 b/s/Hz can be achieved at SNR of 5.5 dB, and bandwidth efficiency up to 8 b/s/Hz can also be achieved at a reasonable SNR of lower than 16.2 dB. These encouraging results show that MIMO-OFDM creates a new way to achieve high bandwidth efficiency without sacrificing additional power or bandwidth.

Conclusions

In this article MIMO-OFDM key techniques are introduced. Some of our considerations in MIMO-OFDM system design are also given, focusing on frame structure, CE, and comparisons of STC and spatial multiplexing. The proposed frame structure with scattered pilots is especially suited for high-data-rate transmission at high mobility. Based on comparisons of STC and spatial multiplexing, qualitative criteria in terms of data rate, application environment, and antenna configuration are proposed to choose STC or spatial multiplexing. Link level simulation results for the designed MIMO-OFDM spatial multiplexing system present encouraging performance. The high bandwidth efficiency obtained shows that MIMO-OFDM is a potential candidate for future broadband wireless access.

References

[1] V. Tarokh, H. Jafarkhani, and A. R. Calderbank, "Space-Time Block Codes from Orthogonal Designs," *IEEE Trans. Info. Theory*, vol. 45, no. 5, Jul 1999, pp. 1456–67.

[2] V. Tarokh, N. Seshadri, and A. R. Calderbank, "Space-time Codes for High Data Rate Wireless Communication: Performance Criterion and Code Construction," *IEEE Trans. Info. Theory*, vol. 44, no. 2, Mar. 1998, pp. 744–65.

[3] G. D. Golden *et al.*, "Detection Algorithm and Initial Laboratory Results Using V-BLAST Space-Time Communication Architecture," *Elect. Lett.*, vol. 35, no.1, Jan. 1999.

[4] J. Ha *et al.*, "LDPC-coded OFDM with Alamouti/SVD Diversity Technique," *Wireless Pers. Commun.*, vol. 23, no. 1, Oct. 2002, pp. 183–94.

[5] A. N. Mody and G. L. Stuber, "Synchronization for MIMO OFDM Systems," *Proc. GLOBECOM 2001*, pp. 509–13.

[6] Y. Li, N. Seshadri, and S. Ariyavisitakul, "Channel Estimation for OFDM System with Transmitter Diversity in Mobile Wireless Channels," *IEEE JSAC*, vol. 17, no. 3, Mar. 1999, pp. 461–70.

[7] Y. Li, "Simplified Channel Estimation for OFDM Systems with Multiple Transmit Antennas," *IEEE Trans. Wireless Commun.*, vol. 1, no. 1, Jan. 2002, pp. 67–75.

[8] 3GPP TR 25.996 V6.1.0, "Spatial Channel Model for Multiple Input Multiple Output (MIMO) Simulations."

[9] S. M. Alamouti, "A Simple Transmit Diversity technique for Wireless Communications," *IEEE JSAC*, vol. 16, no. 8, Oct. 1998, pp. 1451–58.

[10] A. Stamoulis, S. N. Diggavi, and N. Al-Dhahir, "Intercarrier Interference in MIMO OFDM," *IEEE Trans. Sig. Proc.*, vol. 50, no. 10, Oct. 2002, pp. 2451–64.

Biographies

HONGWEI YANG [M] (hongwei.yang@alcatel-sbell.com.cn) is an engineer in the Research and Innovation Center, Alcatel Shanghai Bell Co., Ltd.,China. He received a Ph.D. degree in communication and information systems from Shanghai Jiao Tong University in 2001. His B.S. and M.S. degrees in electromagnetic measurement and instruments were received from Harbin Institute of Technology, China, in 1996 and 1998, respectively. From 2001 to 2004 he was engaged in 3G and 4G mobile communication R&D projects in Alcatel Shanghai Bell Co., Ltd. His research interests are in the area of wireless and mobile communications.

Petitioner Samsung Ex-1004, 0186

Electronic Acknowledgement Receipt	
EFS ID:	12763296
Application Number:	12999029
International Application Number:	
Confirmation Number:	1213
Title of Invention:	INSERTING AND DECODING REPLICATED DATA SYMBOLS IN WIRELESS COMMUNICATIONS
First Named Inventor/Applicant Name:	Ali Yazdan Panah
Customer Number:	27076
Filer:	Jennifer Lane Spaith/randi rowe
Filer Authorized By:	Jennifer Lane Spaith
Attorney Docket Number:	P215801.WO-US.01
Receipt Date:	11-MAY-2012
Filing Date:	14-DEC-2010
Time Stamp:	19:37:53
Application Type:	U.S. National Stage under 35 USC 371

Payment information:

Submitted with Payment	no

File Listing:

Document Number	Document Description	File Name	File Size(Bytes)/ Message Digest	Multi Part /.zip	Pages (if appl.)
1		US-800279-02-US-REG_20120511_SIDS.pdf	177319 5c4b88f43faab6b2c574ecf8f0677d813585fb74	yes	3

	Multipart Description/PDF files in .zip description				
	Document Description		Start	End	
	Transmittal Letter		1	1	
	Information Disclosure Statement (IDS) Form (SB08)		2	3	
Warnings:					
Information:					
2	Non Patent Literature	US-800279-02-US-NAT_NPL1_Cheon1.pdf	1655339 ae850526a3bdae4029f47a627bed3557193f9398	no	4
Warnings:					
Information:					
3	Non Patent Literature	US-800279-02-US-NAT_NPL2_Cirpan1.pdf	5000448 dec54006a46b86271446e865adef845d4ee44421	no	9
Warnings:					
Information:					
4	Non Patent Literature	US-800279-02-US-NAT_NPL3_Lee1.pdf	3028653 c5cf009a1b83586687a7dd8a1f4229639a3d114	no	5
Warnings:					
Information:					
5	Non Patent Literature	US-800279-02-US-NAT_NPL4_Li1.pdf	5804210 a0bfec6d02156b422f8c114eb466b939d2171d60	no	10
Warnings:					
Information:					
6	Non Patent Literature	US-800279-02-US-NAT_NPL5_Lupdf1.pdf	3052043 70051907793cfdaca3a2d3a57fe744dd39332ef4	no	5
Warnings:					
Information:					
7	Non Patent Literature	US-800279-02-US-NAT_NPL6_Kleider1.pdf	2721179 630da89cc8bd7b7aa49ef92d3e6cb00b1be188da	no	4
Warnings:					
Information:					
8	Non Patent Literature	US-800279-02-US-NAT_NPL7_Stamoulis1.pdf	7354601 a752cb28526281d3392e870a6436ef0197ad1525	no	14
Warnings:					
Information:					

9	Non Patent Literature	US-800279-02-US-NAT_NPL8_Sun1.pdf	3476244 56b4d6d5e621067dfde2deff9df2508030a1c242	no	6
Warnings:					
Information:					
10	Non Patent Literature	US-800279-02-US-NAT_NPL9_Ma1.pdf	2000373 8caa23f166762dfb49d3dec4a891aa31476cfdbc0	no	4
Warnings:					
Information:					
11	Non Patent Literature	US-800279-02-US-NAT_NPL10_Yang1.pdf	15047833 3555b8aedd065f2ab20864e8590c7e22f34a0804	no	8
Warnings:					
Information:					
			Total Files Size (in bytes):	49318242	

This Acknowledgement Receipt evidences receipt on the noted date by the USPTO of the indicated documents, characterized by the applicant, and including page counts, where applicable. It serves as evidence of receipt similar to a Post Card, as described in MPEP 503.

New Applications Under 35 U.S.C. 111

If a new application is being filed and the application includes the necessary components for a filing date (see 37 CFR 1.53(b)-(d) and MPEP 506), a Filing Receipt (37 CFR 1.54) will be issued in due course and the date shown on this Acknowledgement Receipt will establish the filing date of the application.

National Stage of an International Application under 35 U.S.C. 371

If a timely submission to enter the national stage of an international application is compliant with the conditions of 35 U.S.C. 371 and other applicable requirements a Form PCT/DO/EO/903 indicating acceptance of the application as a national stage submission under 35 U.S.C. 371 will be issued in addition to the Filing Receipt, in due course.

New International Application Filed with the USPTO as a Receiving Office

If a new international application is being filed and the international application includes the necessary components for an international filing date (see PCT Article 11 and MPEP 1810), a Notification of the International Application Number and of the International Filing Date (Form PCT/RO/105) will be issued in due course, subject to prescriptions concerning national security, and the date shown on this Acknowledgement Receipt will establish the international filing date of the application.

PATENT

IN THE UNITED STATES PATENT AND TRADEMARK OFFICE

Appl. No.	: 12/999,029	Confirmation No.	: 2611
Applicants	: Ali Yazdan Panah et al.		
Filed	: December 14, 2010	Attorney Docket No.:	P215801.WO-US.01
Art Unit	: 2611	Customer No.	: 27,076
Examiner	: Shuwang Liu		
Title	: INSERTING AND DECODING REPLICATED DATA SYMBOLS IN WIRELESS COMMUNICATION		

SUPPLEMENTAL INFORMATION DISCLOSURE STATEMENT

Mail Stop Amendment
Commissioner for Patents
P.O. Box 1450
Alexandria, VA 22313-1450

Sir:

In accordance with 37 C.F.R. §§ 1.56 and 1.97 through 1.98, applicants wish to make known to the Patent and Trademark Office the references set forth on the attached form PTO/SB/08. Copies of the cited non-patent literature references, as required under 37 C.F.R. § 1.98(a)(2), are attached. Copies of the cited U.S. patents will not be submitted herewith in accordance with the waiver by the Office of the requirement under 37 C.F.R. § 1.98(a)(2)(i) for U.S. national patent applications filed after June 30, 2003.

Please acknowledge receipt of this Information Disclosure Statement and kindly make the cited references of record in the above-identified application.

Respectfully submitted,
DORSEY & WHITNEY LLP

May 11, 2012
Date

Jennifer L. Spaith
Registration No. 51,916

701 Fifth Avenue, Suite 6100
Seattle, WA 98104-7043
Telephone: (206) 903-8800
Facsimile: (206) 299-9288

Petitioner Samsung Ex-1004, 0190

PCT REQUEST

Original (for **SUBMISSION**)

0	**For receiving Office use only**	
0-1	International Application No.	PCT/US10/46106
0-2	International Filing Date	20 AUG 2010(20.08.2010)
0-3	Name of receiving Office and "PCT International Application"	RO/US

0-4	**Form PCT/RO/101 PCT Request**	
0-4-1	Prepared Using	PCT-SAFE [EASY/EFS-Web mode] Version 3.51.045.221 MT/FOP 20100401/0.20.5.18
0-5	**Petition** The undersigned requests that the present international application be processed according to the Patent Cooperation Treaty	
0-6	**Receiving Office (specified by the applicant)**	United States Patent and Trademark Office (USPTO) (RO/US)
0-7	**Applicant's or agent's file reference**	P215801WO01
I	**Title of Invention**	INSERTING AND DECODING REPLICATED DATA SYMBOLS IN WIRELESS COMMUNICATIONS
II	**Applicant**	
II-1	This person is	Applicant only
II-2	Applicant for	All designated States except US
II-4	Name	THE BOARD OF REGENTS OF THE UNIVERSITY OF TEXAS SYSTEM
II-5	Address	201 W. 7th Street Austin, Texas 78701 United States of America
II-6	State of nationality	US
II-7	State of residence	US
III-1	**Applicant and/or inventor**	
III-1-1	This person is	Applicant and inventor
III-1-2	Applicant for	US only
III-1-4	Name (LAST, First)	ALI, Yazdan Panah
III-1-5	Address	502 Elmwood Place #101 Austin, Texas 78705 United States of America
III-1-6	State of nationality	IR
III-1-7	State of residence	US

PCT REQUEST

Original (for **SUBMISSION**)

III-2	**Applicant and/or inventor**	
III-2-1	This person is	Applicant and inventor
III-2-2	Applicant for	US only
III-2-4	Name (LAST, First)	HEATH, JR., Robert W.
III-2-5	Address	2143 Barton Hills Drive Austin, Texas 78704 United States of America
III-2-6	State of nationality	US
III-2-7	State of residence	US
IV-1	**Agent or common representative; or address for correspondence** The person identified below is hereby/ has been appointed to act on behalf of the applicant(s) before the competent International Authorities as:	Agent
IV-1-1	Name	DORSEY AND WHITNEY LLP
IV-1-2	Address	IP Docket - SE 701 Fifth Avenue, Suite 6100 Seattle, Washington 98104-7043 United States of America
IV-1-3	Telephone No.	206-903-8800
IV-1-4	Facsimile No.	206-299-9288
IV-1-5	e-mail	ipdocket-se@dorsey.com
IV-1-5(a)	E-mail authorization The receiving Office, the International Searching Authority, the International Bureau and the International Preliminary Examining Authority are authorized to use this e-mail address, if the Office or Authority so wishes, to send notifications issued in respect of this international application:	as advance copies followed by notifi-cations
IV-2	**Additional agent(s)**	additional agent(s) with same address as first named agent
IV-2-1	Name(s)	BULCHIS,Edward W.(26847); MEIKLEJOHN,Paul T.(26569); PARK,Brian C.(45519); ENG,Kimton N.(43605); STEWART,Douglas(51060); BROWN,James Fearon(60837); MEYER,Ryan(61435); LANE,Jennifer M.(51916)
V	**DESIGNATIONS**	
V-1	**The filing of this request constitutes under Rule 4.9(a), the designation of all Contracting States bound by the PCT on the international filing date, for the grant of every kind of protection available and, where applicable, for the grant of both regional and national patents.**	
VI-1	**Priority Claim**	NONE
VII-1	**International Searching Authority Chosen**	Australian Patent Office (ISA/AU)

PCT REQUEST

Original (for **SUBMISSION**)

VIII	**Declarations**	Number of declarations	
VIII-1	Declaration as to the identity of the inventor	–	
VIII-2	Declaration as to the applicant's entitlement, as at the international filing date, to apply for and be granted a patent	–	
VIII-3	Declaration as to the applicant's entitlement, as at the international filing date, to claim the priority of the earlier application	–	
VIII-4	Declaration of inventorship (only for the purposes of the designation of the United States of America)	–	
VIII-5	Declaration as to non-prejudicial disclosures or exceptions to lack of novelty	–	
IX	**Check list**	Number of sheets	Electronic file(s) attached
IX-1	Request (including declaration sheets)	4	✓
IX-2	Description	21	–
IX-3	Claims	4	–
IX-4	Abstract	1	✓
IX-5	Drawings	7	–
IX-7	TOTAL	37	
	Accompanying Items	Paper document(s) attached	Electronic file(s) attached
IX-8	Fee calculation sheet	✓	–
IX-20	**Figure of the drawings which should accompany the abstract**	1	
IX-21	**Language of filing of the international application**	English	
X-1	**Signature of applicant, agent or common representative**	/Jennifer M. Lane 51916/	
X-1-1	Name (LAST, First)	LANE, Jennifer M.	
X-1-2	Name of signatory		
X-1-3	Capacity		

PCT REQUEST

Original (for **SUBMISSION**)

FOR RECEIVING OFFICE USE ONLY

20-08-2010

10-1	**Date of actual receipt of the purported international application**	20 AUG 2010
10-2	**Drawings:**	
10-2-1	Received	
10-2-2	Not received	
10-3	**Corrected date of actual receipt due to later but timely received papers or drawings completing the purported international application**	
10-4	**Date of timely receipt of the required corrections under PCT Article 11(2)**	
10-5	**International Searching Authority**	ISA/AU
10-6	**Transmittal of search copy delayed until search fee is paid**	

FOR INTERNATIONAL BUREAU USE ONLY

11-1	**Date of receipt of the record copy by the International Bureau**	